1-10-2014 12:00 AM

# The Latte Gold Zone, Kaminak's Coffee Gold Project, Yukon, Canada: Geology, Geochemistry, and Metallogeny

Eric Buitenhuis
*The University of Western Ontario*

Supervisor
Dr. Norman A. Duke
*The University of Western Ontario* Joint Supervisor
Dr. Craig S. Finnigan
*The University of Western Ontario*

Graduate Program in Geology
A thesis submitted in partial fulfillment of the requirements for the degree in Master of Science

# THE LATTE GOLD ZONE, KAMINAK'S COFFEE GOLD PROJECT, YUKON, CANADA: GEOLOGY, GEOCHEMISTRY, AND METALLOGENY

(Thesis format: Monograph)

by

Eric Buitenhuis

Graduate Program in Geology

A thesis submitted in partial fulfillment
of the requirements for the degree of
Master of Science

The School of Graduate and Postdoctoral Studies
The University of Western Ontario
London, Ontario, Canada

# Abstract

The Latte Gold Zone is hosted within complexly tectonically imbricated metamorphic rocks of the Yukon-Tanana terrane. Snowcap assemblage psammitic schist and amphibolite with exotic Slide Mountain ultramafics overthrusts unidentified arc metavolcanics which in turn overthrust the Late Permian Sulphur Creek orthogneiss. Rapid unroofing of the Dawson Range during the Mid-Cretaceous culminated in dextral movement along the Coffee Creek fault system. A set of stacked, ESE–WNW trending, steeply dipping brittle fault structures served as conduits for gold-bearing fluids. Core-logging, detailed petrography, microprobe analysis, and PIMA investigations indicate that Latte is an epizonal orogenic gold deposit. Gold is hosted within arsenian pyrite in association with dolomite and illite, and was deposited by a $CO_2$-$H_2O$-As-Sb-S-Ag-Au fluid between 220 and 250° C which sulphidized metamorphic mica. Primary gold disseminations are locally remobilized by a $CO_2$-rich fluid and re-deposited within arsenian pyrite in breccias and dolomite-quartz veinlets.



## Keywords

Yukon, Orogenic Gold Deposit, Dawson Range, White Gold District, Yukon-Tanana Terrane, Snowcap Assemblage, Whole-Rock Geochemistry, Petrography, Arsenian Pyrite, Sulphidation.

# Acknowledgments

Many thanks go out to my two supervisors, Dr. Norm Duke and Dr. Craig Finnigan. Thanks to Norm for always having an open door and his guidance and willingness to listen to any oddball idea I was bouncing off him at any time. Thanks to Craig for the fantastic geologic guidance and mentoring me through my first few years in the field with Kaminak.

This research could not have been completed without the support of the Kaminak Gold Corporation, who generously funded all research costs over the course of this thesis. The research was also generously supported by a Society of Economic Geologists Graduate Fellowship and the Yukon Geological Survey's Geoffrey Bradshaw Memorial Scholarship, both of which I am extremely thankful for. Huge thanks go out to Bob Barnett for the many hours of probe work and his patience in teaching me the finer points of petrography. Thanks to the Kaminak field team over the last three seasons for their support and many excellent geologic discussions: Tim Smith, Rory Kutluoglu, Craig Finnigan, Adam Fage, Joe Currie, James Scott, and Erik Scheel. Thanks to Rob Carpenter for initially approving the project and sitting Craig and I down to get us to focus our research goals.

Thanks is due for all of the excellent work conducted by previous workers in the Dawson Range and Yukon as a whole. Such an excellent story of mineralization that is emerging in the Dawson Range would not have been possible without the efforts of workers at the Geological Survey of Canada and Yukon Geological Survey. Thanks to Murray Allan and Matias Sanchez for stimulating discussion during their visit to the Coffee Property.

Thanks to Peter for being an awesome friend and keeping me grounded, and to Patrick and Scott for always being ready for a pint. Thanks to the Western Geo group: Imran, Moe, Jon, Adam, Laurie. Finally, thanks to my girlfriend Nicole, my Mother, Father, and brother Evan for their support through all of the ups and downs.

Table of Contents

# List of Tables

# List of Figures

# Chapter 1

## 1 Introduction

In recent years, gold has seen a dramatic increase in value. The current worldwide economic instability has prompted both countries and individuals to purchase gold, driving its price up to the highest levels in history, with a peak at $1895/oz. in September, 2011. The rapidly climbing price of gold spurred global interest in exploration for the precious metal, with a prime example being the explosion of exploration activity in Canada's Yukon Territory.

The 2009 discovery by Underworld Resources (acquired by Kinross Gold Corporation in 2010) of the White Gold property in west-central Yukon approximately 100 km south of Dawson City kick-started a claim-staking rush akin to the Klondike Gold Rush of the late 1800's. Gold found at the White Gold property is structurally controlled and orogenic in character, defining a new style of mineralization within the Dawson Range. In addition to Golden Saddle, other lode-gold occurrences within this region of the Yukon include the Longline occurrence, the Boulevard gold deposit, and the Coffee Project, the subject of this thesis. These gold occurrences have been suggested as the bedrock source for the abundant placer gold fields of the Dawson Range, including the famous Klondike (MacKenzie et al., 2010). While the staking rush has now subsided, some initial claims have been proven to contain very significant gold endowment, including Kaminak Gold Corporation's Coffee Gold Project; an initial NI43-101 compliant resource of 3.2 Moz Au was reported in a December 13, 2012 press release.

The regional contexts of these lode-gold occurrences are poorly understood as they are still in the initial years of exploration and discovery. Work to date has demonstrated that Longline, Boulevard, Golden Saddle, and Coffee do not share common intrusion-related characteristics or morphologies. In particular, both Coffee and Golden Saddle have no known analogues in the region. The Coffee deposit shares very few characteristics with commonly known gold deposits globally, and it even lacks similarity with the Golden Saddle deposit. Coffee is unique in that it is a structurally and

lithologically controlled, Au-only deposit, with metal associations limited to As and Sb, with minor Ag, Ba, and Mo. The source of the mineralizing fluids as well as the source of the Au endowment in these areas is currently a subject of debate.

The present investigation focuses on the host rock setting and documents the nature of mineralization in the Latte zone. Objectives of the study are to: 1) characterize the host rocks, structures, and alteration assemblages present within the Latte zone; 2) re-log down-hole drill core logs from the 2010 and 2011 field seasons in order to provide accurate cross sections for geologic interpretation; 3) determine and describe the mineralization process and constrain its relative age and place within the structural history of the Coffee Property; and 4) compare and contrast mineralization at the Latte zone with that of other gold prospects within the Dawson Range in order to define a metallogenic model for the system.

This study utilizes drill core logs, 35-element ICP-MS assay data, petrographic and electron microprobe analysis and trace-element geochemistry in order to fulfil the above objectives. These techniques have provided new information about the geology and geochemistry of the Latte zone, and allow for the creation of a deposit model for the zone. These data, when combined with previous work on the Coffee property, permits the creation of a preliminary geologic model for the Coffee property as a whole. The study adds to the geological understanding of the very complex White Gold district and sheds new light on a very unique and specific deposit without a direct analogue in the region.

## 1.1 Coffee Property Information and Exploration History

Kaminak's Coffee Gold Project is located within the northwestern Stevenson Ridge map sheet (NTS 115-J, K) (Ryan et al., 2013), approximately 130 km south of Dawson City. It is ~8 km south of the Yukon River and at the headwaters of Dan Man and Halfway creeks, which flow northwards into the river. It consists of 3,021 contiguous claims that are staked under the Yukon Territory Quartz mining act and covers approximately 60,230 hectares. The property is 100% owned by Kaminak Gold Corporation, headquartered in Vancouver, British Columbia.

The geomorphology of the property is characterized by rolling uplands with extremely limited outcrop, with vertical relief ranging from ~300 meters at the Yukon River to ~1300 meters at the top of the Supremo zone. A layer of permafrost soil undisturbed by glaciation overlies bedrock and supports dense vegetation, with the strongest and thickest growth concentrated on southern slopes and within drainages. Multiple creeks flow across the area towards the Yukon River, including Halfway Creek, Dan Man Creek, and the eponymous Coffee Creek, which collects drainage from the southern slopes of the ridge which hosts the main Au deposits.

The Coffee Creek area has seen very little lode gold exploration, although Coffee Creek itself has been sporadically placer mined since the early 1900s. Early work in the area includes limited hard rock reconnaissance exploration in the 1960s and 1970s for porphyry copper targets, and soil and silt sampling of Coffee Creek in 1981 (Jilson, 2000). This sampling indicated "uniformly high, double digit arsenic values" near the confluence of the Yukon River and Coffee Creek.

Silt and soil sampling was conducted by Deltango Gold Ltd. in 1999 and they concluded that further work should be undertaken in the area (Jilson, 2000). This was followed by a small exploration program conducted by consultants from Prospector International Resources in 1999-2000. Their program consisted of stream sediment sampling of subsidiary drainages of Coffee Creek, contour and ridgeline soil sampling, sampling of outcrop, and minor fluid inclusion work. The 1999 program identified a soil geochemical anomaly which was refined in 2000 to cover a 400 by 900 meter area. Further soil sampling in addition to mechanized trench sampling was recommended (Jaworski and Meyer, 2000; Jaworski and Vanwermeskerken, 2001).

Work in 2006 and 2007 by prospector Shawn Ryan defined a gold-in-soil geochemical anomaly through ridge and spur soil sampling traverses on the Coffee claims (Ryan, 2007; Ryan, 2008). This region of the Dawson Range is unglaciated and soil samples can be inferred to reflect bedrock below a thin layer of overburden (Duk-Rodkin, 1999). Kaminak Gold Corp. executed an option agreement with Shawn Ryan in June, 2009, to acquire the Coffee project. Kaminak began exploration on the property by expanding the

soil sampling grid and identifying targets including the Supremo, Latte, Double Double, Kona, and Espresso zones. Trench sampling along with geological mapping and prospecting was conducted at each zone. Drill programs were conducted in 2010, 2011, 2012, and to present day, and the new Americano, Sugar, Macchiato, and Arabica prospects were added as further zones of gold enrichment.

## 1.2 Coffee Property Geology

The property lies within the Yukon-Tanana terrane (YTT) and part of the Tintina gold belt (TGB) which is host to several gold and base metal deposits (Smith, et al., 1999; Bakke, 1995; Bakke et al., 2000; Maloof et al., 2001; Hart et al., 2002; Joyce, 2002; Marsh et al., 1999, 2003; Mair et al., 2000, 2006; Goldfarb et al., 2007; Mckenzie, 2013; Bailey, 2013). Rocks in the Coffee area are divided into two main, west-northwest trending, moderate to shallowly south to southwest-dipping assemblages. Mafic metasedimentary and metavolcanic rocks of the Devono-Mississippian Snowcap and an unknown arc assemblage overlie and intertongue with augen orthogneiss of the Permian-aged Sulphur Creek suite. The area of the project is bound to the southwest by the Coffee Creek monzogranite, which intruded into the Dawson Range Batholith. Both intrusive phases are part of the Mid-Cretaceous Whitehorse Plutonic Suite.

Gold mineralization on the Coffee property is structurally controlled. The Latte zone is hosted within a main WNW-ESE trending structure. This structure consists of a corridor of semi-brittle to brittle faults dipping steeply to the southwest with a later brittle overprint expressed as fault gouge and breccias. The structural corridor is a splay related to the Coffee Creek fault, which is in turn a splay off of the Big Creek fault to the southeast. The Big Creek fault originated as a result of thrusting in the Permian followed by a transition in the mid-Cretaceous to dextral strike-slip movement (M.G. Sanchez, personal communication 2013). This structure extends to the northwest with numerous splays, including the Coffee Creek fault, "horse-tailing" off of its deep structural root (Sanchez, 2013). These fault systems have been subjected to later episodes of reactivation as a result of Tertiary-age dextral movement along the Tintina and Denali faults **(**Johnston, 1999; Mackenzie and Craw, 2010). The Latte zone is mineralized over several kilometers along strike and is considered the most prospective gold target on the Coffee

property to date. Other notable prospects comprise the Supremo, Double Double, Kona, and Americano zones. These occur on brittle, N-S and NNE-SSW trending fault-fracture systems occasionally intruded by post-metamorphic dikes.

## 1.3 Previous and On-going Work in the Project Area

Significant research, including geological mapping, has been conducted within the Stewart River map sheet (NTS 115-N, O) as a result of the Geological Survey of Canada's Ancient Pacific Margin NATMAP research program (Ryan and Gordey, 2001a, 2001b, 2002a, 2002b, 2004; Ryan et al., 2003; Shives et al., 2002; Ruks et al., 2006; Berman et al., 2007). As the Coffee Property is located 10 km south of the Yukon River and approximately 12 km south of the border with the Stewart River map sheet, much of the data acquired within that region (geochronology, regional metamorphism and P-T evolution) can be applied to the area of the Coffee Project. Academic research within the northeast corner of the Stevenson Ridge map sheet where the Coffee Project is located is limited.

Mapping has been carried out within the region of the Coffee Project by several authors (Tempelman-Kluit, 1974; Mortensen, 1990, 1992, 1996), including the newly published Stevenson Ridge map sheet (115-J, K) (Ryan et al., 2013). Regional geochronology conducted by Berman et al. (2007) includes samples of the Dawson Range batholith and Coffee Creek granite and a date for the Sulphur Creek orthogneiss outcropping on the Kaminak claims.

Recent study on gold deposits in the immediate area includes a MSc thesis in progress at the University of British Columbia by G. McKenzie, and paper (McKenzie et al., 2013) on the Boulevard gold prospect approximately 10km to the southwest. An MSc thesis (Bailey, 2013) and paper (Allan et al., 2013) are available for the Golden Saddle deposit 40 km to the north. The Boulevard prospect is located in the Independence Creek area of the Dawson Range, 10 km southwest of the Coffee Project. The work completed on the Boulevard gold prospect identified a mid-Cretaceous, orogenic gold system with sheeted quartz-sulphide-carbonate veins and fault breccia hosted within mafic schist (McKenzie et al., 2013). The deposit is dated between 96-95 Ma through Re-Os dating on

molybdenite and Ar-Ar dating on hydrothermal sericite in close spatial association with gold mineralization. Kinross Gold Corporation's Golden Saddle deposit is identified as an amagmatic, structurally and lithologically controlled orogenic gold deposit (Bailey, 2013). Gold is hosted by pyrite and quartz-carbonate-illite veins and is accompanied by Au-Ag-Pb-S-Te enrichment. Re-Os dating on molybdenite in gold-bearing veins resulted in model ages of 163-155 Ma, placing the Golden Saddle mineralization within the Late Jurassic (Bailey, 2013).

Previous research on the Coffee Project itself includes a 2011 paper by Wainwright et al. covering the initial geologic understanding of the deposit, and a BSc thesis on the Supremo gold zone (Cruikshank, 2011). A BSc thesis is in progress by L. Boyce at the University of Alberta on the Double Double zone. Coffee was initially classified as a structurally-controlled and possibly intrusion-related gold deposit with steeply dipping structural corridors characterized by silicification, sericitization, and clay alteration with variable As-Ag-Sb-Ba-Mo enrichment. The gold mineralized structures at Coffee are generally similar in character property-wide and occasionally contain andesite and dacite dikes as well as polyphase brecciation of varying style. Gold is hosted within disseminated arsenian pyrite and arsenopyrite and vein-style mineralization is noticeably absent, although pre-mineralization quartz veining is present throughout the host rocks (Wainwright et al., 2011).

## 1.4 Nomenclature

The Coffee Gold Project has been ascribed to the White Gold *district*, a region which was initially defined as placer and lode gold mineralization of similar character to the Golden Saddle deposit (MacKenzie and Craw, 2010). This district is bound by the Indian River to the north, various placer creeks to the west which drain eastwards into the White and Yukon Rivers, by the Black Hills and Scroggie Creek drainages to the east, and to the south by the Yukon River (Bailey, 2013). Coffee lies just south of the Yukon River and as it shares some characteristics with Golden Saddle, it is included within the bounds of the White Gold district.

The Coffee Gold *project* comprises all 3,021 contiguous claims staked under the Yukon Territory Quartz mining act and covers 60,230 hectares. This continuous block of staked ground lies just south of the Yukon River. The Coffee Gold project contains multiple gold prospects termed *zones*. Examples include the Latte, Supremo, Double Double, and Kona zones. These zones include both drilled and undrilled Au-in-soil anomalies occurring across the claim block variously hosted in granite, schist, and gneiss. Zones which were included in the published resource include: Supremo, Latte, Double Double, and Kona (Kaminak Gold Corporation, 2012).

The Latte *zone* is defined as a single NI 43-101 compliant resource (Kaminak Gold Corporation, 2012). It is located at the southwest apex of the "Golden Triangle", a set of structures which comprise a roughly east-west striking corridor which hosts the Latte and Double Double zones, as well as the roughly north-striking Supremo structures. The Latte mineralization is hosted entirely within metasedimentary and metavolcanic schistose rocks.

## 1.5 Methodology

A sample suite consisting of over 114 samples and >75 polished thin sections was collected from the Latte zone. Selective sampling of drill holes was completed based on detailed core logging completed by the author and Kaminak team over the 2010, 2011, and 2012 drill seasons. Representative material was selected to characterize each lithology seen within the Latte zone as well as provide samples for whole rock geochemical analysis.

All samples are identified following the naming convention ascribed to diamond drill holes by Kaminak Gold Corporation beginning in 2010 with the addition of the sample depth. For example, a sample taken from the 82$^{nd}$ diamond drill hole on the property from 177.5m depth is labelled 82-117.5. No samples from reverse-circulation drill holes are included within this study. All sections are thus identified for petrographic and microprobe analysis.

Most samples were collected in August, 2011 from boxes of cut half-core after in-field re-logging of three strategic drill holes: CFD0082, CFD0105, and CFD0114. Additional samples were taken from drill holes which intersected lithologies not present in the three holes selected for investigation. In particular, serpentinite and mineralized intervals that were intersected in the 2012 drill season or in the 2010 drill season in order to create a complete sample suite. Samples were not selected at set intervals, but rather selected to represent each lithology and the varying alteration styles. Least-altered amphibolite and ultramafic samples were submitted for geochemical analysis. Detailed petrographic analysis was completed on all samples and subsets were subjected to whole rock geochemical analysis and microprobe analysis.

A large field component of this thesis entailed the re-logging of drill holes at Latte. This began with the above mentioned drill-holes, but through the usage of available 35 element inductively coupled plasma atomic emission spectroscopy (ICP-AES) data, included general re-logging of the Latte zone. ICP-AES analysis was performed by ALS Chemex Laboratories in Vancouver, Canada. Analysis included crushing and sieving each meter of drill core to 85 % -200 mesh ASTM (-75 microns), aqua regia rock digestion, in addition to standard fire assay for Au. The 35 Element ICP-AES provides a suitable reconnaissance geochemical filter for usage in bulk re-logging. A number of elements can be plotted down-hole in order to identify alteration relationships, which quickly and cheaply aid in geochemical discrimination of gold zones. Host lithology can also be roughly ascertained through varying elemental ratios regardless of the level of hydrothermal alteration.

Twenty-three least-altered samples were selected from the Latte zone to establish their protolith and sources against known databases of amphibolite within the Yukon-Alaska region and YTT. The samples follow a basic naming convention from L001-L021, each linked to a corresponding thin section. Samples were submitted to ALS Chemex Laboratories in Vancouver, Canada, with sample preparation completed at ALS Chemex Laboratories in Sudbury, Canada. Fourteen elements were detected through lithium metaborate fusion with ICP-AES. Carbon and sulfur were detected by combustion furnace. Trace elements including the full rare earth suite were determined

after three acid digestions with an ICP-AES finish. Resistive elements were treated to a lithium borate fusion. Base metals were determined by a four acid digestion. An aqua regia digestion was applied to the volatile gold-related trace elements, with gold analyzed separately through fire assay.

Electron microprobe analysis (EPMA) was performed with two main goals: 1) characterization of biotite and amphibole chemistry to determine their alteration and the relationship between both minerals; 2) to obtain white mica chemistries to compare with previously reported data by Cruikshank (2011). Analyses were carried out on a 5-spectrometer JEOL 733 at R.L. Barnett Geological in Lambeth, Ontario.

A further suite of mineralized and un-mineralized samples from various zones across the Coffee Project were selected during the 2012 field season. These samples were selected in order to compare alteration mineralogy from the Supremo, Latte, and Double Double zones with that seen at the Sugar zone at the eastern end of the Coffee property. Samples were submitted to Laurentian Goldfields Ltd. for analysis. Samples follow a different naming convention, where abbreviations for the zones are as follows: Latte, LAT; Supremo, SUP; Double Double, DD; and Sugar, SUG. Samples from zones other than Latte are not discussed within this study.

This study utilized a number of additional resources provided by Kaminak Gold Corporation. These supplemental datasets include:

1) The 35-element ICP-AES geochemical data, as described above in the methodology. This data provided the base information for the geochemical re-logging of the Latte zone.

2) A suite of whole-rock geochemical analysis of various rocks from the Coffee Project, collected during the 2010 field season. Samples were sent to ALS Laboratories in Vancouver, BC, and included samples from the Kona, Latte, Supremo, and Double Double zones.

3) The Kaminak Coffee Project drill database. Drill holes studied in this thesis are contained within a database of all (>350) diamond drill holes from the project. Nearly all

drill holes at the Latte zone were oriented and the database contains all data associated with each hole.

## 1.6 Thesis Structure

This thesis contains 7 chapters and 6 appendices. Chapter 1 presents a general introduction and overview of the Coffee Gold Project, then the thesis objectives and methodology. Chapter 2 describes the regional and local geology, from the evolution of the Yukon-Tanana terrane to the geology of the Coffee Property. Chapter 3 describes the architecture and host rocks of the Latte gold zone. Chapter 4 presents the geochemistry of the host rocks at Latte in addition to the geochemistry of crosscutting dikes across the Coffee property. Chapter 5 describes the mineralization textures at Latte. Chapter 6 discusses the results of the previous chapters and suggests a geological model for the formation of the Latte zone. Chapter 7 presents a brief summary and recommendations for future exploration.

# Chapter 2

## 2 Regional Geologic Setting

The Yukon Cordillera is a complex amalgamation of terranes which formed along the western margin of ancestral North America. This chapter serves to introduce the tectonic setting that is host to the Coffee Gold Project. The accretionary history of the terranes of the Yukon Cordillera will be reviewed. This is followed by discussion of the geology of the Yukon-Tanana terrane (YTT), the White Gold district, and finally the local geology of the Coffee Gold Project area. Mineralization styles of the Tintina Gold Province (TGP) and White Gold District as documented in the literature are then synopsized. A complete geochronological study of the evolution of the Yukon Cordillera and Yukon-Tanana Terrane can be found in the works of Berman (2007) and Beranek and Mortensen (2011).

## 2.1 The Yukon Cordillera

The North American Cordillera comprising the Yukon/Alaska segment consists of superimposed arc terranes with the oldest located nearest the western margin of Laurentia. The terranes of the Canadian Cordillera are divided into groups to allow regional correlation by Colpron et al. (2007), into basinal and miogeoclinal terranes, pericratonic Intermontane terranes which include Yukon-Tanana, Stikinian, Quesnellian, Cache Creek, and Slide Mountain terranes, the Insular terranes, including Alexander and Wrangellia, and the Late Accreted and Northern Alaska terranes (Figure 2.1). These terranes display varying affinities between the native North American margin and exotic regions. Laurentia comprises the cratonic margin, miogeoclinal platforms and marginal basins, as well as the parautochthonous Cassiar and Kootenay terranes (Colpron et al., 2007). Slices of oceanic Slide Mountain terrane preserved on the westernmost margin are evidence for the Late Devonian - Permian closure of an oceanic basin which separated Laurentia from the juvenile arc terranes to the west. These pericratonic terranes, including Yukon Tanana, Quesnellia, and Stikinia, are interpreted as a succession of Devonian - Permian arcs which amalgamated outboard of the Laurentian margin. These terranes are bound to the west by the Cache Creek terrane,

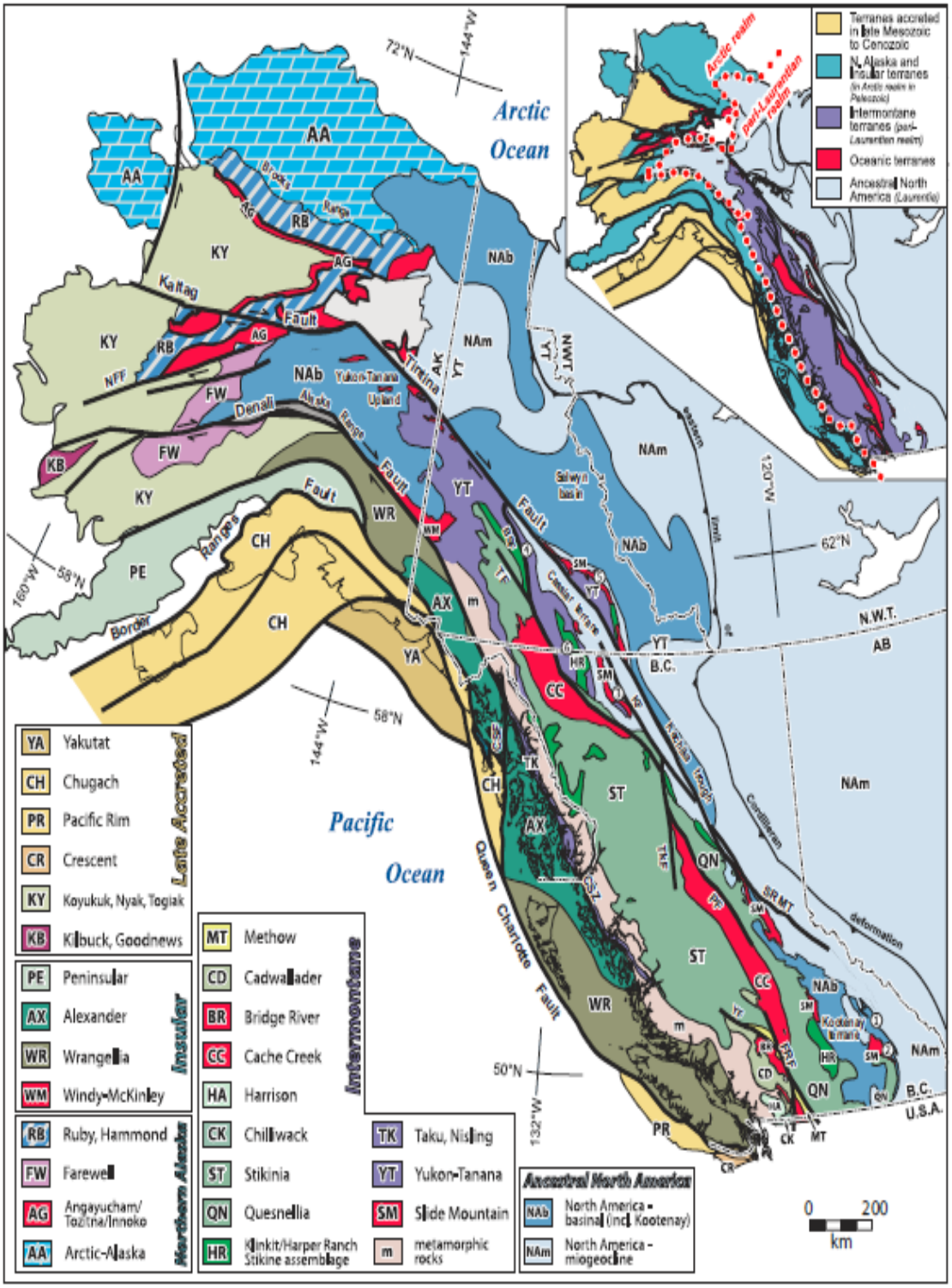


**Figure 2.1: Terrane map of the Canadian and Alaskan Cordillera, from Colpron et al. (2007)**

which displays exotic Tethyian affinities. It is interpreted to have been included within the pericratonic belt through oroclinal enclosure during accretion to Laurentia (Ross and Ross, 1983; Mihalynuk et al., 1994). The Wrangellia and Alexander terranes, known as the outboard Insular terranes, show no affinity to the Laurentian margin and instead display faunal and isotopic affinity to Siberia and Barentia (Bazard et al., 1995; Nokleberg et al., 2000; Bradley et al., 2003; Bradley et al., 2006). These terranes are correlated to the Farewell terrane in Alaska as well as to the Arctic-Alaska terranes. They developed mainly in the Arctic realm and were transported to a southern paleolatitude to a position west of the Intermontane terranes (Smith et al., 2001). The outermost Pacific Rim terranes consist of accreted arcs, seamounts, and accretionary complexes dominated by trench sediments. These terranes were accreted in the latest Mesozoic to the Paleogene, and all developed on or near the current Cordilleran margin (Colpron et al., 2007).

## 2.2 Assembling the Yukon Cordillera

In the Late Devonian, an arc developed on the western margin of Laurentia due to east-dipping subduction of old oceanic crust, beginning at 375 Ma in Alaska (Colpron et al., 2006a; Dusel-Bacon et al., 2006). By 365-360 Ma, a large belt of alkali-feldspar granite to monzogranite intruded along much of the arcs length (Mortensen, 1992; Piercey et al., 2006; Ruks et al., 2006). The arc matured until it's back-arc region rifted during the Late Devonian - Early Mississippian to create the Slide Mountain Ocean, a restricted ocean basin in the extensional environment between the tectonostratigraphic base of the YTT and the western margin of Laurentia (Templeman-Kluit, 1979; Colpron et al., 2006a, Nelson et al., 2006). The Stikinian and Quesnellian arc terranes developed outboard of the Laurentian margin. The Cache Creek terrane, which displays Tethyian affinity, was also incorporated into the developing outboard arc amalgamation making up the dominantly exotic Intermontane terranes (Yukon Tanana, Stikinia, Quesnellia) (Ross and Ross, 1983; Colpron et al., 2006a, Colpron et al., 2007).

Westerly subduction during the Early to Middle Permian began the consumption of Slide Mountain Ocean and generated the Klondike arc during a period of magmatism which spanned 265-253 Ma (Villeneuve et al., 2003; Breitsprecher and Mortensen, 2004;

Ruks et al., 2006; Berman et al., 2007; Beranek and Mortensen, 2011). This is recorded in a belt of eclogite and blueschist exposed along the eastern margin of the YTT. These rocks display geochemical affinity between mid-ocean ridge (MORB) and within plate basalts (Creaser et al., 1997; Erdmer et al., 1998; Fallas et al., 1998; Creaser et al., 1999; Beranek and Mortenson, 2011). Complete closure caused obduction of Slide Mountain ophiolite onto the western Laurentian margin as well as local incorporation of slices of Slide Mountain within the Intermontane terranes (Figure 2.2).

Numerous dates record the collision of the Intermontane terranes with the Laurentian margin. Berman et al. (2007) cite TIMS U-Pb geochronological data from the Minto area ~120 km SE of the Stewart River map area. The data reveals low - P metamorphism, tectonic burial, deformation, mineralization, and rapid exhumation occurring between 198 ± 2 and 195 ± 1 Ma as the main collision between the Intermontane terranes and Laurentia (Tafti and Mortensen, 2004; Berman et al., 2007). Beranek and Mortensen (2011) identify arc-derived detrital zircons in Early to Middle Triassic (251-235 Ma) sedimentary rocks which overlie the Laurentian continental margin in addition to detrital zircon from Laurentia in regionally-extensive Late Triassic (235-200 Ma) strata which overlie the accreted terranes (Hansen and Dusel-Bacon, 1998; Unterschutz et al., 2002; Beranek et al., 2010a, Beranek et al., 2010b). Based on these results, the authors conclude that collision occurred by 252.5 Ma, with westward subduction and obduction of Slide Mountain Ocean beginning at an age of 274 Ma: the maximum age of eclogite and blueschist interpreted to have formed within the subduction zone during the flip in subduction polarity from east-dipping to west-dipping (Erdmer et al., 1998; Fallas et al., 1998; Beranek and Mortenson, 2011). It is clear that the collision of the Intermontane terranes with the Laurentian margin occurred over a broad time domain, beginning during the Late Permian to Early Triassic with orogenic activity continuing until the Early to Middle Jurassic.

Following the collision of the Intermontane terranes and Laurentia, east-dipping subduction was reinstated along the western margin of the newly docked terranes (Colpron et al., 2007; Berman et al., 2007; Beranek et al., 2011). This introduced the later

arc terranes, including Alexander, Farewell, Arctic Alaska, Wrangellia, and Cache Creek (Colpron et al., 2006a, Nelson et al., 2006; Colpron et al., 2007;

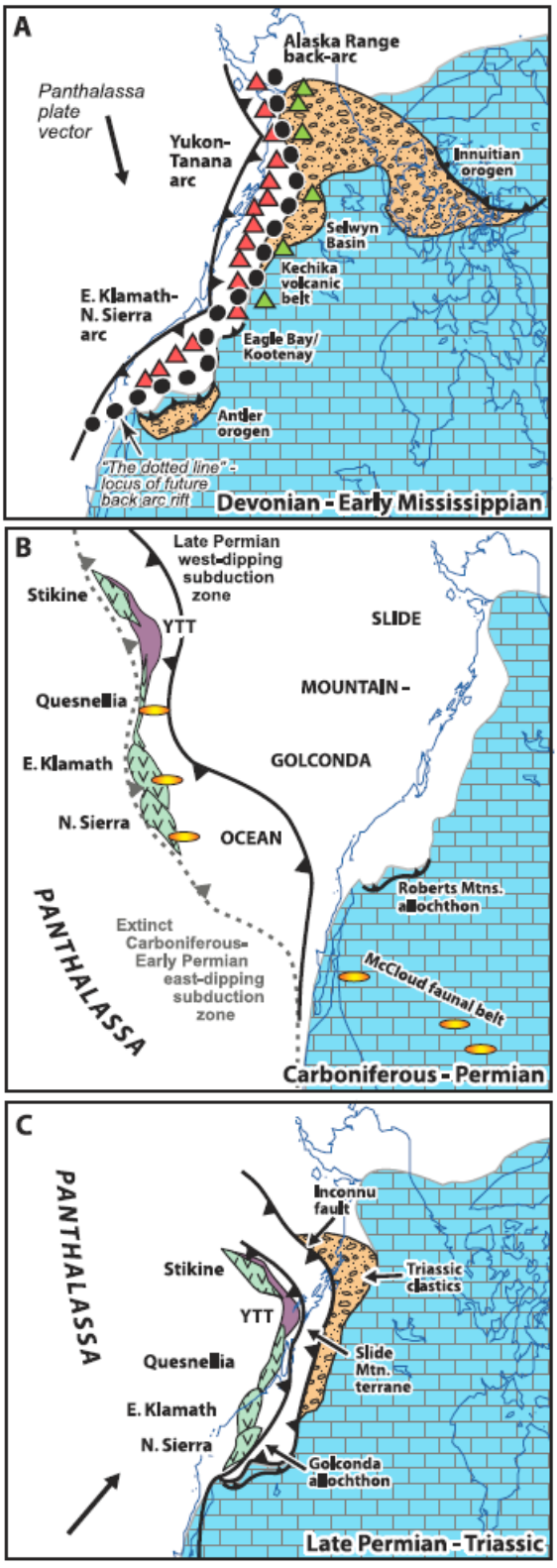


**Figure 2.2: Schematic diagram displaying the creation and closure of Slide Mountain Ocean along the North American continental margin. From Colpron et al. (2007)**

Piercey and Colpron, 2009). Final terrane accretion in the Yukon consisted of the Yakutat terrane, composed of Cretaceous flysch and melange as well as later igneous rocks and basaltic volcanics, and the Chugach terrane, an accretionary complex which sits structurally above the Yakutat (Plafker, 1987; Haeussler et al., 2003; Pavlis and Roeske, 2007; Amato and Pavlis, 2010).

Regional extension and exhumation began in the Early Cretaceous following crustal thickening during terrane emplacement. This is recorded in $^{40}Ar/^{39}Ar$ cooling ages in hornblende, muscovite, and biotite from the Lake George assemblage of the Yukon-Tanana Uplands, Alaska (Dusel Bacon et al., 2002). A number of post-accretionary magmatic events occurred throughout the Yukon Cordillera, some possibly due to Cordilleran-wide extension. Key magmatic events include: the St. Elias suite, intruding the Insular and Chugach terranes (145-135 Ma); the Kluane Ranges suite, intruding Wrangellia and Alexander (118-108 Ma); the Dawson Range and Whitehorse suite and it's extrusive equivalent the Mount Nansen Group in the Intermontane terranes (112-98 Ma); the Tungsten (97-94 Ma), Mayo (95-92 Ma), and Tombstone (92-90 Ma) suites northeast of the Tintina fault intruding the Selwyn basin; the Carmacks Group (70-68 Ma) and Ruby Range suite (64-56 Ma) (Hart et al., 2004). Many of these suites are tied to varying styles of gold mineralization and provide the backbone for the intrusion-related gold model which is applied to many deposits of the Tintina Gold Province (Hart et al., 2004; Hart et al., 2008).

## 2.3 The Yukon-Tanana Terrane (YTT)

The Yukon-Tanana Terrane (YTT) consists of variably metamorphosed Proterozoic and Paleozoic sedimentary and igneous rocks subdivided into four main tectonic assemblages (Colpron et. al, 2006a; Piercey and Colpron, 2009). These assemblages stratigraphically begin with the basal Snowcap assemblage which is overlain by three unconformity bounded volcanic and volcaniclastic magmatic arcs. These include the Finlayson assemblage (Upper Devonian - Lower Mississippian), Klinkit assemblage (mid-Mississippian to Lower Permian), and the Klondike assemblage (Middle to Upper

Permian), which all display arc affinity (Colpron et al., 2007) (Figure 2.3). All three arc assemblages are coeval with oceanic rocks of the Slide Mountain terrane, remnants of which are found sporadically throughout the YTT, especially along the eastern margin (Piercey and Colpron, 2009).

The Snowcap assemblage has been interpreted by numerous authors as a rifted fragment of the western margin of Laurentia (Templeman-Kluit, 1979; Colpron et al., 2006a, 2006b, 2007; Nelson et al., 2006). It is the structurally lowest and oldest component of the YTT and is composed of dominantly metasedimentary rocks including psammitic schist, quartzite, carbonaceous schist, calc-silicate rocks in addition to marble and local groupings of amphibolite, greenstone, and ultramafic rocks. It is interpreted that a crystalline basement was delaminated during orogenesis sometime during the Late Paleozoic and not preserved (Cook and Erdmer, 2005; Murphy et al., 2006; Piercey and Colpron, 2009) (Figure 2.3).

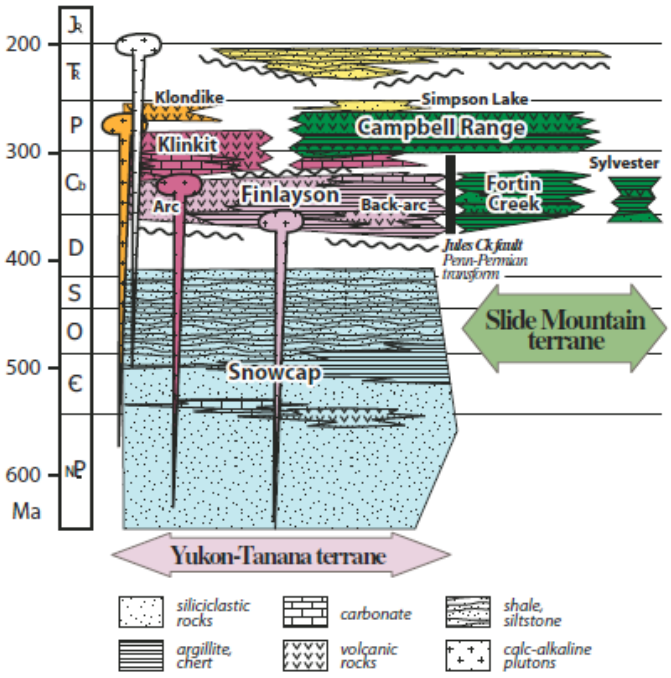


**Figure 2.3: Stratigraphic diagram of the Yukon-Tanana terrane with the Slide Mountain terrane separating it from the North American margin. The Snowcap assemblage is the structurally and stratigraphically lowest component of the YTT, and would have rest above a crystalline basement which was removed during orogenesis. Figure from Piercey and Colpron (2009).**

The YTT is bound by two crustal-scale transform faults: the Tintina Fault to the northeast, and the Denali Fault to the southwest. The Tintina Fault strikes NNW-SSE from northern British Columbia through the Yukon into Alaska. Many subsidiary faults which are also Eocene in age, converge to the northwest into the Tintina (Gabrielese et al., 2006). While the entire cumulative displacement of the outermost parts of the Cordillera is estimated at 860 km, the Tintina Fault is responsible for approximately 430 km of dextral displacement between the Late Cretaceous and Eocene (Gabrielese et al., 2006). In the YTT, the Teslin Fault accounts for approximately 125 km of dextral offset in northern BC. However in the heart of the YTT, near the Minto mine, no displacement is apparent and the fault seems to terminate (Gabrielese et al., 2006; Bennett et al., 2010). Regional second-order structures including the Tadru, Big Salmon, and d'Abbadie faults can be reconstructed and shown to have accommodated the missing offset northeast of the Teslin fault **(**Bennett et al., 2010). Northwest trending structures persist beyond the apparent termination of the Teslin Fault into the Dawson Range. These structures as well as Cretaceous magmatism in the Dawson Range are interpreted as being related to late extension in the region (Bennett et al., 2010).

## 2.4 Deformational Events

Numerous deformational and metamorphic events occurred during the structural evolution of the northern Cordillera. Within the Yukon-Tanana there are five regionally recognizable deformational events, each producing a foliation or metamorphic fabric (MacKenzie et al., 2008). These deformational events have been designated $D_1$-$D_5$, and this tectonic framework is used within this thesis.

$D_1$ deformation is a result of the initial development of an arc sequence on the siliclastic Snowcap assemblage beginning in the Late Devonian (375 Ma) (Dusel-Bacon et al., 2006; Berman et al., 2007). This deformation is difficult to restrict to a specific magmatic event during the arc's formation and evolution, however deformation and exhumation of the Stewart River region can be roughly constrained to an age of 345 Ma (Villeneuve et al., 2003; Berman et al., 2007). This places $D_1$ deformation within a window of 375-345 Ma, with its true source unknown. $D_1$ deformation and $S_1$ metamorphic foliation is rarely observed within the White Gold region of the YTT as

very poorly preserved early folds subparallel to the dominant $S_2$ overprint. Some workers suggest that visible $S_1$ foliation seen in rocks in the White Gold region is actually an earlier component of $S_2$ foliation which has been dominantly wiped out by the $D_2$ deformational event (Beranek and Mortenson, 2011; Bailey, 2013). As the foliation is so poorly preserved, it is currently unknown whether it is a product of the ancient arc formation and subsequent exhumation, or the early component of $D_2$ deformation.

$D_2$ deformation represents the peak metamorphic event within the region. It is constrained to the Klondike orogeny of Beranek and Mortenson (2011) which occurred during closure of the Slide Mountain ocean and collision of the Yukon-Tanana terrane with the Laurentian margin from 260-252.5 Ma (Berman et al., 2007; Beranek and Mortenson, 2011). Deformation and metamorphism consists of upper greenschist to lower amphibolite facies metamorphism across the entire region, with garnet found within rocks near the White River and rarely at the Coffee Property within the Sulphur Creek augen orthogneiss (Berman et al., 2007; Beranek and Mortenson, 2011; Cruikshank, 2011; Bailey, 2013). This deformation event overprinted previous $D_1/S_1$ foliation with a regionally extensive $S_2$ foliation defined by alignment of mica and amphibole grains.

$D_3$ deformation overprints the regional $S_2$ foliation with $F_3$ folds. These are slightly inclined and vary from open to tight folds which plunge shallowly with respect to the $S_2$ foliation (Bailey, 2013). These folds are accompanied by low-angle thrust faulting to the northeast at the Coffee Property resulting in internal duplication and dismembering of the various units of the YTT (MacKenzie and Craw, 2010). This low-angle thrusting locally produced mylonitic textures along sets of stacked thrust faults, in addition to movement along structures transposing lithological contacts parallel to the $S_2$ foliation. These thrust faults locally dismember Slide Mountain ophiolite (MacKenzie et al., 2008; MacKenzie and Craw, 2010; 2012). $D_3$ deformation is a result of continued accretion of the YTT onto the North American continental margin and culminates with the complete closure of the Slide Mountain Ocean by the Early to Middle Jurassic.

$D_4$ deformation is recorded dominantly within the Golden Saddle and Klondike domains as $F_4$ generation brittle-ductile kink/buckle folds which are observed to overprint $F_3$ folds in some areas (MacKenzie et al., 2008; Bailey, 2013). The timing of $D_4$ deformation is constrained to approximately 185-170 Ma by $^{40}Ar/^{39}Ar$ dating on mica. Amphibolite south of Thistle Creek yield two populations of hornblende cooling ages, both at 180 Ma (Villeneuve et al., 2003; Berman et al., 2007; Bailey, 2013). This deformation is interpreted as the result of extension due to rapid exhumation of the tectonically thickened YTT.

$D_5$ deformation in the Coffee Creek area is characterized by multiple sets of steeply dipping brittle fractures and dextral normal faults which create extensional horst and graben structures. These faults were caused by splays off the regional-scale Big Creek fault to the southeast of the Coffee Creek area. They are interpreted to be mid-Cretaceous in age, active syn-to-post emplacement of both the Dawson Range batholith (~100 Ma) and the Coffee Creek granite (~98 Ma) (Johnston, 1999; Sanchez, 2013). Brittle fractures are exploited by dacite and andesite dikes at the Coffee Property, and are present within the Coffee Creek granite, indicating continued movement and/or reactivity post-emplacement of the granite.

The transpositional fabric present at the Coffee Property has not been dated. This fabric could potentially be the result of $D_2$ deformation, or even related to the rapid uplift and exhumation of the Dawson Range during the Mid-Cretaceous. This issue can be resolved by $^{40}Ar/^{39}Ar$ dating of white mica, biotite, and amphibole which defined the transpositional foliation at Coffee.

## 2.5 Local Geology

An arcuate belt of gold mineralization through the YTT is referred to as the Tintina Gold Province (Figure 2.4). This belt stretches through Yukon and Alaska, covering an area of greater than 150,000 $km^2$. It includes the historically significant placer districts such as the Klondike (Goldfarb et al., 2007). The belt is over 2000 km in length and includes such major deposits in the Yukon as Clear Creek, Scheelite Dome, Dublin Gulch, and Brewery Creek (Hart et al., 2002, Goldfarb et al., 2007).

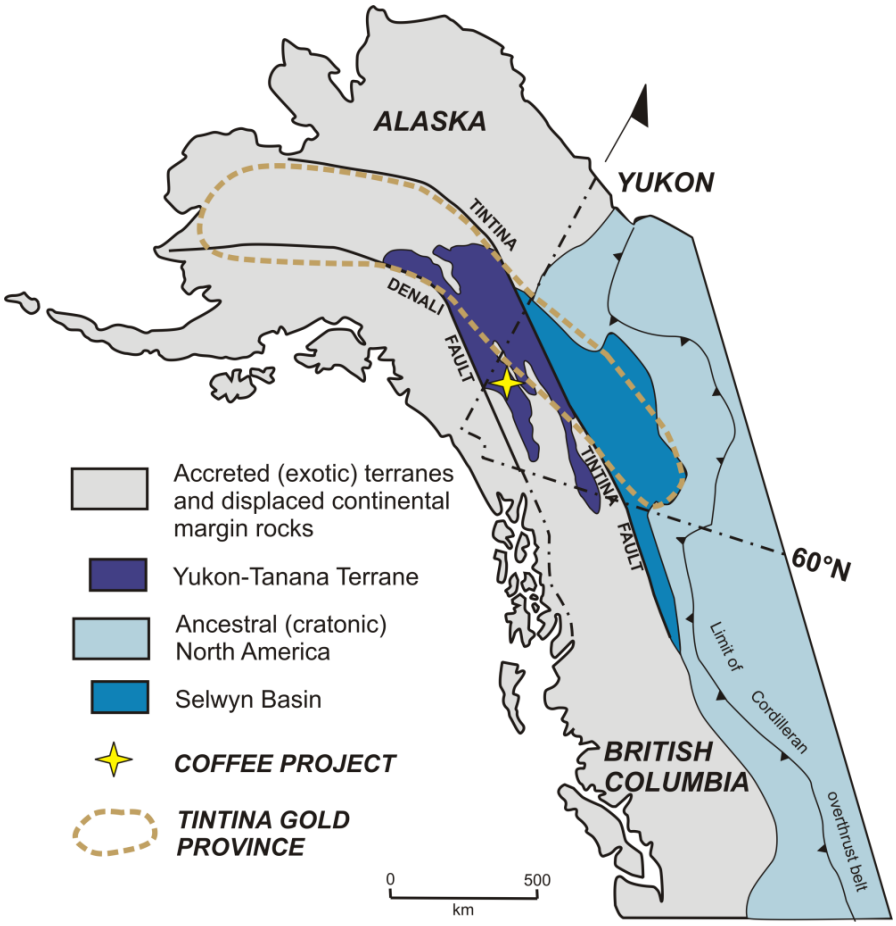


**Figure 2.4: Map of the Cordillera with the generalized outline of the Tintina Gold Province superimposed. The Tintina and Denali faults are marked, in addition to the location of the Coffee Gold Project as indicated by the gold star. Modified from Mair et al. (2006).**

Exploration for lode sources for the placer gold deposits has been on-going historically. Improvement to regional infrastructure and increasing technological advancement has allowed for economic recovery of lower grade (<1 g/t Au) resources including Alaska's Fort Knox deposit (Bakke et al., 2000; Goldfarb et al., 2007).

The Coffee Gold Project occurs at the southern margin of the White Gold District within the Dawson Range. This district encompasses Kinross Gold Corporation's Golden Saddle deposit and is roughly centered upon the convergence of the Yukon and White rivers (Figure 2.5). The region consists of the Paleozoic schists and gneisses of the YTT. Greenschist to lower-amphibolite facies metamorphism in the Late Permian between 260 and 252.5 Ma is attributed to the Klondike orogeny (Beranek and Mortenson, 2011).

These rocks were subsequently intruded by numerous intrusions ranging in age from Jurassic to Eocene (Colpron et al., 2006a). From the Late Permian into the early Jurassic the schists and gneisses were tectonically stacked along foliation-parallel thrust faults, incorporating slices of mafic and ultramafic components of the Slide Mountain terrane. These thrust slices are regional in scale and poorly exposed, marked by laterally traceable ultramafic lenses and serpentinite (MacKenzie and Craw, 2010).

Extensional tectonism during the mid-Cretaceous led to exhumation of the metamorphic infrastructure and allowed for emplacement of numerous intrusive bodies, chiefly the Dawson Range batholith and Coffee Creek granite (MacKenzie and Craw, 2010; McKenzie and Craw, 2012). The Dawson Range batholith is over 250 km in length and 50 km in width with a surface area of > 10 000 $km^2$. It intrudes the metamorphic assemblages of the Yukon- Tanana terrane (Johnston, 1999). The Dawson Range batholith is composed of a dominant quartz diorite phase in addition to multiple porphyritic granitic phases, one of which is the Coffee Creek granite. This granite is observed to intrude the Dawson Range batholith as a later phase. The emplacement of the batholith is constrained by U-Pb zircon dating on the quartz diorite phase giving a zircon crystallization age of 105 Ma. K-Ar hornblende and biotite cooling ages of 100 Ma are reported for the granitic phases. The Coffee Creek granite has an emplacement age of 98.2 +/- 1.3 Ma. (Johnston, 1995, 1999; A. J. Wainwright and A. Simmons, unpublished data, 2010; McKenzie et al., 2013).

Regional extension during the emplacement of the Dawson Range batholith was accommodated by activation of the Big Creek fault. This extends > 300 km through west-central Yukon and generally follows the northern boundary of the Dawson Range batholith (Johnston, 1999). The fault is interpreted as a Jurassic thrust which was overturned and reactivated in the Mid-Cretaceous as a west-northwest trending dextral strike-slip fault (Sanchez et al., 2013). The Big Creek fault accounts for a minimum of 20 km of dextral offset in the region. It pre-dates the Upper Cretaceous basalt flows of the

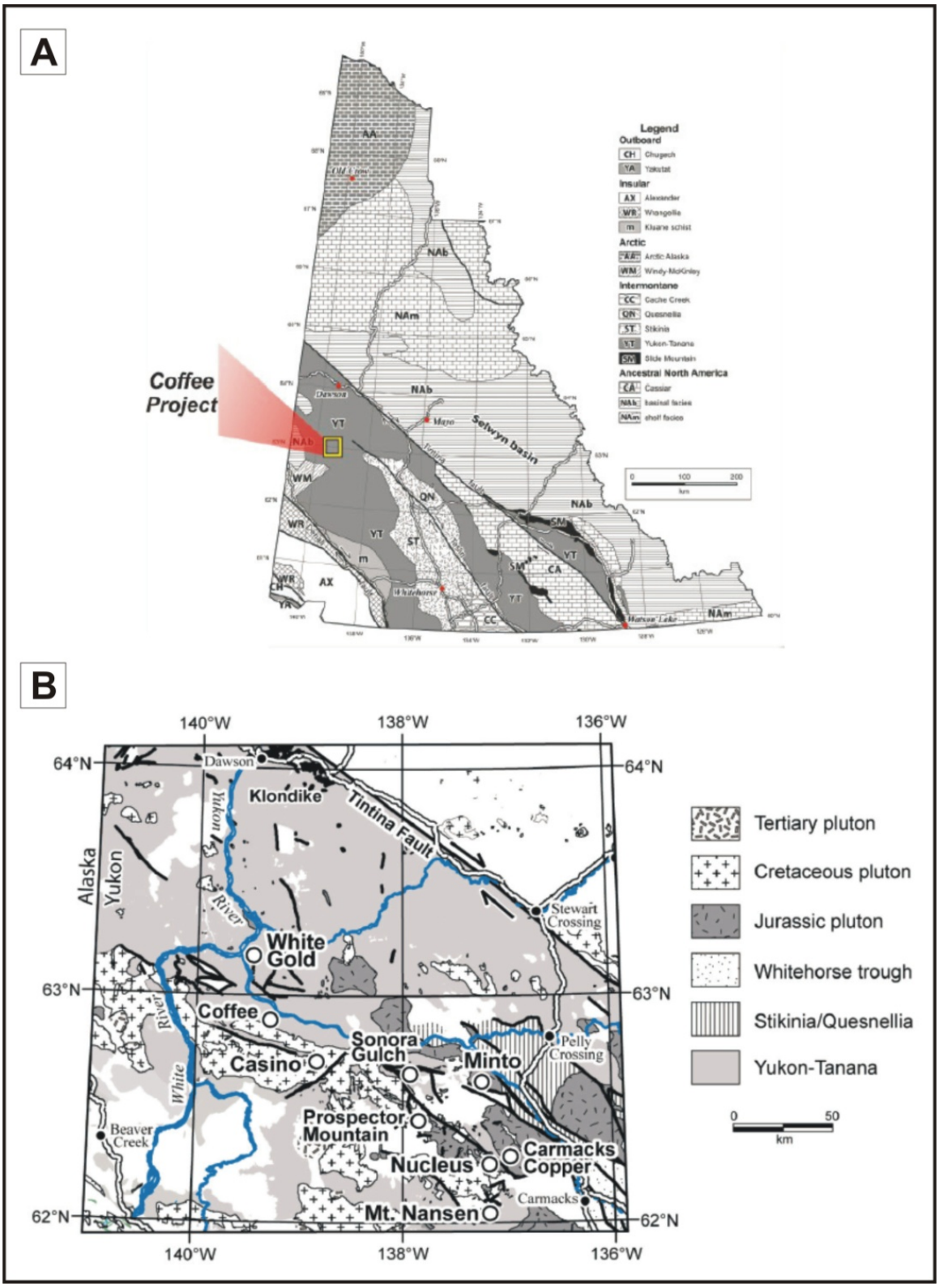


**Figure 2.5: Location of the Coffee property: A) Within the Yukon and B) Within the White Gold district. From Wainwright et al. (2011).**

Carmacks Group dated at 70 Ma (Grond et al., 1984; Johnston, 1999, Hart et al., 2004).

In the immediate Coffee Project area, numerous dextral strike slip faults are interpreted as splays off of the Big Creek fault. The Coffee Creek fault strikes roughly northwest along the northern boundary of the Coffee Creek granite and has an unknown amount of dextral strike-slip displacement. The Coffee Creek South fault splays off the Coffee Creek fault, continuing west where the Coffee Creek fault horsetails to the northwest (Sanchez et al., 2013). In the domain bound by these faults, stress is accommodated by multiple generations of brittle faults off the main shear zone, termed faults of order 1 - 4 based on the order in which they were formed (Figure 2.6).

Regional first order faults which trend west-northwest form the P shears in a Riedel shear system (Bennett et al., 2010; Wainwright et al., 2011). Secondary NNE trending structures are common and are the complimentary R shears to the first-order shears (Bennett et al., 2010). Higher orders of faults strike NNW, ENE, and NNE as seen in Figure 2.6. This fault zone geometry occurs throughout the Dawson Range. Such fault splays control the gold mineralization at Kinross's Golden Saddle, Northern Freegold's Nucleus, and Kaminak's Coffee deposits (Bennett et al., 2010, Campbell et al., 2010; Wainwright et al., 2011).

Strike-slip displacement continued until the Eocene. There is ~450 km of strike-slip displacement on the Tintina fault. Minor uplift through the Tertiary resulted in the formation of placer gold deposits (Gabrielese et al., 2006; MacKenzie and Craw, 2010).

## 2.6 Regional Mineralization

The Yukon-Tanana terrane is host to multiple styles of syngenetic mineral deposits including sedimentary exhalative (SEDEX), volcanogenic massive sulphide (VMS) and Mississippi Valley-type (MVT) deposits. These deposit styles relate to episodes of rifting and magmatism during Late Devonian - Permian subduction (Nelson and Colpron, 2007; Bailey, 2013). The most economic VMS deposits occur in the YTT north of the Tintina fault (ex. Wolverine Zn). The recently identified Touleary VMS prospect was discovered

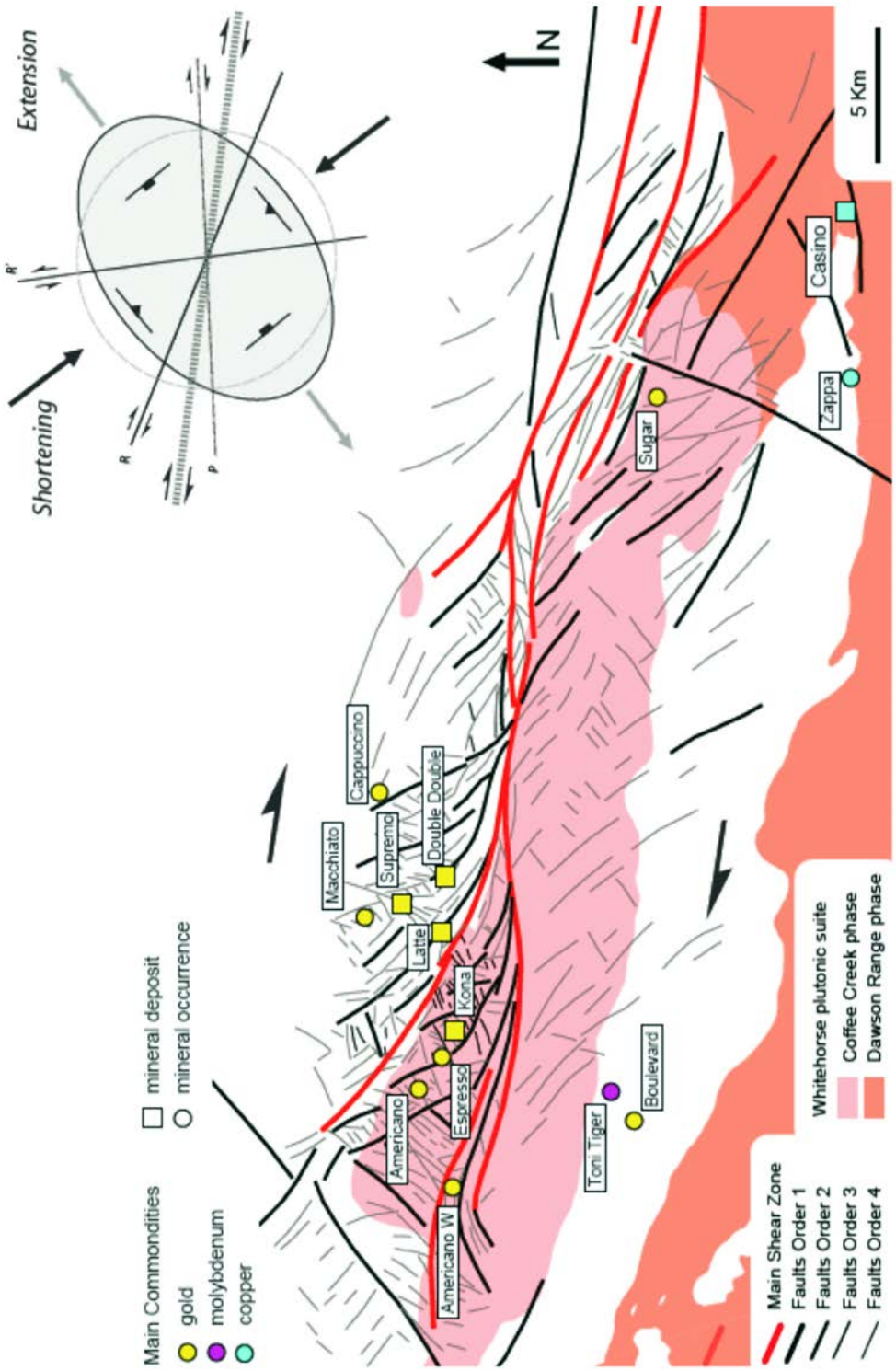


**Figure 2.6: Fault structures within the region of the Coffee Property. Mineralized deposits and prospects are marked, and a region of shortening and NE trending extension is visible. Faults are marked from main shear zones to faults of order 1-4. From Sanchez et al. (2013).**

by Arcus Development Group in 2011. This prospect lies immediately north of Kaminak's claims on the northern bank of the Yukon River. It consists of high grade Cu-Ag-Au-Zn mineralization hosted within sericitized tuffaceous felsic-to-intermediate volcaniclastic rocks (Arcus Development Group, 2011). Mineralization consists of moderate to heavy disseminations and semi-massive to massive bands of pyrite. Aggregates of coarsely recrystallized chalcopyrite and rarer covellite occur parallel to foliation (Arcus Development Group, 2011).

The Tintina Gold Province (TGP) contains many economic mineral deposits of varying character. These can be broadly subdivided into two main groupings: 1) syngenetic sedimentary and volcanogenic deposits; and 2) epigenetic deposits including structurally-hosted orogenic and intrusion-related gold deposits (Bailey, 2013). Epigenetic deposits can be further subdivided by age and style. Orogenic gold deposits occurring in the vicinity of the Coffee Project are of two ages: 1) structurally controlled Jurassic to Early Cretaceous veins in Klondike schists and structurally-hosted deposits in the White Gold region; and 2) mid to late Cretaceous lode gold deposits within the Dawson and Moosehorn Ranges (Joyce, 2002; McKenzie et al., 2013). The deposits of particular interest include the Golden Saddle deposit, the nearby Boulevard prospect, and the Longline occurrence within the Moosehorn Range.

The Golden Saddle deposit, located approximately 40 km north of the Coffee Property contains a resource of 1.4 Moz Au (Weiershäuser et al., 2010) . This deposit occurs within Late Paleozoic metamorphosed rocks of the Yukon-Tanana terrane. Metavolcanic and metaplutonic rocks form the hanging wall of a north-striking thrust fault, while metasiliciclastic rocks form the footwall (MacKenzie and Craw, 2010; MacKenzie et al., 2010; Bailey, 2013). Mineralization is focused at the intersection of the thrust fault with a system of Jurassic east-striking sinistral transpressional faults (Bailey, 2013). A series of northeast-striking and northwest-dipping faults controls the economic gold mineralization. Gold related alteration consists of quartz-carbonate-illite with gold-bearing pyrite. The dominant trace element enrichment consists of Au-Ag-Pb-S-Te. The timing of mineralization is coincident with regional uplift and extension which occurred

during the Jurassic. It is constrained by $^{187}Re/^{187}Os$ ages of 163-155 Ma for molybdenite occurring in gold-bearing veins.

The nearby Boulevard gold prospect occurring 10 km southwest of the Coffee property on Independence Gold Corporations Snowcap Property owned by Independence Gold Corporation has recently been investigated by McKenzie et al., (2013) (Figure 2.7).

Boulevard consists of sheeted, gold-rich quartz-sulphide-carbonate veins and fault breccia hosted within mafic schist. On the same property, the Toni Tiger molybdenum showing comprises quartz-molybdenite veins cutting Late Permian meta-aplite and an undated garnet-pyroxene skarn (McKenzie et al., 2013). Geochronological work by McKenzie et al. (2013) reported $^{187}Re/^{187}Os$ model ages of 95.0 +/- 0.4 Ma for molybdenite at the Toni Tiger showing. A 95.9 +/- 0.9 Ma $^{40}Ar/^{39}Ar$ cooling age is reported for hydrothermal sericite directly linked to gold mineralization at Boulevard. The deposit is modelled as a mid-Cretaceous orogenic gold system tied to exhumation of the Dawson Range shortly after intrusion of the Dawson Range batholith. This exhumation was accompanied by brittle deformation, fluid flow, and gold-molybdenite mineralization (McKenzie et al., 2013).

In the Moosehorn Range near the Yukon-Alaska border, gold-bearing quartz veins occur in dilational zones within a broad compressional setting. Gold is hosted within sheeted quartz veins emplaced along shallowly ENE dipping, NNW-striking brittle reverse faults within the Dawson Range batholith. Vein mineralogy includes galena, sphalerite, arsenopyrite, pyrite, boulangerite, tetrahedrite, native gold, and scheelite. Bonanza gold grades within the veins are as high as ~30 g/t (Joyce, 2002). $^{40}Ar/^{39}Ar$ dating on hydrothermal muscovite within gold-bearing quartz vein selvages reports ages of 93-92 Ma (Joyce, 2002).

The nearby Casino Cu-Mo-Au porphyry owned by Western Copper and Gold contains 976M tonnes of proven and probable mill-ore, containing 4.3 B lb of Cu, 7.4 Moz Au, 483 M lb Mo, and 53.8 Moz Ag (Huss et al., 2013). It is located approximately 30 km to the southeast of the Coffee Project. The Casino porphyry complex was

explosively brecciated and created a hydrothermal system circulating outwards from a central plug

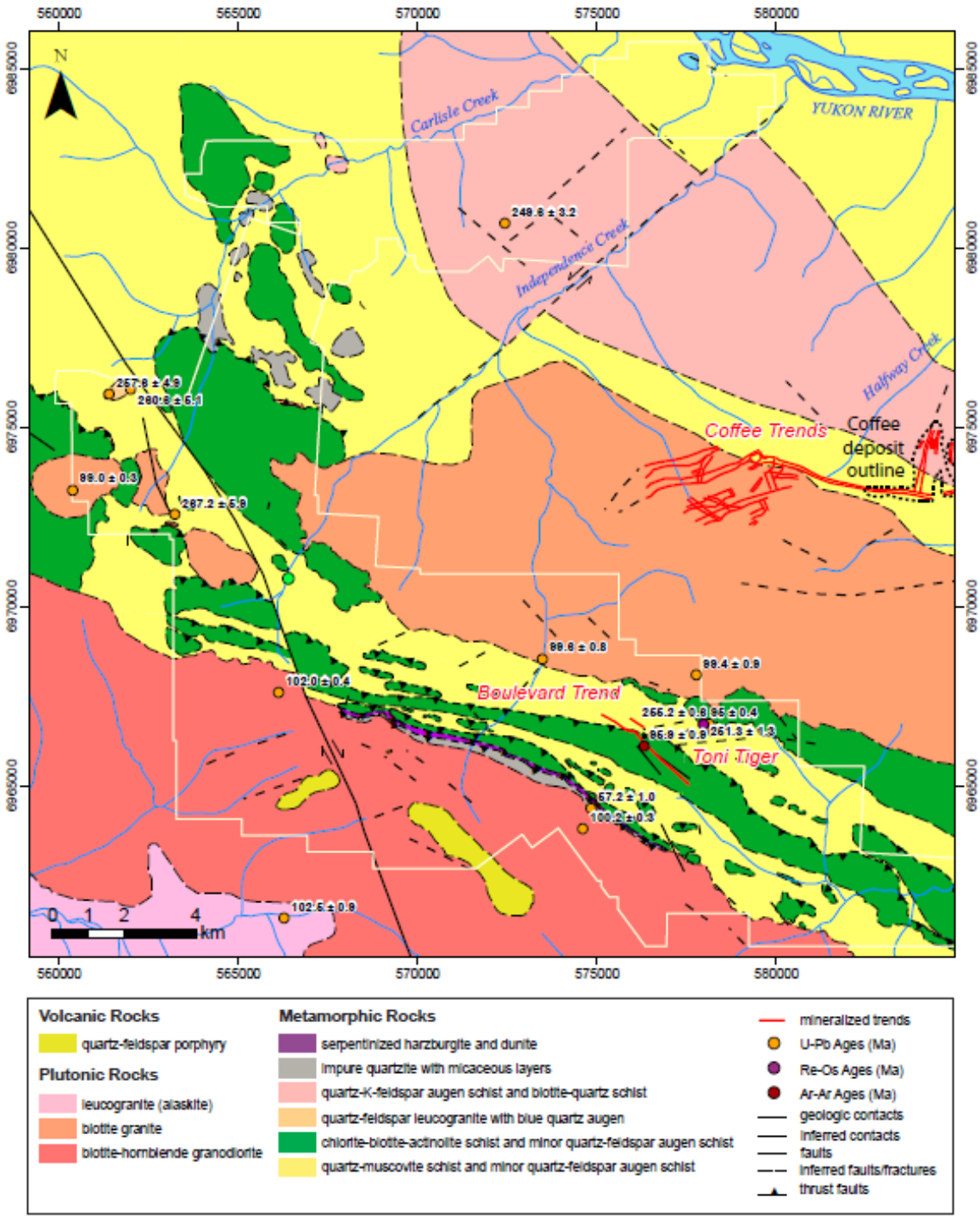


**Figure 2.7: Map of the Boulevard prospect in relation to the location of the Coffee Project. From McKenzie et al. (2013).**

into the bordering Dawson Range batholith. It developed a classic porphyry alteration halo which zones concentrically upwards and outwards (Godwin, 1975). The feldspar porphyry has been dated at ~70 Ma. No epithermal mineralization has yet been tied or linked to the intrusion of the Casino porphyry.

## 2.7 The Coffee Gold Project

The Coffee Gold Project is located approximately 130 km south of Dawson City (Figure 2.8). The Coffee property is underlain by a sequence of shallowly to moderately southwest dipping metamorphic rocks of the Yukon-Tanana Terrane, which exhibit at least two dominant metamorphic fabrics (MacKenzie et al., 2008; Wainwright et al., 2011). Three main lithological groupings underlie the central Supremo, Latte, Double Double, and Kona gold zones. An augen gneiss panel is overthrust by a panel of biotite schist and amphibolite, all of which strike west-northwest and dip south-southwest. These occur on the northern side of the Coffee Creek granite (Figure 2.9). All three groupings have been assigned local names, and a further breakdown of the geological makeup of each lithological group follows.

The northernmost panel consists dominantly of a quartz-feldspar +/- biotite and muscovite augen gneiss. Augens generally reach up to 1 cm in size and are defined by dominantly white mica laths which wrap around K-spar megacrysts and define the foliation within the gneiss panels. Small lenses up to 10 meters in size of biotite-feldspar (+/-quartz, muscovite) schist are intercalated and make about 30% of the rock panel (Wainwright et al., 2011). Limited geochronological work by Kaminak personnel at Stanford University, California, USA, reported an age of 257.9 Ma +/- 3.5 for the augen gneiss at Coffee (A.J. Wainwright and A. Simmons, unpublished data, 2010).

A biotite schist panel structurally overlies the augen gneiss panel. This unit strikes through the central portion of the Coffee Property. It is a moderately to strongly foliated biotite-feldspar (+/- quartz, +/- muscovite) schist. It is variably calcareous, with marble bands ranging in apparent thickness from 3 cm up to 1 m. Near the marble banding, the

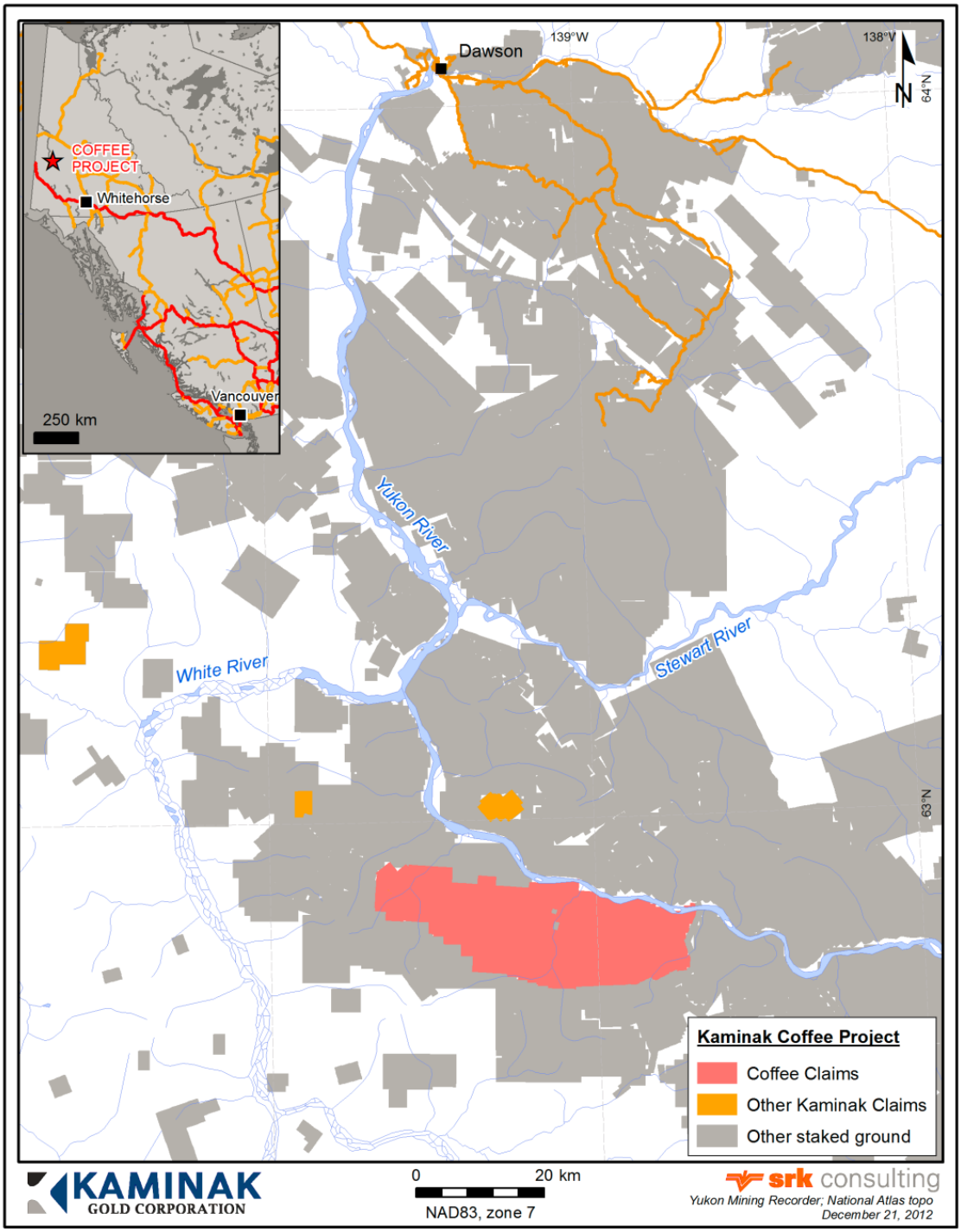


**Figure 2.8: Map of Kaminak's claims: Coffee claims are in red, other claims in the region are in orange. From Chartier et al. (2013).**

bordering schist is moderately to strongly calcareous. Carbonate veining as well as pervasive carbonate flooding are indicative of a very strong CO2-rich fluid event in the region. At the footwall of the schistose units is a mafic panel which locally consists of a deformed metagabbro intermixed on the 10 cm to > 15 m scale with finely foliated amphibolite. Also present are structurally continuous, >20 m thick serpentinized ultramafic panels of tectonic character.

The Coffee Creek granite is dated at 98.2 +/- 1.3 Ma and assigned to the Whitehorse plutonic suite (A J. Wainwright and A. Simmons, unpublished data, 2010). This date agrees with the geological interpretation of Templeman-Kluit (1974), and recent work at the Boulevard property by McKenzie et al. (2013) that the Coffee granite was emplaced just after the Dawson Range batholith (100.2 +/- .3 Ma to 102.5 +/- .9 Ma), a large biotite-hornblende granodiorite immediately adjacent to the Coffee Creek granite (McKenzie et al., 2013). In addition to the three main rock groupings, various dikes crosscut both thrust panels and the Coffee Creek granite. Dikes include variably altered dacite and andesite (MacKenzie et al., 2013).

Lode gold mineralization on the Coffee property is structurally controlled. This mineralization is gold-only and characterized by extensive silica, sericite/illite, and dolomite/carbonate alteration. Deep weathering has resulted in extensive development of clay minerals (Wainwright et al., 2011). Gold is hosted in arsenian pyrite and is distributed throughout the entire pyrite grain. There are a number of gold zones on the property. The Supremo, Latte, Double Double, and Kona zones are described briefly below based on the work of Wainwright et al. (2011), Chartier et al. (2013), and the author.

The Supremo zone is dominantly hosted within the Sulphur Creek augen orthogneiss panel. It is composed of a set of narrow, brittle structures which dip steeply (80 degrees to near-vertical) to the east and strike roughly to the north. Mineralized structures progress from west to east from T1 through T8, named after the initial trenches which intersected them at surface. The dominant T3 structure forms a central structural corridor with gold in matrix-supported breccias with silicified dacite dike clasts. Supremo

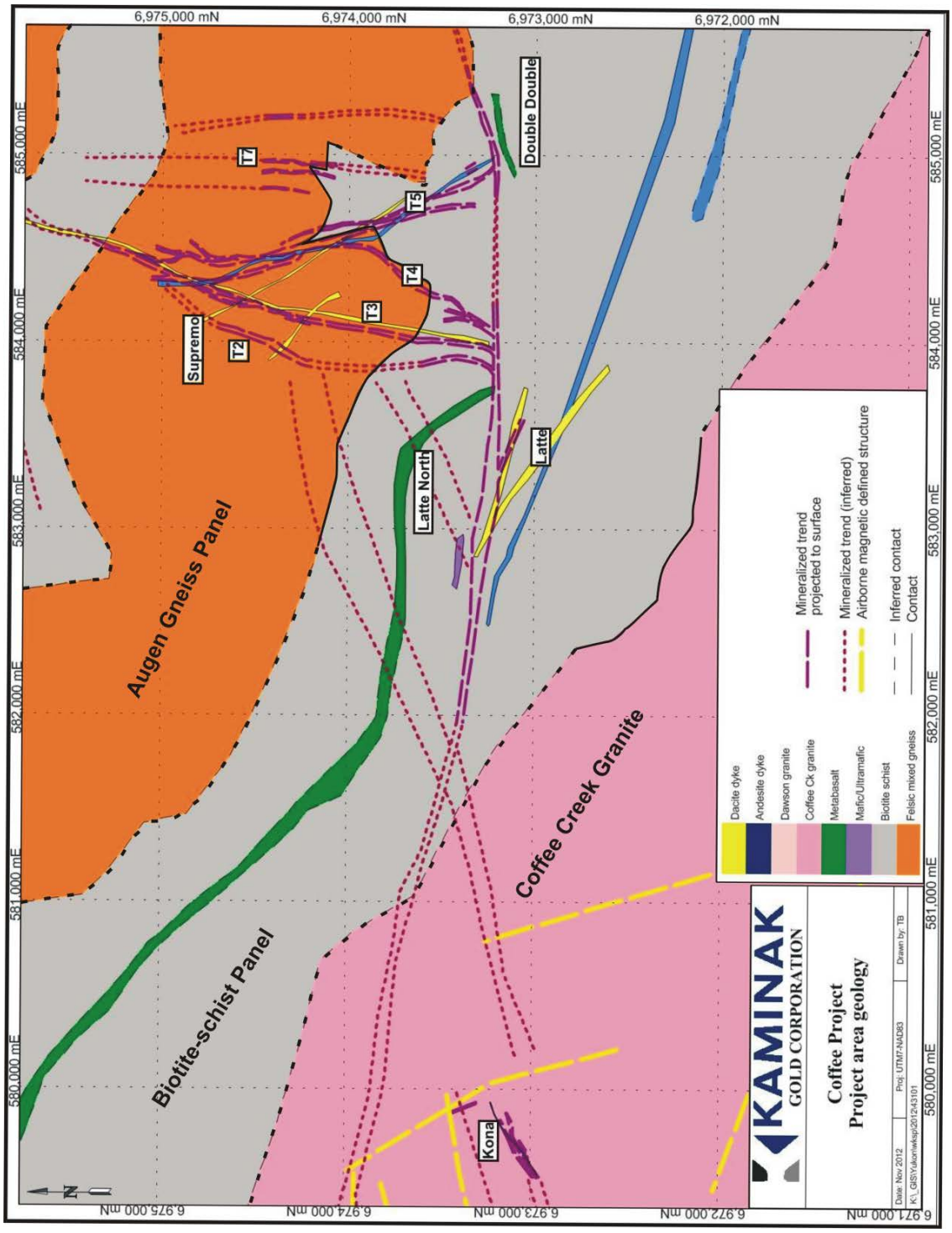


**Figure 2.9: Map of the Coffee Property main rock panels. Mineralized trends are shown as purple dashed lines. From Chartier et al. (2013).**

structures terminate against the large, roughly east-west trending structural corridor to the south in what is termed the Connector zone, but remain open along strike to the north and at depth.

The Latte zone occurs within the biotite-schist panel to the southwest of the augen gneiss panel and the Supremo structures. The Latte zone is a semi-brittle to brittle structural corridor with numerous stacked fault zones dipping moderately to steeply to the southwest, and striking east-south east. Mineralization is characterized by disseminations of arsenian pyrite off of these faults into schistose rocks. Various breccias and dacite dikes occur locally. The Latte structure extends for a strike length of >1.5 km and remains open to the west. It connects roughly to the east with the Double Double zone. The Double Double zone contains some of the highest grade mineralization on the Coffee Property. It follows a series of steeply south-dipping to near-vertical thin structures striking east, which flip to a northern dip to the west. Gold is hosted in matrix-supported breccias. Strong disseminations of arsenian pyrite occur along mica foliations in fragments and the bordering host. The Double Double zone remains open to the east. The Kona zone is hosted within the Coffee Creek granite approximately 4 km to the west of the Supremo zone. Disseminated arsenian pyrite occurs within structural corridors with common dacite dikes.

Gold mineralization at the Coffee property is divided into three categories based on level of oxidation: oxide, transitional, and sulphide. Gold is sited within arsenian pyrite grains. Oxidation of the pyrite releases gold out of the pyrite structure, and allows for easy gold recovery through heap leaching. The oxidation profile at Coffee varies greatly across the deposit but consists of near-surface, oxide-facies gold mineralization to a minimum depth of 50 meters to over 300 meters below surface. This oxide-facies mineralization is amenable to open-pit, heap leach mining methods, and is found in all zones at the Coffee property. Transitional facies mineralization contains a mixture of un-oxidized or partly oxidized sulphides, and yields slightly lower gold recovery through acid heap leaching. The sulphide facies mineralization found at depth is un-oxidized and does not yield significant gold recovery through the acid heap leach method. As the

sulphide-facies mineralization at Coffee is unobstructed by oxidation, it allows for accurate petrographic interpretation of gold ore prior to oxidation.

Pathfinders for mineralization at Coffee include strong As-Sb enrichment, with minor and variable Ag-Ba-Mo enrichment. Due to the lack of glaciation in the project area, gold-in-soil anomalies and As-Sb enrichment have proven to be a direct indicator of the gold-bearing potential of underlying bedrock.

# Chapter 3

## 3 Host Rocks and Architecture of the Latte Gold Zone

Existing research into the petrogenesis of the host rock assemblage at the Coffee Gold Project is very limited. To date, no detailed petrographic descriptions or geochemical analyses have been carried out beyond Kaminak technical reports (Wainwright et al., 2011; Chartier et al., 2013). In order to understand the lithological and structural controls on gold mineralization, it is vitally important that the rocks in the Latte zone are characterized. Lithological units are documented petrographically in order to establish the metamorphic/hydrothermal setting of the gold mineralization.

Since drilling began in the 2010 field season, Kaminak has collected 35-element ICP-AES data for each meter drilled on the Coffee property. This assay data includes not only a fire-assay for Au, but full 35-element bulk rock data for each meter interval. This data has proven to be a great aid in targeting drill holes through the down-hole mapping of Au-As-Sb geochemical signatures. While a comprehensive whole-rock geochemical analysis takes a month or more to receive, assay data has a much quicker turnaround and has been utilized in real-time to aid in drill targeting. This bulk rock data can also be used to designate geochemical markers for different lithologies as well as differing alteration styles, and the data allows for quick discrimination of mineralized zones.

Core logging is the key component of the drill program. It is essential to properly identify units in order to constrain exploration efforts. At the Latte zone, the subtle differences between some geological units may be missed by loggers, but can be corrected through scrutiny of the ICP data in conjunction with core photographs. This "re-logging" was carried out to create a geological interpretation used in targeting strategy. At Latte, a complete 35-element ICP-AES database exists for almost every drill hole (n = 82). The author used specific geochemical markers for mafic and ultramafic lithologies which were under represented in drill logs in an attempt to standardize all drill logs to create a coherent and useful cross section of the Latte zone.

An understanding of the origin of the hosts and their place within the regional geotectonic framework is of paramount importance. This chapter presents petrographic descriptions

of each unit present at the Latte zone, demonstrates how 35 element ICP-AES data provides support on lithological identification on the meter scale, identifies the tectonic stratigraphy of the Latte host rocks, and presents two representative cross sections of the Latte zone.

## 3.1 Tectonic Stratigraphy of the Latte Zone

The Latte zone is hosted within the biotite schist panel. This comprises a sequence of schistose rocks overlying a mafic metavolcanic assemblage, forming the Upper and Lower Latte packages. Upper Latte is defined by quartz-biotite-feldspar ± calcite schist interleaved with quartz-muscovite-feldspar schist. Lower Latte contains a complex amalgamation of metavolcanic rocks including amphibole-biotite schist, amphibolite, and metagabbro. A serpentinized ultramafic unit is in tectonic contact with the interior of the Upper Latte package. Two suites of dikes intrude the Latte area: mafic andesitic dikes and felsic dacite dikes. In certain areas of the Latte zone it is possible to drill through the Lower Latte package into the Supremo augen gneiss. A generalized Latte tectonic stratigraphy is shown in Figure 3.1.

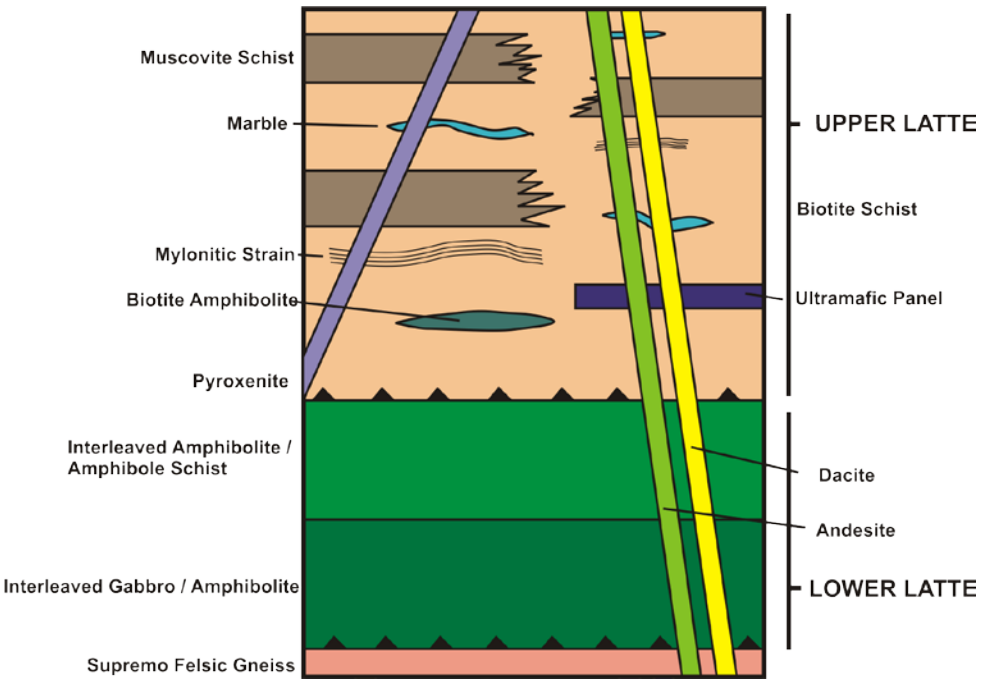


**Figure 3.1: Latte zone tectonic stratigraphy, showing the Upper and Lower Latte assemblages. The Latte panel is thrust over the Supremo felsic gneiss.**

The Latte panel dips moderately to the south- southwest (35-55/180-210). Host rock foliation is relatively constant throughout. Foliation measurements taken from oriented drill core have been averaged on a traverse from Latte west to Latte east along drill sections and reported in Table 3.1. Foliation of the schistose rocks undergoes a slight steepening within the middle of the Latte zone; beginning at 583175 mE and easing off by 583820 mE. This variation in both strike and dip of the host package is minimal and representative of strain during thrust emplacement of the host panels during the Jurassic, as well as flexure due to the WNW striking low amplitude antiform on the property.

Within both Upper and Lower Latte, average foliation recorded in oriented drill core shows a gradual change in trend from west to east. It changes from dipping moderately (~40 degrees) at ~186 degrees in the westernmost portion of Latte from 582550 mE to 582950 mE, steepening to ~50 degrees to ~205 degrees) near the central portion of Latte around 583050 mE to 583650 mE. Continuing east, the foliation reverts to the initial southern, moderate dip from 583750 mE to 584200 mE (Table 3.1).

**Table 3.1: Average structural measurements of foliation taken from oriented drill core spanning the Latte zone from west to east.**

| Easting (mE) | Dip | Dip Direction |
|---|---|---|
| 582550 | 42.7 | 184.9 |
| 582650 | 36.5 | 186.5 |
| 582750 | 38.6 | 195.6 |
| 582800 | 32.5 | 183.3 |
| 582850 | 37.3 | 189.5 |
| 582900 | 39.2 | 186.6 |
| 582950 | 38 | 186.7 |
| 583050 | 41.9 | 207.7 |
| 583140 | 37.3 | 209.3 |
| 583175 | 44.5 | 209 |
| 583350 | 49.6 | 195.8 |
| 583450 | 57.5 | 192.3 |
| 583550 | 46.1 | 190.3 |
| 583650 | 48.3 | 192 |
| 583750 | 54.3 | 177.2 |
| 583820 | 42.5 | 190 |
| 583900 | 46.5 | 170.3 |
| 584000 | 40 | 185 |
| 584200 | 41.3 | 197.5 |

## 3.2 Descriptions of Lithological Units in the Latte Zone

Detailed information about the mineralogy and textures of the different rocks of the Latte zone follows below. Rock units are divided into three packages based on tectonic provenance and petrographic characteristics: 1) Upper Latte psammitic schist and metavolcanics; 2) Lower Latte mafic metavolcanics; and 3) dikes and ultramafic rocks.

### *Upper Latte – Biotite Schist*

Twenty-nine samples of biotite (± feldspar ± quartz ± muscovite ± carbonate) schist were examined from both the eastern and western regions of the Latte zone (Figure 3.2). The rocks are variably retrogressed depending on their location relative to areas of Permian metamorphic strain and mineralized intervals.

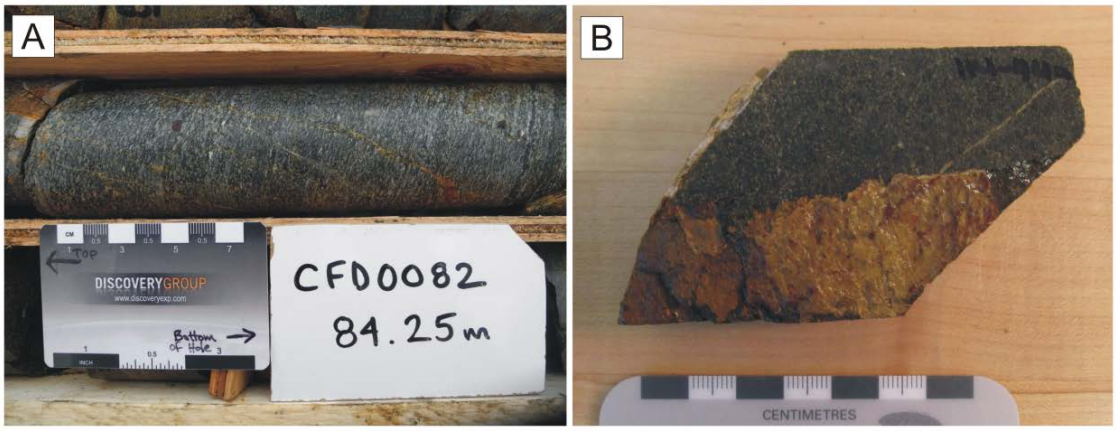


**Figure 3.2: Photos of biotite schist hand samples. A) Full core sample, CFD0082, 84.25m; B) Cut half core, sample 114-44**

The schistose texture is defined by interconnected biotite laths which wrap around relict and replaced "augens" of quartz and sericitized feldspar (Figure 3.3). This defines the dominant $S_2$ foliation within the Coffee area. Biotite is variably chloritized. Augens vary in size, but are generally < 1mm in size. Texturally, the biotite schist varies in strain level from schistose to mylonitic fabrics grading into ribbon-quartz mylonite (described below). Retrogression of the biotite schist results in variable amounts of chlorite replacement of biotite. Biotite grains also show exsolution of ilmenite ($FeTiO_3$). There is near-complete replacement of feldspars by illite/sericite, carbonate, and quartz. Rare fine

grained and blocky potassium feldspar grains and epidote are trace components. Where the biotite schist has high quartz content, it occurs in association with augens of altered feldspar. Locally, quartz occurs as ribbons separated by the micaceous foliation and domains locally display cataclastic (brittle) textures.

Samples can also be rich in carbonate, with late crosscutting carbonate veining, but fine grained carbonate occurs within the foliation of the rock itself as small carbonate pods (<.25 cm). Marble bands are only observed within the biotite-chlorite schist package and are finely recrystallized and range from white to weakly pink in colour. The marble bands typically occur in localized groupings where band frequency increases to multiple thin (3-10 cm) bands per meter. The largest bands have not been observed to be laterally continuous between drill holes, however a large pod of marble observed to the south of Latte near the contact with the Coffee Creek granite is laterally extensive. Late carbonate veining crosscuts all features of the host.

Oxidation within the biotite-chlorite schist occurs along fractures through relatively un-oxidized samples, and pervasively along foliation throughout samples exposed to the strongest oxidation profiles at Coffee. Metamorphic cubic and blebby pyrite is a common constituent of the rock occurring along foliation, appearing brassy in un-oxidized samples and a dark orange-red colouration when oxidized. In weakly oxidized schist, cubes of pyrite display oxidized rims and brassy cores.

### *Upper Latte – Muscovite Schist*

Volumetrically minor muscovite schist is interleaved with biotite schist in the Upper Latte package. It is rarely laterally traceable across drill sections, suggesting it is the product of a different, less mafic protolith which was sporadically deposited in the pre-metamorphic environment. Muscovite schist is composed of quartz, muscovite, sericite, and relict feldspar. The schistose texture is made up of white mica, quartz, and sericitized feldspars, with up to 10% biotite present along foliation (Figure 3.4). The white mica reaches grain sizes of up

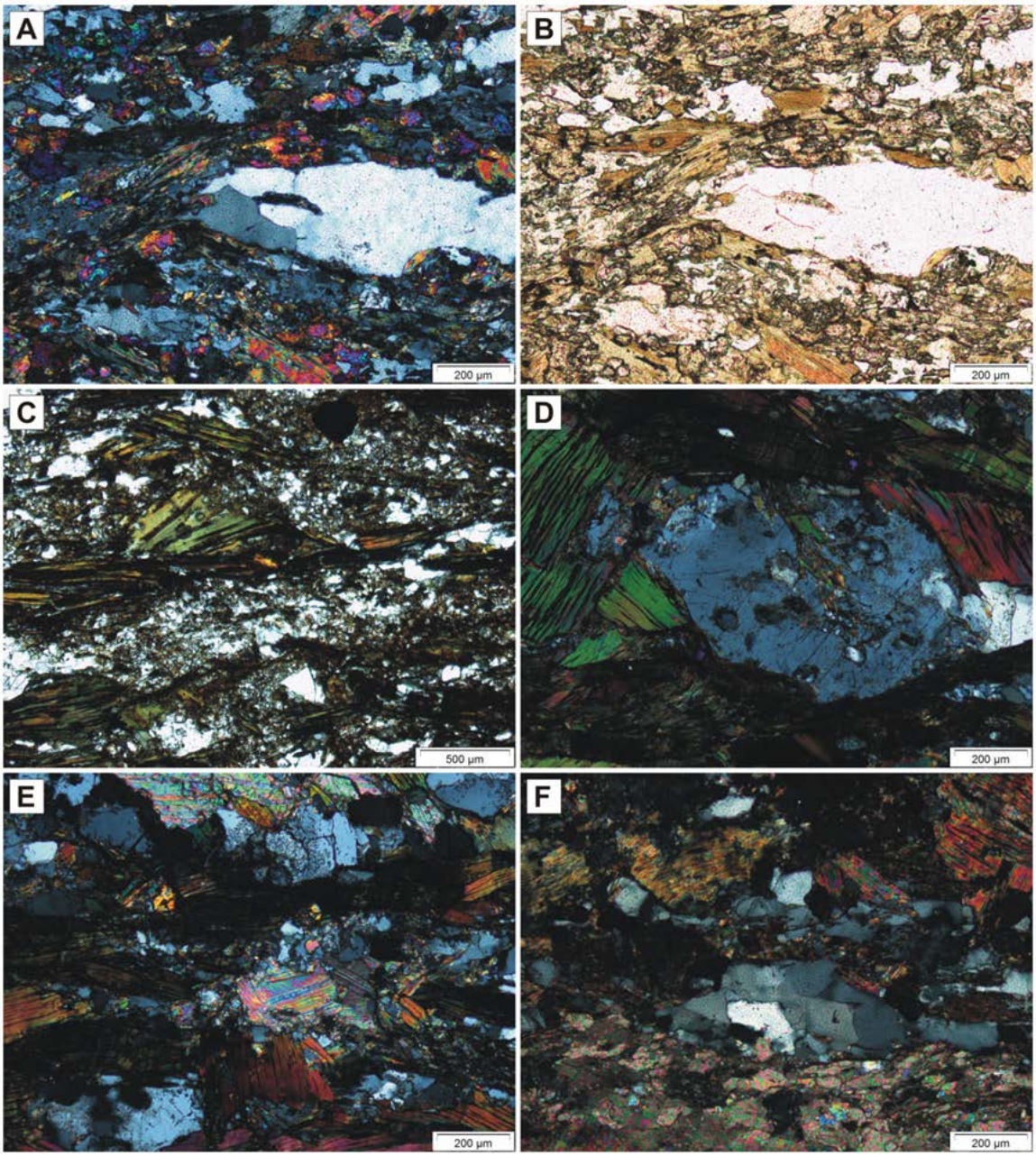


**Figure 3.3: Representative photomicrographs of samples of biotite schist from across the Latte zone, scale bars in lower right of each image. A) 57-167.5 , quartz-rich biotite schist with fine biotite laths, cross-polarized light (XPL) B) 57-167.5, same as last, plane-polarized light (PPL) C) 97-45, strong sericite-clay alteration of feldspars around coarser biotite flakes, XPL D) 97-92, large and feldspar porphyroblast with coarse biotite wrapping around, XPL E) 97-92 exhibiting pockets of carbonate minerals, XPL F) 114-12B, schist adjacent to thin marble band at bottom of photomicrograph, XPL.**

to 2mm. Feldspar porphyroblasts/augens are not as well developed as in portions of the biotite schist, but are also variably sericitized and clay altered. Minor cubic brassy pyrite is present as a pre-metamorphic foliation-concordant feature as seen in the biotite schist. Rare fine grained ilmenite (< .1mm) is present along mica foliation. The minor biotite present within the muscovite schist is readily replaced by chlorite. Samples which experience the strongest retrogression see feldspars completely replaced by sericite and clay minerals.

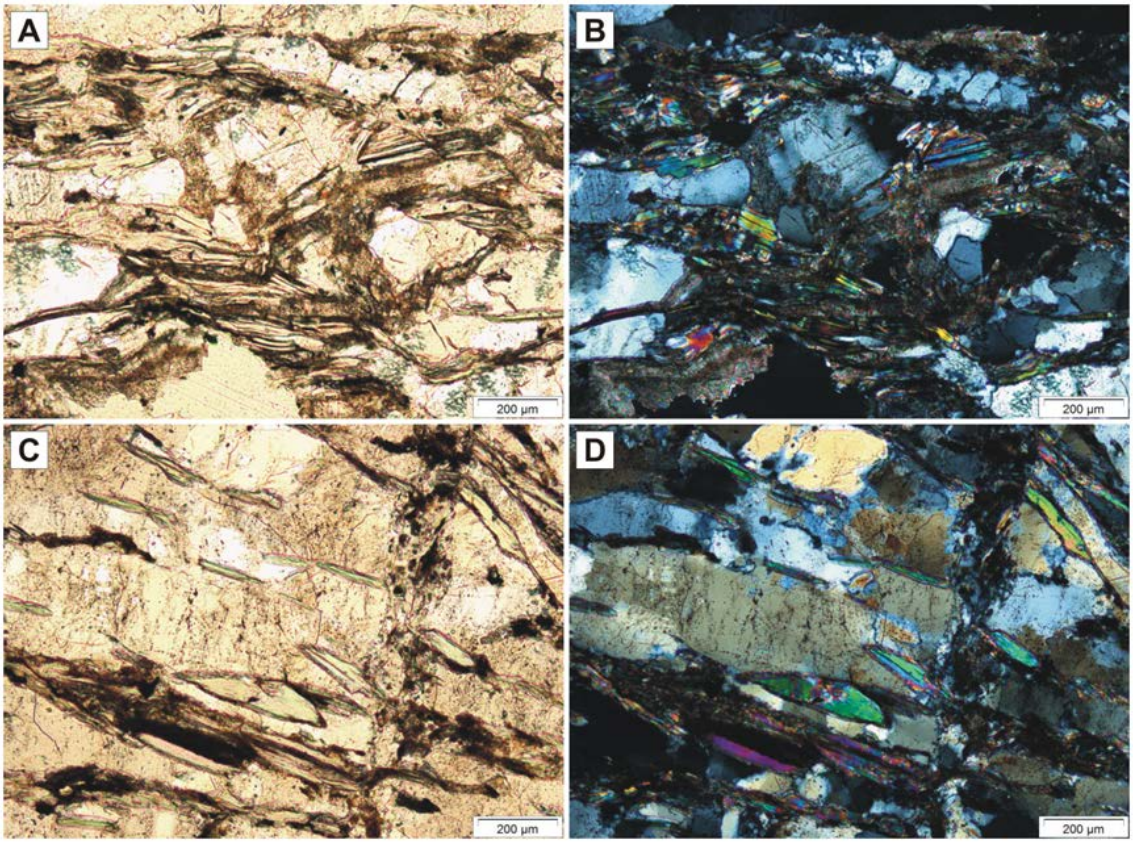


**Figure 3.4: Representative photomicrographs of a sample of muscovite schist from across the Latte zone, scale bars in lower right of each image. A)105-206, domains of quartz and feldspar with strained white mica and clay alteration PPL B) Same image as previous, X XPL C) 105-206, different location on sample: large quartz domains with recrystallized margins and short (.2 mm) mica laths within and surrounding PPL D) Same image as previous, XPL.**

### *Upper Latte – Ribbon Quartz Mylonite*

Ribbon quartz mylonite (RQM) is a drill core logging designation used to refer to schistose units (biotite schist, felsic schist) which appear to contain ribbons of quartz paralleling the dominant $S_2$ foliation (Figure 3.5). These ribbon-quartz mylonites are found throughout the schistose Upper Latte package, but are best preserved at depth where strain and sericitic alteration is not overprinted by near-surface clay alteration and oxidation. In hand sample, fine quartz ribbons are visible separated by fine-grained sericite. Rare fine-grained (< .25 mm) brassy cubic pyrite is present. Mylonitic textures are observed to occur coplanar with the $S_2$ foliation. Sericitic alteration forms along the metamorphic foliation. This sericitization and mylonitization is interpreted to be unrelated to Coffee-style mineralization. This strain manifests itself on a variable scale in drill core within the schists. RQM's are generally <10 cm to multi-meters in width.

Under microscopic analysis, quartz ribbons locally display cataclastic textures and evidence of recrystallization. The high strain implies they were formed during regional $D_2$ deformation, and subsequently recrystallized and subjected to later brittle deformation. Laths of mica are completely replaced by fine-grained sericite and trace chlorite.

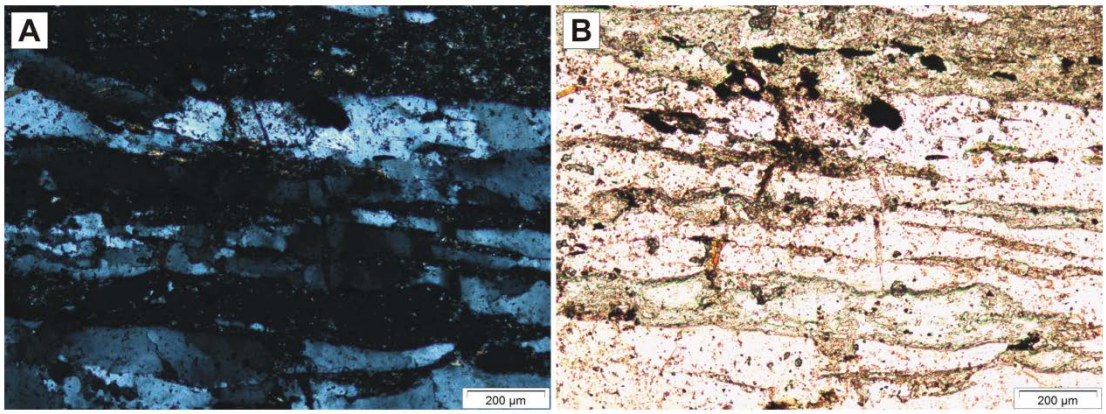


**Figure 3.5: Representative photomicrographs of a sample of ribbon-quartz mylonite. A) 114-58.5, recrystallized quartz ribbons without brittle/cataclastic features are separated by thin regions of strongly sericitized and clay altered white mica. Minor opaques, most likely pyrite. XPL B) Same image as in A, PPL**

### *Upper Latte – Biotite Amphibolite*

Thin intervals of amphibolite are present within biotite schist in the Upper Latte package (Figure 3.6: A, B). These intervals comprise < 20% of the sequence. Massive amphibolite forms dark green-black units within the biotite schist at Latte but has not been observed within intervals of muscovite schist. They generally contain 80-90% hornblende, 10-20% biotite, and rare plagioclase and quartz. Weak to moderate foliation is defined by alignment of amphibole.

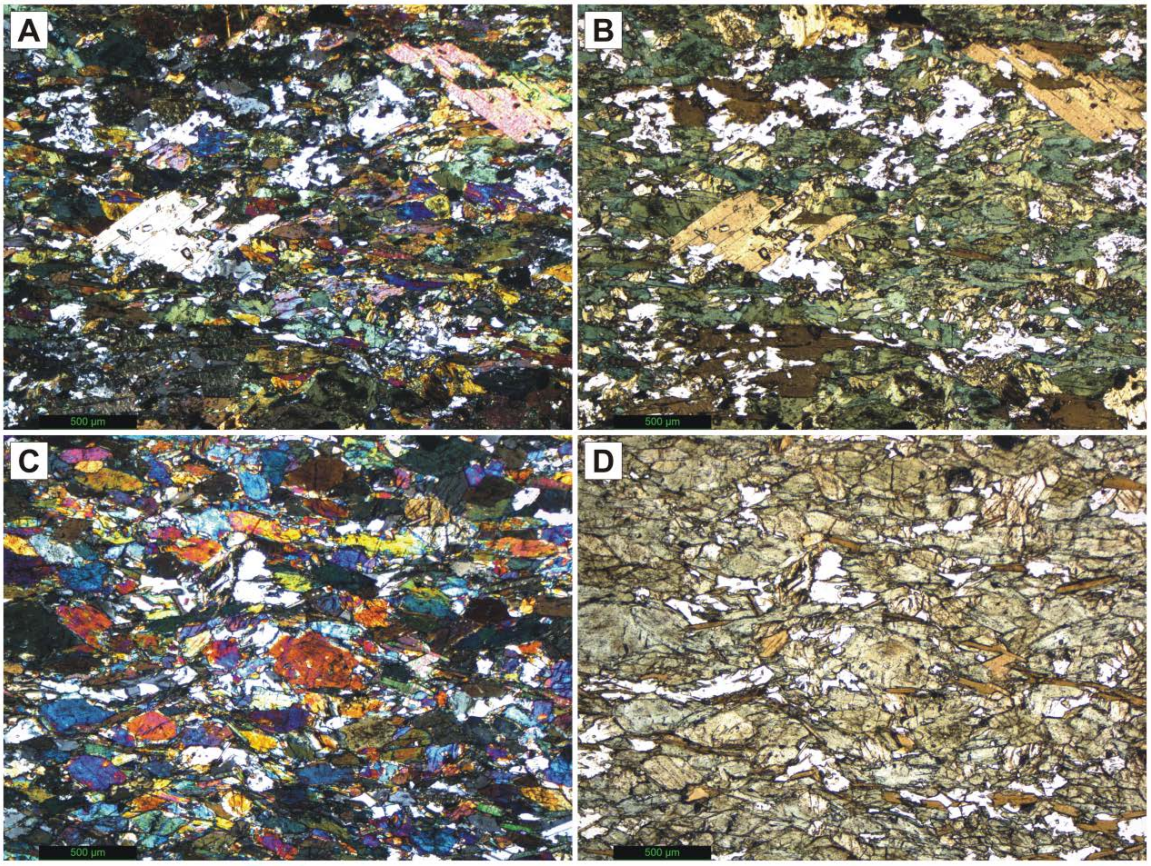


**Figure 3.6: Representative photomicrographs of Latte amphibolite/metabasalt. A) Sample 82-170.6, Upper Latte metabasalt, coarse brown biotite laths within fine grained and foliated hornblende, XPL; B) Same as A, PPL; C) Sample 114-296, Lower Latte metabasalt, massive but fine grained hornblende with minor biotite. Sample is interlayered with coarse metagabbro, XPL. D) Same as C, PPL.**

Amphibole is fine grained (< 0.5 mm) while biotite laths are generally larger in size (1 mm). Minor fine grained quartz and feldspar is found within the amphibolite. Greenschist-facies retrogression is manifested by coarse epidote after amphibole, and

weak to moderate chlorite replacement of biotite. Rare leucoxene is observed as an alteration product after very minor ilmenite.

### *Lower Latte – Amphibolite*

Lower Latte is composed of two dominant mafic units. A layer of amphibolite petrographically similar to the Upper Latte amphibolite is prevalent and intermixed with metagabbro. Contacts between metagabbro and amphibolite in Lower Latte are sharply defined and occur on a 10 cm to multi-meter scale. Fine grained hornblende comprising a massive rock appears dark black to dark green in hand and core samples. Foliation is defined by the hornblende and flakes of biotite. The amphibolite contains up to 15% biotite occurring as fine laths up to 0.25 mm in size. Minor fine grained quartz and feldspar is present within the rock. (Figure 3.6: C, D).

The amphibolite is variably retrogressed, with up to 30% replacement of biotite by chlorite, and coarse epidote replacing amphibole. In areas of strong retrogression, epidote can locally replace up to 60% of the amphibole. These areas appear in drill core as patches of intense epidote replacement. While superficially similar to the Upper Latte metabasalts, they are geochemically distinct and will be discussed in the following chapter.

### *Lower Latte – Metagabbro*

The metagabbro units display varying textures on the meter scale, with banded domains of relict plagioclase grading to coarser and more weakly to unfoliated gabbroic textures (Figure 3.7). Domains of metagabbro are commonly interleaved with metabasalt and amphibolite within the Lower Latte sequence. Coarse hornblende crystals (2 mm) range from radiating laths to "shredded" subhedral crystals. Plagioclase is heavily altered and replaced by sericite. It may be coarse and unfoliated or deformed into thin ribbons with a mylonitic appearance (Figure 3.8). Hornblende is variably strained leading to sub-grain development. Within individual hornblende grains, relict domains remain, which are overprinted by the amphibolite-facies metamorphism and greenschist facies retrogression. The matrix to the large amphibole crystals contains an altered and

retrogressed mixture of plagioclase, fine grained and deformed amphibole, and chlorite and carbonate.

These metagabbroic intervals occur in conjunction with finer grained, massive amphibolite. Both rocks are composed of hornblende; however the finer grained rocks resemble dikes or sills which intruded the coarser metagabbroic rocks. Both rocks are interleaved on a fine scale, with coarse metagabbro cut by the massive and fine grained amphibolite on the decimeter to meter scale. Both rocks exhibit the $S_2$ regional foliation, defined by alignment of fine amphibole grains within the amphibolite, and by coarse and shredded hornblende crystals within the metagabbro.

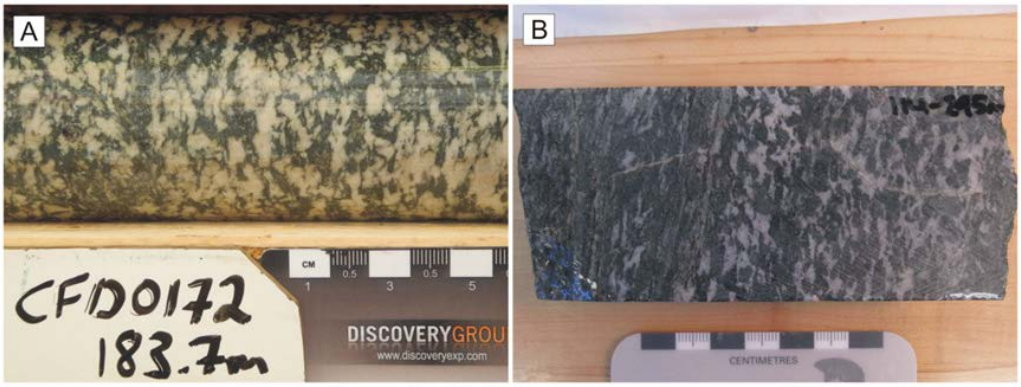


**Figure 3.7: A) Unfoliated metagabbro from CFD0172 at 183.7m down hole, core sample. B) Sample 114-295, analysed in this study, showing strong to weak foliation from left to right.**

## *Ultramafic Rocks*

The ultramafic rocks at Latte can be subdivided into two groups based on their size and character. The first grouping consists of a slice of ultramafic replaced by magnesite which reaches >20 m in thickness and is traceable along multiple drill sections. The second grouping consists of thin tectonic slivers (1-3 m) of heavily altered ultramafic (talc schist, listwanite).

Thick slices (>20m) of strongly chloritized and serpentinized ultramafic rocks, which have been almost completely carbonated to magnesite ($MgCO_3$), are intersected in a number of drill holes (Figure 3.9). Upper and lower contacts observed in drill core are sharp and appear to be tectonic in character. The units contains large (2 mm) crystals of

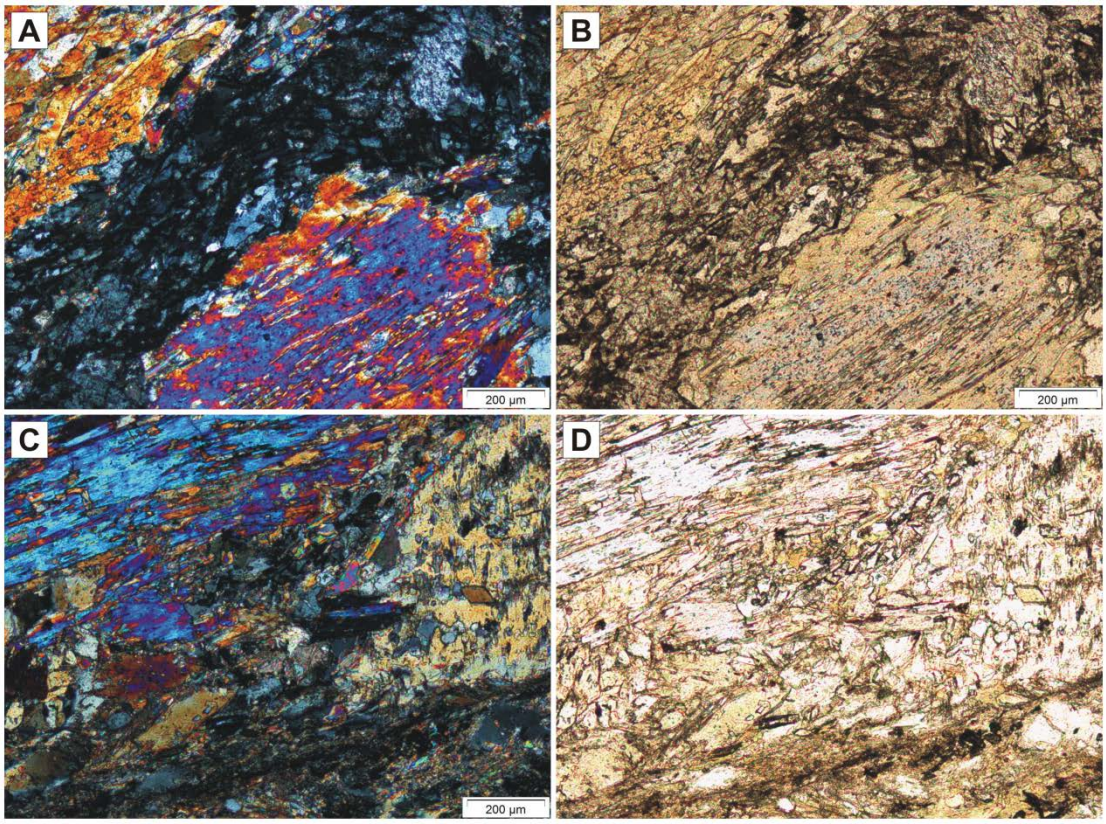


**Figure 3.8: Representative photomicrographs of Latte metagabbro. A) Sample 114-295, coarse hornblende crystals with moderate actinolite overprint, XPL; B) Same as A, PPL; C) Sample 10-180, coarse, shredded hornblende crystals with actinolite, XPL; D) Same as C, PPL. All scale bars 200 microns.**

magnesite with very well developed 60/120 degree cleavage rimmed by fine grained, lath-shaped talc. Samples are altered to clay along fractures, and contain large domains of chlorite and acicular talc and serpentine in the groundmass.

Coarse aggregates of magnetite replace large grains of the magnesite, and fine disseminations are spread throughout the groundmass (< .1 mm). These ultramafic bodies are both weakly foliated and unfoliated, with rounded/semi-euhedral magnesite crystals appearing shredded within foliated units. Samples which appear relatively fresh in hand sample (ex. 113-120.4, Figure 3.10) are generally strongly serpentinized and pervasively altered to magnesite (Figure 3.9). The slices of this ultramafic at Latte can be dismembered along section and appear to have tectonic contacts with the surrounding host.

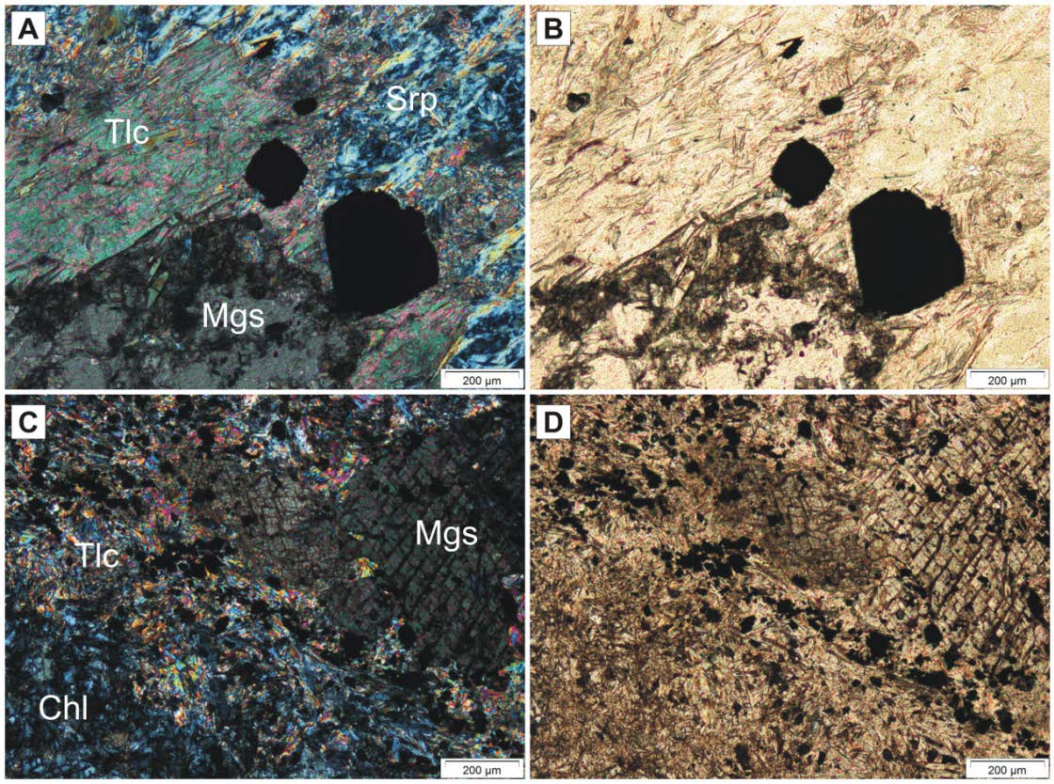


**Figure 3.9: Representative photomicrographs of Latte magnesite. A) Sample 82-135, coarse crystals of magnesite surrounded by talc within a serpentine matrix, XPL; B) Same as A, PPL; C) Sample 113-120.4, coarse magnesite crystals with fine talc and chlorite within t the groundmass, XPL; D) Same as C, PPL. All scale bars are 200 microns.**

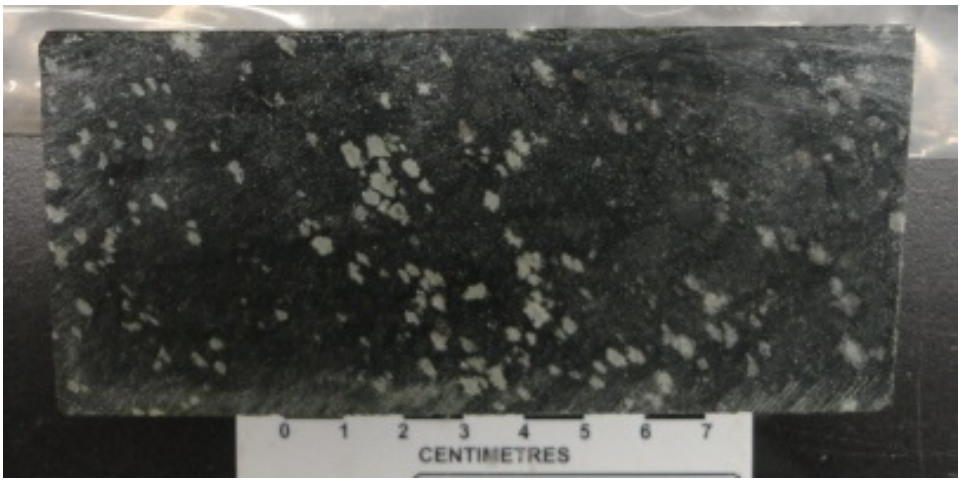


**Figure 3.10: Fresh-looking sample of ultramafic from CFD0113 at 120.4m down hole. The sample is identical to A) in Figure 3.9 under the microscope.**

Thin ultramafic slivers are found throughout Latte and are easily identifiable within drill core. They are strongly deformed and commonly exhibit recumbent folding and a strong sense of shear (Figure 3.11). The recumbent folds are interpreted to be of the $F_3$ generation ($D_3$ deformation and thrust stacking) with the ultramafics readily accommodating strain due to rheological differences with the surrounding mafic and schistose hosts (Figure 3.12). These thin slivers are usually found within the lower panels of the biotite schist intervals in Upper Latte.

The thin ultramafics contain coarse laths of actinolite (up to 2 mm) in close association with talc and serpentine. Blocky grains of magnesite are present in samples which have experienced a high level of retrogression. Minor feldspar has been dominantly replaced by coarse grained epidote (1 mm). Sulphide mineralogy is variable and consists of subhedral pyrite and pyrrhotite grains which are commonly intergrown.

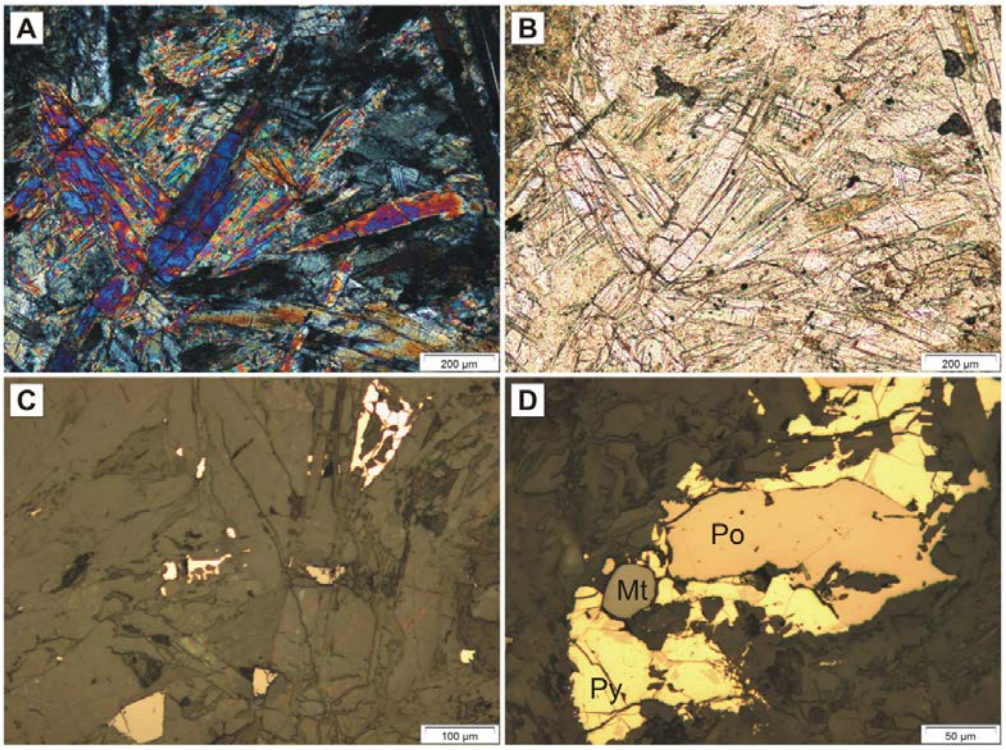


**Figure 3.11: Representative photomicrographs of heavily altered ultramafic slivers from the Latte zone, all images from sample 35-253. A) Laths of actinolite in association with talc, XPL; B) Same as A, PPL; C) Reflected light image of sulphides in the ultramafics: visible pyrite and pyrrhotite, RL; D) Close up of intergrown pyrite and pyrrhotite with accessory magnetite, 50 micron scale bar. All other images 200 micron scale bar.**

**Figure 3.12: Core box photo of CFD0164 from 31.8-36.14m. The yellow marked ~1m interval is a thin and heavily altered, folded, and sheared ultramafic sliver.**

## *Late Dikes*

Late dikes at the Coffee Property typically exploit existing structures and areas of weakness in the host which are generally mineralized structures. Volumetrically significant dikes are present in both mineralized and un-mineralized areas of the Latte zone, generally striking in an easterly direction in Latte west and a northerly direction in Latte east.

Dikes of both andesitic and dacitic compositions are found at Latte and are generally strongly clay-sericite altered. Andesite dikes are typically aphanitic, though rare andesite porphyries are intersected with euhedral feldspar phenocrysts up to 3 mm in width and easily visible in hand sample. They are black in colour with grey-blue coloured feldspar phenocrysts. The groundmass of the dikes is extremely fine grained and contains fine feldspar crystals and a large clay component. Dacite dikes are almost exclusively aphanitic. Feldspars phenocrysts are rarely visible in hand sample. They are a light grey colour in hand sample and are usually bleached white by pervasive clay alteration. Primary igneous texture is sometimes difficult to detect. Due to oxidation, the dacite dikes are easily distinguished by a lisegang-banded oxidation pattern.

In both andesite and dacite dikes, subhedral feldspar phenocrysts (.3 - 3 mm), strongly altered to sericite and fine quartz (.2 mm), occur dispersed among the groundmass (Figure 3.13). Preserved plagioclase in andesite dikes occasionally exhibit polysynthetic twinning. The dominant clay alteration in both dikes is kaolinite, which obscures the fine textures. Dikes occasionally contain fine carbonate veinlets which

terminate at contacts with the host lithology, implying at least minor post-emplacement movement.

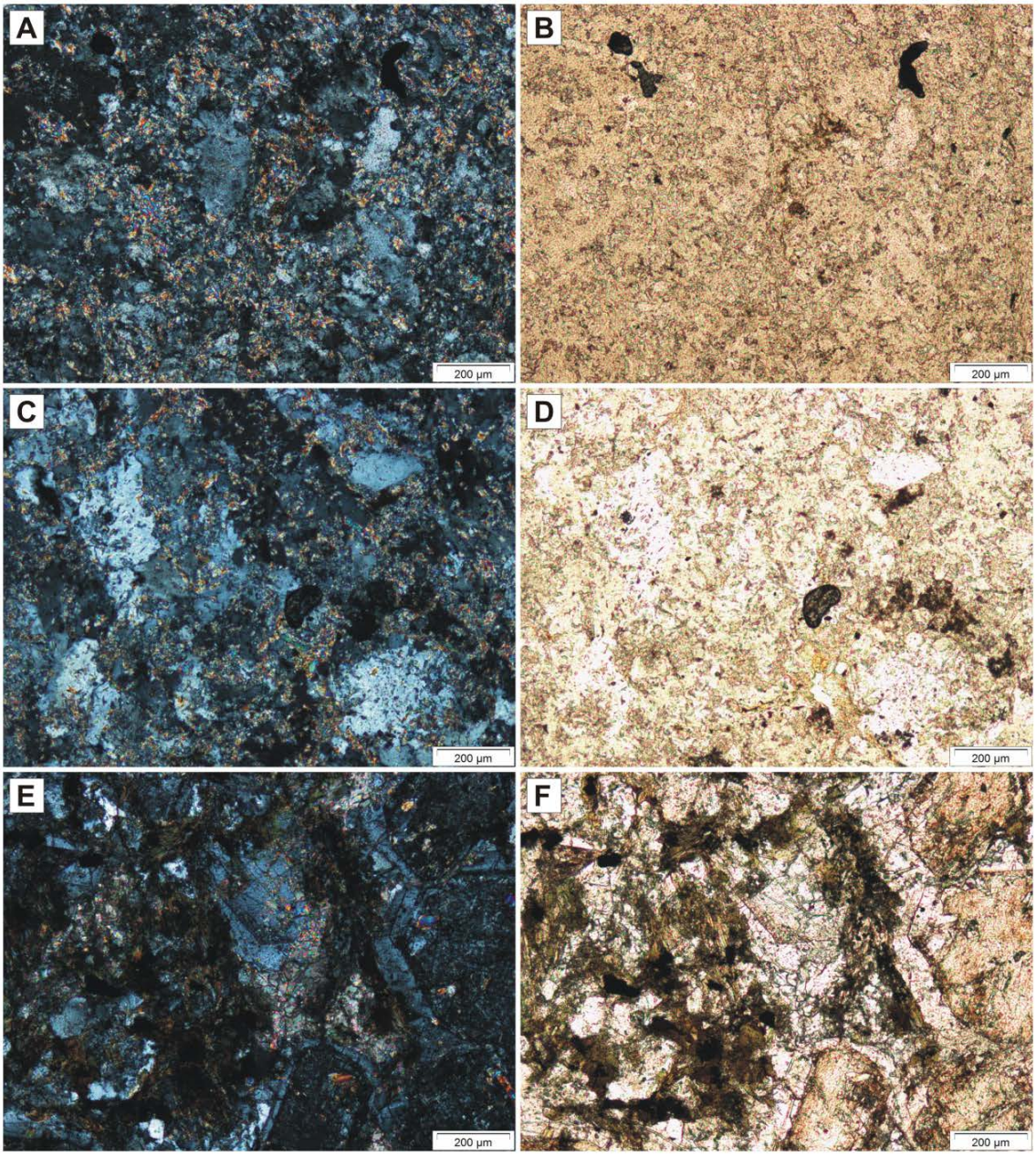


**Figure 3.13: Representative photomicrographs of Latte dikes: A, B) Sample 6-80, dacite, XPL, PPL; C,D) Sample 7-66, dacite, XPL, PPL; E,F) Sample 99-84.5, andesite, XPL, PPL. All scale bars 200 microns.**

## 3.3 35-Element ICP-AES Re-logging of Latte Zone Drill Logs

A complete 35 element ICP-AES assay database exists for each drill hole in the Latte zone. This database was utilized to aid in re-logging of the Latte zone by attempting to determine geochemical signatures for the above named lithologies. The ICP-AES analysis provides a detailed yet efficient chemical breakdown of each 1 m drill core sample. Analysis of the complete dataset revealed a number of useful geochemical markers used to quickly and simply classify rocks which may have been misrepresented during in-field drill core logging. By applying these geochemical filters to the data set a more accurate picture of the complete cross-sectional geology of the Latte zone emerges than what was initially available from drill logs direct from the field. This provides a valuable standard which can greatly aid in drill targeting and the understanding of the Latte zone.

The units which were most easily distinguished chemically and also the most misinterpreted during drill core logging were the amphibolite/metabasalt units, metagabbro, and ultramafics. Rocks at Latte are generally very difficult to distinguish visually due to pervasive alteration. Rough geochemical markers included an approximation of Mg number (Mg/Mg+Fe), P, Ca, Ti, Cr, and Ni content. These units are found within both the Upper and Lower Latte packages, with a distinct geochemical change at the beginning of the Lower Latte sequence. In order to distinguish the lithological units at Latte while logging drill core, a set of lithological codes created during the 2010 season has been employed. For the mafic and ultramafic units, a number of codes have been in use with varying meanings and have been miss-applied. For the purpose of the newly re-logged Latte 3D model in Appendix F, refer to Table 3.2 when interpreting cross section data.

The different metabasaltic rocks at Latte are distinguishable by their ICP chemistry. Three different mafic assemblages can be defined: the Upper Latte metabasalt, the Lower Latte metabasalt, and the Lower Latte metagabbro/metabasalt. In order to distinguish between these different units a number of filters were applied. The Mg # (Mg/Mg+Fe) was calculated from ICP-MS results (Table 3.3). In order to be categorized

**Table 3.2: Short-form core logging designations used during the 2010-2011 field seasons, used within this study.**

| Core Logging Designation | Lithology |
|---|---|
| MBSLT | Amphibolite/Metabasalt |
| UX | Metagabbro |
| RU | Magnesite/Talc Schist/Pyroxenite |
| BtS | Biotite schist |
| MsS | Muscovite-sericite schist |
| BtS_carb | Biotite schist + carbonate |
| IV | Andesite dyke |
| FC | Dacite dyke |
| FG | Felsic gneiss |
| RQM | Ribbon quartz mylonite |
| YC | Silicified-clast breccia |
| YO | Breccia-other |
| HU | Hydrothermally unrecognizable |
| PyF | Pyritic Fault |

generally as a metabasalt/amphibolite or metagabbro under this classification, a sample interval must have Mg # greater than 30 and less than 60. In addition to the Mg #, typical Cr and Ni content should be between 40 - 400 ppm and 35 - 200 ppm respectively. Metabasalt and amphibolite were given the distinction "MBSLT" when renaming mis-logged intervals which fit these criteria.

The Upper Latte metabasalts displayed Mg #'s on the low end of the scale defined above, and could be identified by increased Ca content (3-9 wt. %) and marked jumps in P content (> 1000 ppm) relative to the adjacent biotite schist units. Lower Latte metabasalt contains greater Cr content (>200 ppm) and higher Mg # (40-50) than comparative Upper Latte metabasalt (ex. Sample 114-272). The third grouping consists of the Lower Latte interlayered metabasalt and metagabbro. While texturally distinct, these rocks are chemically equivalent with a Mg # of approximately 40-60, and an elevated Ca content relative to the Lower Latte metabasalt described previously. An additional tool in re-logging was visual inspection of historical core box photos to identify the distinct white banding or zones of plagioclase seen in the samples. As the metagabbro is visually distinct from both the Upper Latte amphibolite and coarse hornblende dominant metabasalt, it was given the lithological designation "UX".

**Table 3.3: Summary table of parameters used to aid in distinguishing Latte mafic rocks from background biotite.**

| Unit | Cr | Ni | Mg# | Other characteristics |
|---|---|---|---|---|
| Upper Latte metabasalt | <150 | <100 | 30-40 | >1000 ppm P |
| Lower Latte biotite-rich metabasalt | >200 | 35-200 | 40-50 | N/A |
| Lower Latte interleaved metabasalt and metagabbro | <150 | <100 | 40-60 | Elevated Ca, depleted Fe |

All ultramafic units were discovered and corrected during re-logging by applying Mg#, Cr, and Ni filters to the data. By setting these chemical filters to Mg# > 60, Cr > 600 ppm, and Ni > 600 ppm, ultramafic lithologies were easily distinguished. A wide (up to 20 m) ultramafic body which correlates as much as 400 m between sections was discovered with both Cr and Ni content exceeding 1300 ppm, and Mg# averaging 75, and peaking at 81 in drill holes CFD0080, 82, 91, 94, 96, 107, 113, 116, 118, 126, 164, 169, and CFD0174 (Figure 3.14). In addition, lowering the threshold Cr and Ni values revealed many thin units of ultramafic character on the 1 m scale that were not identified during core logging (ex. Figure 3.12).

Other units within the Latte zone can also be easily chemically distinguished, including both dacite and andesite dikes. These units are generally easily identifiable in drill core and have not been significantly mis-logged.

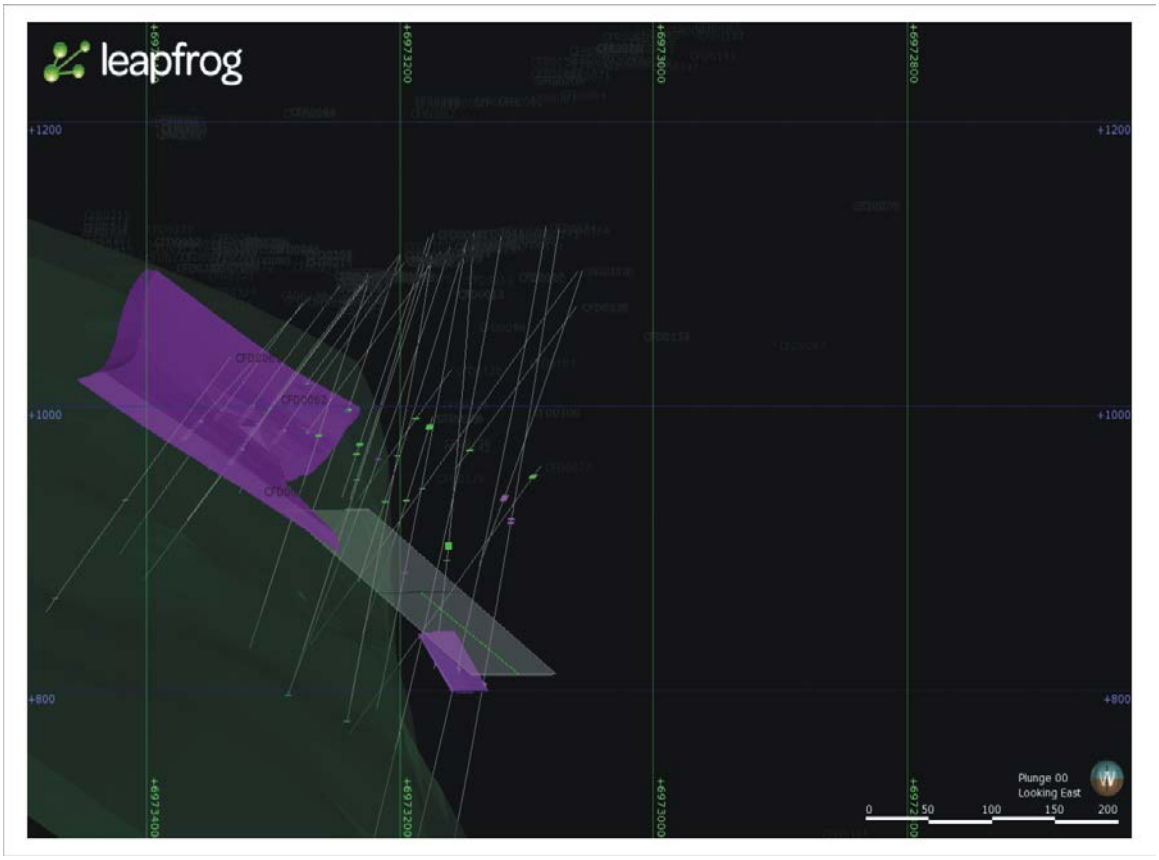


**Figure 3.14: Leapfrog 3-D image of the Latte zone, looking east. The purple panels represent the thick ultramafic body observed in drill core. The panels are emplaced roughly along foliation, and the down-dropped panel has possibly been faulted off of the upper. The green at the structural footwall represents the footwall metabasalts/metagabbros of Lower Latte.**

## 3.4 Architecture of the Latte Zone

The Latte Zone is delineated by both reverse circulation and diamond drilling for a strike length of over 1.5 km. All of the drill holes were collared on and penetrated into the schistose Upper Latte panel. This panel extends to the northwest before terminating against an inferred fault contact with a panel of Klondike Schist. To the east it pinches out between the Sulphur Creek orthogneiss (Supremo orthogneiss) and the Coffee Creek granite. Structural features of the Latte zone prior to mineralization can be discussed chronologically. First, the foliation of the host rocks was established during the Permian during the Klondike orogeny. Secondly, slices of Yukon-Tanana rocks were thrust emplaced to the northeast during the Jurassic. Finally, late ductile to brittle faulting

occurred from the Mid-Cretaceous to the Eocene. The late structural framework will be discussed in detail in Chapter 5 and not discussed here.

NE verging thrust emplacement and folding is common throughout the Dawson Range and identified at Latte (MacKenzie et al., 2008). Thrust emplacement is best exemplified by the entrainment of exotic ultramafic rocks at Coffee. The major ultramafic slice seen at Latte is weakly foliated to unfoliated, and is emplaced coplanar to the regional $S_2$ foliation. As described above, contacts with the thick, tabular ultramafic bodies are tectonic in character. The lack of strong foliation within the units in comparison to the thin ultramafic slivers, which display internal folding and strong deformation, differentiates the thick bodies as a different rock than the thinner ultramafics. Weak foliation observed in some samples of the thick ultramafic is found along the margin of the units and is interpreted as a component of strain imparted to the thick ultramafic during tectonic thrust emplacement. Interior portions of these rocks are unfoliated. The stratigraphic variation between Upper and Lower Latte is distinct, and representative of two differing rock assemblages.

These differing rock panels are prominent in cross sections of the Latte zone, as well as within the Leapfrog 3D model provided as a Leapfrog Viewer file (Appendix F). Section 582900mE in the western portion of the Latte zone displays a typical cut through the western Latte stratigraphy (Figure 3.15). Six diamond drill holes penetrate through the Upper Latte schistose panel, which contains zones of increased strain, logged as ribbon quartz mylonite. Rare thin ultramafics are present in the upper stratigraphy as well as common andesite and dacite dikes, which generally cut through mineralized structures. These are not shown on this section for clarity, but run roughly west-east and dip steeply to the south-southwest. Panels of amphibolite are intersected in both the Upper and Lower Latte intervals. A thick panel of ultramafic rock was intersected in CFD0107 and CFD0113, the two northernmost drill holes on the section, but was not cut by CFD0110, which was drilled off the same pad as CFD0107 but at a steeper dip (-70 degrees). This indicates that the ultramafic is a discontinuous panel, tectonically emplaced. Cross sections to the east and west of 582900mE also exhibit the same morphology.

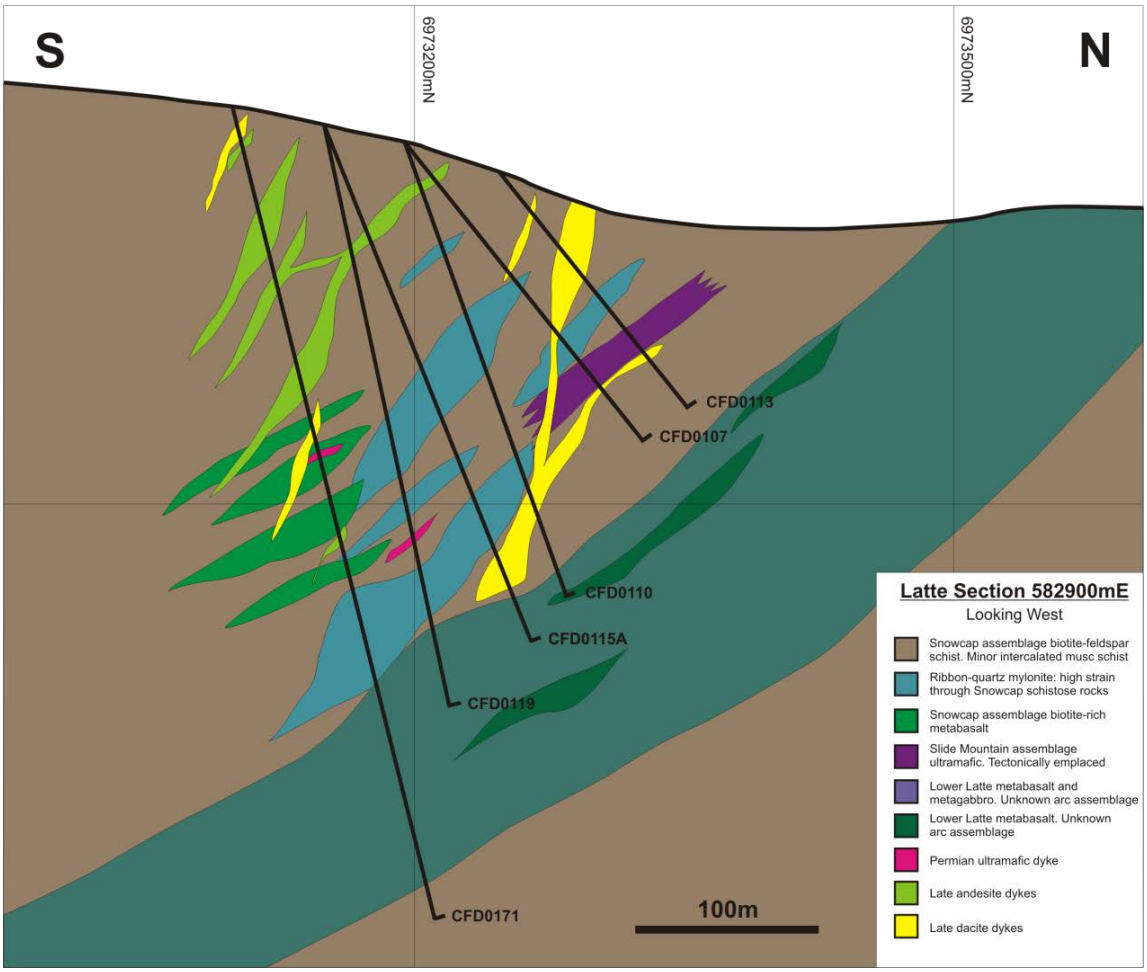


**Figure 3.15: Cross section of Latte west on the 582900mE easting, looking west. Upper Latte is cut by common andesite and dacite dikes, and is in tectonic contact with the panel of Lower Latte metabasalt and metagabbro. A panel of Slide Mountain assemblage ultramafic is intersected in CFD0113 and CFD0107.**

A representative cross section through Latte east at 583450mE shows the same tectonic arrangement of schistose rocks overthrusting a metavolcanic panel (Figure 3.16). The Lower Latte metavolcanic panel appears to thin slightly to the east. Also notable is the relative lack of diking in the eastern drill section: only rare andesite and no dacite dikes were intersected by the six drill holes on the 583450mE section. CFD0114 shows a slight discontinuity in the Lower Latte panel, with two bodies of the footwall metavolcanic package interleaved with an interval of biotite schist. Minor strain is evident in the upper portions of the Latte stratigraphy compared to the western section.

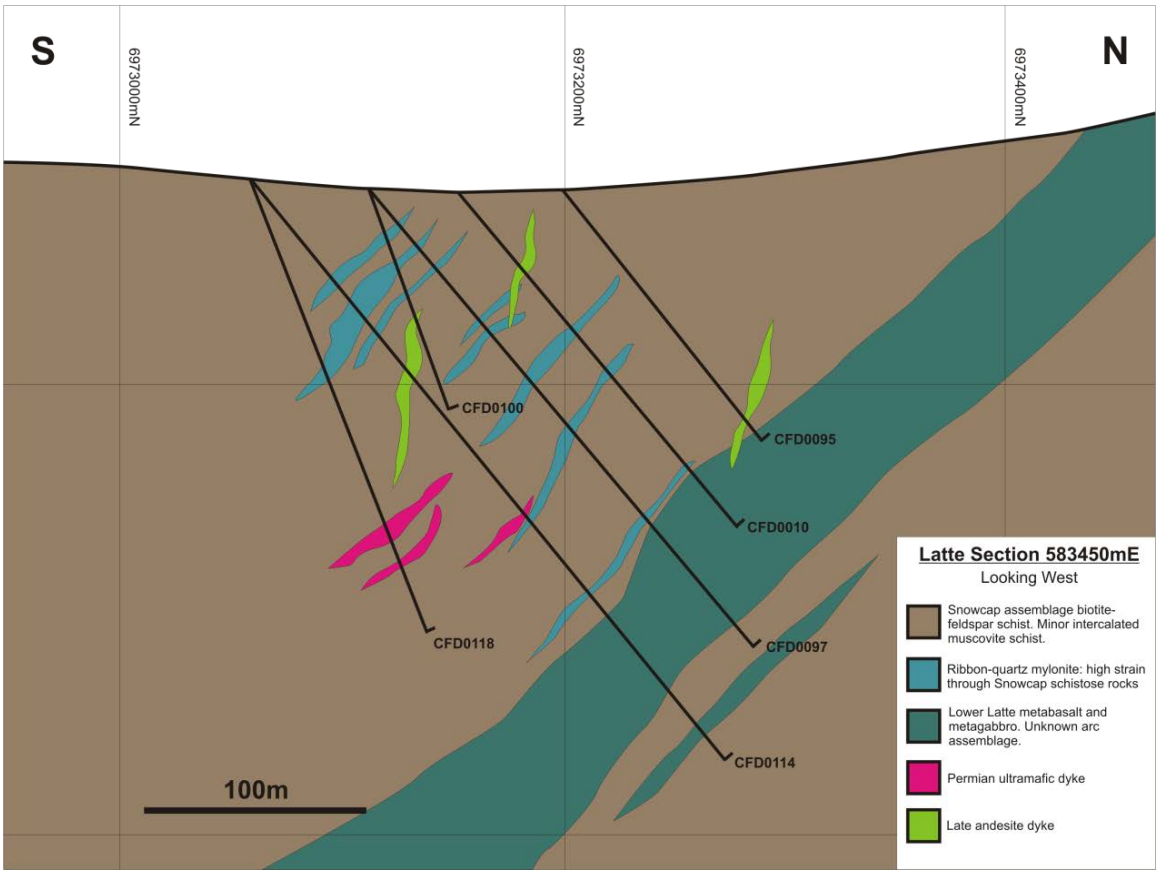


**Figure: 3.16 Cross section of Latte east on the 583450mE easting. Note the absence of common dikes and the similar morphology of the Lower Latte panel to Latte west. The dikes in the eastern portion of Latte most likely strike N-S, and are not represented as well in drill core. The tectonically emplaced ultramafic slice (Slide Mountain) is not present on this section.**

# Chapter 4

## 4 Geochemistry of the Latte Host Rocks

Twenty-three samples were submitted for research grade whole-rock geochemical analysis (Table 4.1). These samples have been grouped roughly by rock type, with 10 amphibolites, 7 ultramafics, 3 dikes, and 1 marble. The amphibolite samples were chosen in an attempt to determine their original tectonic provenance and source. This was accomplished utilizing the methods applied by Dusel-Bacon and Cooper (1999) in the Yukon Tanana Uplands in east-central Alaska. The ultramafics were sampled in order to determine geochemical characteristics which may distinguish different magmatic suites. Dikes were chosen to bolster the limited geochemical database at Coffee and compare their trace element signatures with that of the nearby Coffee Creek granite. Petrographic descriptions for each sample can be found in Appendix A, the whole-rock geochemical data can be found in Appendix B. The results are described below.

**Table 4.1: Summary of samples analysed in this chapter. Each sample was given a code, ex. L001, to simplify sample notation while working with numerous plots and charts**

| Analysis | Sample | Description |
|---|---|---|
| L001 | 6-80m | Dacite dike |
| L002 | 7-66m | Dacite dike |
| L003 | 7-157.8m | Altered ultramafic dike |
| L004 | 10-180m | Foliated metagabbro |
| L005 | 35-253m | High Cr mafic |
| L006 | 38-254m | High Cr mafic |
| L007 | 40-206.9m | High Cr mafic |
| L008 | 40-234.8m | Talc schist/listwanite |
| L009 | 49-255.7m | High Cr mafic |
| L010 | 57-128m | High Cr mafic |
| L011 | 57-167.5m | Lower Latte mafic |
| L012 | 61-131.15m | Altered Cr mafic |
| L013 | 73-9.8m | Ultramafic |
| L014 | 82-141.6m | Ultramafic |
| L015 | 82-168m | Marble |
| L016 | 82-170.6m | Metabasalt |
| L017 | 99-84.5m | Andesite dike |
| L018 | 113-120.4m | Ultramafic |
| L019 | 114-44m | Biotite schist |
| L020 | 114-272m | Metabasalt |
| L021 | 114-296m | Metabasalt |
| L022 | 20-42m | Supremo andesite dike |
| L023 | 53-40m | Kona dacite dike |

## 4.1 Amphibolite Geochemistry

The whole rock geochemical results on amphibolites are plotted on 5 diagrams designed to assign a tectonic classification to rocks with basaltic protoliths. All ten samples are shown on each plot regardless of how well the data clusters in the set tectonic fields. A general classification diagram is first used to discriminate volcanic rock type, followed by extended-REE plots and three ternary discrimination diagrams. The volatile-free normalized (anhydrous) $SiO_2$ content ranges from a minimum of 44.9% in sample L006 to a high of 60.2% in sample L007. It should be noted that two samples (L007, L011) contain >55% $SiO_2$, and therefore exceed the maximum silica content of a basalt. The current $SiO_2$ content of each rock may not represent the initial composition due to high levels of alteration and metamorphism in the Latte zone.

The volcanic rock classification diagram of Winchester and Floyd (1977) plots $Zr/TiO_2$ against Nb/Y (Figure 4.1). The diagram is designed to determine original igneous rock type and classify the samples as alkaline or subalkaline. Nine of ten amphibolite samples plot within the charts area. Samples L004, L010, and L021 plot

within the subalkaline basalt field while samples L005, L011, L019, and L020 plot within the andesite/basalt field. Sample L016 plots alone within the alkaline basalt field. Sample L007 is an outlier which plots in the rhyodacite/dacite field. No samples plot within the andesite field, with the majority plotting in the andesite/basalt field (n = 3) and the subalkaline basalt field (n = 3).

Samples are then plotted on extended-rare earth element (REE) spider diagrams. The diagrams are normalized to primordial mantle using the normalization of McDonough et al., (1992). Element order along the bottom of the spidergrams is from Jenner (1996). Elements increase in compatibility (favour the solid phase during melting or crystallization) from left to right along the bottom of the diagrams. Figure 4.2 displays all 10 samples on the same extended-REE plot. REE abundance is generally low for all samples. Samples L004, L006, and L010 all plot with primitive signatures and marked depletions in Zr. The rest of the samples display 3 distinct patterns. A depletion of Nb and Ta relative to Th and La is present in samples L005, L007, L011, L019 and L020, with depletion of elements past La. In contrast, sample L016 is enriched in Nb and Ta

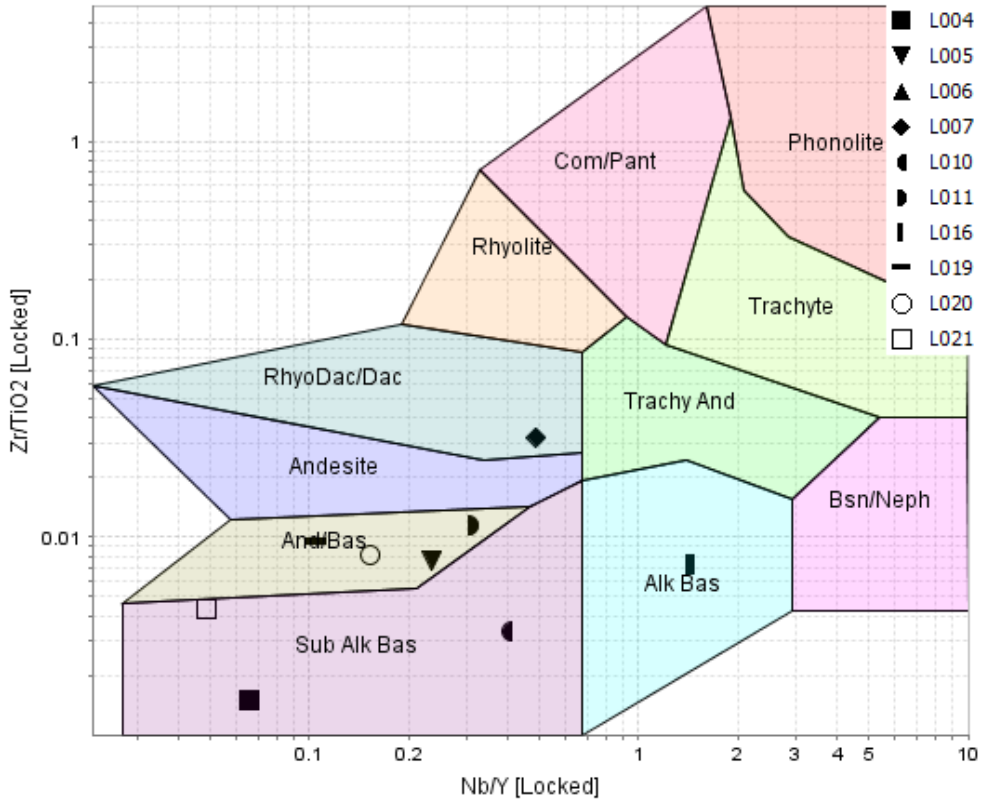


**Figure 4.1: Latte amphibolite samples plotting in the volcanic rock classification diagram of Winchester and Floyd (1977).**

relative to Th and La, forming a gentle hump. With the low-REE-abundance, sample L021 is slightly depleted in the LREE elements relative to the HREE elements and shows a slight enrichment in Th. Samples L004, L006, and L010 that plot near primordial abundances are strongly depleted in Zr and Ti, and show significant Eu enrichment. Samples which demonstrate diagnostic REE patterns are plotted on Figure 4.3 for clarity.

All 10 samples were plotted in the Ti/100 - Zr - Yx3 ternary discrimination diagram of Pearce and Cann (1973) (Figure 4.4). Samples L004, L005, L006, L010, and L021 all plot right of the basalt discrimination fields. Sample L007 plots towards the Zr apex left of the continental alkaline basalt (CAB) field. Sample L011 plots within the CAB field, L016 plots alone in the within-plate basalt (WPB) field, and L019 and L020 plot together within the MORB, island-arc tholeiite (IAT) and CAB fields. Sample L011 and L09 plot near the join between the CAB and MORB and IAT fields.

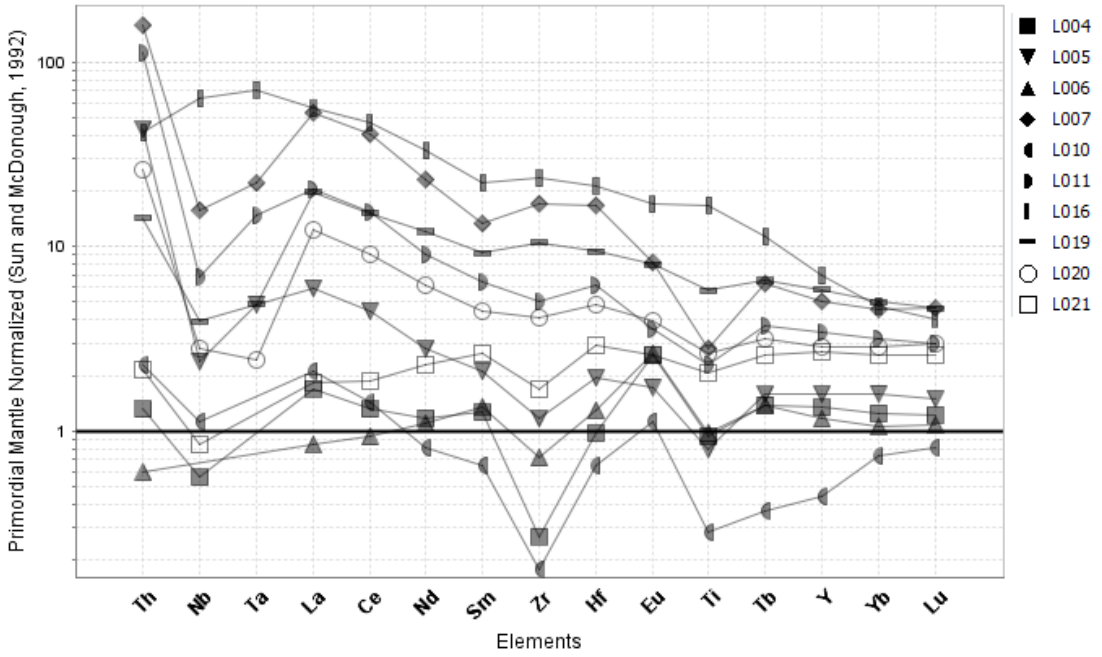


**Figure 4.2: Primordial mantle normalized (McDonough et al., 1992) extended-REE spidergram for all 10 Latte amphibolite samples.**

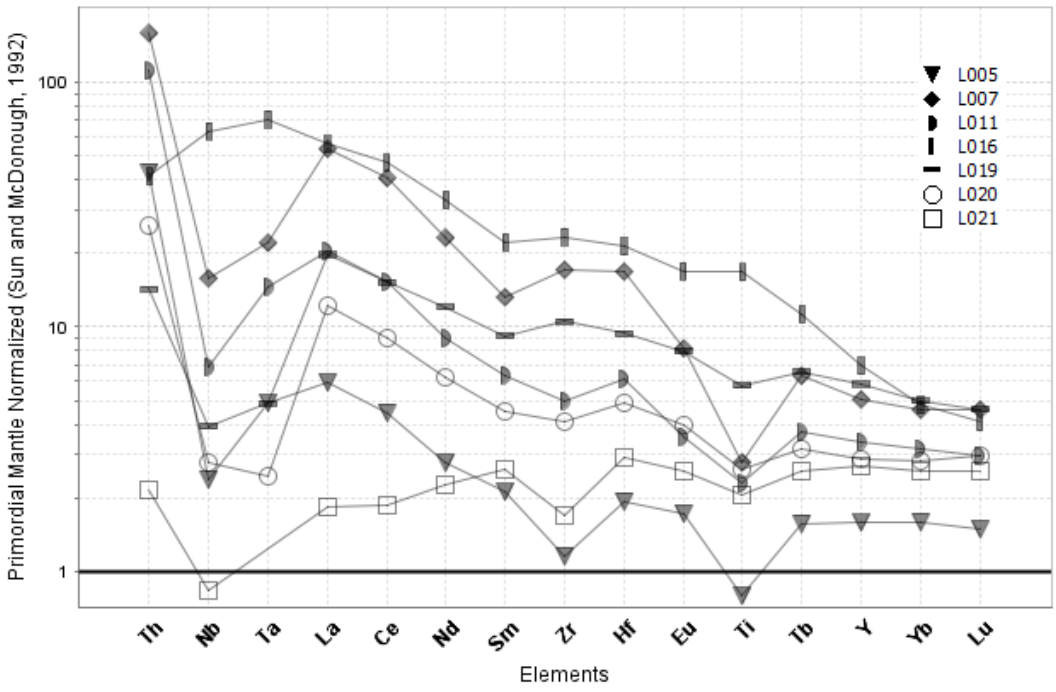


**Figure 4.3: Primordial mantle normalized (Sun and McDonough, 1992) extended-REE spidergram for Latte samples which exhibit modern arc, alkali basalt, and MORB signatures for clarity.**

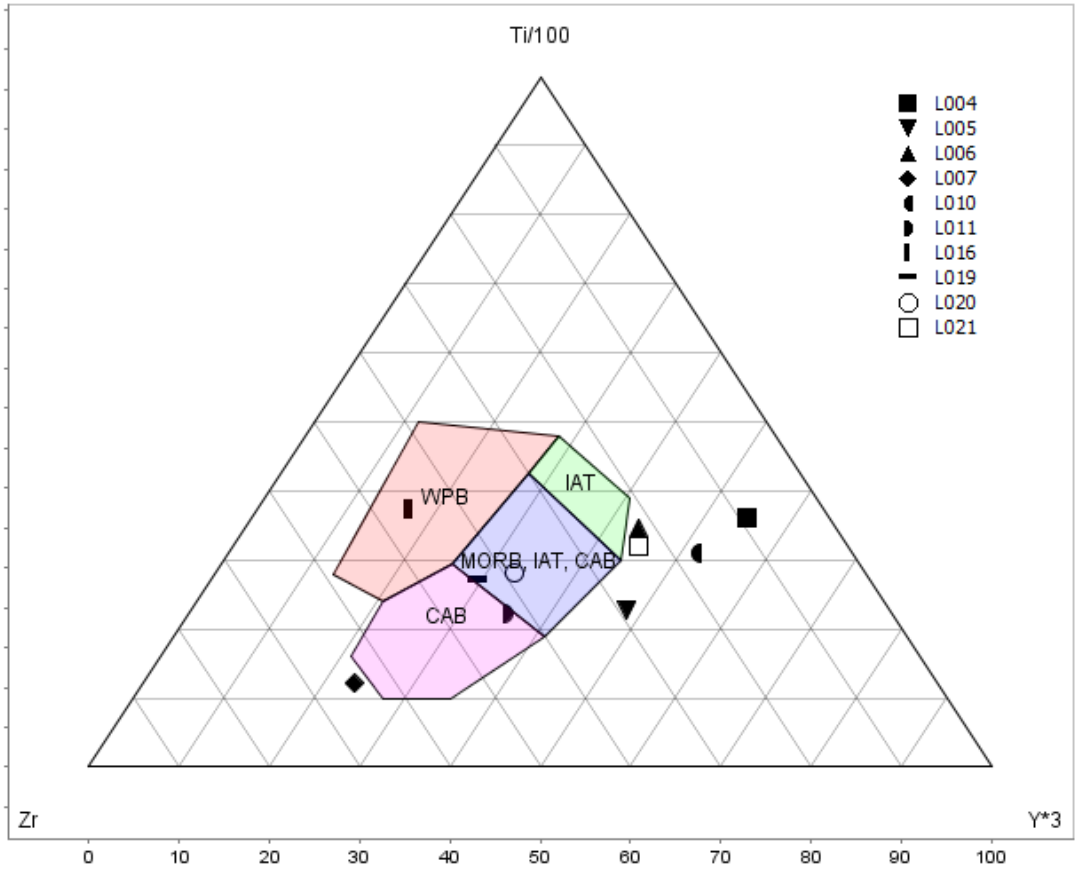


**Figure 4.4: Basalt Ti-Zr-Y discrimination diagram of Pearce and Cann (1973) with all 10 Latte amphibolite samples plotted.**

The ternary (Nb x 2 - Zr/4 - Y) diagram of Meschede (1986) distinguishes between normal MORB (N-MORB) and enriched MORB (E-MORB) (Figure 4.5). Sample L016 plots in the within-plate alkali basalt (WPAB) field, while sample L007, plots slightly on the WPAB+WPT field with a lower Nb value. Sample L019 plots directly on the WPT + volcanic arc basalt (VAB) join. Samples L020 and L021 plot as N-MORB while L005 and L011 plot as E-MORB. Samples L010 and L004 both plot outside of all fields while sample L006 does not plot on the diagram due to Nb content which is below detection.

The Y/15 - La/10 - Nb/8 ternary of Cabanis and Lecolle (1989) is used to separate arc rocks from MORB (Figure 4.6). Samples plotting along the left (Y - La) side of the diagram originate at destructive-type plate boundaries (arc) while those plotting along the right side (Y - Nb) originate from within-plate, anorogenic, or extensional tectonic

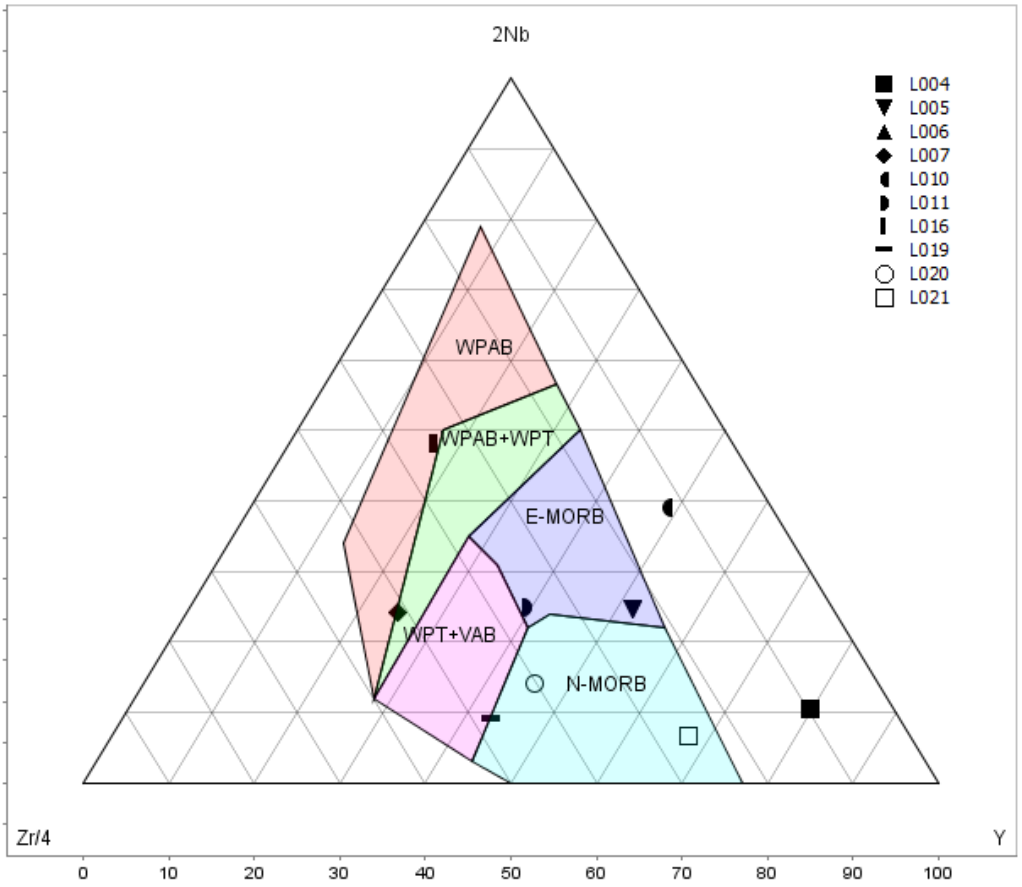


**Figure 4.5: Basalt Nb-Zr-Y discrimination diagram of Meschede (1986) with all 10 Latte amphibolite samples plotted. Sample L006 does not appear due to Nb levels below detection.**

settings. On this diagram amphibolite samples display a dominant arc-related tectonic setting as 7 of 9 samples plot within the arc series on the Y - La side. Sample L004 plots in the arc tholeiite field, and samples L005, L007, L011, L019, and L020 all plot within the arc calc-alkaline field. Samples L010 and L016 plot within the orogenic continental domain. Sample L021 plots within the arc tholeiite domain.

## 4.2 Geochemistry of Dikes from Latte and the Coffee Property

Three dikes were sampled from the Latte zone, a single fresh andesitic dike selected from the Supremo zone, and a single altered and mineralized dacite dike selected from the Kona zone. These samples were combined with whole-rock geochemical data collected by Kaminak during the 2010 field season, and the combined batch is used to characterize the dike suite. Samples are listed in Table 4.2. Total samples span the Latte, Supremo,

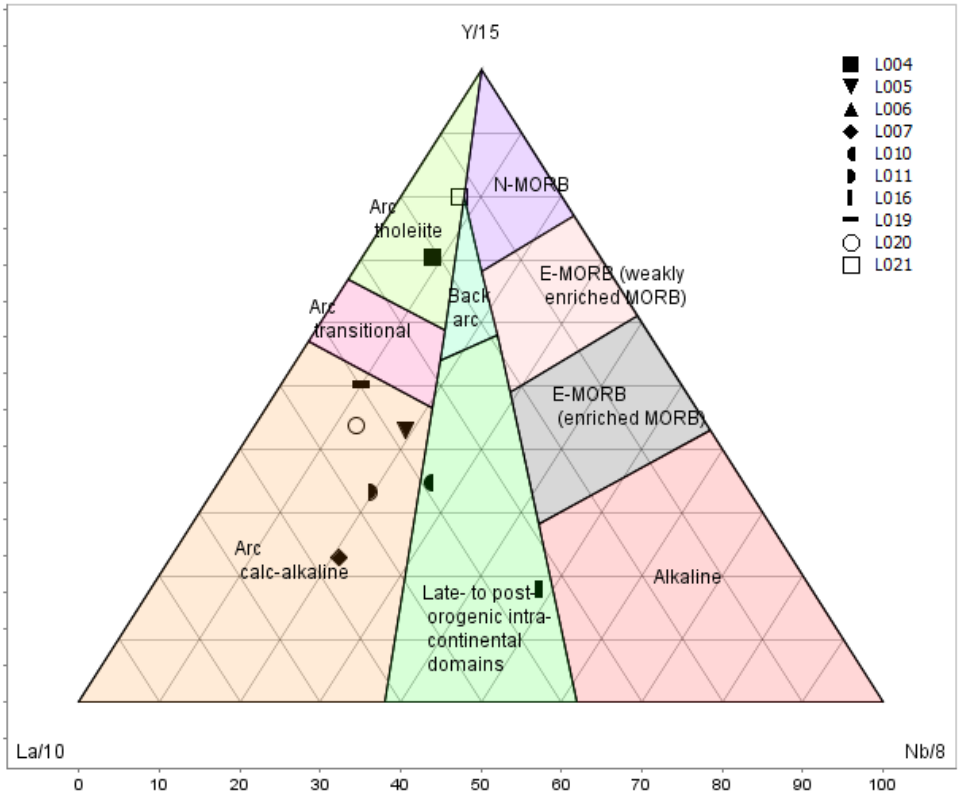


**Figure 4.6: Tectonic classification of mafic igneous rocks diagram of Cabanis and Lecolle (1989). All 10 Latte amphibolite samples are plotted. Sample L006 does not appear due to Nb levels below detection.**

and Kona zones on the Coffee property, with n = 18. Representative sample photos of each sample type are displayed in Figures 4.7 & 4.8. The goal of this geochemical study is to determine if the dikes across the Coffee Property are genetically and geochemically related to the Coffee granite.

Following the previous investigation of amphibolites all dike samples excluding samples of the Coffee granite were plotted on the volcanic rock classification diagram of Winchester and Floyd (1977) (Figure 4.9). All mafic-intermediate dikes plot roughly within the same region of the diagram. The Supremo and Latte andesites plot within the andesite field (L017, L022, I308668), while the single Kona andesite (I308672) plots slightly above the rhyodacite/dacite field. Two of the Supremo intermediate dikes (59446, 59449) and the single diorite sample from Supremo (59551) plot within the andesite/basalt field with slightly lower $Zr/TiO_2$ ratios than those of the andesitic dikes.

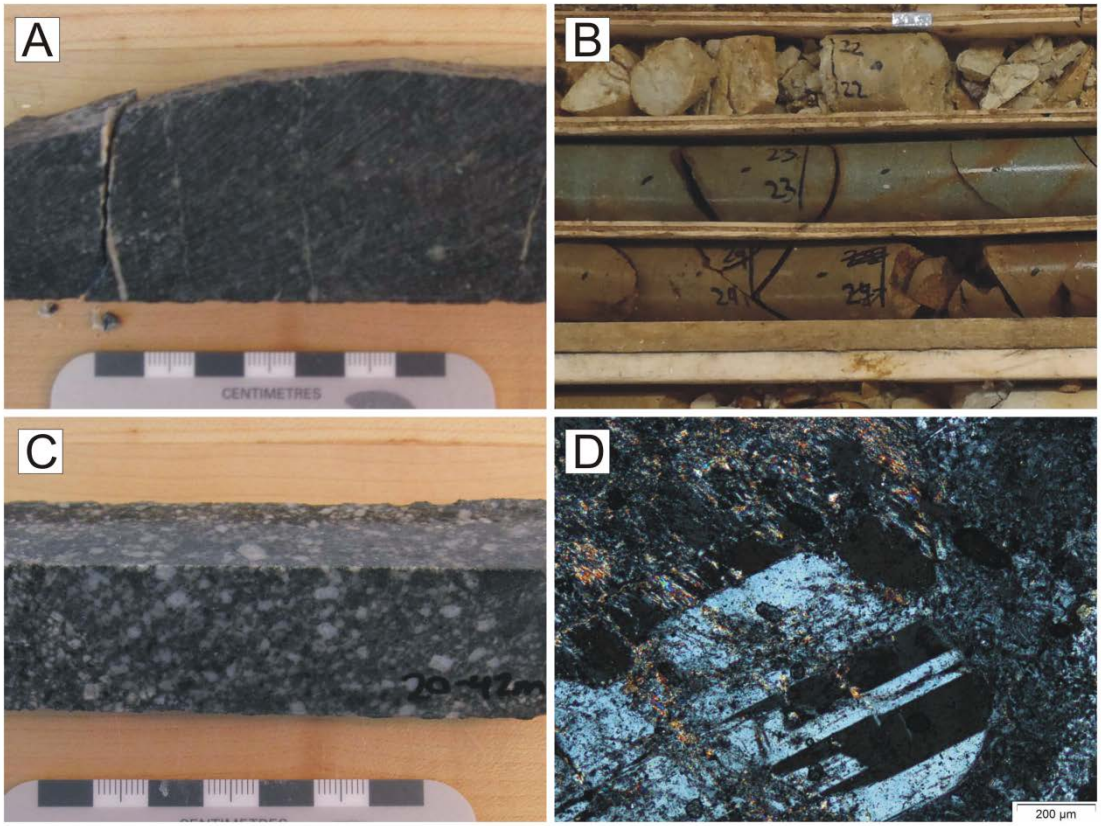


**Figure 4.7: Example photographs of andesite dike samples: A) hand sample photograph of 99-84.5; B) Core box photograph of sample 51-23, selected for geochemical analysis in 2010; C) hand sample photograph of 20-42; D) photomicrograph of feldspar phenocryst in sample 20-42, XPL.**

A single Supremo intermediate dike plots alone in the sub alkaline basalt field while another plots directly beside the fresh Supremo andesites. Sample L001, a Latte dacite dike, plots alone in the rhyolite field while the second Latte dacite plots in the rhyodacite/dacite field. Both Kona dacite dikes plot in the trachyte/andesite field.

Dike samples were plotted on the total alkali silica (TAS) diagram of Le Maitre et al. (1989) in order to refine classification (Figure 4.10). Supremo andesite dikes plot in a tight cluster along with the single Kona andesite and one Supremo intermediate. All plot within the andesite field with the exception of sample L022, which has a $SiO_2$ content that places it in the dacite field (64 %). Two of the Supremo zone intermediate dikes plot within the basaltic andesite field and one within the andesite field. The last intermediate dike, sample 59353, plots in association with the cluster of andesite dikes from Supremo and Kona in the upper portion of the andesite field. The single Latte andesite plots within

**Table 4.2: Sample IDs and locations for all dikes used in this study. Samples with a LXXX designation were collected by the author, all other data was collected by Kaminak in the 2010 field season. N/A refers to grab samples.**

| Sample ID | Zone | Unit | Drill hole | Depth (m) | Au (g/t) |
|---|---|---|---|---|---|
| L001 | Latte | Dacite | CFD0006 | 80 | 0.234 |
| L002 | Latte | Dacite | CFD0007 | 66 | 1.1 |
| L017 | Latte | Andesite | CFD0099 | 84.5 | - |
| L023 | Kona | Dacite | CFD0053 | 40 | 0.189 |
| I308672 | Kona | Andesite | CFD0051 | 23 | - |
| I308673 | Kona | Dacite | CFD0051 | 16 | - |
| L022 | Supremo | Andesite | CFD0020 | 42 | - |
| I308668 | Supremo | Andesite | CFD0020 | 45 | - |
| 400421 | Supremo | Intermediate | N/A | N/A | - |
| 59353 | Supremo | Intermediate | N/A | N/A | - |
| 59446 | Supremo | Intermediate | N/A | N/A | - |
| 59449 | Supremo | Intermediate | N/A | N/A | - |
| 59551 | Supremo | Diorite | N/A | N/A | - |
| I308657 | Kona | Granite | CFD0046 | 71 | - |
| I308658 | Kona | Granite | CFD0046 | 92 | - |
| 400378 | Kona | Granite | N/A | N/A | - |
| 78816B | Kona | Granite | N/A | N/A | - |
| 78816A | Kona | Granite | N/A | N/A | - |

the basaltic andesite compositional field, just below the join with the basaltic trachyandesite field. The sample of Supremo diorite plots alone in the basaltic trachyandesite field, with near identical total alkali levels as those in the Supremo andesites but with an approximately 10% lower silica content. Both Kona dacite samples plot within the dacite field. The Latte dacite samples plot off the right margin (80% $SiO_2$ content limit) of the diagram, and show an average of 3.00 % total alkali content.

All 13 dike samples were plotted on a primordial mantle normalized REE spider plot using the element order and normalizing values of Sun and McDonough (1989) (Figure 4.11). A smooth concave-up curve is demonstrated from LREE to HREE. The dikes therefore follow a very similar depletion pattern. Intermediate sample 59446 from Supremo is an outlier with depletion in La, Ce, and Pr relative to the entire dike suite. Figure 4.12 further refines the data by isolating mafic-intermediate dikes from the dacite samples. On A, all mafic dikes display similar enrichment in La and Ce, but diverge at Pr, with one set of samples clearly becoming more depleted in the REEs relative to the other, stabilizing at Eu and continuing to the right of Eu in two distinct

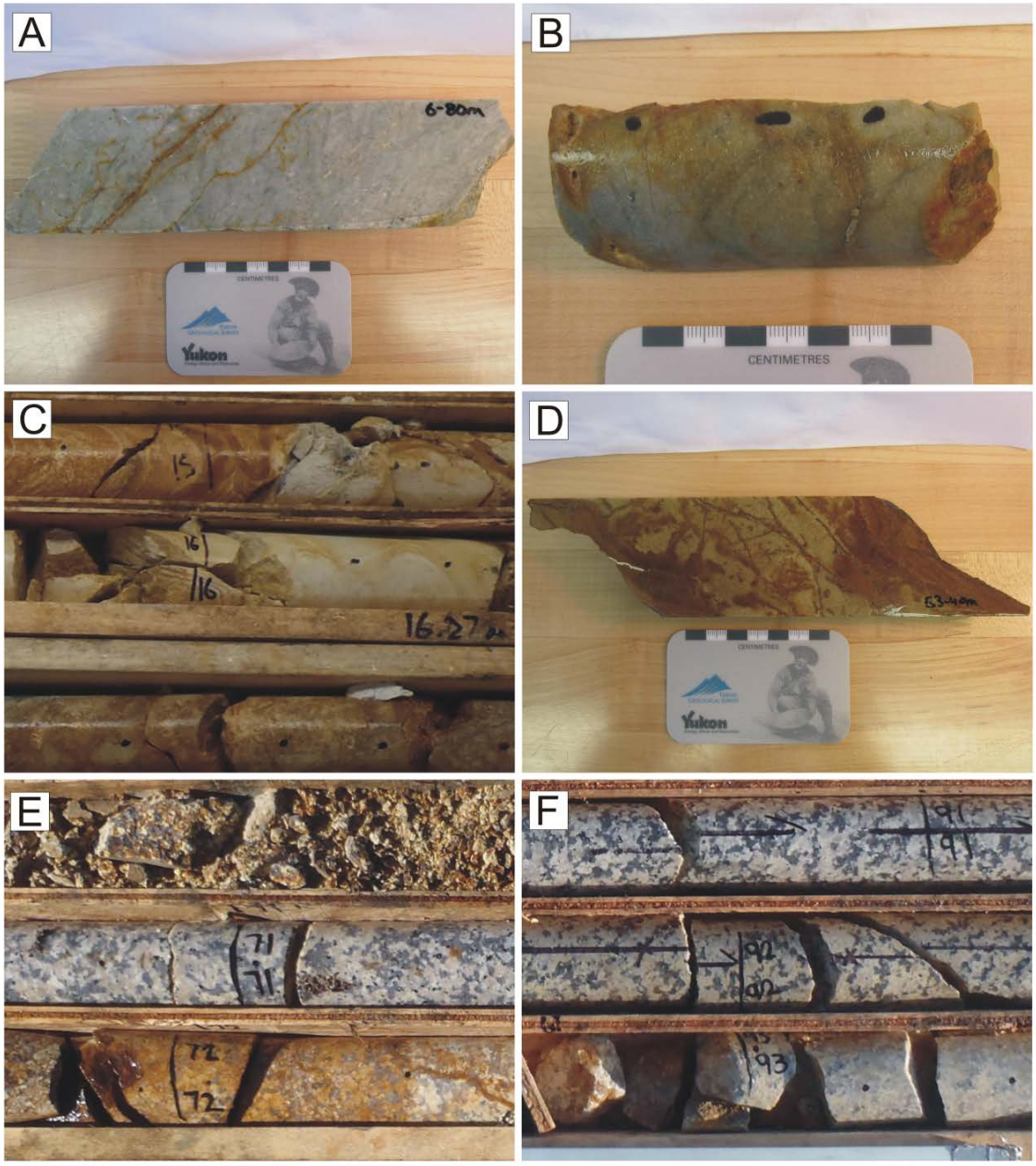


**Figure 4.8: Example photographs of dacite dike and granite samples: A) 6-80, weakly mineralized Latte dacite, B) 7-66, mineralized Latte dacite, C) CFD0051 – 16m, Kona dacite analysed in 2010, D) 53-40, mineralized Kona dacite, E) CFD0046-71m, fresh Coffee Creek granite from Kona, F) CFD0046-92, fresh Coffee Creek granite from Kona.**

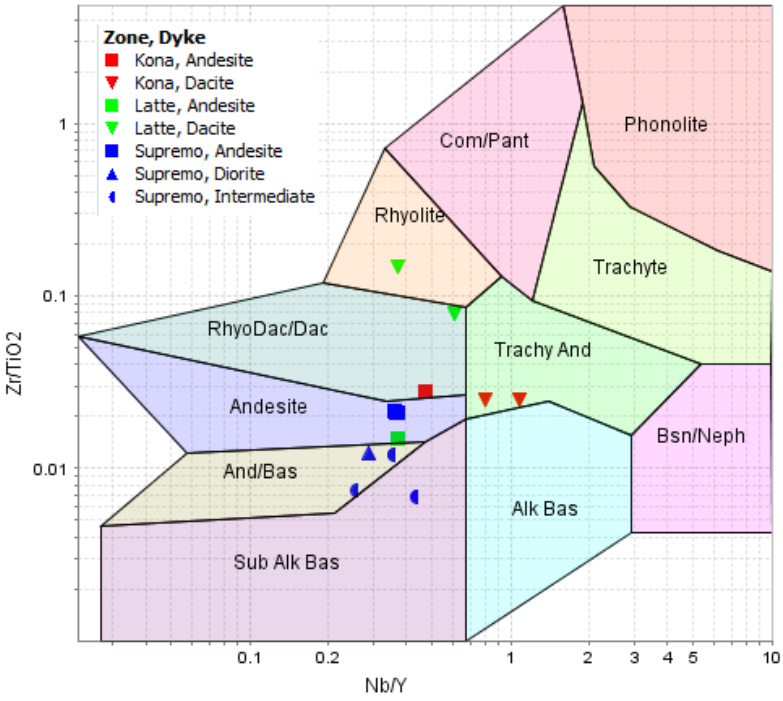


**Figure 4.9: All Coffee Property dikes plotted on the volcanic rock classification diagram of Winchester and Floyd (1977). Samples from Kona are in red, Latte in green, and Supremo in blue. Each dike type is prescribed a corresponding shape**

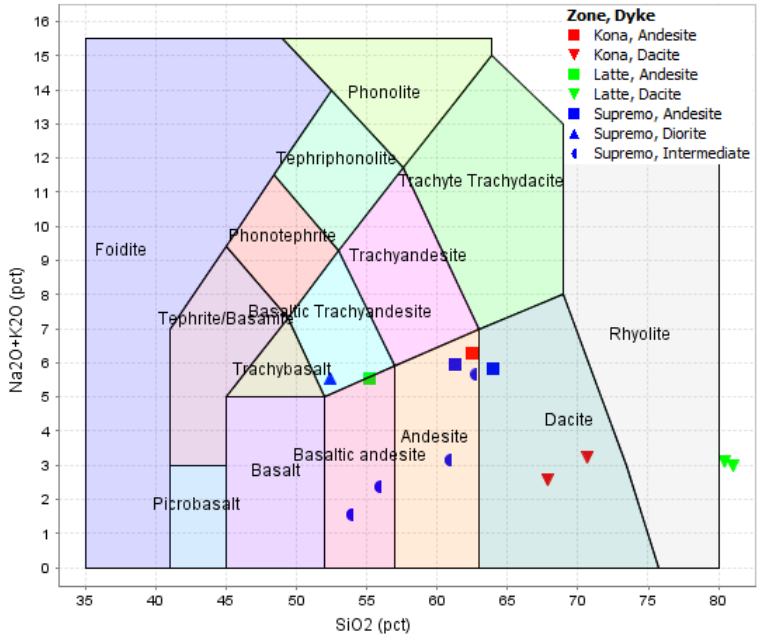


**Figure 4.10: All Coffee Property dikes plotted on the Total Alkali Silica (TAS) diagram of Le Maitre et al. (1989). Samples from Kona are in red, Latte in green, and Supremo in blue. Each dike type is prescribed a corresponding shape.**

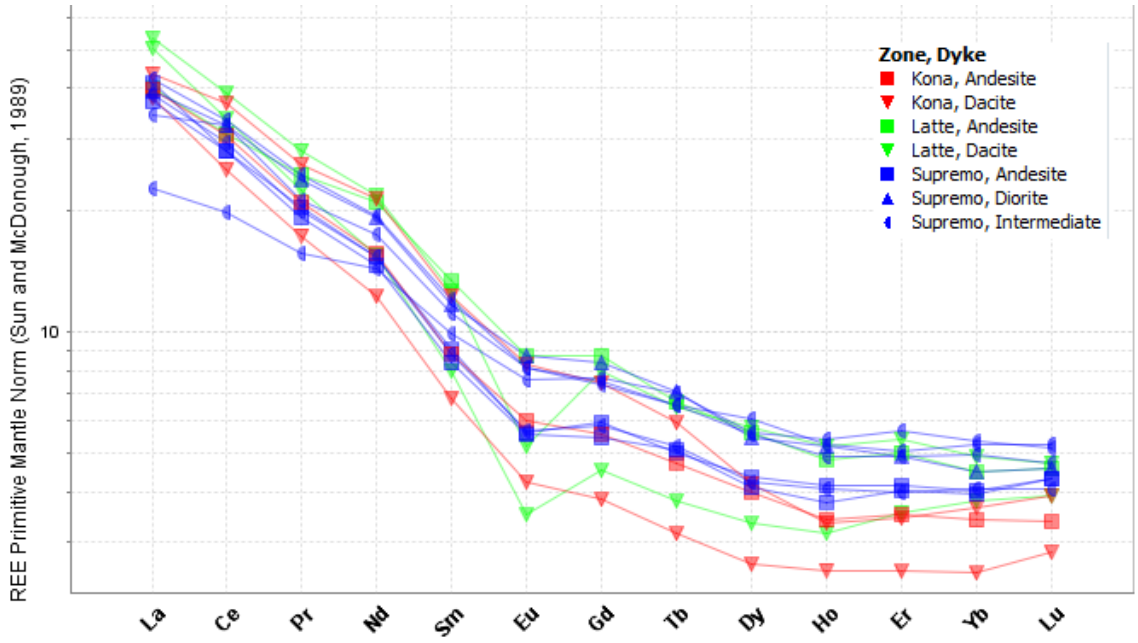


**Figure 4.11: Primordial mantle normalized (Sun and McDonough, 1989) REE spider plot for all 13 Coffee property dikes (Supremo, Kona, Latte).**

geochemical compositions. The enriched sample group contains three Supremo intermediate dike samples (400421, 59449, and 59446), the Supremo diorite (59551), and the Latte andesite (L017). The group of samples depleted in HREE relative to the first set includes the sample of Kona andesite (I308672), two Supremo andesites (L022, I308668), and one Supremo intermediate dike (59353). On Figure 4.12 B) the dacite dikes show similar patterns. Also, a similar divergence in samples is noted, interestingly with samples from the same zone (Kona, Latte) displaying the diverging depletion patterns. A strong negative Eu anomaly is present in both Latte dacites.

Samples of the Coffee granite were plotted on the TAS diagram of Wilson (1989) (Figure 4.13). This diagram is the intrusive equivalent of Figure 4.10. Three samples of Coffee Creek granite from Kona granite appear within the plot area. Sample I308658 plots as granite, and samples I308657 and 78816A plot as alkali granite. Sample 400378 plots on the extreme right edge of the plot, and sample 78816B plots off of the grid. Both of these samples are mineralized and have low total alkalis (sample 400378: 4.68% $Na_2O+K_2O$, 75.53% $SiO_2$; sample 78816: 0.77% $Na_2O+K_2O$, 93.71% $SiO_2$).

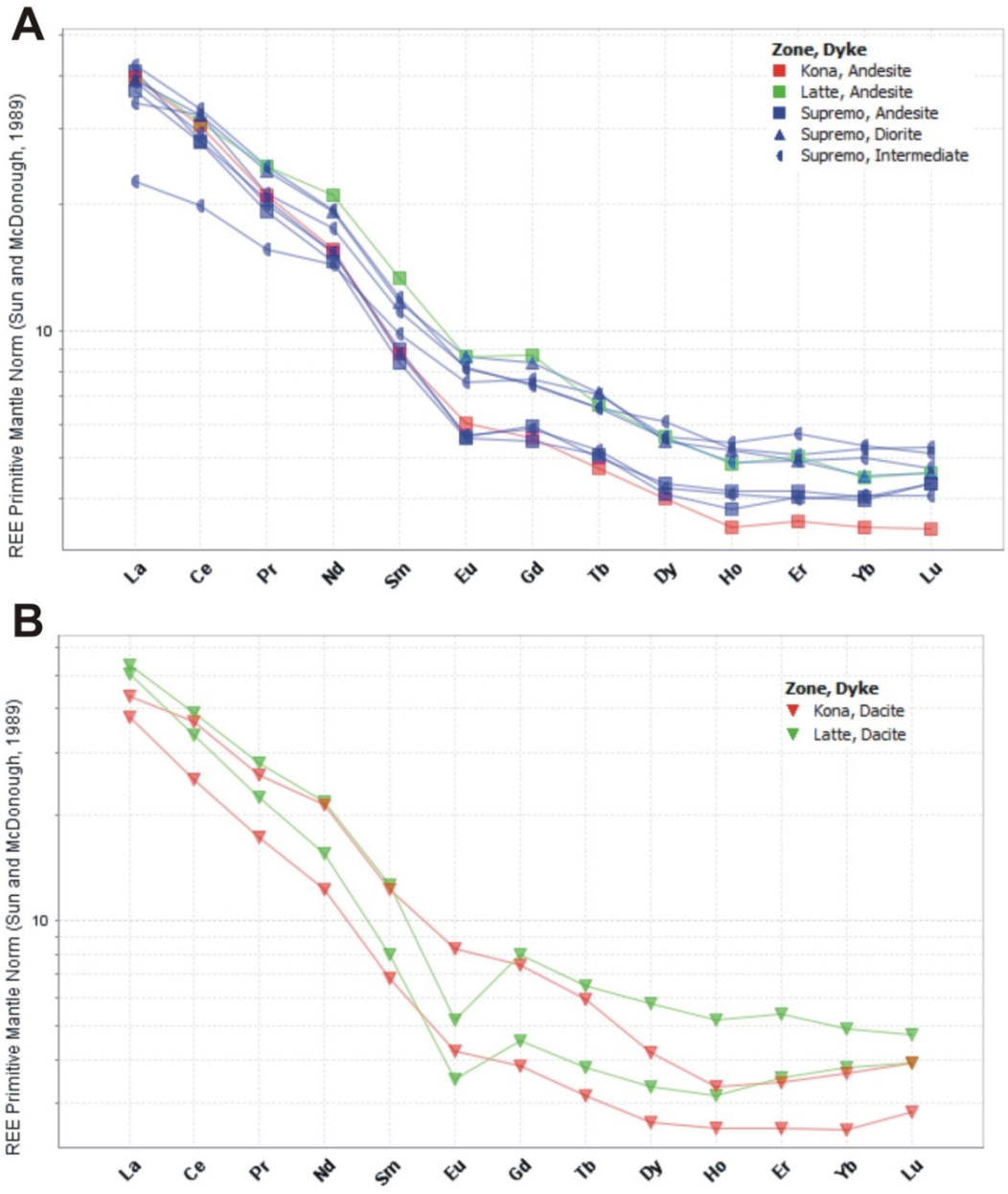


**Figure 4.12: Primordial mantle normalized (Sun and McDonough, 1989) REE spider plots from Figure 4.11 displaying A) only dikes of andesitic, dioritic, and intermediate compositions; and B) dikes of dacitic compositions Note that two geochemically distinct groups can be seen towards the right of the diagram. The Latte dacites display negative Eu anomalies.**

In order to determine if a genetic relationship exists between dikes at the Coffee property and the Coffee granite, selected samples were plotted on immobile element ratio bivariate plots. As the elements used in these plots are considered immobile, they shed light on the initial magmatic source of each intrusive suite (Figure 4.14). The dikes plot

separately from the granite samples, with the exception of the two Latte dacite dikes which group roughly with the granitic samples. All dikes plot with low Nb/Ti ratios with the exception the same Latte dacites. The granite samples and Latte dacites have higher Nb/Ti ratios and plot together with two samples considered outliers (78816A, 78816B) which display even higher Nb/Ti.

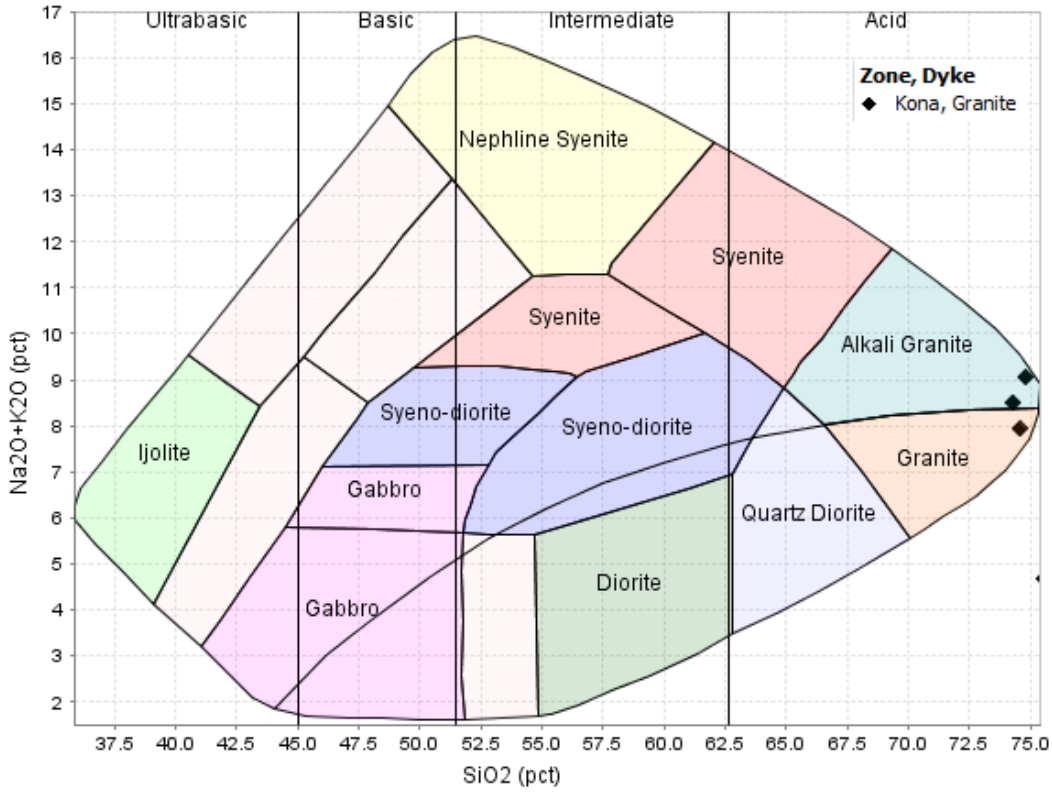


**Figure 4.13: Kona granite samples plotted on the intrusive plutonic Total Alkali Silica (TAS) diagram of Cox et al. (1979), adapted by Wilson (1989). Three samples plot within the discrimination fields, while two samples are not visible.**

Five separations of dikes are clearly visible in this plot (Figure 4.15). The Kona andesite and dacite samples plot together with a Ti/Zr ratio of near 40, and Nb/Ti slightly below .002. The Supremo andesite samples and one intermediate sample (59353) plot with Ti/Zr of approximately 47 and slightly lower Nb/Ti. The Latte andesite sample (L017) plots separately but along the same negative trend. The Supremo diorite and a single intermediate dike sample (59449) plot tightly with a Ti/Zr ratio of 82.5, and a lower Nb/Ti of .0007. The two Supremo intermediate dikes (59446, 400421) plot at approximately the same Nb/Ti ratio (.00065) but different Ti/Zr. Sample 59446 exhibits a

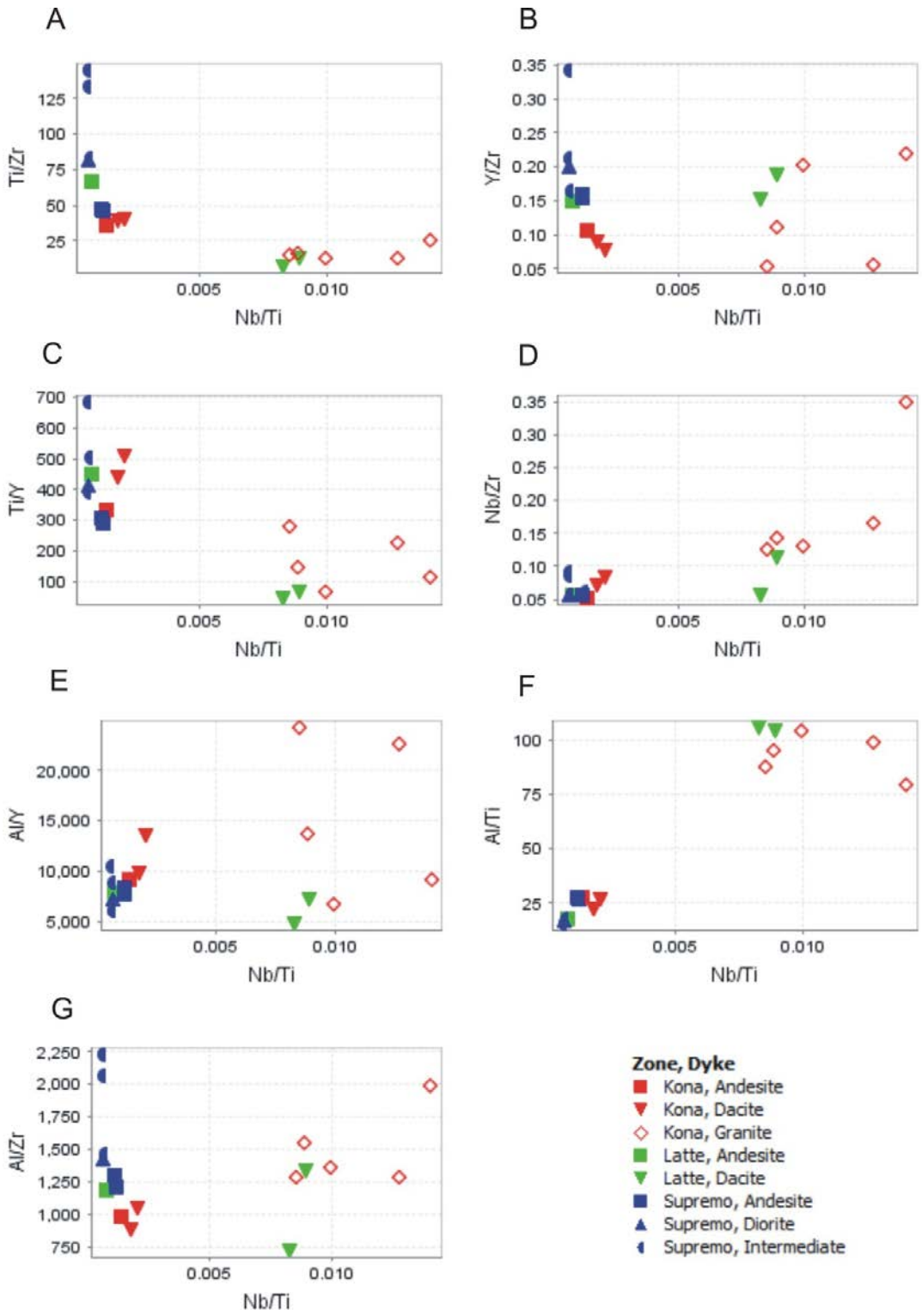


**Figure 4.14: Immobile element ratio plots for dike and granite samples from the Latte, Supremo, and Kona zones. All ratios are plotted against Nb/Ti on the X axis, vs: A) Ti/Zr, B) Y/Zr, C) Ti/Y, D) Nb/Zr, E) Al/Y, F) Al/Ti, G) Al/Zr.**

Ti/Zr ratio of about 133, and sample 400421 has a Ti/Zr ratio of 145.

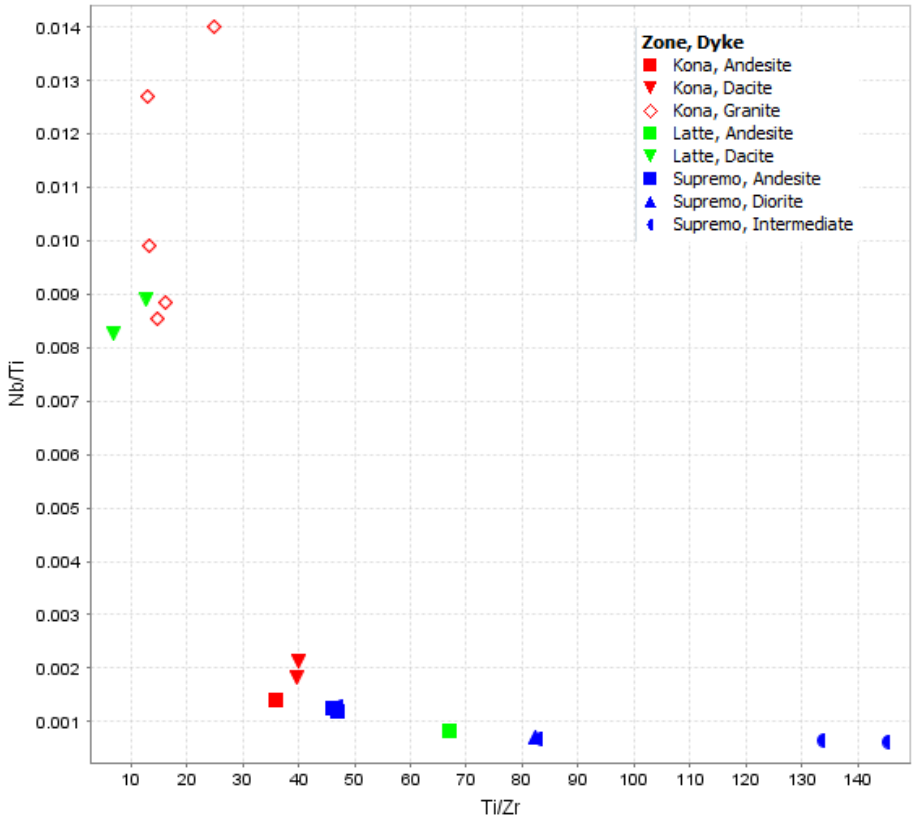


**Figure 4.15: Immobile element ratio plot of Ti/Zr vs. Nb/Ti (modified from Figure 4.15), A) for dike and granite samples from the Latte, Supremo, and Kona zones. Each suite of dikes plots with differing Ti/Zr ratios.**

## 4.3 Geochemistry of Ultramafic Rocks in the Latte Zone

Ultramafic rocks in the Latte zone are altered to the point where rock protolith is completely unrecognizable. Plots of $SiO_2$ vs. Mg # (Mg/(Mg+Fe)) and $SiO_2$ vs. Cr and Ni are presented here in an attempt to genetically link ultramafic samples. Figure 4.16 plots a $SiO_2$ vs. Mg # (Mg/(Mg+Fe)) binary which shows good correlation among samples L013, L014, and L018. All three plot with near-identical values. Samples L008, L009, and L012 plot nearby with higher $SiO_2$ content, while sample L003 plots alone as an outlier with very low $SiO_2$ content, but similar Mg #. In Figure 4.17, a $SiO_2$ vs. Cr binary shows that chrome content within the samples varies. Samples L012, L013, L014, and L018 plot with over 2500 ppm Cr. Samples L008 and L009 have 1500 ppm Cr, and L003

plots as an outlier due to high carbonate content. Figure 4.18 plots a $SiO_2$ vs. Ni binary and shows a similar pattern. Samples L014 and L018 both plot tightly together with > 2000 ppm Ni. Sample L003 remains an outlier, while samples L009, L012, and L013 all plot with 1500 ppm Ni. L008 is notably Ni-poor relative to the other ultramafic samples.

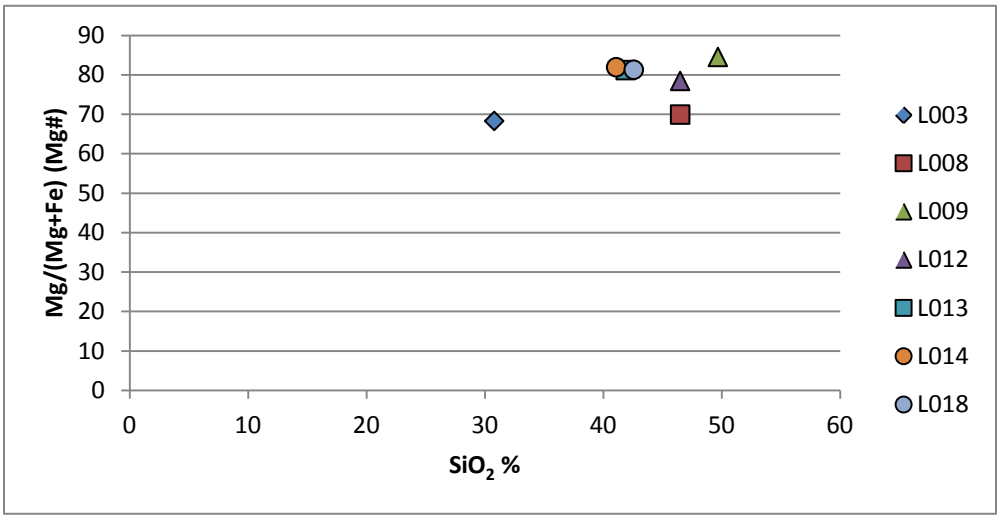


**Figure 4.16: Plot of $SiO_2$% vs. Mg # for ultramafic rocks from the Latte zone.**

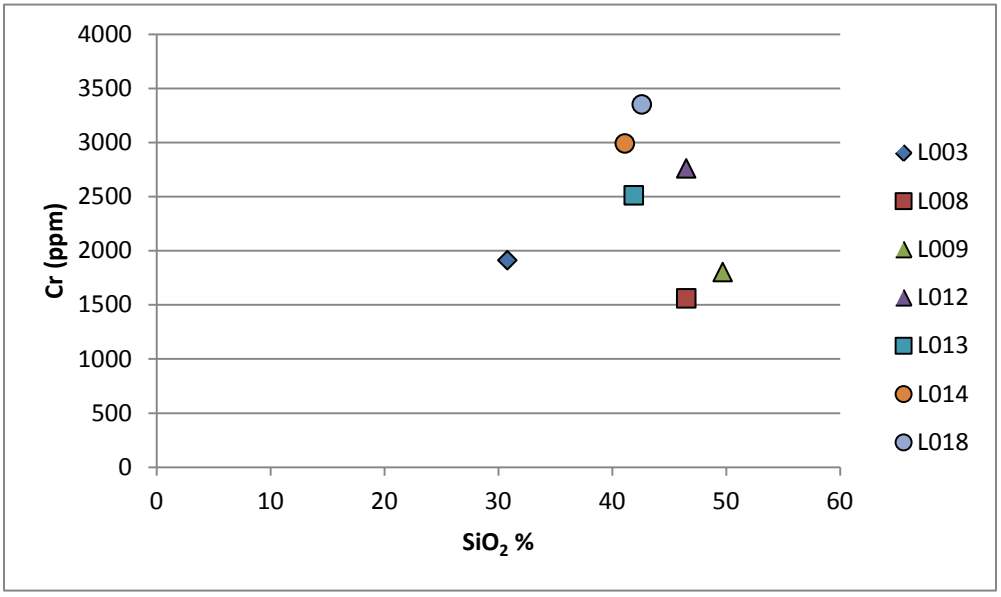


**Figure 4.17: Plot of $SiO_2$% vs. Cr (ppm) for ultramafic rocks from the Latte zone.**

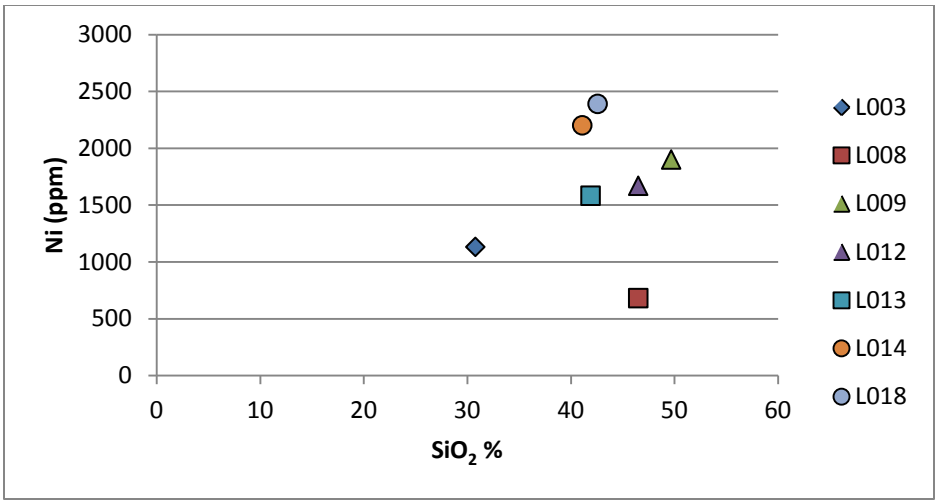


**Figure 4.18: Plot of $SiO_2$% vs. Ni (ppm) for ultramafic rocks from the Latte zone**

An immobile element binary plot of Y/Nb vs. Zr/Nb for Latte ultramafics demonstrates similar separation (Figure 4.19). Five samples are plotted with the omission of sample L012 (Nb below detection) and sample L013 (Zr below detection). Samples L014 and L018 remain grouped near the origin with Zr/Nb < 5. Samples L003 and L008

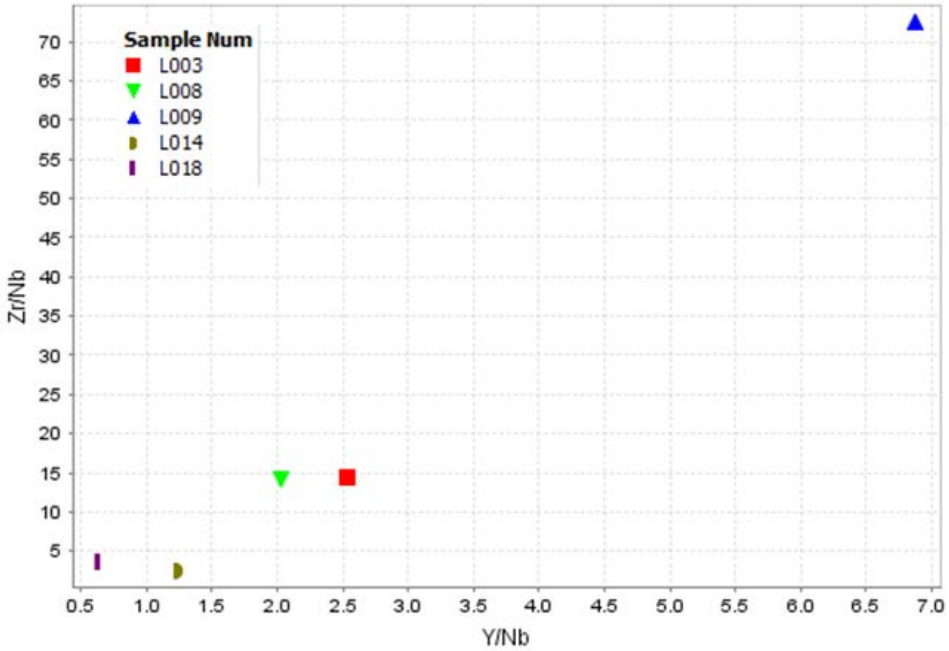


**Figure 4.19: Plot of Y/Nb vs. Zr/Nb for ultramafic samples from the Latte zone. Three groupings are visible, with samples L014 and L018 plotting near the origin, L003 and L008 plotting together with higher Y/Nb and Zr/Nb, and sample L009 plotting opposite the origin.**

plot with higher Y/Nb (> 2.0) and Zr/Nb of 15. Sample L009 has an extreme Zr/Nb ratio almost 5 times greater than others, and a Y/Nb ratio approximately 2.5 times greater than the same closest grouping (L003, L008).

## 4.4 EPMA Mineral Chemistry of Latte Host Rocks

Detailed mineral chemistry has been collected on biotite and amphibole grains from two drill holes representing Latte west (CFD0082) and Latte east (CFD0114). These provide Latte-wide amphibole and biotite mineral chemistry databases, which shed light on the metamorphic and hydrothermal conditions. All mineral grains examined are selected from unmineralized intervals of drill core. Complete probe data is listed in Appendix C.

### *Biotite Mineral Chemistry*

Nine samples of unmineralized, biotite-bearing rocks from CFD0082 (Latte west) and CFD0114 (Latte east) were selected for analysis. Samples consisted of five samples of quartz-biotite schist, two biotite-rich amphibolites, and two samples of Lower Latte amphibolite and metagabbro. All samples were plotted on the "ideal biotite plane" diagram of Guidotti (1984) (Figure 4.20). The binary plots aluminium in the octahedral site along the horizontal axis against Mg/(Fe + Mg) along the vertical axis. The biotite-phlogopite division at Mg:Fe = 2:1 is from Deer et al., (1966). Biotite end-members are also shown for clarity and context.

Four main distinctions are evident. A cluster of samples occurs directly on the biotite-phlogopite tie line. All three of these samples are typical biotite-schist samples, with 2 samples from CFD0114, and one sample from CFD0082 (samples 82-161.2, 114-44, 114-144) (Figure 4.20). Two samples from the same drill hole, 114-295 and 114-296, plot in the phlogopite field with Mg/(Fe + Mg) ratios of > 0.7. These samples contain a minimal biotite component and are a coarse-grained and strained metagabbro (114-295) and a fine grained amphibolite (114-296) in close proximity to each other (Figure 4.21). A third, more iron-rich cluster occurs within the biotite field, with quartz-biotite schist with abundant carbonate alteration (114-179) and an amphibolite with a 15% green

biotite component (82-170.6). Sample 114-296 is 95% amphibole and contains trace biotite. Sample 82-223 is the most iron-rich of all biotite grains analysed. This is a sample of the Supremo augen orthogneiss from the bottom of CFD0082.

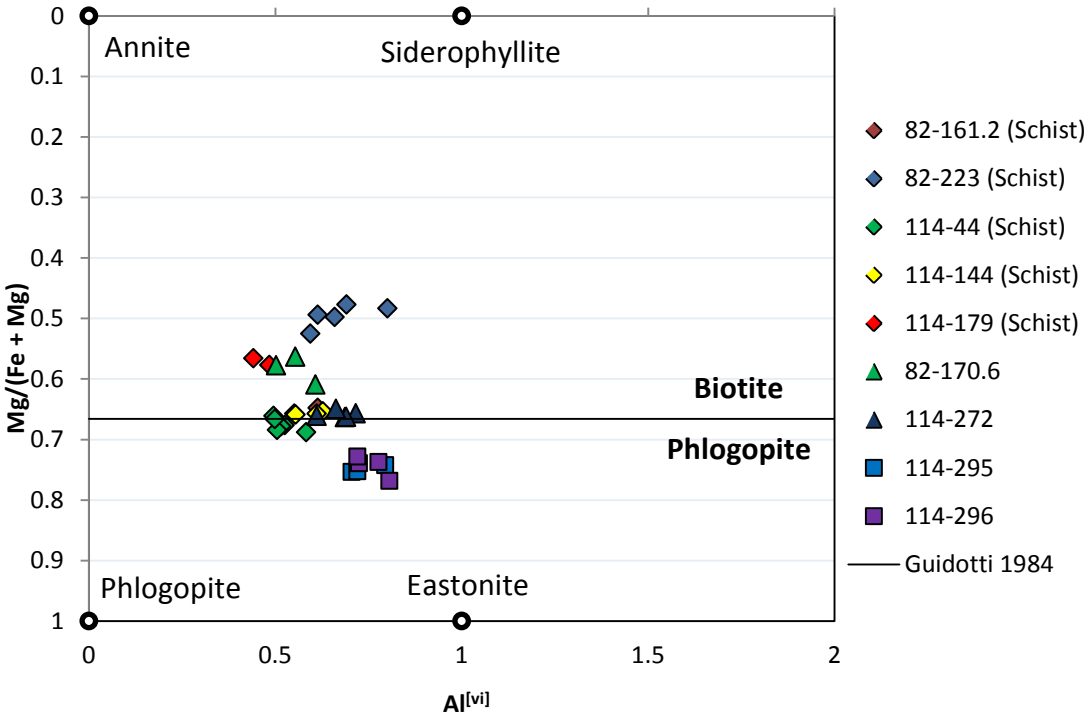


**Figure 4.20: "Ideal biotite plane" diagram of Guidotti (1984). The biotite-phlogopite field boundary is based off an Mg:Fe ratio of 2:1 from Deer et al., (1966).**

## *Amphibole Mineral Chemistry*

Four un-mineralized samples were selected for microprobe analysis of amphibole. Each sample analysed represents a different style of amphibole-bearing rock within the Latte zone. Sample 82-170.6 contains approximately 85% amphibole with 15% Fe-rich biotite, but occurs within an interval of varying biotite/amphibole concentrations. Sample 114-272 contains abundant phlogopitic biotite with a strong foliation defined by the biotite and amphibole. Samples 114-295 and 114-296 both contain >90% amphibole, with 114-295 displaying coarse amphibole crystals overprinted by retrogression and shear, while 114-296 is 95% amphibole with massive, weakly foliated texture.

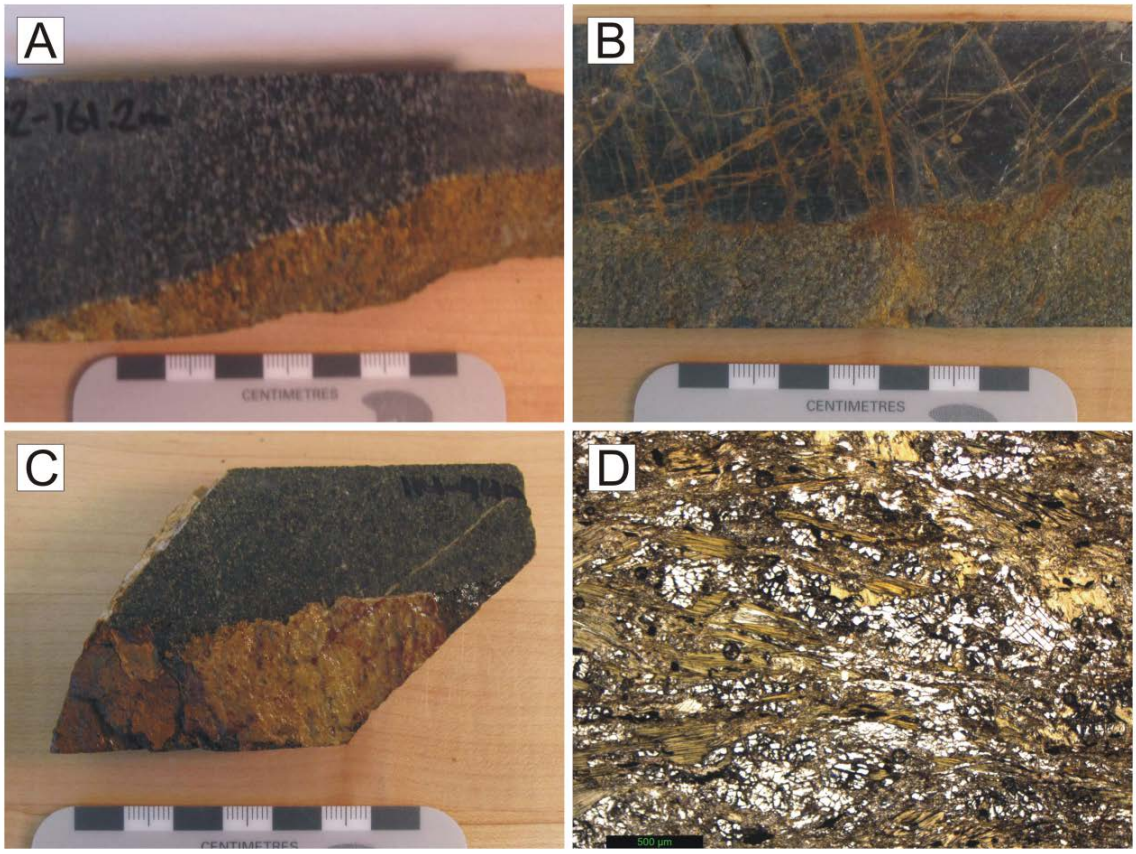


**Figure 4.21: Samples of qtz-bt schist analysed by microprobe in this study: A) Sample 82-161.2; B) Sample 114-114 upper portion of sample is a fine grained andesite dike, not analysed; C) Sample 114-44; D) Thin section image of 114-44, plane-polarized light.**

Analyses were plotted on Figure 4.22. This binary plots Al occupancy in the tetrahedral site vs. total alkalis (Na in the A-site + K), on the discrimination classification of Heitanen (1974). It shows increasing retrogression from top right to bottom left. Samples and analyses which plot along the actinolite-hornblende tie line represent metamorphic amphibole compositions. Decreasing Al is a result of subsequent hydrothermal retrogression. Samples 82-170.6 and 114-272 contain amphibole which plots as hornblende. Al depletion is documented on amphibole grain margins. Sample 114-272 displays lower alkali content than 82-170.6. Samples 114-295 and 114-296 show more pervasive retrogression to actinolite.

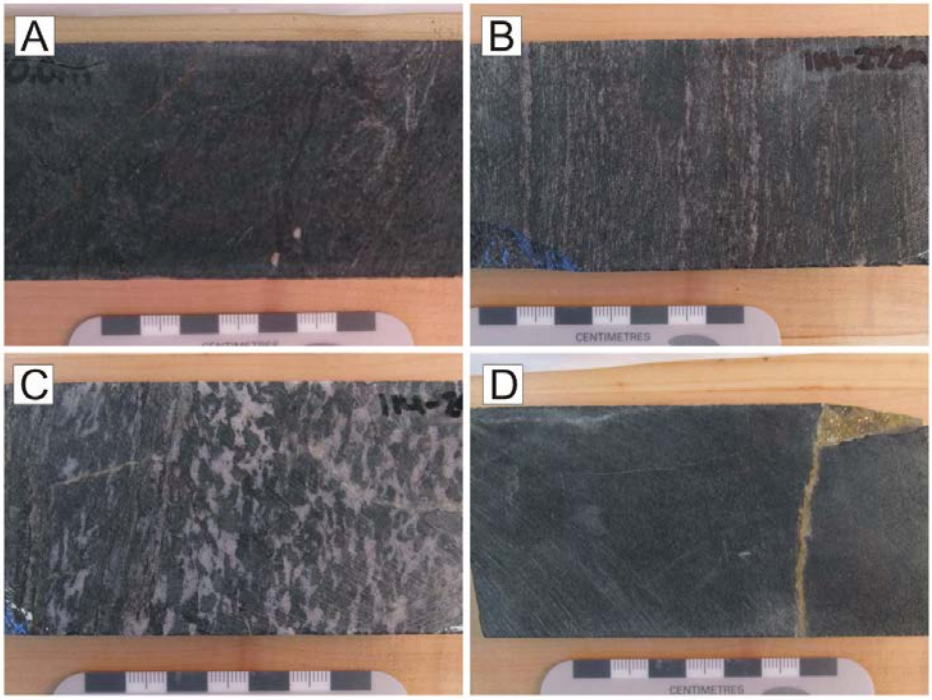


**Figure 4.22: Samples of amphibolite and metabasalt/metagabbro analysed by microprobe in this study: A) Sample 82-170.6; B) Sample 114-272; C) Sample 114-295; D) Sample 114-296.**

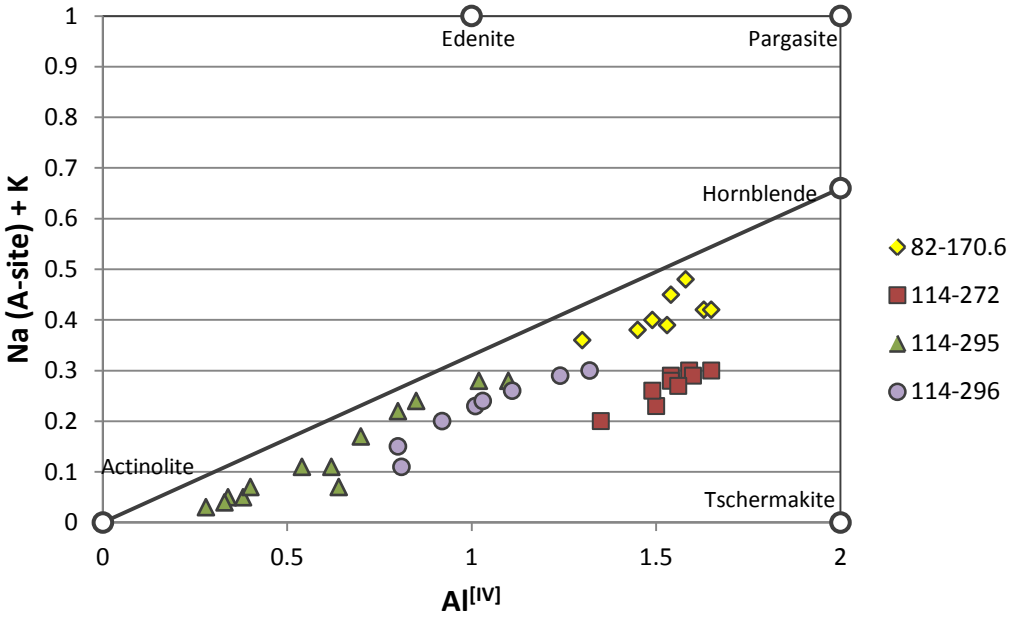


**Figure 4.23: Plot of tetrahedral site Al vs. Total Alkalis for amphibole grains from four samples from the Latte zone. Scatter of data points to the origin of the chart indicates retrogression from original metamorphic or igneous composition.**

Both samples have been grouped together in Figure 4.24 in order to show differences between metamorphic Al content and the retrogressive overprint. A clear trend is visible in both samples towards the origin with greater retrogression. Cores of amphibole preserve the initial composition of amphibole within sample 114-295 prior to pervasive retrogression (Figure 4.25). In sample 114-296, similar high Al core compositions are present; however amphibole composition at peak or near-peak metamorphic conditions is overprinted by retrogressive amphibole compositions lower in both tetrahedral Al and alkali content.

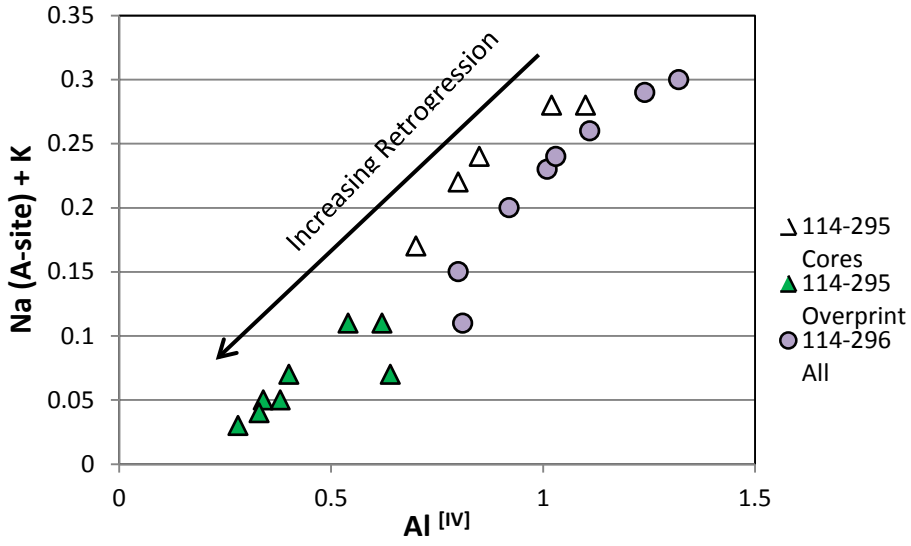


**Figure 4.24: Enlargement of Figure 4.23 emphasizing samples 114-295 and 114-296. Analyses which plot in the upper right of the chart represent peak metamorphic conditions.**

Amphibole analyses for each of the four samples were also plotted on the amphibole discrimination diagram of Leake et al. (1997) (Figure 4.26). This binary plots atomic Si content vs. $Mg/(Mg + Fe^{2+})$. Samples 82-170.6 and 114-272 both plot slightly left of the tschermakite - magnesiohornblende divide, with 114-272 containing a greater Mg content. Both samples display remarkably similar patterns reflecting weak retrogression. All analyses from 114-296 plot within the magnesiohornblende field, with $Mg/(Mg + Fe^{2+})$ ratios > 0.73. Analyses from 114-295 also plot within the magnesiohornblende field migrating right into the tremolite-actinolite fields due to retrogression. Five analyses from 114-295 plot within the actinolite field. The analyses in

the magnesiohornblende field correspond to metamorphic cores (lowest Si content, slightly lower Mg/(Mg + $Fe^{2+}$)) and the subsequent hydrothermal retrogression. This is highlighted in Figure 4.27, following the same nomenclature as Figure 4.26. Increase in retrogression causes an increase in the Ca content in the amphiboles.

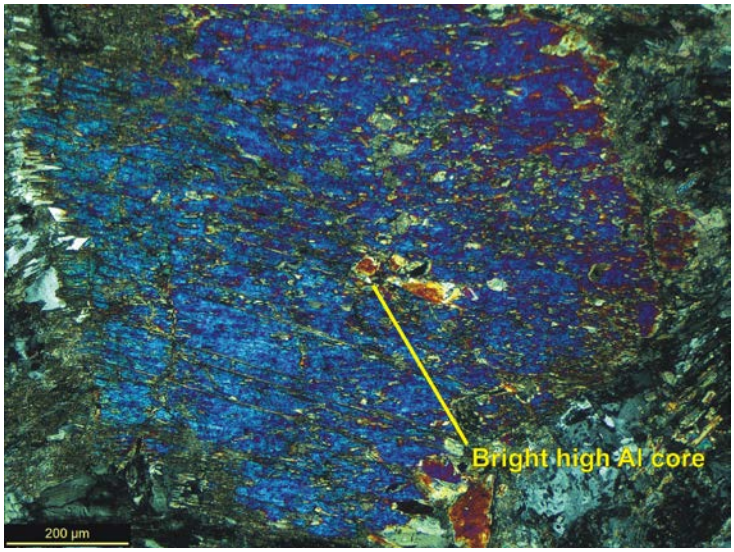


**Figure 4.25: Photomicrograph of coarse amphibole grain from sample 114-295. The bright orange spot within the central part of the grain is a preserved high Al core, indicative of initial metamorphic composition.**

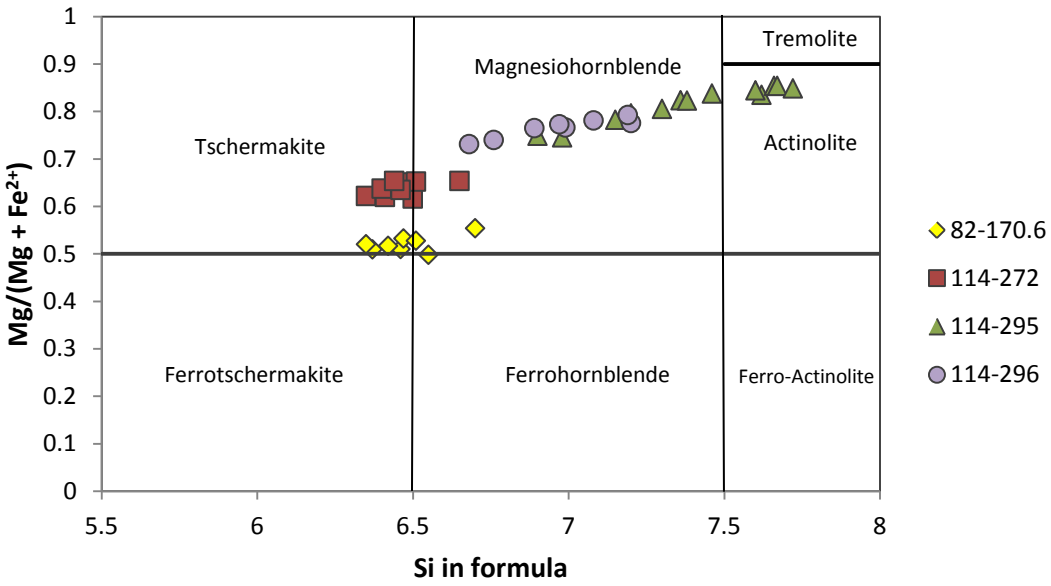


**Figure 4.26: Amphibole discrimination diagram of Leake et al. (1997).**

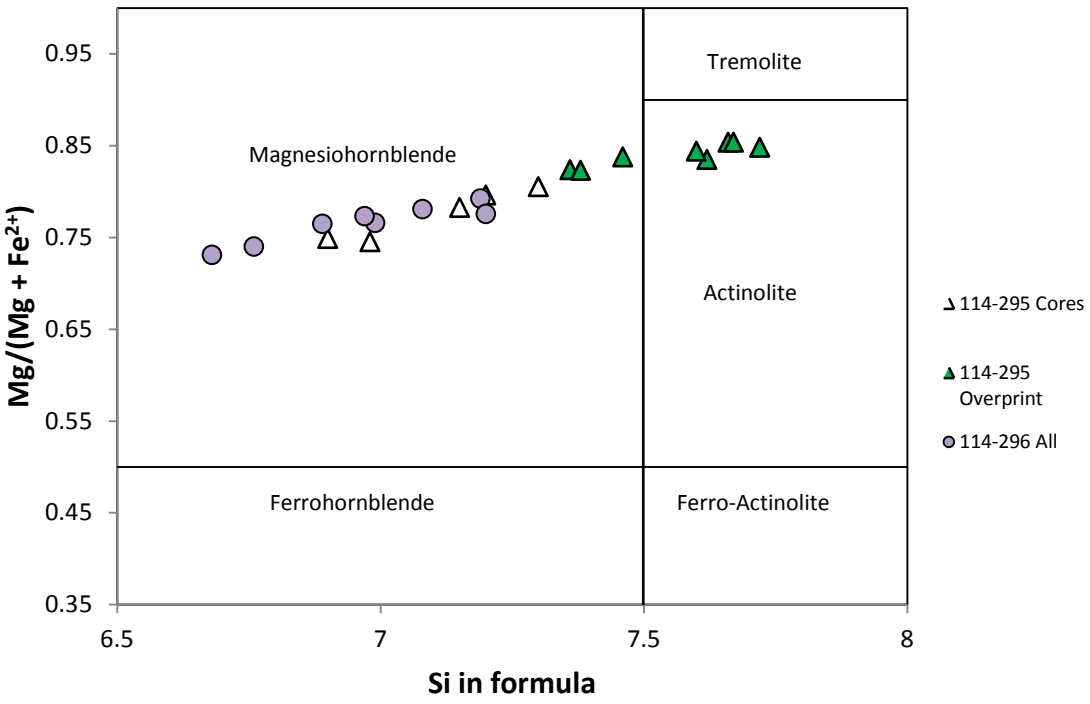


**Figure 4.27: Enlargement of amphibole discrimination diagram of Leake et al. (1997). Samples 114-295 and 114-296 are plotted together, with igneous cores analysed in 114-295 appearing as white triangles, with the subsequent retrogressive overprint to actinolite clear.**

Figure 4.28 plots Ti vs. Si. As Si increases in the grain, Ti decreases greatly. Samples (preserved at metamorphic grade) with weak retrogression have uniform Ti content, at approximately 0.045 - 0.05 for sample 82-170.6 and 0.03 - 0.035 for 114-272. The strong retrogressive overprint in samples 114-295 is clearly exemplified by the depletion of Ti within analyses of amphibole margins.

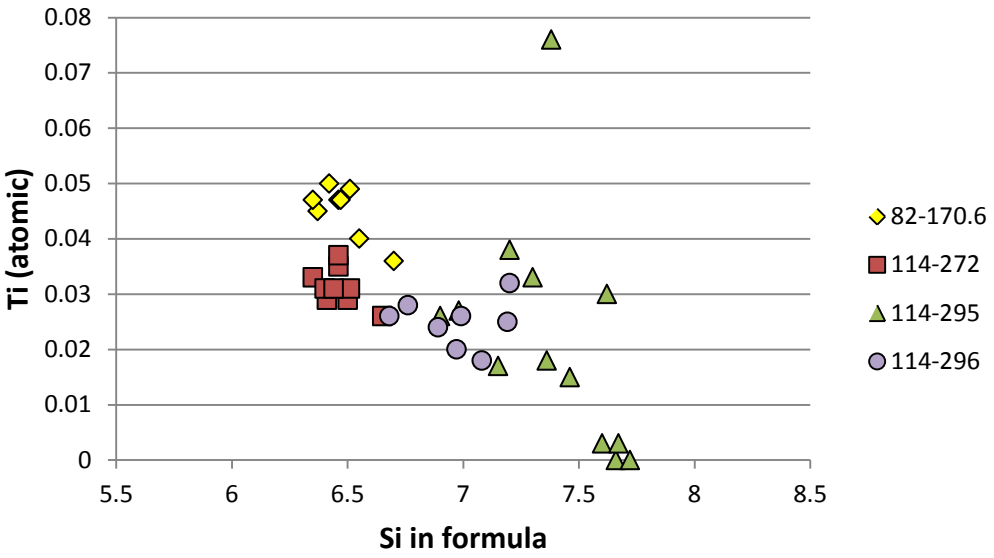


**Figure 4.28 Plot of Si vs. atomic Ti for amphibole grains from the Latte zone. Later retrogressive amphibole contains little-to-no Ti, while two different Ti concentrations are visible in amphibolites preserved at peak metamorphic grade (82-170.6 and 114-272).**

# Chapter 5

## 5 Mineralization at the Latte Gold Zone

The Latte zone represents the southwest apex of the "Golden Triangle", the intersection of the central three gold zones on the Coffee property. It consists of the Supremo zone at the north, Latte in the southwest, and the Double Double zone to the southeast. Mineralization within the Latte zone is hosted within moderately to steeply SSW dipping (65 to 85 degrees) stacked structures. It consists of structurally controlled disseminations through the Upper Latte panel and narrow higher grade structures in the Lower Latte panel. This chapter will discuss the structural control on the Latte gold zone, the styles of mineralization, vein assemblages, and alteration. Comments are made on the influence of lithology on mineralization.

### 5.1 Structural Control on Mineralization in the Latte Zone

Structural control on mineralization at Coffee is an extremely important component of the mineralizing system. Mineralization is controlled by a WNW to NW-trending dextral strike slip fault system comprising the Coffee Creek fault. This fault system consists of three regional-scale WNW-trending dextral strike slip faults or shear zones, in addition to multiple sets of dextral oblique-extensional, NW-trending splays (Figure 5.1). The Coffee Creek fault sets are considered to be a splay system off of the regional-scale Big Creek fault, located to the south east. In the immediate Coffee property area two large shear zones, the Coffee Creek fault and the Coffee Creek south fault, are parent to numerous horse tailing splays. A series of NE to NNE trending faults accommodating sinistral shear account for the mineralization at Supremo, Macchiato, and Kona.

Two dominant structural sets are observed to host mineralization. The Supremo zone is hosted within the Sulphur Creek orthogneiss in generally NNE-trending and steeply dipping brittle structures. In contrast, the Latte gold zone is hosted within schistose metasediments and mineralization occurs in moderately-to-steeply SSW-dipping, ESE-striking brittle-ductile structures. The Latte structures appear to splay off the first order NW-trending fault zones as seen in Figure 5.1. No shear fabrics or

observable high strain is visible in association with the steep, mineralized Latte structures.

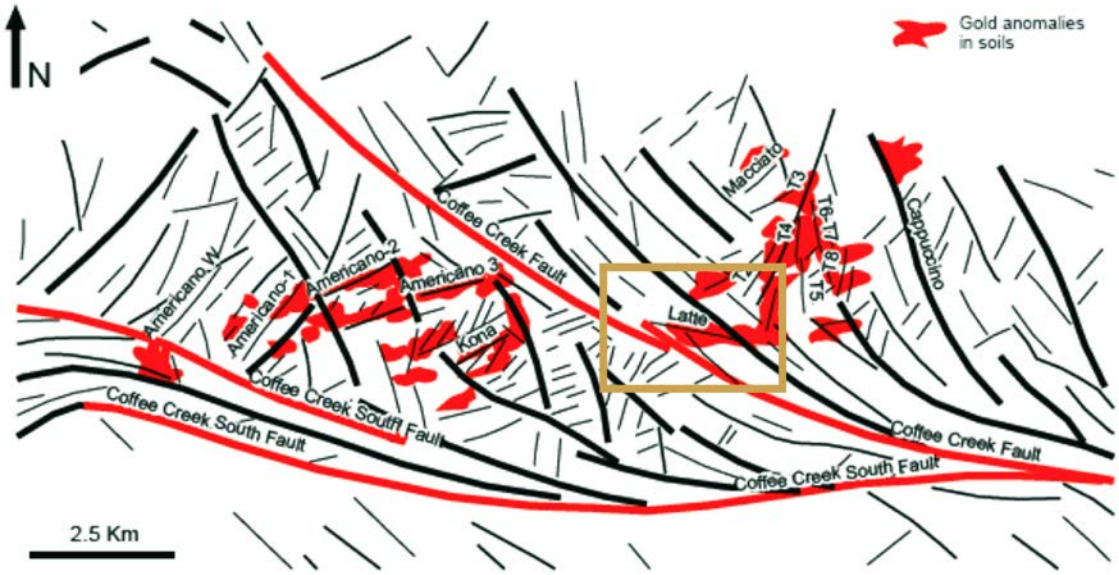


**Figure 5.1: Local Coffee Creek fault array. The Latte fault splay is highlighted within the gold box. Note it is a splay off a 1st order NW-trending fault, but not a regional shear zone (red). Modified after Sanchez et al., 2013.**

## *Latte Deposit Structure*

Gold mineralization at Latte is generally confined to a structural corridor up to 100 m wide, comprising numerous stacked structures. In the western portion of the Latte zone, broad panels of disseminated mineralization makes up the bulk of the deposit. This panel strikes ~100° and contains 5 or greater separate ore shoots which merge and separate along section. A second structure striking ~85° splays off of the main splay at approximately 583000mE and this dips near-vertically to the south. This structure continues along an 80-90° trend before entering the Connector zone, the intersection of NE and NNE striking structures of the Supremo zone with the mineralized structures of the Latte zone and Double-Double to the east. Total traceable length of the mineralized Latte structure reaches a strike length of 1550 metres.

The gold mineralization is exposed at surface and all structures remain open at depth (Figure 5.2). Step-back deep drilling during the 2011 season intersected mineralization at depths of up to 450 metres-below-surface in CFD0164 along the same structural trend.


**Figure 5.2: Surface expression of Latte mineralization. Looking east. A mineralized corridor dips SSW. Geotool for scale.**

The Latte zone was initially identified as an east-west trend of gold-in-soil anomalies corresponding to the surface expression of the mineralized structures (Figure 5.3). Where the soil anomaly dropped off to the west, step out drilling indicated the continuation of the structure with no significant surface expression for an additional 650 metres as of 2013.

A cross section of the bulk lode gold mineralization in Latte west is provided in Figure 5.4. Mineralization is intersected near-surface and as deep as 356 metres down-hole in CFD0171 (~335 m below surface), the furthest step-back drill hole on the section. Approximately 3 distinct ore shoots are intersected near surface before merging into a

bulk mineralized zone comprising the main lode. At depth, the structure breaks into three ore shoots. Mineralization in Latte east varies slightly from the west, with a pair of steeply dipping ore shoots branching off from the main Latte lode (Figure 5.5). Where the original Latte lode consisted of a bulk domain of strong mineralization, the main Latte structure has now broken into three stacked planar structures. The secondary splay branches off on a more eastward trend and with a much steeper dip. Two separate corridors of mineralization are visible.

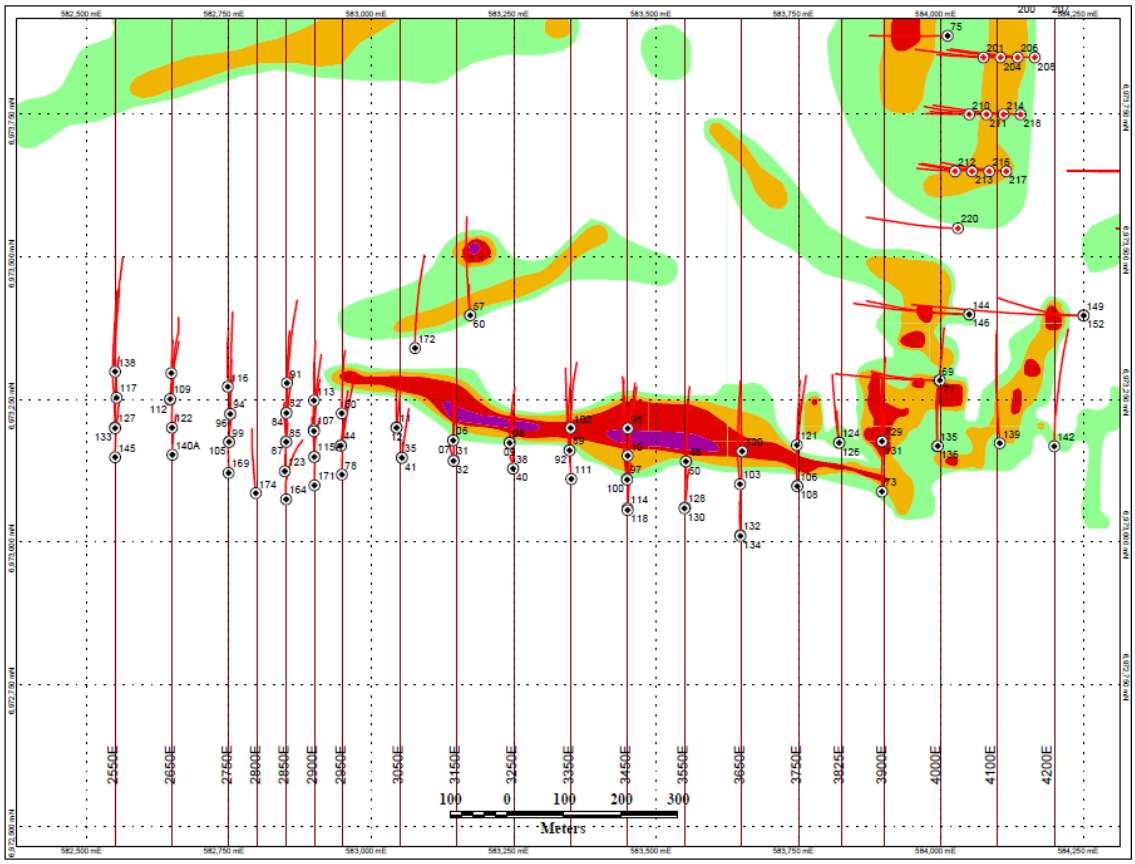


**Figure 5.3: Plan view of Latte zone drill collars current to 2012 drilling. Note the bulk of Latte west holes were drilled off of the strong Au-in-soil anomaly. These holes contain the bulk of the Latte lode and have no surface expression.**

The largest mineralized intervals at Latte occur in the western portion of the zone as demonstrated on the longitudinal section (Figure 5.6). The main Latte lode consists of broad disseminated mineralization through a schistose host with the majority of mineralized intervals consisting of >75 gram-metres Au. Mineralization in the eastern

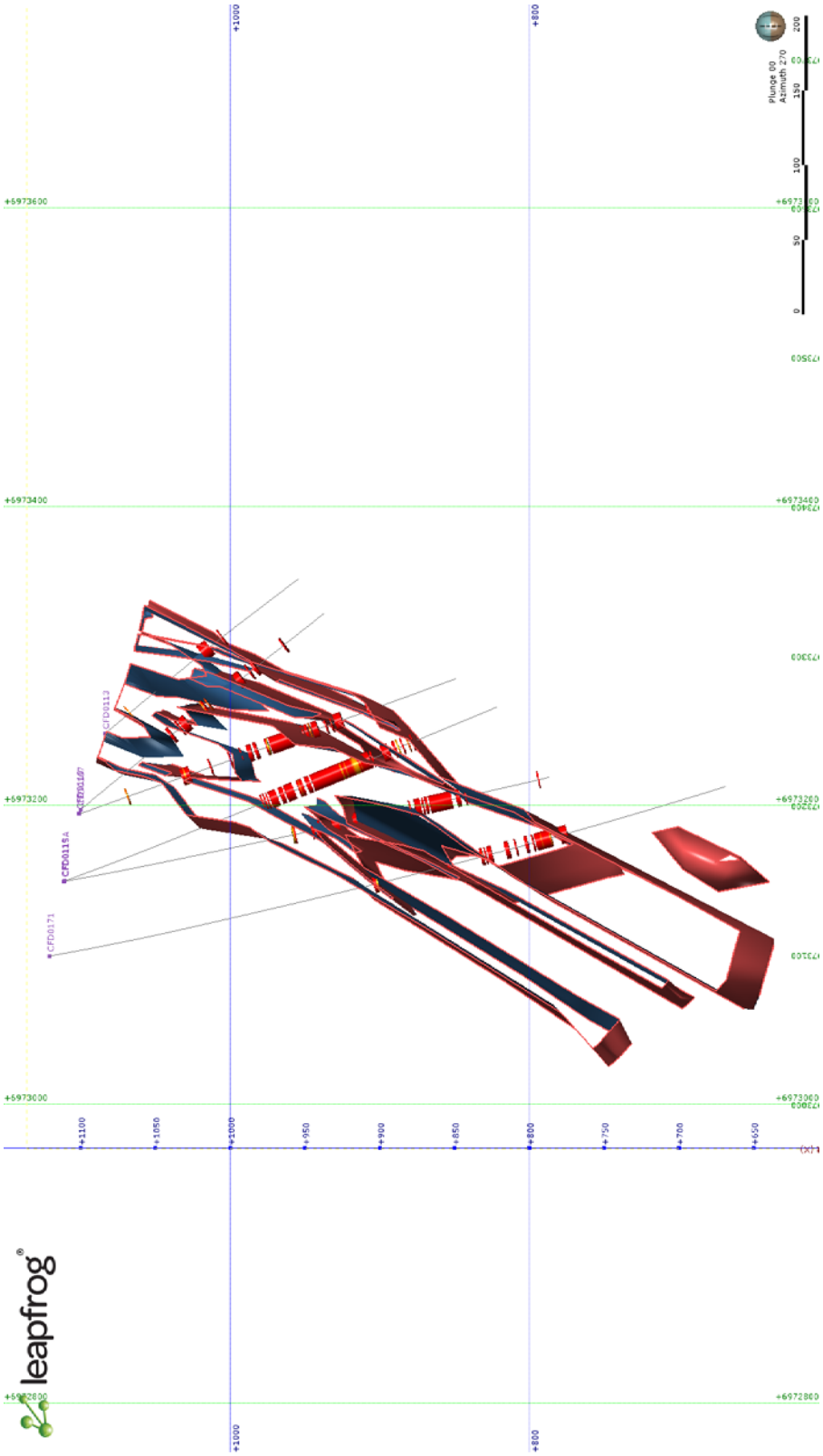


**Figure 5.4: Leapfrog 3D cross section of section 582900 mE, looking west. Structures dip moderately-steeply to the SSW, with a main lode of mineralization occurring directly in the middle of the wireframe.**

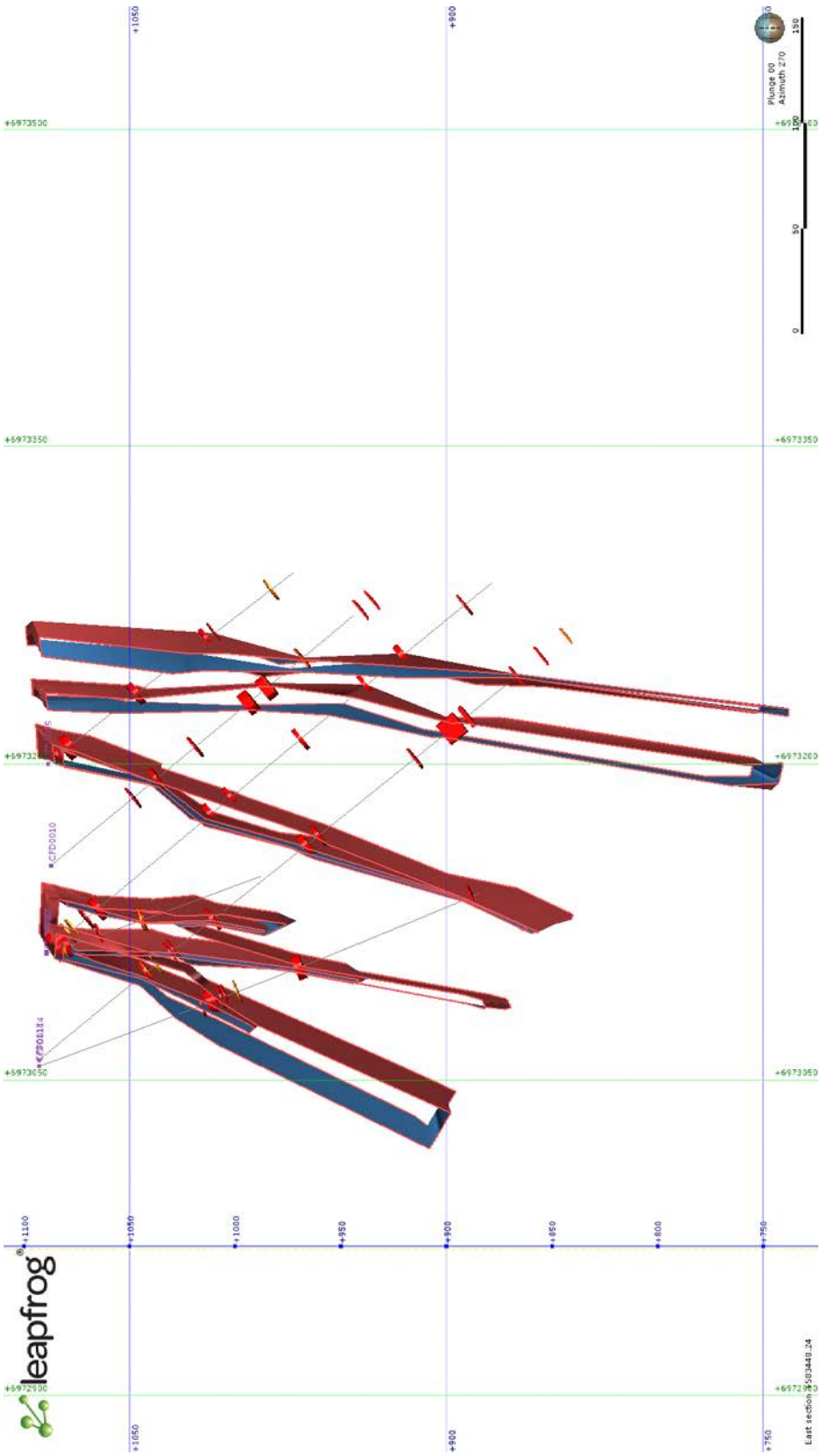


**Figure 5.5 Leapfrog 3D cross section of section 583450 mE, looking west. Structures in the eastern portion of the Latte zone dip steeply to the SSW and separate into 4 distinct corridors.**

portion of Latte consists of intervals averaging 25-75 gram-metres Au. The geometry of the mineralized structures varies from west to east as described above, with the thinner structures of the east yielding less Au.

## *Reactivation of Mineralized Structures*

Mineralization at Latte consists of at least two distinct styles, with common breccia and brittle deformation overprinting an initial disseminated phase of mineralization. This later brittle overprint is visible in multiple morphologies and will be discussed later in this chapter. It is clear, however, that the structural corridor at Latte was active post-mineralization. The duration of structural reactivation is unknown, however, regional fault structures such as the Tintina and Denali faults were active through the Eocene and remain active to this day.

## *Latte Oxidation Profiles*

Mineralization at the Coffee property is variably oxidized, with extensive weathering of Fe-rich sulphide minerals within host rocks by oxidizing meteoric fluids. These surface fluids percolated down the mineralized structures, leading to oxidation of both ore zones and host rocks to varying degrees.

Four oxidation profiles are defined on the Coffee property: oxide, upper transitional, lower transitional, and sulphide facies. Classification of drill core into each zone is completed by visual inspection of the degree of oxidation of drill core. Oxide facies rock is fully oxidized, with replacement of all sulphide minerals with Fe-oxides such as limonite-goethite and hematite. Oxidation by weathering in addition to saprolitization to form clay minerals such as kaolinite tends to destroy original rock texture and greatly hinders identification of host rocks. All mineralized zones at Coffee and Latte experience at least some degree of oxidation to a minimum extent of 50 metres below surface to greater than 330 metres.

Sulphide facies is found in both un-mineralized country rock and mineralized intervals. Within the country rock, it is characterized by near-complete preservation of

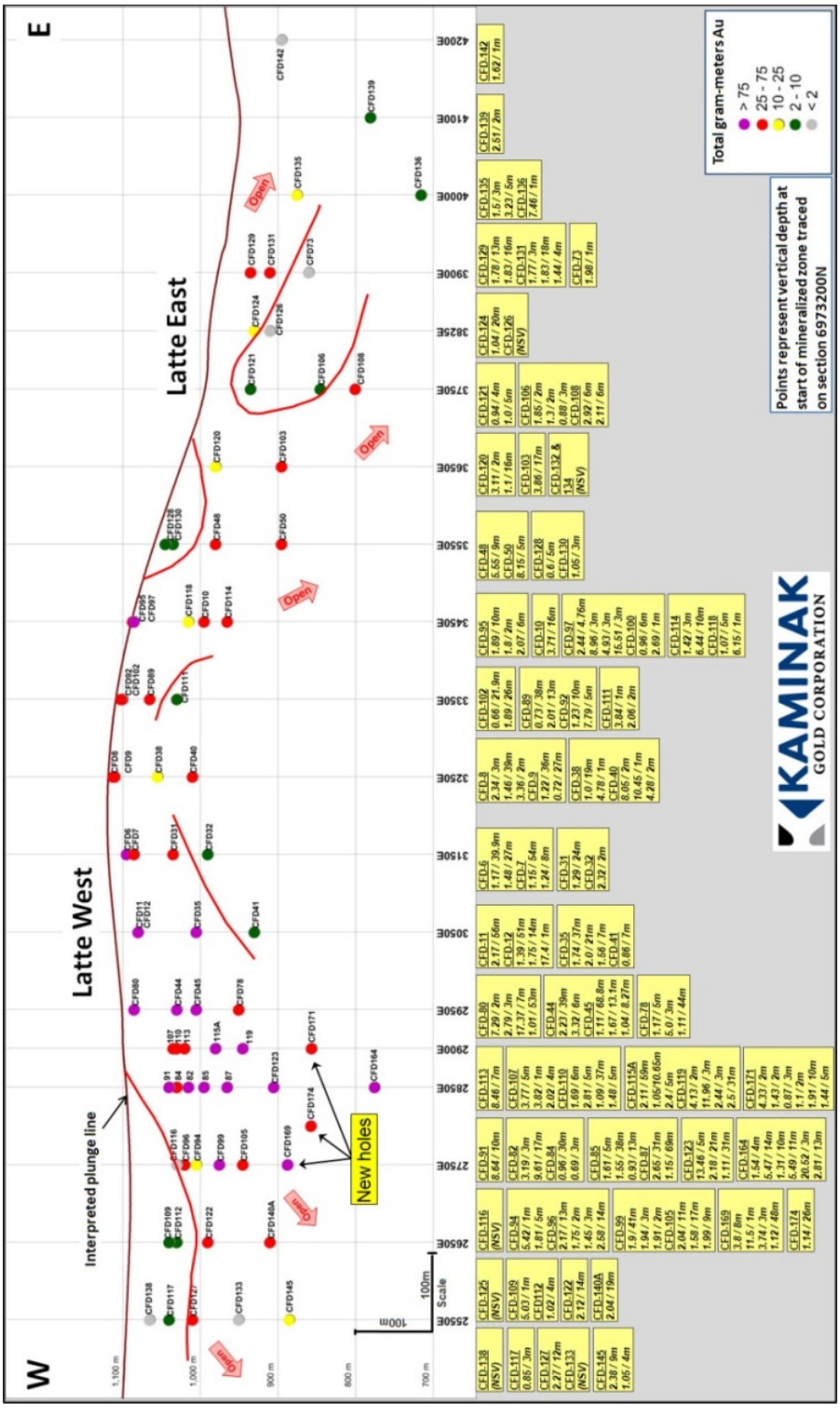


**Figure 5.6: Longitudinal cross section of the Latte zone based off of drilling to 2012. Latte west contains a region of strong, bulk, disseminated mineralization. This region is termed the Latte lode, with many holes returning >75 gram-metres Au.**

original metamorphic textures and mineralogy. Feldspars are only slightly clay-altered and ferromagnesian silicate minerals remain un-oxidized. Cubic metamorphic pyrite displays a brassy, metallic lustre. This un-oxidized country rock is found distal to mineralized structures and extends from surface to depth. Mineralized sulphide facies rock is composed of fresh gangue and alteration products with no oxidation. Dolomite, sericite/illite, silica, and late clay alteration minerals are fresh and clearly distinguishable. Au-phase sulphide minerals (arsenian-pyrite, arsenopyrite) are fresh and are un-oxidized. Latte rocks are dominantly oxidized, however a significant portion of mineralization is considered sulphide facies. Sulphide facies mineralization can be found at various depths throughout Latte, however most intervals are intersected at depth. As sulphide facies mineralization is untouched by texture-destructive late oxidation, it is ideal for identifying the original mineralizing processes active at the Latte zone.

## 5.2 Disseminated Mineralization at Latte

Gold mineralization at the Latte zone is composed of an initial disseminated style overprinted by later brecciation and late fluid ingress. Mica-rich host rock is the main host for Au, with a three phase mineral reaction resulting in Au precipitation. Disseminated mineralization is responsible for the majority of Au mineralization within the Latte zone, most notably the long, continuous intersections found in Latte west. Sulphide-facies disseminated mineralization is generally preserved at depth, where textural obliteration by oxidizing meteoric fluids was avoided. Au is hosted within rims of As-rich (up to 15 wt. %), extremely fine pyrite, with microscopic inclusions within the pyrite structure (Figure 5.7). Deposition occurs as a result of complete sulphidation of mica; dominantly biotite but also phengite depending on the schistose host.

Mineralized rocks retain the textures of original mica-schist, however, the original mica is pseudomorphously replaced by dolomite and fine grained Ti-rich phengitic mica (Figure 5.8). Arsenian-pyrite and arsenopyrite are fine grained (up to 0.25 mm) and occur disseminated along the original schistosity. Recystallized quartz boudins define the tectonic fabric within the host. Titanium within the original host biotite is removed during mineral consumption and reincorporated into mineralization-phase white mica and rutile.

A third mica phase forms a lath-like morphology on rims of mineralization-phase white mica.

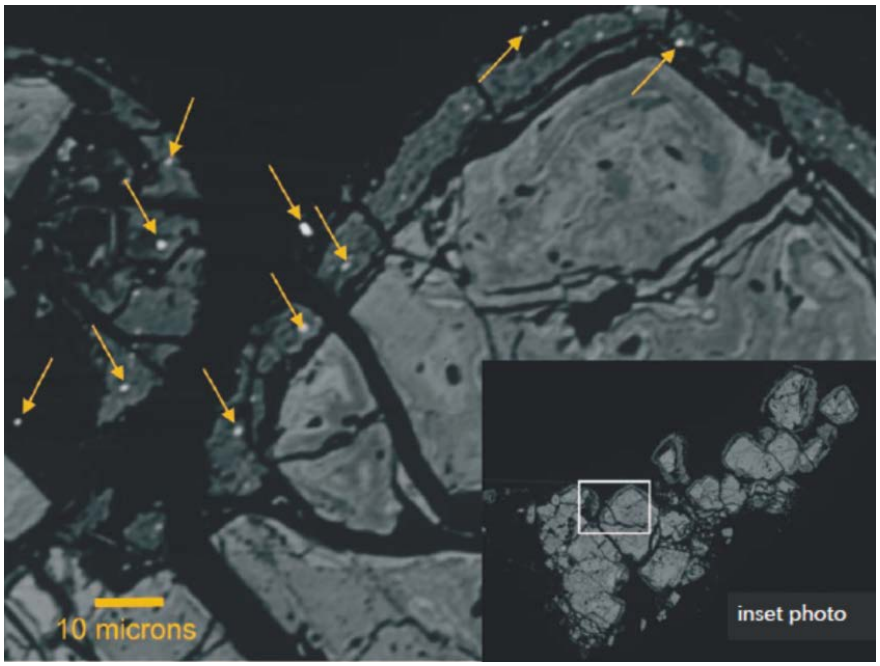


**Figure 5.7: Super fine Au hosted within As-rich pyrite. Oxidation (dark rim) has liberated the Au from within the As-Py mineral structure, where it has most likely substituted interchangeably with S.**

## *The Mica Sulphidation Reaction*

Au deposition is linked to two generations of hydrothermal white mica. Background metamorphic biotite or phengite is consumed in the reaction. Biotite ranges in composition from near-equal FeO – MgO content to phlogopite or Fe-biotite members. Both biotite and muscovite contain appreciable Ti and Cr, indicative of a metamorphic parentage defining the dominant metamorphic foliation.

The first step of the reaction begins with fresh metamorphic white mica and biotite interacting with the mineralizing fluid. The fluid was rich in $CO_2$, S, As, Sb, and Au as evidenced by the mineralization assemblage. Reaction products include dolomite, muscovite/illite, and As-rich pyrite. The Fe within the parent mica is consumed by a simple sulphidation reaction involving S and Au (+ As and Sb). The metamorphic mica is completely replaced by white mica which retains the Mg, Ti, and Cr content of the parent

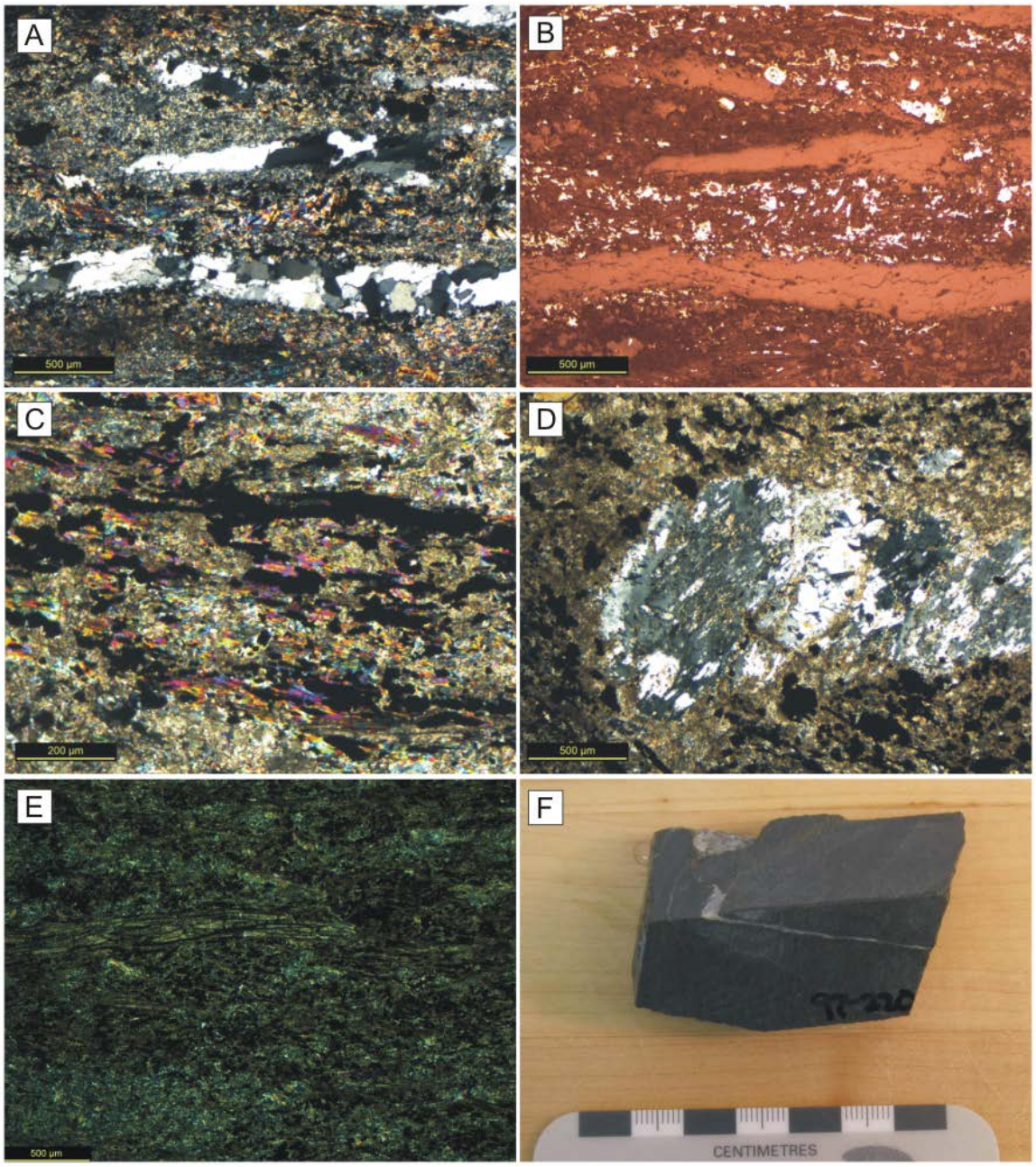


**Figure 5.8: Disseminated mineralization within the Latte zone. A) 164-464, XPL; B) Same as A, RL; C) 164-469, XPL; D) 164-469, relatively fresh feldspar porphyroblast surrounded by completely replaced mica and As-Py, XPL; E) 97-220, fine As-Py sulphidation, XPL; F) 97-220, hand sample.**

biotite lath. Au-bearing arsenian pyrite occurs along relict foliation planes. This mica phase is designated Hydrothermal 1 (HT1) for clarity. This first step of the reaction leaves sericite/illite white mica containing abundant fine grained arsenian pyrite which hosts Au. A general chemical equation for the mica sulphidation reaction is shown in Reaction 5.1.


**Reaction 5.1: Simplified mica sulphidation reaction: metamorphic biotite and phengite reacts with a heated ore fluid to form HT1 ore-phase illite/muscovite and extremely As-rich pyrite containing up to wt.% Au.**

In high-grade intervals this reaction runs to completion with no metamorphic mica compositions preserved. In intervals which did not experience complete sulphidation, relict metamorphic mica is preserved. Accessory minerals include arsenopyrite, also defining the parent mica foliation, dolomite which replaces silicate minerals, and sericite/illite and dolomite completely replacing feldspar porphyroblasts. Rare tetrahedrite has been observed at depth associated with this phase of mineralization, as well as fine-grained rutile. This alteration phase results in complete metasomatism of the previously schistose host, and HT1-phase alteration minerals dominate the mineralogy of Latte ore.

Continued fluid influx results in further white mica formation. This phase is composed of fine laths and overgrowths of sericite around HT1 white mica and is classified as Hydrothermal 2 (HT2) mica phase. The mica exhibits a habit of fine, highly birefringent laths and is commonly observed within domains of pure dolomite or in association with superfine chalcedonic silica influx (Figure 5.9). No further formation of sulphide is observed in association with the HT2 white mica species.

## *White Mica Mineral Chemistry*

White mica within both mineralized and un-mineralized thin section samples were selected for EPMA analysis in order to determine the chemical composition of the

various phases of mica (biotite mineral chemistry was reported in Chapter 3). Plots of octahedral site occupancy of Ti, Cr, Fe, Mg, and Mn vs. octahedral Al content are presented for mineralized and un-mineralized samples in Figure 5.10.

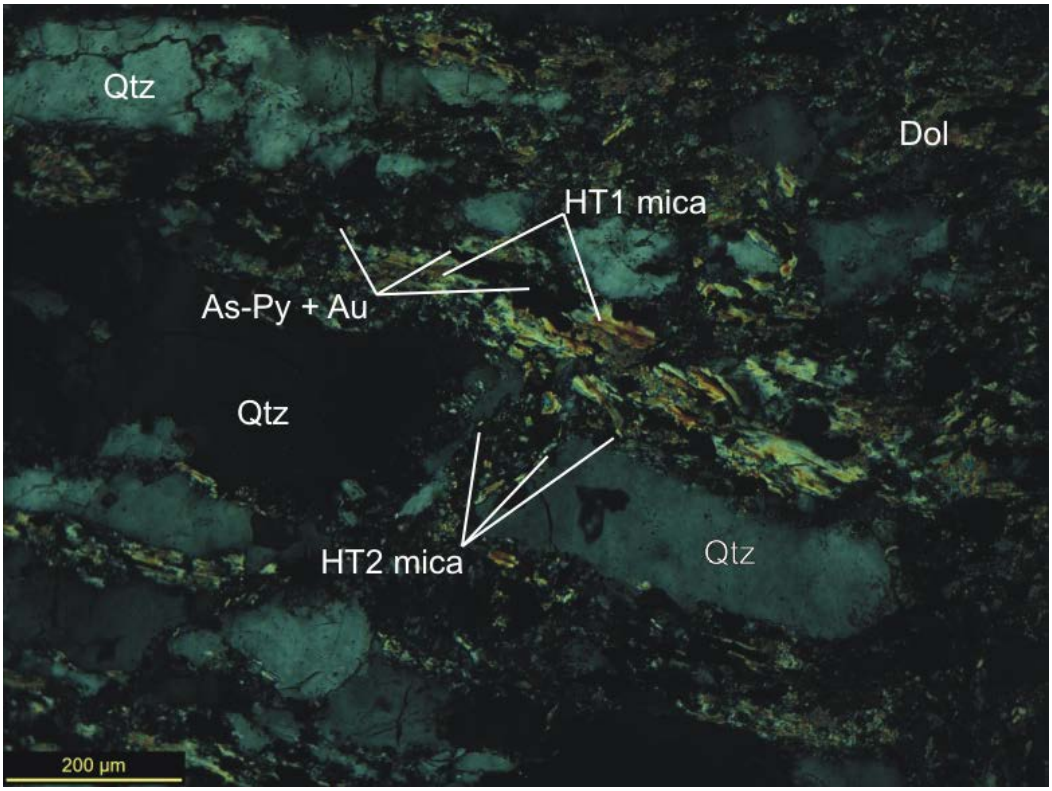


**Figure 5.9: Photomicrograph of sample 82-117.5, showing HT1 white mica (main laths) with opaque As-Py along foliation. Fine laths of HT2 phase white mica are found along the margins and forming out of solution with quartz.**

The compositional data for all three white mica species plot in discrete regions. White mica of metamorphic parentage contains high Ti, Cr, Fe, Mg, and Mn in the octahedral site and low octahedral Al. These compositions plot as phengitic in the lower right. In contrast, purely hydrothermal HT2 white mica plots in the upper left of the plot, with high Al occupancy in the octahedral site and low Ti, Cr, Fe, Mg, and Mn. The HT1 hydrothermal white mica (mineralization-phase) plots as an intermediate phase between the two end members.

Of the six samples analysed, two samples contain no appreciable Au mineralization. Sample 114-114 contains undetectable Au concentrations and plots in the

extreme bottom right of the plot with all mica analysed exhibiting phengitic compositions. Sample 82-223 also contains Au below detection, however mica grains analysed plot in two main groupings. Two analyses are phengitic while an anomalous cluster plots within the compositional range of HT1 hydrothermal white mica near high grade gold ore (Sample 97-220, 32 g/t Au).

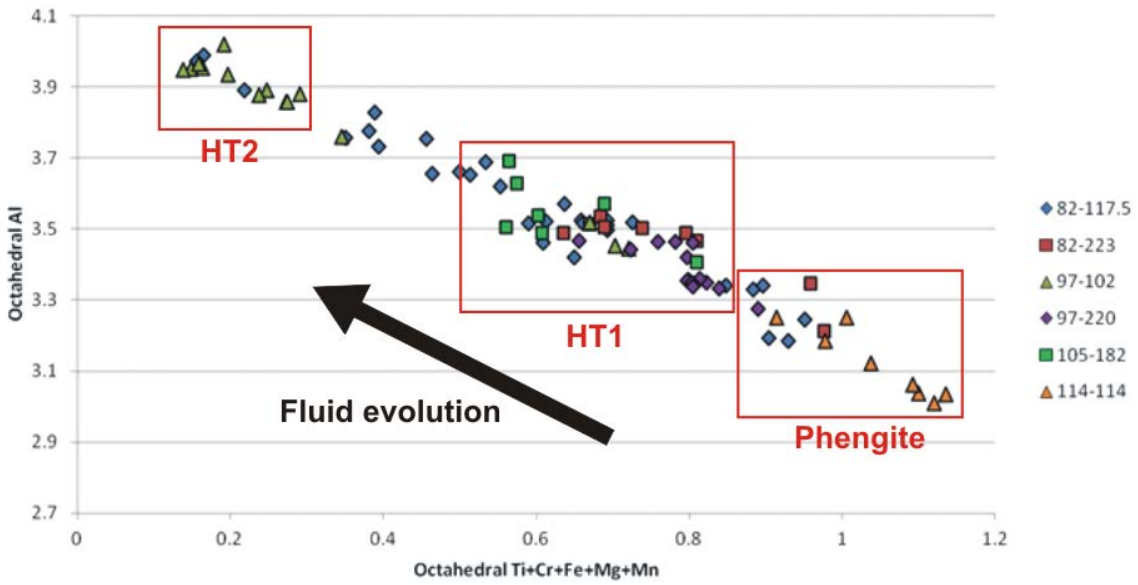


**Figure 5.10: Plot of octahedral-site Ti, Cr, Fe, Mg, & Mn vs. octahedral-site Al occupancy. Mica of primary, metamorphic compositions plots in the lower right (low octahedral Al). With increasing fluid interaction, HT1 phase mica replaces original phengitic compositions, culminating with purely hydrothermal mica (HT2) with high octahedral Al. As-Py sulphide deposition is associated with HT1 white mica.**

Mineralized samples display a wide variability in white mica composition. All mineralized samples contain white mica of HT1 compositions while only sample 82-117.5 contains any relict mica of metamorphic origin. The remainder of the analysed samples all contained HT1 white mica with an overprint of HT2 white mica. Sample 82-117.5 is an excellent example of the three stage reaction, with relict cores of phengitic mica overprinted by HT1 mineralization-phase white mica, all overprinted by HT2 late hydrothermal mica. This alteration sequence is well illustrated in Figure 5.11, with 5 representative analyses reported in Table 5.1. Chemical compositions of each mica phase as analysed in the mineralized and un-mineralized samples from the Latte zone are reported in Appendix C.

**Table 5.1: Representative analyses of white mica from sample 82-117.5. Spots correspond to annotations on Figure 5.11, while spots in brackets ex. (X) correspond to the full analyses in Appendix C.**

| Representative White-Mica Analyses: 82-117.5 | | | | | |
|---|---|---|---|---|---|
| **Spot** | **1** (17) | **2** (20) | **3** (22) | **4** (25) | **5** (28) |
| SI | 6.383 | 6.658 | 6.7 | 6.71 | 6.616 |
| AL (4) | 1.617 | 1.342 | 1.3 | 1.29 | 1.384 |
| AL (6) | 3.244 | 3.517 | 3.52 | 3.57 | 3.99 |
| TI | 0.019 | 0.161 | 0.139 | 0.137 | 0 |
| CR | 0 | 0.011 | 0.002 | 0.007 | 0.007 |
| FE | 0.361 | 0.07 | 0.112 | 0.07 | 0.009 |
| MG | 0.57 | 0.419 | 0.471 | 0.423 | 0.149 |
| MN | 0 | 0 | 0.001 | 0 | 0 |
| GA | 0 | 0.004 | 0.003 | 0.006 | 0.017 |
| BA | 0.002 | 0 | 0 | 0 | 0 |
| K | 1.833 | 1.108 | 0.989 | 0.993 | 1.021 |
| NA | 0.105 | 0.012 | 0.01 | 0.012 | 0.012 |
| O | 22 | 22 | 22 | 22 | 22 |
| FE | 38.74 | 14.28 | 19.24 | 14.16 | 5.94 |
| MG | 61.26 | 85.72 | 80.76 | 85.84 | 94.06 |
| F/M | 0.632 | 0.167 | 0.24 | 0.165 | 0.063 |
| F/FM | 0.387 | 0.143 | 0.194 | 0.142 | 0.059 |

## *PIMA Analysis*

Samples of altered rock were selected from across the Coffee property in order to determine mineralogical differences between mineralized and un-mineralized rocks. Samples included oxidized and un-oxidized rock, and were subjected to portable infrared mineral analysis (PIMA) spectral analysis. Results are summarized in Table 5.2.

All mineralized samples analysed at Coffee contain two alteration minerals, illite and kaolinite, with some intervals also containing palygorskite. Illite is detected in samples which are not mineralized, although these samples experienced high levels of alteration and interacted with the mineralizing fluid as evidenced by elevated As (ex. Sample DD233-184.7, 185.3). Minerals detected only within mineralized zones include gypsum (rare), phengite, and jarosite, a hydrous sulphate of potassium and iron, commonly occurring with limonite and goethite.

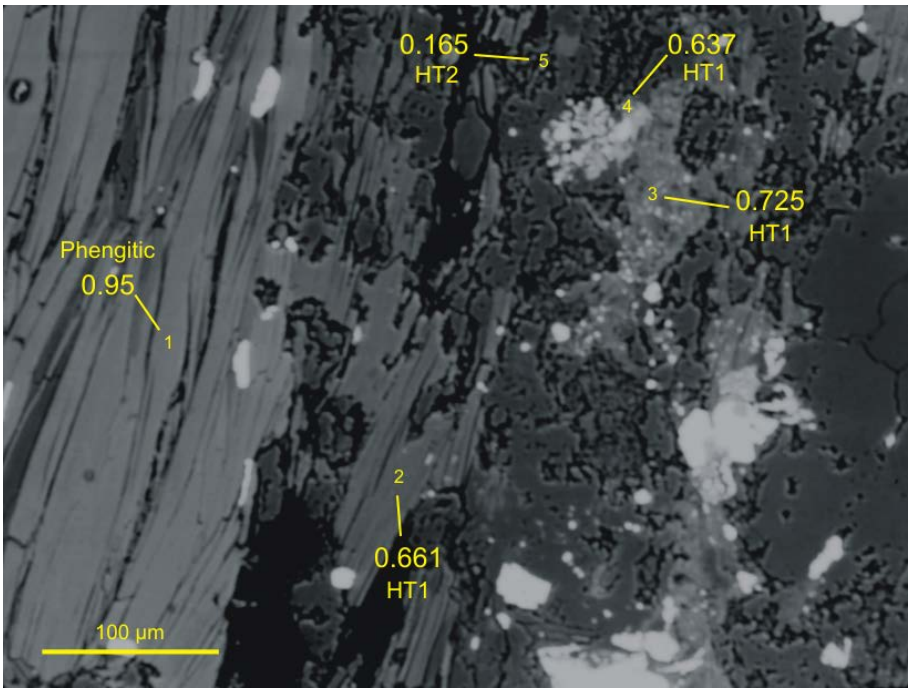


**Figure 5.11: Representative EPMA spot analyses on sample 82-117.5. Analyses progress from phengitic host mica, to HT1 overprint and replacement, to very fine HT2 white mica as a final phase. Number values represent total octahedral-site Ti, Cr, Fe, Mg, & Mn content.**

**Table 5.2: Summary of minerals detected by PIMA analysis within mineralized rocks at the Latte zone.**

| Sample | Lithology | Grade (g/t) | Min. 1 | Min. 2 |
|---|---|---|---|---|
| LAT85-205.50 | PyF | 3.34 | Illite | |
| | | | Illite | |
| | | | Illite | Kaolinite |
| | | | Illite | Kaolinite |
| LAT82-55.50 | HU | 1.56 | Kaolinite | |
| | | | Kaolinite | |
| LAT82-94.60 | RQM | 4.44 | Illite | |
| | | | Illite | |
| | | | Gypsum | Illite |
| LAT82-131.50 | RQM | 0.337 | Illite | |
| | | | Illite | Jarosite |
| | | | Illite | Jarosite |
| LAT82-133.40 | RQM | 2.12 | Kaolinite | Illite |
| | | | Illite | Gypsum |
| LAT78-268.40 | YC | 0.6 | Illite | |
| | | | Illite | |
| LAT78-270.50 | HU | 0.366 | Muscovite | Gypsum |
| | | | Muscovite | Kaolinite |
| | | | Kaolinite | Gypsum |
| LAT89-111.50 | YC | 4.23 | Illite | Palygorskite |
| | | | Illite | Phengite |
| | | | Illite | Kaolinite |
| LAT102-50.0 | RQM | 1.475 | Illite | |
| | | | Illite | |
| | | | Illite | |

Many altered but un-mineralized intervals on the Coffee property appear visually similar to mineralized intervals. Strong oxidation and clay alteration is common with no associated gold mineralization. PIMA results for two samples representative of this difference reveal distinctly different mineralogies. A sample from CFD0089 111.5m assayed at 4.23 g/t Au from 111 – 112m. This sample is strongly clay altered and oxidized. Minerals detected by PIMA analysis include illite, phengite, palygorskite, and kaolinite. In contrast, a sample from CFD0102 30.9m down hole did not contain significant Au by fire assay (0.023 g/t Au from 30 – 31m), yet is also strongly clay altered and oxidized. Minerals detected within this sample were restricted to kaolinite and opal. Un-mineralized samples with strong alteration contained a variety of additional alteration products not related to mineralization including: halloysite, montmorillonite, dickite, opal, talc, serpentine, Mg-chlorite, Mg-clays, ankerite, and epidote (Table 5.3).

**Table 5.3: Summary of minerals detected by PIMA analysis within un-mineralized rocks at the Latte zone**

| Sample | Lithology | Grade (g/t) | Min. 1 | Min. 2 |
|---|---|---|---|---|
| LAT82-134.70 | SZ | 0.028 | Serpentine | Talc |
| | | | Talc | |
| | | | Serpentine | Talc |
| LAT89-46.70 | RQM | 0.086 | Dickite | Muscovite |
| | | | Muscovite | Dickite |
| | | | Muscovite | Dickite |
| | | | Muscovite | Dickite |
| LAT89-47.80 | HU | 0.082 | Kaolinite | Paragonite |
| | | | Kaolinite | |
| LAT102-30.90 | HU | 0.023 | Kaolinite | Opal |
| | | | Kaolinite | Opal |
| | | | Kaolinite | |

## 5.3 Brecciation and Remobilization of Gold

Gold mineralization is commonly associated with brecciated intervals. Three phases of brecciation are identified in the Latte zone, each associated with differing fluid compositions after the deposition of Au within As-rich pyrite. A first phase of brecciation occurs after intense $CO_2$-rich fluid interaction with previously mineralized intervals which leads to reabsorption of Au-bearing sulphide minerals by the fluid. A second style of brecciation consists of silica/rock-flour matrix breccia development which is not

associated with mineralization. The final phase consists of Fe-carbonate brecciation unrelated to mineralization.

## *Intense $CO_2$ Fluidization of Mineralized Intervals*

At Latte, mineralized intervals at depth are observed to consist of complete replacement of parent mica by hydrothermal muscovite/illite. This reaction occurs in conjunction with intense $CO_2$-rich fluid-rock interaction which results in strong dolomitization. In some mineralized intervals this reaction proceeds until no remaining primary silicate minerals are present, leaving dolomite, hydrothermal white mica, Au-bearing As-rich pyrite, and strands of primary quartz which define the original foliation. In the most heavily altered intervals there is polyphase dolomite veining (Figure 5.12).

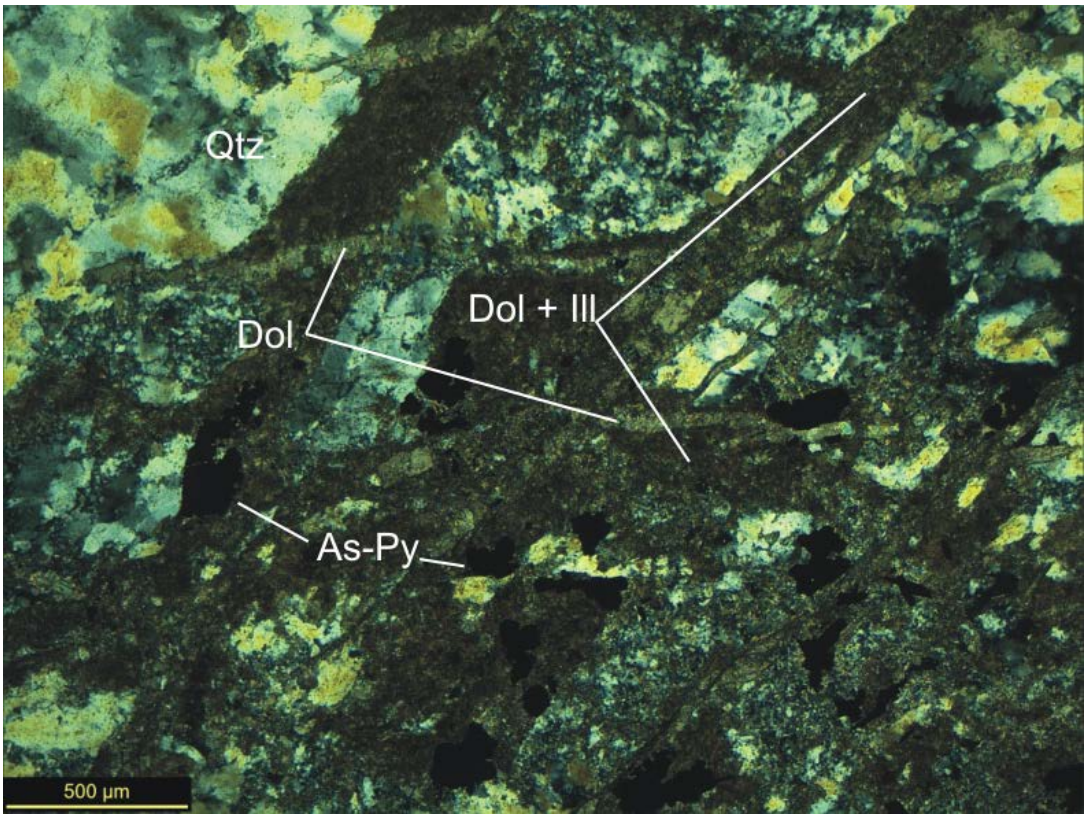


**Figure 5.12: Photomicrograph of sample 99-157, XPL. Multiple phases of dolomite are present within the mineralized interval.**

Intervals of such intense fluid-rock interaction become completely overprinted by dolomite and exhibit significant remobilization of Au-bearing sulphide minerals. The

carbonate-rich fluid reacts with the host during continuing dolomitization and leaches As-rich pyrite and arsenopyrite from the previously mineralized host. This sulphide is later recrystallized along the margins of carbonate-quartz veins (Figure 5.13).

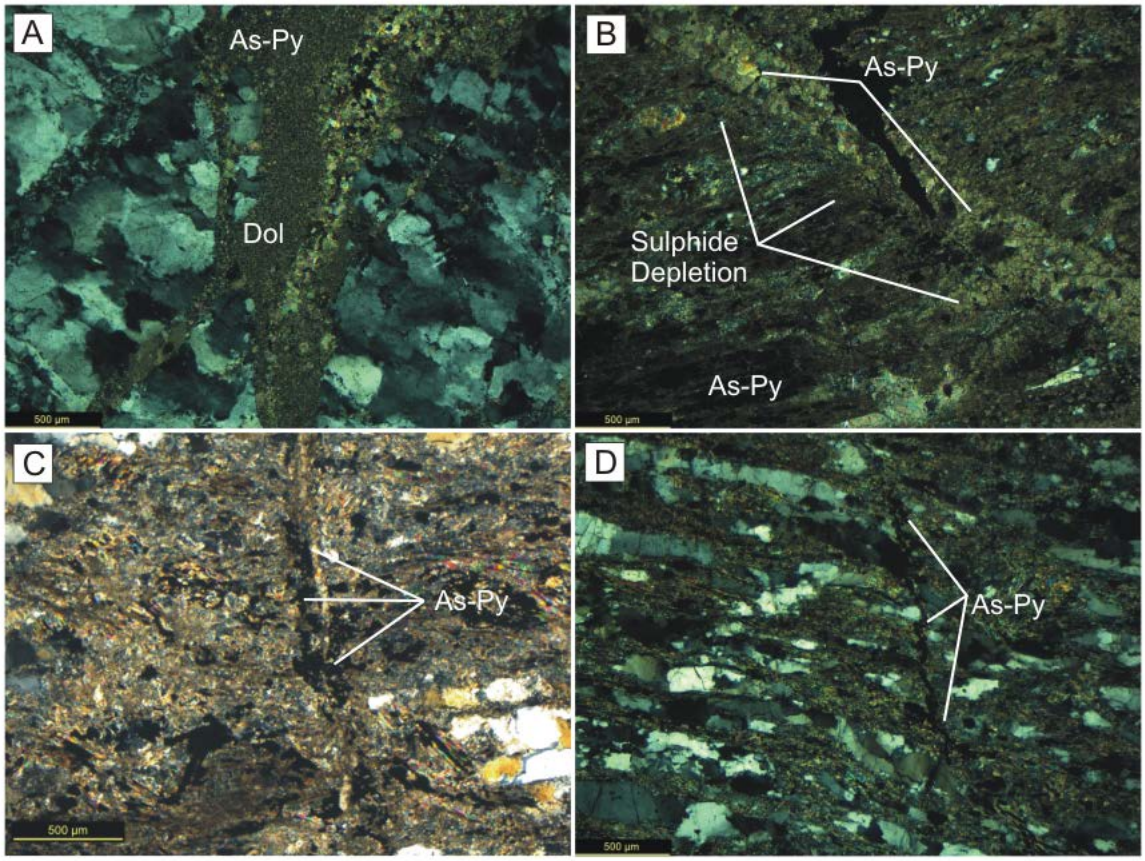


**Figure 5.13: Photomicrographs of remobilized sulphide. A) 99-157, two phases of dolomite cut a recrystallized quartz vein, XPL; B) 97-102, a dolomite vein cuts through mineralized host, consuming foliation-controlled sulphide, XPL; C) 164-364, re-precipitation of sulphide along a fine dolomite veinlet's margins, XPL; D) 82-117.5, Thin veinlet of sulphide and dolomite cutting host foliation, XPL.**

These veinlets are readily observed within sulphide-facies intervals throughout the most heavily dolomite/illite altered host rocks within the Latte zone. Veinlets observed in hand sample are grey in appearance due to the extremely fine-grained nature of the sulphide (Figure 5.14). Silica within the veinlets is obtained through the previous consumption of silicate minerals during complete dolomitization.

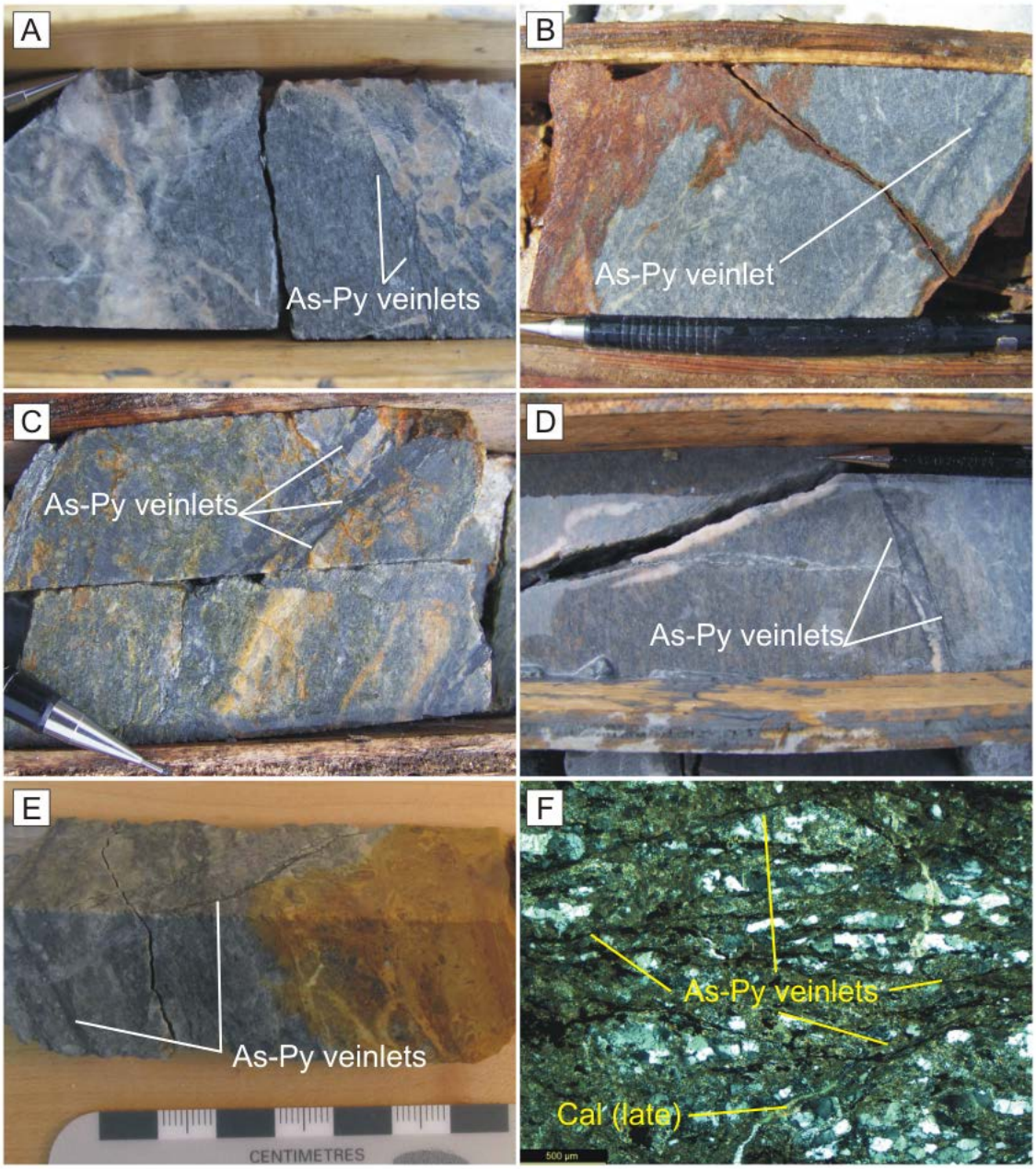


**Figure 5.14: Core photos of remobilized sulphide: A) 85-133.6m (15.6 g/t Au); B) 89-57.7m, 6.48 g/t Au; C) 115A-149.5m, 20 g/t Au; D) 119-186.3m, 7.07 g/t Au; E) 97-30m, 2.07 g/t Au; F) 97-30, photomicrograph of thin sulphide veinlets, XPL**

These domains of intense alteration are common throughout the Latte zone and are best preserved at depth, where late oxidative meteoric fluids have not overprinted the sulphide-rich intervals.

## *Sulphide-matrix Breccia and "Pyritic Faults"*

Numerous intervals at depth within the Latte zone consist of monomictic breccia of heavily altered host rock supported by a fine matrix of sulphide and clay minerals. These breccias are rarely preserved, and are usually found in conjunction with non-cohesive pyritic faults. These sulphide-matrix breccias are generally immature and usually appear as concentrations of very fine "sooty" As-rich pyrite with a steel/sooty grey colouration. These concentrations of As-pyrite are commonly clay altered and share the same colouration and morphology as the thin As-pyrite rich veinlets which commonly cut heavily altered intervals. The sulphide minerals within these intervals are carried by a carbonate + quartz fluid which both brecciates host intervals and forms patches of heavily concentrated sulphide minerals (Figure 5.15, Figure 5.16). Pyritic faults are so-named due to their lack of cohesiveness and strong clay alteration. Sulphide content within these intervals is estimated at up to 20%. Petrographic study of both sulphide-matrix breccia and pyritic faults is difficult due to the heavy alteration experienced by the host. Samples are generally not competent enough to create a thin section and are reduced to rubble and mud after in-field core splitting for assay samples.

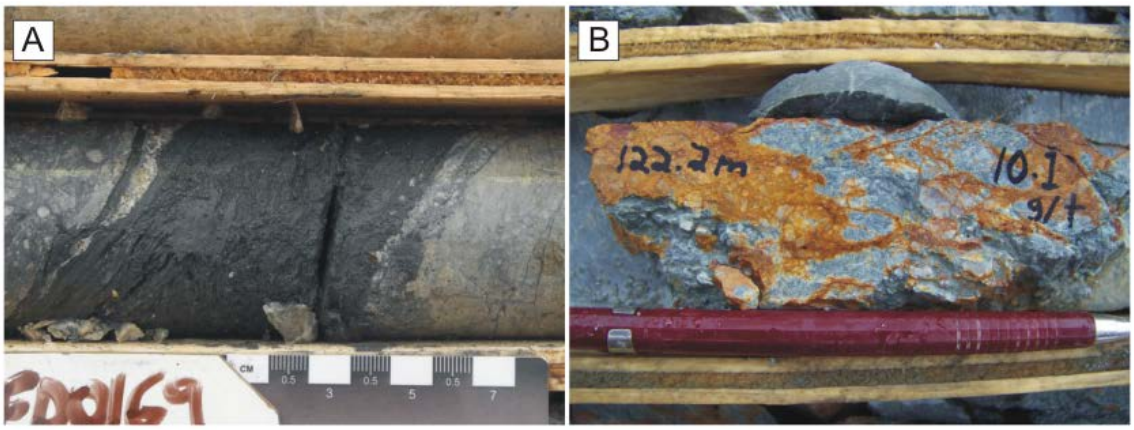


**Figure 5.15: Core photographs of: A) pyritic fault in CFD0169 at 237.8m. Fine sulphide/clay domain within heavily altered host; B) sulphide-matrix breccia from CFD0010 at 122.2m.**

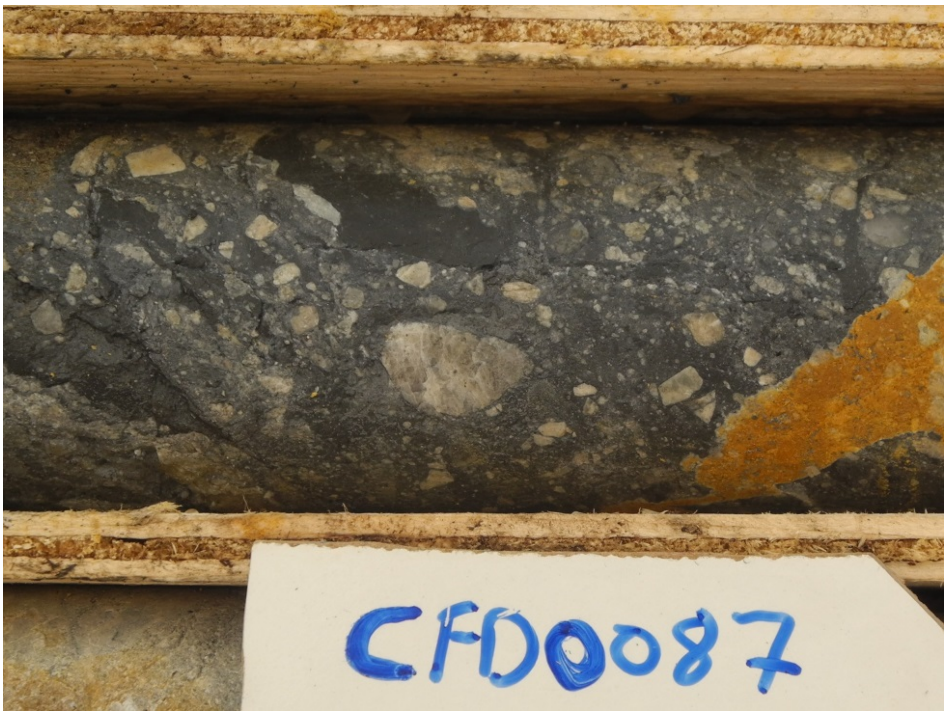


**Figure 5.16: Core photograph of a sulphide-matrix breccia in drill hole CFD0087 at 130.40m down hole. Approximately 20% of the breccia matrix is composed of fine, "sooty" arsenian pyrite hosting Au.**

## *Post-mineralization Brecciation*

Breccias which contain angular monomictic clasts of mineralized host rock are common at Latte. These breccias cut through schistose host rocks which have been mineralized by the mica sulphidation reaction (Figure 5.17). The matrix to these later breccias appears similar in appearance to a sulphide-matrix breccia, however it is composed of extremely fine rock flour and comminuted fragments of the host. These breccias are formed by a mixture of fluid-action and tectonic milling. Fine grained sulphide is found within the breccia matrix in association with ground-up host rock. Mineralization is chiefly hosted within the clasts. Notably, these breccias do not contain significant carbonate content: cementation of the breccias is achieved by silicification of the breccia matrix. All carbonate minerals within the interval are fine grained fragments of marble within the host.

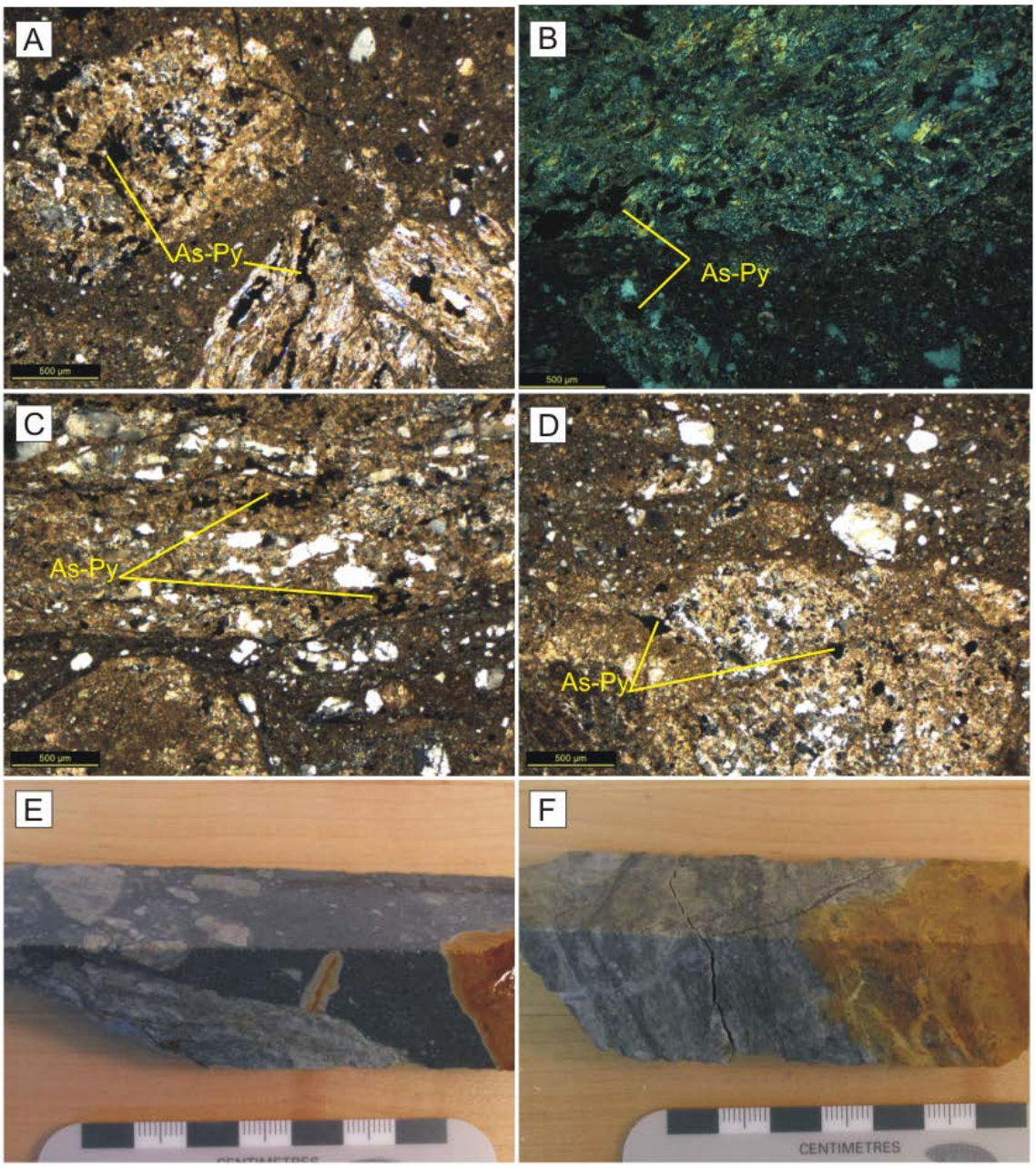


**Figure 5.17: Examples of late, post-disseminated mineralization brecciation with no sulphide influx. A) 114-162, clasts of mineralized wall rock within a super-fine rock flour/silica matrix, XPL; B) 114-162, same as A; C) 97-30, breccia corridor with super-fine rock flour/silica matrix and mineralized clasts/wall rock, XPL; D) same as C, XPL; E) hand sample of A, B; F) hand sample of C, D**

Wide intervals of brecciation with a nearly pure Fe-carbonate matrix are intersected in the upper portions of the Latte zone. These intervals are heavily oxidized and dominantly un-mineralized. Clasts are variably angular to sub-rounded and are

usually matrix supported depending on the maturity of the brecciated interval (Figure 5.18). This Fe-carbonate matrix brecciation is occasionally observed to cut mineralized intervals, appearing as the carbonate matrix equivalent of brittle, silica/rock flour matrix breccias as described above. No mineralization-phase sulphide or oxide minerals are present within or are carried by this carbonate fluid phase.

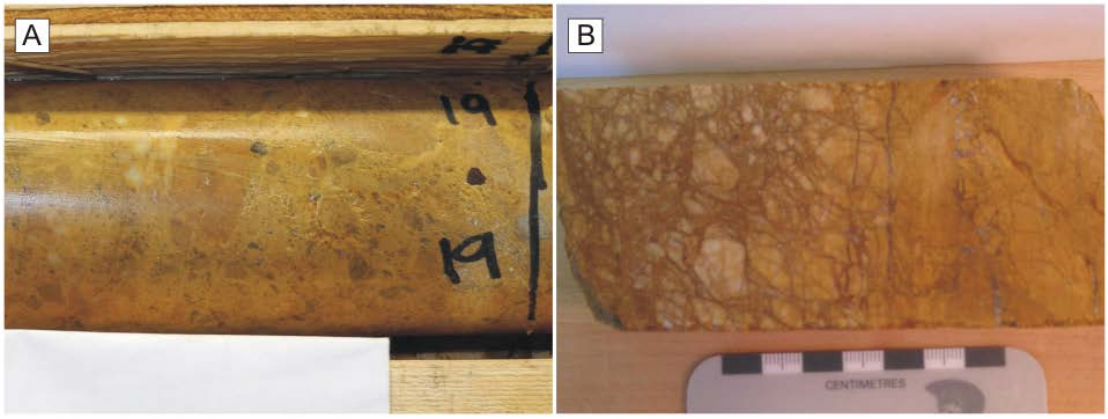


**Figure 5.18: Sample of Fe-carbonate matrix breccia. A) full core from CFD0082 at 18.9m; B) cut face of sample 82-17.8, in very close proximity to A.**

## 5.4 Vein Assemblages

At Latte, veins are subdivided into different types based on vein mineralogy and chronologic order. Five generations are observed and are ordered from V1 – V5 as summarized in Table 5.4.

**Table 5.4: Summary of vein assemblages observed at Latte. Modified after Allan et al., 2013**

| | Mineralogy | Alteration | Age |
|---|---|---|---|
| V1 | Qtz | - | Late Permian |
| V2 | Qtz ± Kfs ± Py | Weak Kfs, py | Jurassic |
| V3 | Dol-Py ± Qtz | Dol, ill | Cretaceous |
| V4 | Fe-carb | Fe-carb | Cretaceous |
| V5 | Cal | - | Cretaceous |

*V1 Quartz Veins*

V1 quartz veins were formed prior to the $D_2$ deformational event. The veins consist of milky, opaque-white quartz and are found very commonly throughout the schistose rock

panel which hosts Latte. These veins were transposed to conform to the regional $S_2$ foliation and now lie foliation-concordant. Veins vary in size from 1cm to approximately 50cm as intersected in drill core.

*V2: Quartz-Kspar Veins*

A second suite of veins cuts the Latte zone and consists of milky quartz ± K-feldspar ± pyrite veins with highly irregular margins. These veins cut $S_2$ foliation and vary in size from ~5cm to >1m in width. V2 veins are sometimes observed with pod-like, "blotchy" margins. Patchy domains of K-feldspar occur within the vein.

*V3: Ore-stage Dolomite-Pyrite Veins*

V3 veins consist of dolomite ± As-pyrite ± quartz, with massive to banded dolomite and common super-fine arsenian pyrite. Blocky grains of hydrothermal quartz are observed, however dolomite remains the dominant mineral. Super fine arsenian pyrite hosting Au commonly occurs along vein margins. Strong concentrations of arsenian pyrite occur locally in areas. This vein generation provides the matrix for sulphide-matrix breccias as described previously. V3 veins are commonly called "sooty-sulphide" veinlets where thin (<1cm), and are considered equivalent to the strong concentrations of super-fine sulphide commonly referred to as "pyritic faults". V3 generation veins are generally only observed within and closely proximal to heavily altered mineralized zones.

*V4: Ferroan Carbonate Veins*

Thin (<1 – 5mm) veinlets of Fe-carbonate commonly cut un-mineralized metamorphic rocks at Latte, but are not observed to inject heavily altered ore-stage rocks and veins (V3). These veinlets are visually identical to the Fe-carbonate un-mineralized breccias found crosscutting the Latte stratigraphy.

*V5: Calcite Veinlets*

Thin white calcite veins crosscut all other lithologies in the Latte zone. These veins are generally <1cm in width, but can be occur up to 30cm in width. V5 veins locally display open space and infill textures with multiple generations of coarse, bladed calcite. Local

white-calcite matrix brecciation is observed at Latte and is attributed to high-energy V5 formation.

## 5.5 Metal Associations

Latte displays an interesting set of metal associations. All gold zones at the Coffee property exhibit a very clear association between mineralization and arsenic and antimony (Figure 5.19). Latte specifically shows a weak positive correlation between gold-silver and gold-calcium and an average gold-to-silver ratio of 1:5 (Figure 5.20). No other significant elemental correlations are observed within the Latte zone. Therefore, mineralization at Latte is gold-only and shows strong positive correlation with As, and Sb, and weak positive correlation with Ca and Ag.

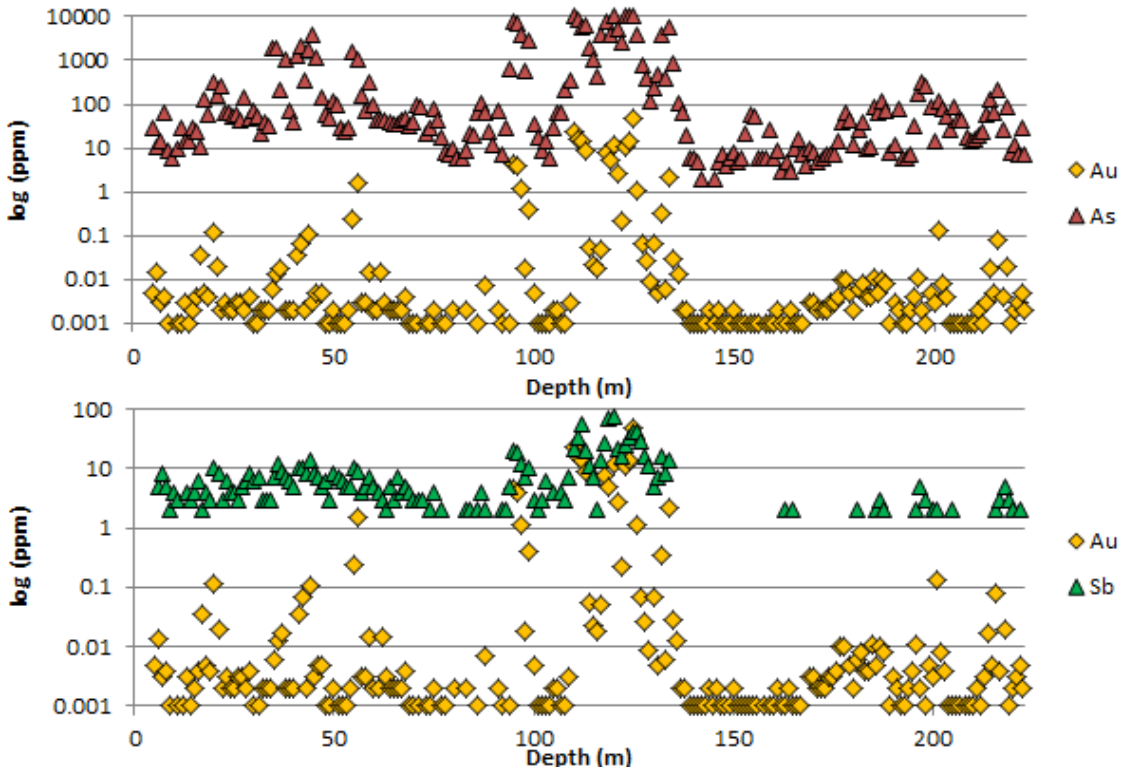


**Figure 5.19: Down hole logarithmic plots from CFD0082. An obvious correlation between Au, As, and Sb is seen and has been an excellent exploration vector while drilling at Coffee.**

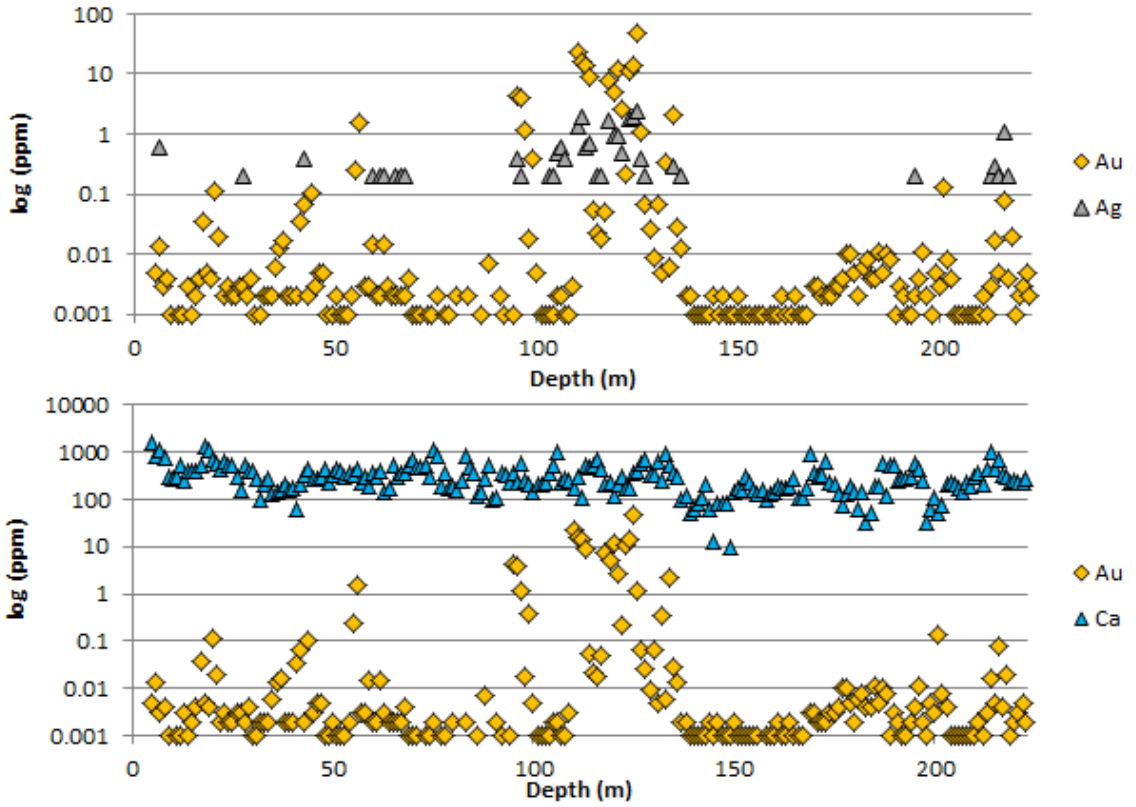


**Figure 5.20 Down hole logarithmic plots from CFD0082. A correlation is observed between Au and Ag at Latte. Correlation between Au and Ca is generally weak, but locally strong.**

## 5.6 Influence of Lithology on Gold Mineralization

Mineralization at Latte is driven by the sulphidation of mica to form arsenian pyrite which hosts gold. Thus, a key component of the mineralization reaction is mica-rich schist. Some lithologies in the Latte package are not amenable to mineralization and act as aquitards for mineralizing fluid. In addition, the permeability of a potential host rock to reactive mineralizing fluids plays a major part in the distribution and extent of Au-rich intervals at Latte.

### *Ultramafic Rocks as Aquitards for Au-rich Fluid*

Ultramafic rocks at Latte are typically poor host rocks for Au mineralization. A thick tectonically emplaced slice of ultramafic rock is intersected by a number of drill holes (ex. CFD0082, CFD0113). This ultramafic slice contains significant magnesite, indicating strong fluid-rock interaction with a $CO_2$-rich fluid (Figure 5.21). No gold

mineralization is intersected within the ultramafic despite the strong carbonate replacement. “Pooling” of high-grade gold mineralization can be observed in the hanging wall of the thrust-emplaced ultramafic slices (Figure 5.22). Gold mineralization in Figure 5.22 is modelled as grade shells using 0.5, 1.0, 2.0, and 4.0 gram/ton cut offs.


**Figure 5.21: Sample 82-141.6, Serpentinite. This unit has not been observed to be mineralized at Latte.**

The purple ultramafic is seen to be intersected by three drill holes looking east on section 582850mE (Figure 5.22). A high-grade pod of mineralization which follows the general steep Latte structural trend (striking ESE, dipping steeply to SSW) is truncated by the ultramafic slice. Though the ultramafic is severely altered by $CO_2$-rich fluid, it is un-mineralized and potentially pools mineralizing fluid on its hanging wall side.

## *Marble as an Aquitard for Au-rich Fluid*

Marble bands and horizons are extremely common in Upper Latte schistose rocks. Where cut by a mineralized structure marble is unreactive with the Au-rich mineralizing fluids, and appears to act as an impenetrable barrier. In areas where marble bands are closely interlayered with biotite/muscovite schist, mineralized fluid is channelled through the schistose rocks leading to sulphidation of the mica and deposition of arsenian pyrite (Figure 5.23). This containment can occur on fine scales. As observed in CFD0346, sulphidation of biotite occurs between fine marble bands 40cm away from an identical interval with no mineralization (Figure 5.24).

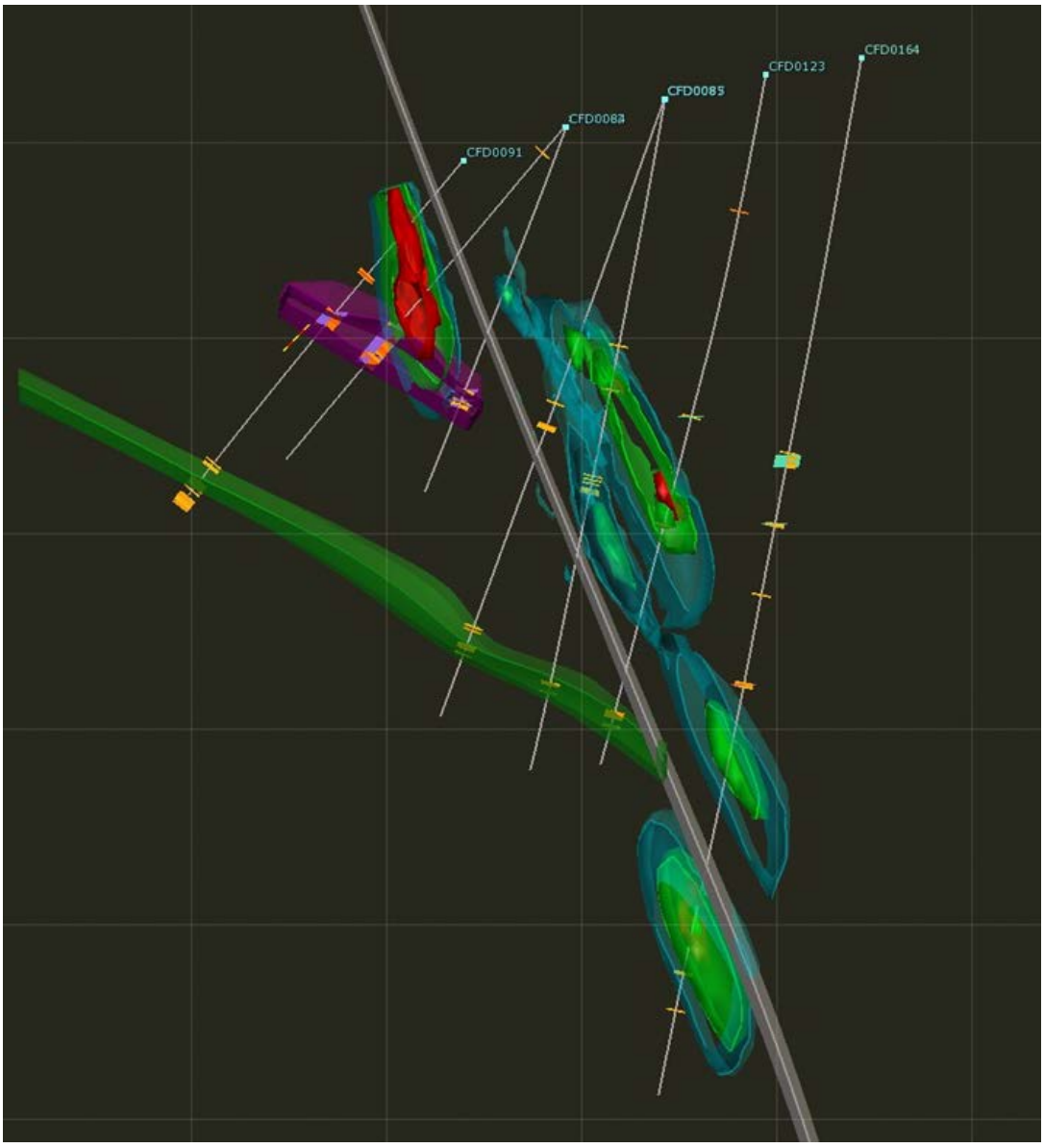


**Figure 5.22: Leapfrog 3D cross section of section 582850 mE, looking east. The purple body sits below a pod of high grade mineralization in the hanging wall, and is un-mineralized itself. The panel appears to impede fluid flow. Gold mineralization is modelled as grade shells using 0.5, 1.0, 2.0, and 4.0 gram/ton cut offs.**


**Figure 5.23: Sulphide-facies mineralization hosted within strong marble banding in CFD0079 at 78m down hole.**

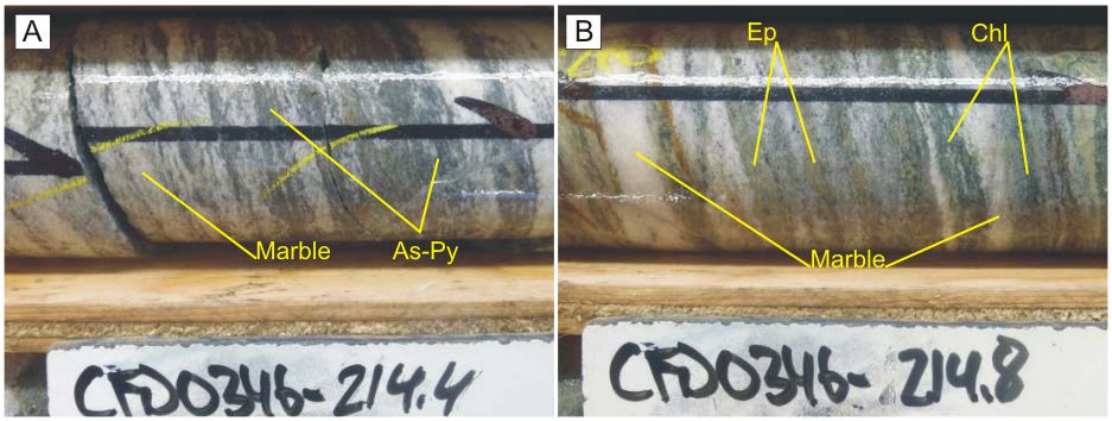


**Figure 5.24: Marble bands host and channel mineralizing fluids along small intervals. CFD0346: A) strong sulphidation of mica layers within marble bands in a biotite schist unit at 214.4m down hole; B) un-mineralized biotite schist with chlorite and epidote alteration 40cm down-hole from A.**

## *Mica-poor Host Rocks*

The widest and highest-grade mineralization occurs within the schistose rocks of Upper Latte. In contrast, gold mineralization within the Lower Latte mafic rocks is much more tightly constrained. Mafic rocks in Lower Latte are mica-poor. As described earlier in this chapter, gold deposition at Latte is controlled by sulphidation of metamorphic mica

and later redistribution by $CO_2$-rich fluid. Mica content of the varying amphibolitic and metagabbroic rocks at Latte is restricted to less than 15% in Upper and Lower Latte amphibolites and 5% or less within the metagabbro which dominates Lower Latte. In comparison, Upper Latte schistose rocks contain an average of more than 80% mica.

When the mineralizing fluid comes into contact with these mica-poor rocks, less mica is available to react with the fluid and induce arsenian pyrite (and Au) deposition. However, within the Lower Latte mafic package, rare and thin intervals of schistose rock are intersected. If cut by a structure which channels the fluid, these highly reactive, mica-rich rocks are preferentially mineralized over amphibole-dominant mafic rocks. Amphibole does not react with mineralizing fluid at the Latte zone. Mineralization within the Lower Latte sequence is generally confined to thin intervals of schistose rock present within amphibole-dominant mafics.

A distinct permeability difference can be observed between mafic rocks and schistose metasediment at Latte. Wide and broad disseminated mineralization as intersected in Latte west is found within schistose-dominant areas. Petrographic examination of the schistose rocks at Latte shows strong interconnectivity between laths of mica (Figure 5.25). As mineralizing fluid passes through a conduit at Latte it reacts with mica in the host rock. In very mica-rich host rocks, this fluid would begin to bleed outwards out of the conduit into the host by reacting with interconnected grains of mica.

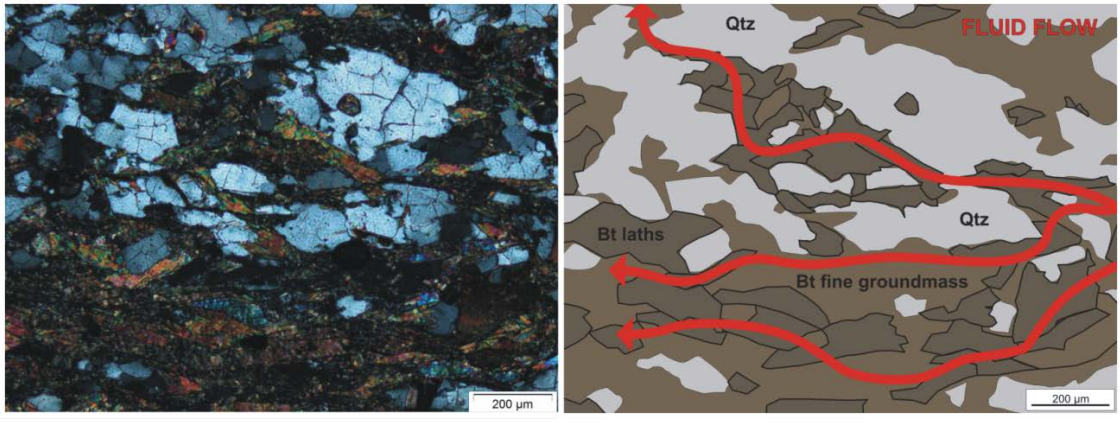


**Figure 5.25: A) Sample 105-139, biotite schist with interconnected laths of biotite. B) Cartoon simplification of A, demonstrating the path ore-stage fluid would take to consume biotite and precipitate As-Py with Au. The interconnected micas provide an optimal and permeable path for the fluid.**

This results in the complete sulphidation and replacement of metamorphic mica in broad panels along wide schistose corridors. Fluid reacts with the mica proximal to the fluid source or conduit, and then pervades throughout the host rock reacting with adjacent mica laths (as illustrated in Figure 5.25). Where mica connectivity is poor (rocks with lower overall mica content), the fluid does not pervade as easily or widely. In amphibole-dominant mafic rocks, this fluid does not react with amphibole and cannot reach the rarer mica, thus hindering gold deposition.

# Chapter 6

## 6 Discussion

The host rocks have been subdivided into the Upper and Lower Latte packages. Upper Latte consists of interleaved biotite and muscovite schist with rare amphibolite and structurally overlies the Lower Latte package. The transition from the Upper sequence to the Lower sequence correlates with a spike in Mg # between biotite-rich metasediment and amphibole-rich metavolcanic rocks. The contact between the Upper and Lower sequences dips moderately to the southwest. It is stratigraphically higher in the northeast of the Latte zone (Figure 6.1). The Lower Latte sequence is composed of two main rock units: amphibolite with minor biotite content, and intermixed amphibolite and metagabbro. The Lower Latte sequence is of variable thickness, and can be in tectonic contact with either the Supremo orthogneiss or Upper Latte schistose rocks. Lower Latte is identified as a thick tectonic slice.

## 6.1 Host Rock Assemblages

Geologic mapping by Ryan et al., (2013) has assigned the thick domain of schistose rocks which makes up the Latte zone to the Snowcap assemblage. This is an assembly of schist and rare mafic metavolcanics which demonstrate geochemical affinity with the ancestral North American margin. The Snowcap assemblage is composed of mixed psammitic schist, quartzite, dark grey carbonaceous schist, calc-silicate rocks, and local mafic metavolcanics. It is interpreted as pre-Late Devonian age metamorphosed continental margin sediment with rare layers of basaltic flows (Piercey and Colpron, 2009). The rocks also are variably calcareous and contain common bands or layers of marble, locally traceable as 50-100m thick horizons (Piercey and Colpron, 2009). Rocks of the Upper Latte sequence at Coffee are classified as Snowcap assemblage schist due to similar lithology. No quartzite or carbonaceous schist units are observed at Latte.

In contrast, Lower Latte rocks form a distinctly separate unit from the Upper Latte schists. This sequence consists of two distinct metabasaltic rocks, as well as coarse and variably foliated metagabbro. While mafic metavolcanics are observed within the

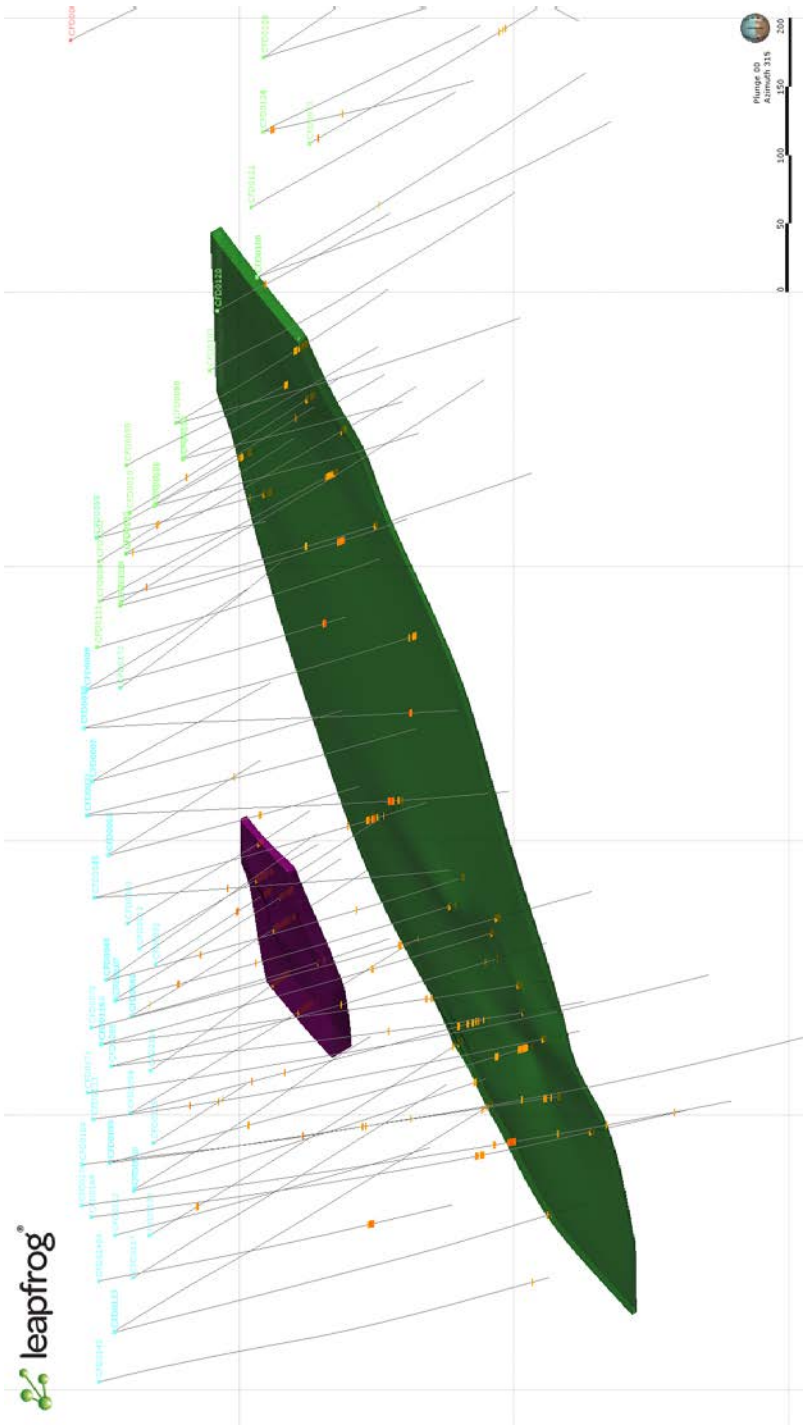


**Figure 6.1: Leapfrog 3-D image of the Latte zone looking northeast. The green panel represents the sudden change in rock package from Upper Latte Snowcap assemblage schist above, to Lower Latte mafic metavolcanics below. Dip of the panel follows regional tectonic imbrication and closely approximates foliation in the Latte zone rocks (moderately to the southwest). Orange markers on drill holes represent Mg # >70. The panel of Slide Mountain ultramafic rock is the purple polygon.**

Snowcap assemblage as 1-10m horizons, no large bodies of metagabbro are documented (Piercey and Colpron, 2009). Three overlying arc sequences form the remainder of the YTT: the Finlayson, Klinkit, and Klondike assemblages. Comparison of metabasalt from the Upper Latte sequence with metabasalt in Lower Latte reveals a greater biotite content in the Upper Latte rocks, in addition to more Fe-rich biotite. Geochemical differences between the two panels of rocks will be examined later in this chapter. The change in lithology from schistose rocks to a thick panel of mafic metavolcanics with distinct petrographic differences in addition to sharp geochemical changes suggests that the Lower Latte panel is not a part of the Snowcap assemblage. It is instead suggested that Lower Latte is a tectonic slice of arc rocks of the Finlayson, Klondike, or Klinkit assemblages.

The thick ultramafic bodies found within the Latte zone are weakly foliated to unfoliated and appear to be in tectonic contact with the surrounding host. This morphology is well documented in the Klondike region by MacKenzie and Craw (2012) and MacKenzie et al., (2013), where serpentinized ultramafic slabs are tectonically emplaced along low angle thrust faults during the Jurassic. These slabs are postulated to be large, tectonically emplaced slices of Slide Mountain assemblage ultramafics (MacKenzie et al., 2013). Slices of ultramafics are discontinuous both at Latte and within the Klondike region, most likely due to dismemberment during tectonic emplacement.

Rocks at Latte and the Coffee property have undergone multiple episodes of deformation and metamorphism. Two major prograde deformational events affected the area before the Cretaceous: the Klondike orogeny ca. 250 Ma, and the Jurassic thrust-assembly of the Dawson Range rocks. These metamorphic events affected all rocks greater than approximately 180 Ma. The Klondike orogeny is preserved by amphibolite facies mineralogy, while Jurassic thrust-assembly is visible in greenschist facies mineralogy in some areas of the Latte zone. Typical prograde metamorphic mineral assemblages for each both events are identified in Table 6.1.

**Table 6.1: Generalized metamorphic mineralogy of Latte host rocks.**

| Lithology | Klondike Orogeny Mineralogy (Amphibolite Facies) | Jurassic Thrust-Assembly Mineralogy (Greenschist Facies) |
|---|---|---|
| Biotite Schist | Biotite, quartz, feldspar | Chlorite, epidote, albite, sericite, ± carbonate |
| Muscovite Schist | Phengite, quartz, feldspar | Albite, sericite, ± carbonate |
| Amphibolite (Upper and Lower Latte) | Hornblende, biotite, quartz | Chlorite, epidote, weak actinolite, ± carbonate |
| Ultramafic slices | None: avoided amphibolite facies metamorphsim | Magnesite, talc, serpentine, chlorite, magnetite |
| Metagabbro and Amphibolite (Lower Latte) | Hornblende, biotite, quartz | Actionlite, epidote, chlorite, ± carbonate |

The Permian Klondike orogeny is generally suggested to be responsible for the $D_2$ metamorphic event (MacKenzie and Craw, 2010; Bailey, 2013). This event is defined by the corresponding regional $S_2$ foliation visible in the mafic and schistose rocks at Latte, excluding serpentinite and the late dikes. Rocks experienced mid/upper-amphibolite facies metamorphism as evidenced by the uniform presence of amphibole in all mafic rocks at Latte. No garnet has been observed within rocks in the Latte package, although rare garnet has been observed within the Supremo orthogneiss (Cruikshank, 2011). As such, the peak metamorphic grade achieved at Coffee is amphibolite facies.

A secondary regional metamorphic event occurred within the Jurassic during thrust stacking of packages of schist and gneiss within the Dawson Range. This event occurred at approximately 180 Ma and consisted of low-angle thrust stacking of dismembered components of the YTT along the previously defined $S_2$ fabric. This low angle emplacement is a potential source of the domains of foliation parallel strain recorded at Coffee as RQM zones. Metamorphic grade peaked at greenschist facies and is represented by chlorite and epidote replacement (Table 6.1). It is possible that original $D_2$ metamorphic minerals are overprinted or reset by this secondary event, however no significant mineralogical change is detected and it is visually impossible to distinguish between the two events. Slightly north of the Coffee property, amphibole grains within amphibolite at Thistle Creek record Ar-Ar mica cooling ages of ~180 Ma, implying at least a resetting in metamorphic age and possibly even the age of the dominant metamorphic event (Villeneuve et al., 2003).

No geochronology has been conducted on the schistose rocks of the Latte package to determine the age of the transpositional foliation. There are therefore three potential sources for the dominant foliation: 1) the Late Permian $D_2$ deformational event ($S_2$ foliation), 2) low-angle foliation due to Jurassic thrust assembly, and 3) transpositional foliation due to Mid-Cretaceous rapid unroofing. There is significant variability in age of rocks surrounding the Coffee Creek area. In addition to the Jurassic age of amphibole at Thistle Creek to the north, a Late Permian date was reported by McKenzie et al. (2013) for quartz-biotite schist at the Boulevard prospect to the southwest. No Cretaceous age has been reported within the Yukon, although Dusel-Bacon et al. (2002) reported Early Cretaceous ages for hornblende, biotite, and muscovite in the Lake George assemblage of the Yukon-Tanana Upland in Alaska.

## *Assembly of the Latte Host Rocks*

During the mid-Paleozoic, the Finlayson and Klinkit assemblages were being deposited onto the Snowcap assemblage outboard of the North American margin (Piercey and Colpron, 2009). Slide Mountain Ocean formed between the Yukon-Tanana terrane and the ancestral North American margin during this time. A reverse in subduction polarity resulted in the closing of Slide Mountain Ocean and the tectonic event termed the Klondike Orogeny and associated Klondike assemblage arc volcanism occurring ~260 Ma. Klondike assemblage magmatic activity was also responsible for the Sulphur Creek monzogranite; the foliated augen gneiss of the Supremo zone at Coffee in contact with the Latte schistose rocks. The monzogranite was emplaced at 257.9 +/- 3.5 Ma and shares the same $S_2$ foliation as the surrounding schistose rocks due to the $D_2$ deformational event (Klondike orogeny). During the closure of Slide Mountain Ocean, slices of Slide Mountain terrane ophiolite were incorporated into the YTT, with complete closure occurring during the Jurassic. Peak metamorphic grade experienced during the $D_2$ deformational event was approximately mid-amphibolite facies, though rocks to the north of Coffee in the Klondike region only reached upper-greenschist facies (MacKenzie and Craw, 2012).

The complex mixture of arc metavolcanics and metasedimentary rocks of the YTT experienced orogenic collision with the North American continental margin during the Jurassic, when complete closure of the Slide Mountain Ocean occurred (Mackenzie et al., 2013). This Jurassic collision resulted in internal tectonic imbrication of the Yukon-Tanana terrane with localized greenschist facies metamorphism in addition to emplacement of slices of Slide Mountain ultramafic rock along low angle thrust faults and folds. This episode imparted the $D_3$ and $D_4$ structural features to the Yukon-Tanana rocks.

The complex internal duplication of the YTT during Jurassic orogenesis accounts for the reverse stratigraphic order of host rocks within the Latte zone. Packages of rock at Latte are emplaced along low angle Jurassic thrust faults during this orogenic event, which accounts for the appearance of Snowcap assemblage schist (Upper Latte) stratigraphically above the mafic metavolcanics of an as-of-yet unknown arc sequence (Lower Latte). These Jurassic thrust faults also incorporated a slice of Slide Mountain assemblage ultramafic within the Upper Latte tectonic stratigraphy. The greenschist facies overprint within the Latte zone which consists of chlorite and epidote alteration is attributed to the late stages of this Jurassic thrusting. This retrogression occurs at the end stage of brittle-ductile, foliation-parallel shearing during thrust emplacement. Localized regions of high shear, termed Ribbon Quartz Mylonite by Kaminak workers, are constrained to the planes of thrust faulting and are not temporally related to mineralization at Latte.

The tectonic assembly of the Latte zone host rocks is a complex but not unique occurrence. Other examples within the Dawson Range include the Klondike region, as well as the Moose Creek thrust to the southwest. Thrust emplacement of tectonic units and packages of rock within the Klondike region is discussed in detail by Mackenzie et al., (2008). To the southwest, the post-Triassic and NE-vergent Moose Creek thrust juxtaposes the Late Devonian and older Scottie Creek formation with a large panel of Permian Klondike schist to the northeast (Ryan et al., 2013). A panel of identical Klondike schist occurs to the northwest of the Coffee property in fault contact with the package of Snowcap assemblage schist that hosts the Latte zone.

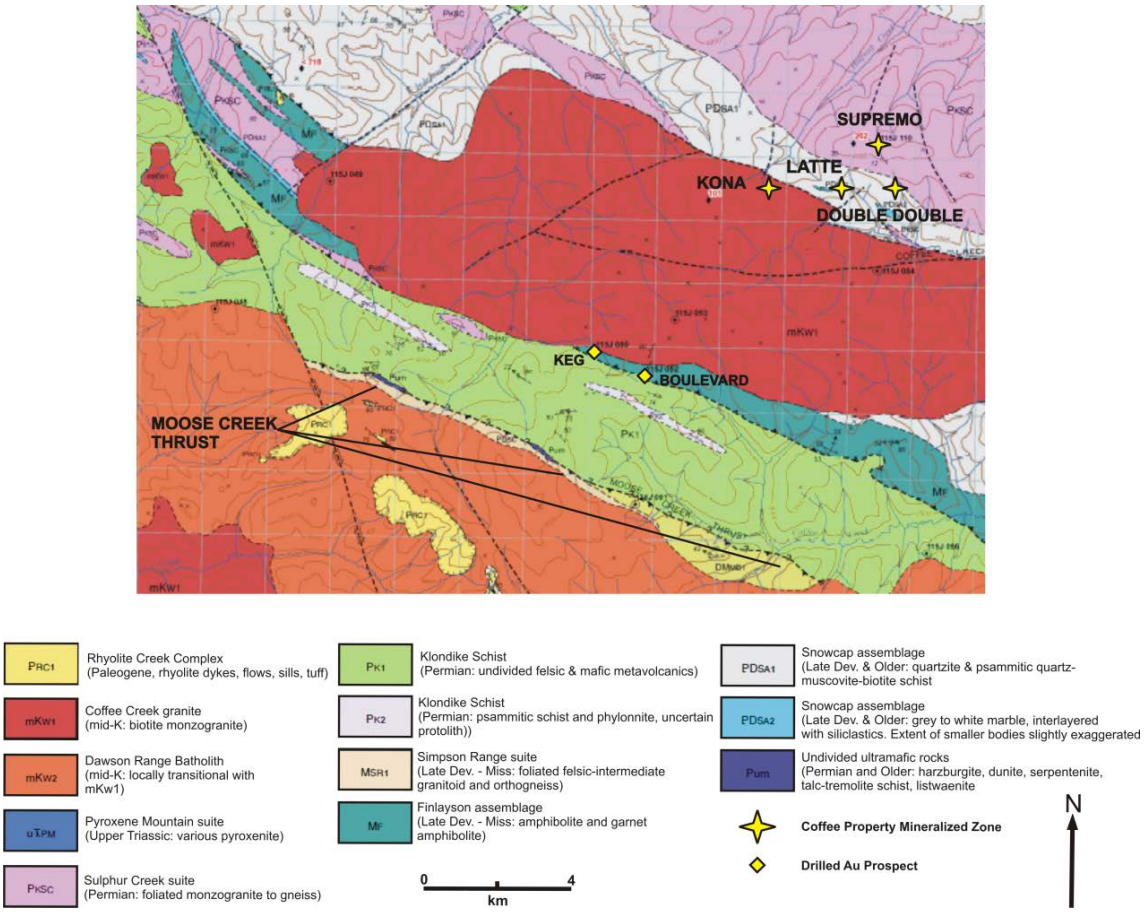


**Figure 6.2: Map of the Dawson Range with the Moose Creek thrust fault marked. The incorporation of ultramafic thrust slices in the Latte package along roughly NE-trending thrust faults mimics the incorporation of Permian ultramafic pods along the Moose Creek thrust to the SE of the Coffee property. Modified after Ryan et al., (2013).**

Thin pods of Permian aged ultramafic rock are tectonically emplaced along the Moose Creek thrust, most likely members of the Slide Mountain assemblage (Figure 6.2). This geometry is the same as that seen to the north in the Klondike region, and also as seen at Coffee within the Latte zone. These similarities reinforce that the Slide Mountain serpentinite at Latte was tectonically emplaced along a commonly-oriented thrust system.

The origin of the Lower Latte panel of mafic metavolcanic rocks can be attributed to two possible assemblages: the Klondike or Finlayson. Panels of Finlayson assemblage mafic metavolcanics are common in the map area. They occur to the southwest of the Coffee property on the southern margins of the Coffee Creek granite, notably as the host for the Boulevard gold prospect. A portion of Klondike schist exposed to the northwest of

Coffee with Snowcap assemblage schist overlying it in thrust contact. The unit is overthrust at its south-eastern limit by the same panel of Snowcap assemblage schist as hosts the Latte zone. This Klondike schist unit may continue below the Snowcap schist to the southeast and represent the Lower Latte panel.

Dikes at the Latte zone and Coffee property are late in the geologic history of the area and appear to exploit brittle fault structures. Orientation of the dikes appears to be purely controlled by the orientation of strike-slip fault structures. Dikes which appear to strike north in the eastern portion of the Latte zone are potentially following a subsidiary NE-trending mineralized structure designated as Latte North. This structure begins in the eastern portion of Latte. This explains the observed difference between dike orientations in the west and east of Latte.

## 6.2 Geochemistry of the Latte Host Rocks

Several types of rock were geochemically examined, including the amphibolites and ultramafics within the Latte zone, and dikes at Coffee and Latte.

### *Latte Amphibolite*

Samples of foliated amphibolite from the Latte zone were analysed, with four key samples shedding light on the genesis of the mafic rocks within the Latte zone. Most amphibole-rich samples from the Latte zone were heavily altered and retrogressed, although the four key samples were relatively fresh. The key samples were 82-170.6, 114-272, 114-295, and 114-296, representing CFD0082 in the Latte west area and CFD0114 in Latte east. All samples share a roughly common foliation as described within the previous chapter (dipping moderately to the west-southwest), implying that all amphibolites at Latte were present prior to $D_2/D_3$ metamorphism and the $S_2/S_3$ foliation.

The four samples are interpreted to represent three different suites and four individual rock types. Sample 82-170.6 and 114-272 are superficially very similar rocks: both are amphibole-dominant, contain up to 15% biotite, and are strongly foliated. Both samples are interpreted as metabasalts; however they are geochemically very distinct. Sample 82-170.6, from the Upper Latte package, is geochemically constrained by this

study as alkali basalt with within-plate and continental rift affinity. Sample 82-170.6 was the only sample to show an enrichment of Nb and Ta, forming an enriched hump that is diagnostic of alkali basalt (Sun and McDonough, 1989; Dusel-Bacon and Cooper, 1999). No arc-related geochemical signatures are found. The sample is inter-layered with metasediment and matches the description of Snowcap assemblage mafic meta-volcanics as defined by Piercey and Colpron (2009) extremely closely (Table 6.2). This metabasalt was most likely formed during an episode of Neoproterozoic - early Paleozoic continental rifting along the western Laurentian margin. Sample 114-272 is from the Lower Latte package and is geochemically constrained as andesitic basalt of N-MORB affinity with an arc calc-alkaline signature. The sample is depleted in LREE and exhibits a distinct Nb-Ta depletion which is diagnostic of arc rocks (Sun and McDonough, 1989; Dusel-Bacon and Cooper, 1999). It is interpreted as a metabasalt formed during arc-volcanism during the formation of either the Klondike or Finlayson assemblages.

The two other key samples were from CFD0114, located in the eastern portion of the Latte zone. They were selected from the lower mafic panel of the Latte zone, which is first intersected in CFD0114 at 255m down-hole. Samples 114-295 and 114-296 are

**Table 6.2: Select geochemical data for mafic meta-volcanic rocks from the Finlayson Assemblage, Snowcap Assemblage, and the Latte zone. Note the similarity between Snowcap rocks and sample 82-170.6. Latte mafic rocks appear to be enriched in Cr relative to the other suites.**

| **Region** | **Finlayson Lake Mafics** | | | **Snowcap Mafics** | | **Latte Amphibolite** | | | |
|---|---|---|---|---|---|---|---|---|---|
| **Group** | *2A* | *2B* | *2C* | *Amph.* | *Grn.Stone* | *82-170* | *114-272* | *114-296* | *10-180* |
| **Mg#** | 65.41 | 55.88 | 55.93 | 35.86 | 34.01 | 37.44 | 38.93 | 59.35 | 61.08 |
| **$SiO_2$** | 53.78 | 49.23 | 48.51 | 47.51 | 46.56 | 47.6 | 53.8 | 49.9 | 44.6 |
| **$TiO_2$** | 0.36 | 1.74 | 1.07 | 2.09 | 2.49 | 3.57 | 0.56 | 0.44 | 0.2 |
| **Zr/Y** | 1.57 | 5.36 | 2.67 | 4.76 | 6.23 | 8.32 | 3.51 | 1.54 | 0.49 |
| **Zr** | 14 | 149 | 67 | 160 | 252 | 262 | 46 | 19 | 3 |
| **Nb** | <LD | 18 | 1 | 21 | 29 | 45.1 | 2 | 0.6 | 0.4 |
| **Ni** | 133 | 47 | 45 | 127 | 60 | 174 | 42 | 224 | 112 |
| **Cr** | 324 | 185 | 133 | 250 | 90 | 410 | 190 | 1250 | 930 |

taken from within a complex metabasaltic/metagabbroic unit. The samples are nearly identical geochemically. Whole-rock geochemistry was conducted on sample 114-296, however not on 114-295. Based on field relationships and petrographic study, sample 10-

180 can be selected to represent 114-295 in whole-rock data (Figure 6.3). These metabasaltic samples are interpreted as subvolcanic dikes of subalkaline basalt with arc tholeiite affinity, with the metagabbroic samples being the coarse grained intrusive equivalent of the same melt source.

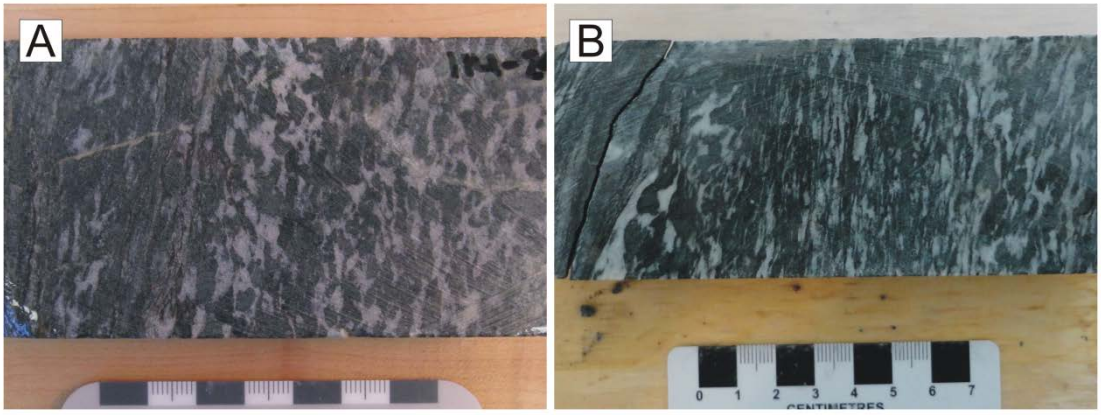


**Figure 6.3: Sample photographs of equivalent metagabbroic samples from the Latte zone: A) 114-295, amphiboles analysed on microprobe; B) 10-180, sample analysed for whole-rock geochemistry. Both samples are petrographically identical and part of the same mafic panel in the Latte zone.**

Based on the geochemistry and building on the petrographic data and drill logs, there are two general panels of rocks within the Latte zone: Upper Latte, dominantly composed of metasediment and rare metavolcanics, and Lower Latte, composed of mafic metavolcanics and rarer metasediment. The schistose rocks at Latte have been assigned to the Snowcap assemblage. Sample 82-170.6, found within these schistose rocks, geochemically matches with Snowcap assemblage mafic metavolcanics as defined by Piercey et al. (2009). In contrast, the samples from the thick mafic panel, Lower Latte, are much more Mg-rich and are arc-related. As the panel is thick and continuous across the entire lower portion of the Latte zone it is interpreted as a tectonic slice of mafic metavolcanic rocks with arc signatures. Based on the regional geology this panel could either represent Finlayson assemblage metavolcanics, diagnostic of the Yukon-Tanana terrane, or a slice of Klondike assemblage mafic metavolcanics. Both are arc assemblages and are present within the region: Finlayson assemblage rocks outcrop to the north-east and southwest of the Coffee property, and Klondike assemblage rocks outcrop to the east

and west of the property. This footwall mafic panel also influences areas of mineralization, as will be discussed later in this chapter.

Ultramafic rocks at the Coffee property tend to be extremely altered. As such, interpreting geochemical data is difficult, as whole-rock compositions are rarely representative of the sample prior to alteration. Slices of ultramafic rocks were emplaced across the entire Latte zone during Jurassic thrust assembly of the Latte package (MacKenzie and Craw, 2012). Thrust emplacement of ultramafic rocks is well documented to the southwest of the Coffee Property along the Moose Creek thrust. Ultramafic lenses of variable thickness incorporated between Permian Klondike schist and the Late Devonian Scottie Creek formation, a similar rock package to the Snowcap assemblage schist (Ryan et al., 2013). The ultramafic slices at Latte are type examples of Slide Mountain assemblage serpentinite as defined by MacKenzie and Craw (2012).

All dikes in this study are interpreted as components of the Whitehorse Plutonic Suite, the magmatic suite responsible for the Coffee Creek granite and the Dawson Range batholith. At Kona, both dacite and andesite dikes are observed to cut the Coffee Creek granite. This constrains at least one series of dikes, both felsic and mafic, to younger than ~98 Ma. The Kona andesite dike shares geochemical affinity with the Supremo andesite samples from CFD0020. This andesite dike from CFD0020 was dated to 101.7 +/- 1.3 Ma by U-Pb zircon dating, and was emplaced within felsic gneiss (A J. Wainwright and A. Simmons, unpublished data, 2010). One of the mineralized Latte dacite dikes was dated to 104 +/- 1.5 Ma (A J. Wainwright and A. Simmons, unpublished data, 2010). This sample is one of the two which share a common magmatic source with the Coffee Creek granite. This date is within error of the upper age limit of emplacement of the Coffee Creek granite (approximately 101 Ma, dating by McKenzie et al. (2013)).

During the emplacement of the Coffee Creek Granite, a mafic and felsic dike component of the Whitehorse Plutonic suite was active. Based on the geochemical data, dacitic diking related to the Coffee granite occurred in the Coffee region syn-to-pre-emplacement of the granite as well as post-emplacement. Mafic dikes at Coffee are related to an evolving magmatic chamber rather than the exact same source as the granite. Two main geochemical groups of dikes can be identified from this single magmatic source, with one group slightly more enriched in REE than the other. The current

youngest age recorded for a dike on the Coffee property, in very limited geochronological study, is 101.7 +/- 1.3 Ma. Dikes on the property have been observed to occupy structural corridors hosting mineralization suggesting that diking continued post emplacement of the Coffee Creek granite, exploiting brittle structures. Regardless, all dike samples analysed in this study are related to intrusive activity constrained roughly from 104 Ma to 98 Ma or less. The possibility exists that a portion of the dikes present on the property are related to younger regional magmatic events, ex. Carmacks volcanism ca. 70 Ma (Godwin, 1975).

## 6.3 Latte Mineralization

The Latte gold zone is strongly controlled by a set of project-scale WNW-NW trending dextral strike-slip faults called the Coffee Creek fault system. This fault system initiated movement during the Mid-Cretaceous as a subsidiary splay of the larger, regional-scale Big Creek fault (Sanchez et al., 2013). The Big Creek fault is interpreted as an old Jurassic-aged thrust fault which was subsequently rotated and pulled into a near-vertical orientation and reactivated as a dextral strike slip fault during the Mid-Cretaceous (M.G. Sanchez, personal communication). This fault is responsible for significant dextral offset, much of which would have been transferred NW to the Coffee Creek faults in the Mid-Cretaceous. A series of NE to NNE trending brittle-normal faults accommodate the sinistral shear applied by the dextral strike-slip movement of the larger Coffee Creek faults. These faults generally are found within the Supremo felsic gneiss panel due to the brittle nature of the orthogneiss.

The Latte structures strike ESE and are mineralized for over 1550 metres. Due to the mineralogy and texture of disseminated, first-phase mineralization at Latte, it is inferred that the initial steep Latte corridors were formed as a normal fault zone with very little movement. No significant lateral or normal movement can be inferred from the Latte structures, and later brecciation overprints an initial fault zone which formed near the brittle-ductile transition. Structures are observed to cut through all lithologies on the property and were multiply reactivated after the initial disseminated mineralization event. The initial event is inferred to have occurred at the ductile-brittle transition during Mid-

Cretaceous unroofing of the Dawson Range, while later brecciation is indicative of continued movement along the Latte structures within a brittle regime. Mid-Cretaceous uplift and extension has been observed at the Boulevard and Longline gold deposits.

The structural history of the Coffee Creek fault system is poorly studied, however field evidence indicates a protracted history of movement and reactivation of existing fault structures. Significant movement along the main Coffee Creek faults is required for two reasons. The Coffee Creek south fault runs along the contact of the Coffee Creek granite, offsetting the schistose rock package with the granite for an unknown distance. If no significant movement occurred along this fault surface after the emplacement of the granite (98.2 +/- 1.3 Ma), a substantial thermal halo and extensive contact metamorphism would be expected in the schistose and mafic rocks due to the proximity of the pluton. This is not observed in the Latte rock package except for a weakly developed region of hornfelsing exposed near the contact. Secondly, the granite itself is mineralized, indicating that the fault system was active after cooling of the pluton.

### *Disseminated Mineralization and Mica Sulphidation*

The discovery of “sooty sulphide” rich mineralized intervals during early drilling at Latte allowed for observation of mineralized intervals before destruction by oxidation due to late meteoric fluid influx. The initial phase of mineralization at Latte consisted of strong fluid-rock interaction within a relatively static normal fault corridor. The fluid contained a dominant elemental assemblage of As, Sb, $CO_2$, and Au, with minor Ag and rare Cu. Fluid flow was controlled by the steep Latte fault structure, and is observed to have fully utilized the corridor, as alteration and mineralization is found at all levels along the structure.

This fluid reacted with mica within host rocks adjacent to the fluid conduit, resulting in the sulphidation of Fe within the metamorphic parent mica and formation of Au-rich arsenian pyrite and Ti-rich white mica (illite) which pseudomorphs the parent mica. This initial hydrothermal mica has been designated HT1. In addition to the sulphidation reaction, strong dolomitization of silicate minerals occurred. This reaction is

only observed within mineralized zones and is responsible for the initial deposition of Au at Latte. While no mass balance calculations have been completed, due to the sheer volume of mica-rich rocks within the schistose Latte zone it is assumed that the majority of Au mineralization occurred due to this reaction.

The sulphidation of mica by $CO_2$-rich fluid continued to varying stages of completion. Some mineralized intervals consist completely of illite, dolomite, arsenian pyrite, and primary quartz, while others retain traces of metamorphic mica which escaped full consumption. High-grade disseminated intervals at Latte are assumed to have experienced complete sulphidation and dolomitization, while lower grade disseminated intervals would have either: 1) experienced less fluid interaction, and therefore less Au-bearing arsenian pyrite formation; 2) contained less mica to sulphidize and therefore lower levels of arsenian pyrite formation. Following deposition of HT1 white mica and arsenian pyrite, a second generation of mica of purely hydrothermal composition is observed to form as thin laths directly out of solution. This HT2 hydrothermal mica is extremely fine-grained and observed in close association with dolomite. The deposition of this HT2 mica signals the end of the initial mica sulphidation reaction: no arsenian pyrite is associated with its deposition.

## *Fluid Composition and Alteration Styles*

A slightly acidic and reducing fluid consisting of $H_2O$-$CO_2$-S-As-Sb-Ag is proposed as the ore-stage fluid at Latte. The temperature is roughly constrained to a range of 220 – 250° based on stability ranges of > 220° for illite and 150 - 250° for arsenian pyrite (Hedenquist et al., 1995). Gold is likely carried in an ionic complex with $HS^-$ acting as a ligand, with $CO_2$ acting as a wall rock pH buffer during fluid transport (Benning and Seward, 1996; Phillips and Evans, 2004). The presence of kaolinite as an oxidative overprint suggests a cooler, meteoric source for late oxidative fluids.

Analysis of select drill core samples with a PIMA spectrometer indicated common mineralization-phase mineralogy. All mineralized samples contain illite as the HT1 white mica. The PIMA data well supports the mineral chemistry and petrography.

Mineralization requires the sulphidation of metamorphic phengite or biotite and creation of a secondary, Ti-rich white mica (illite). Kaolinite is present within both mineralized and un-mineralized samples. All samples which contain kaolinite are at least marginally oxidized, and dominantly heavily oxidized. Kaolinite is interpreted as a late clay alteration phase resulting from cool, meteoric, acidic, oxidizing fluid ingress down the Latte structures. Clay alteration within sulphide facies zones (un-oxidized) is considered the result of superfine illite alteration as a result of intense fluid-rock interaction.

### *Remobilization of Gold*

Remobilization of disseminated Au-bearing arsenian pyrite by a $CO_2$-rich fluid occurs following the series of mica replacement. Two possibilities for the source of this fluid can be postulated:

1) The same fluid which caused the mica sulphidation reaction and deposition of Au-bearing arsenian pyrite continues to flow through the Latte structures, consuming HT1 and HT2 phase white mica as well as consuming Au-bearing arsenian pyrite. This fluid completely bleaches previously mineralized schistose intervals and re-deposits Au-bearing arsenian pyrite within dolomite-quartz veins and sooty sulphide “mats”.
2) A secondary $CO_2$-rich fluid flows through the Latte structures and begins to consume HT1 and HT2 phase white mica in addition to consuming Au-bearing arsenian pyrite. This leads to near-complete dolomitization of previously-mineralized intervals and re-deposition of Au-bearing arsenian pyrite in the same manner as the first possibility.

In both cases, a $CO_2$-rich fluid interacts with previously mineralized intervals to remobilize Au. The gold budget of carbonic fluids is not known, however subsequent recrystallization of arsenian pyrite requires Fe, S, As, Au, and Sb. Both scenarios result in the formation of V3-phase dolomite-quartz-arsenian pyrite veins. Carbonate-fluid remobilization explains the abundance of arsenian pyrite veinlets and concentrations seen

throughout heavily altered intervals at depth. The formation of sulphide-matrix breccia suggests that the dolomite-quartz-arsenian pyrite fluid travelled through the system with occasional jumps or drops in fluid pressure. These pressure changes could have been caused by the pumping of fluid through an actively slipping fault zone (Micklethwaite and Cox, 2004). Numerous phases of brecciation followed the remobilization and re-deposition of Au-bearing arsenian pyrite. Due to the heavy cataclasis and alteration experienced by mineralized zones, crosscutting phases of breccia are not observed. The three dominant phases of late brecciation consist of broad intervals of Fe-carbonate matrix brecciation, silica-rock flour matrix brecciation, and late calcite brecciation.

Late Fe-carbonate brecciation is widespread and has been observed to brecciate mineralized intervals, supporting clasts containing disseminated mineralization within a Fe-carbonate (ankerite) matrix. The Fe-carbonate matrix is identical to V4 Fe-carbonate veinlets which are found throughout Latte. As such, the breccias are interpreted as the high-energy equivalent to the thin, fracture-controlled Fe-carbonate veinlets. Silica-rock flour matrix brecciation is common within mineralized intervals, but has also been observed in un-mineralized host rock. The morphology of the breccia indicates that it is a brittle, late event which does not contribute to mineralization. While fine sulphide is found in the groundmass, it is due to intense communition of the breccia clasts, releasing sulphide into the groundmass.

## *Lithological Control*

Mineralization at Latte and Coffee is not only structurally controlled, but lithologically controlled. Numerous rocks within the Latte package are either poor hosts for Au mineralization, or act as aquitards. The thick panel of Slide Mountain assemblage serpentinite intersected in numerous drill holes in Latte west/central is heavily altered, but un-mineralized. This suggests two possible scenarios, either: 1) the serpentinite was permeable to mineralizing fluid, but unreactive as no mica is present; 2) the serpentinite was not permeable to mineralizing fluids resulting in pooling of the fluid on the margins and potential high grade mineralization due to concentration of fluid, and was subsequently altered by a later $CO_2$ rich fluid.

Pre-existing marble layers within the metamorphic stratigraphy were clearly unreactive with the ore fluids. These marble bands acted as impermeable barriers to fluid, only allowing for dolomitization and sulphidation of the intervening micaceous layers. This confinement of the ore fluid potentially allows for greater efficiency in mica sulphidation and Au deposition by forcing the fluid through a confined corridor and promoting maximum mica-fluid interaction. The replacement of silicate minerals by dolomite and white mica results in volume reduction which further increases the ability of the fluid to pervade through the host.

The most obvious lithological control on mineralization at Latte and Coffee is the presence of mica-rich host rocks. The dominant mineralization observed at Latte is due to the sulphidation of mica. This reaction is potentially responsible for all gold mineralization at Latte, with later remobilization. As such, the presence of mica-rich host rocks is vitally important to Au mineralization. Structures which intersect mica-poor host rocks such as metabasalt, metagabbro, or mica-poor ribbon quartz mylonite do not yield significant mineralization. Thin ore zones intersected within the Lower Latte mafic rocks are interpreted as biotite-rich schistose intervals within the mafic metavolcanic package. These schistose intervals are occasionally high-grade, as the ore fluid does not react with the surrounding amphibole-rich rocks. As this fluid comes into contact with permeable and reactive mica-rich schist, it is confined within the schistose lens, resulting in complete replacement of the host, and optimal sulphidation.

## 6.4 Discussion of Genetic Models

The Latte zone, and Coffee deposit as a whole, represents a unique gold system. Latte is a gold-only deposit with no significant base metal correlations. Gold is hosted within extremely As-rich pyrite (up to 15 wt. % As), and is characterized by elevated antimony. Latte also exhibits a weak correlation with gold-silver and gold-calcium in some cases. The mineralizing fluid is $CO_2$-rich and slightly acidic as evidenced by Au-phase illite-sericite and the intense dolomitization of schistose rocks.

Mineralization is both structurally and lithologically controlled, with steeply SSW dipping structural corridors controlling fluid flow, and rock type controlling the major

phase of gold deposition. Deposition of Au-bearing As-rich pyrite is controlled by wall-rock sulphidation reaction requiring a Fe source in the form of metamorphic biotite and phengite. Initial mineralization is not associated with veining, although secondary remobilization of Au-bearing sulphide occurs within a dolomite-quartz vein phase. Orogenic quartz veins reminiscent of Au-bearing Klondike quartz veins and Au-bearing veins at the Golden Saddle deposit are present within the package, but were not responsible for gold mineralization.

Alteration at the Latte zone consists of greenschist-facies retrogressive alteration throughout the host rock package, crosscut by texturally destructive, mineralization-phase dolomite-illite alteration due to fluid influx along structures. Later kaolinite alteration due to oxidizing meteoric fluid ingress overprints most rocks at Coffee but is not related to mineralization. No epithermal-style alteration haloes are observed surrounding mineralized corridors at Latte beyond the initial dolomite-illite alteration phases.

The Latte zone can be summarized by the following features. It is: structurally and lithologically controlled; gold-only; vein-poor; and formed from $CO_2$-S-As-Sb rich fluid. The unique metal geochemistry exhibited by Latte eliminates many of the typical classification for deposits in the region.

A common style of gold system within the Tintina Gold Belt is reduced intrusion-related gold deposits. A typical reduced-intrusion related gold system displays anomalous Bi, W, and Te in addition to low salinity and $CO_2$-rich ore fluids (Hart and Goldfarb, 2005). In addition, these deposits are located proximal to reduced, alkaline, volatile-rich plutons, and have low sulphide content within ores hosted in the igneous bodies. Finally, low grade auriferous sheeted vein systems are typically found within the pluton cupolas. Latte was formed from $CO_2$-rich ore fluids, however the Bi, W, and Te anomalies are not observed. Similarities between mineralization within the Coffee Creek granite at the Kona zone and the Latte zone eliminate the granite as a major heat source. Therefore, Latte is not a reduced intrusion-related gold system. At Latte, fine grained As-rich pyrite hosts micron-scale gold mineralization. The absence of mercury and thallium anomalies

as well as the absence of significant carbonate host rocks eliminates the possibility of Latte being a Carlin-type gold system (Emsbo et al., 2006).

While mineralization at Latte exhibits a weak gold-silver correlation, it does not show any significant gold-base metal correlations. This eliminates the possibility that Latte is a typical epithermal gold system (White and Hedenquist, 1995). A low sulphidation epithermal model can immediately be eliminated as a possibility for the Latte zone, as mineralization is clearly not tied to open-space veining, and disseminated ore is the dominant ore style at Latte. When attempting to apply an epithermal model to Latte, it is immediately apparent that the Latte zone shares characteristics with both low and high sulphidation deposits (Hedenquist et al., 1994). The typical deep, mineralizing fluid assemblage (illite) roughly matches that of low sulphidation deposits; however the disseminated nature of the ore favours high sulphidation deposits. Gold-silver ratios at Latte (5:1) are consistent with epithermal mineralization. However, the absence of base metals property-wide is again not consistent with these systems. The presence of dolomite, illite, a $CO_2$-rich fluid, and disseminated ore, and a lack of any base metal association all illustrate that Latte is not dominantly an epithermal ore deposit. It should be noted, however, that epithermal-like textures not associated with mineralization are observed on the Coffee property. Intervals of chalcedonic quartz brecciation and infill-veins are observed in some areas. These intervals appear to be late and are not related to disseminated mineralization at Latte.

### *Orogenic Gold Deposits*

The term “Orogenic Gold” comprises a large and varied classification of gold deposits. These deposits are broadly defined as epigenetic hydrothermal gold systems which form in varied host rocks at a set range of depths in close association with orogenic belts (Groves et al., 1998). A number of key features of orogenic deposits have been summarized by previous workers (Groves, 1993; Groves et al., 1998; McCuaig and Kerrich, 1998; Phillips and Powell, 2010). Features of orogenic deposits relevant to the Latte zone include:

1) Orogenic mineralization occurs over depths from 2-20 km, a temperature range of 200-700°C, and pressures from 0.5-5 kbar;
2) Mineralization occurs in transpressional or compressional settings commonly along subsidiary structures of major crustal faults;
3) Mineralization is controlled by fault geometry, rock composition, and host rock permeability;
4) Alteration assemblages include ankerite-dolomite-white mica-chlorite at greenschist facies;
5) Sulphide content of the deposits is usually 3-5% pyrite and arsenopyrite, with gold:silver ratios ranging from 10:1 to 1:1. Deposition of ore is controlled by veins and wall rock sulphidation;
6) Typical elemental associations include Au-Ag ± As, B, Bi, Hg, Mo, Sb, Te, W, and minor Cu, Pb, and Zn.
7) Gold is transported in a kilometre-scale regional fluid of low salinity, slightly acidic to near-neutral, and aqueous-carbonic composition as a reduced sulphur complex.

The above listed features are a sample of characteristics of orogenic gold deposits which are observed at the Latte zone. Notable absent characteristics include the absence of sheeted Au-bearing quartz veining and higher mineralization-phase sulphide abundance. It should be noted that not all common characteristics of the orogenic gold classification are required to be met, as the definition is broad and strives to encompass a wide range of deposits.

## *Local Orogenic Gold Deposits*

A number of mineralized prospects are located within the immediate vicinity of the Latte zone. The Boulevard prospect 10 km to the SW of Coffee contains a set of sheeted orogenic quartz-sulphide-carbonate veins hosting gold mineralization within mafic schist. The Toni Tiger molybdenum showing immediately adjacent to Boulevard hosts quartz-molybdenite veins dated to 96-95 Ma. Fluid inclusion study of mineralized quartz veins from both prospects indicates that the prospects are genetically related and formed from

$H_2O$-$CO_2$-NaCl orogenic fluids of low salinity between 279 and 310°C and >1 kbar. The Boulevard prospect retains a distinctly mesothermal-orogenic signature due to the presence of sheeted quartz veins and nearby molybdenite mineralization, in addition to the Au-As-Sb-(Pb-Zb-Cu) metal associations (McKenzie et al., 2013).

The 93-92 Ma Longline deposit is also structurally controlled and contains high-grade Au (~30 g/t) hosted within sheeted quartz veins (Joyce, 2002). Mineralization occurs within dilational zones in a broad compressional setting within shallowly ENE dipping, NNW striking brittle reverse fault structures within the Dawson Range batholith. The alteration assemblage associated with mineralization includes muscovite, sericite, Fe-carbonate, pyrite, arsenopyrite, minor clay, quartz, and tourmaline. Au-bearing quartz veins precipitated from a $H_2O$-$CO_2$-$CFl_4$-NaCl + $N_2$ fluid of moderate salinity between temperatures of 260 and 300°C, at a pressure of approximately 1.3 – 1.9 kbar and a depth of 5-7 km. The source of the fluid is also unknown, as the associated Moosehorn Range intrusions (equivalent to the Coffee Creek granite and Dawson Range batholith) have been determined to not be the source of metals (Joyce, 2002). Both systems represent mesothermal orogenic Au systems with a distinctive mineralogy and similar sheeted vein systems.

## *The Epizonal Orogenic Gold Model*

Based on the evidence presented in this study, an epizonal, early-brittle stage orogenic gold model is proposed for the Latte zone. Mineralizing fluid at Latte likely represents the cooler (220-250°C), shallower extension of regional orogenic mineralizing fluid responsible for mineralization at the Boulevard and Longline prospects. Regional exhumation in the Dawson Range followed shortly after the emplacement of the Dawson Range batholith and Coffee Creek granite (Allan et al., 2013; McKenzie et al., 2013). The exhumation resulted in brittle fracturing as a result of dextral strike-slip movement along the Coffee Creek fault array, and was accompanied by fluid flow and varying mineralization. The rapid uplift and exhumation is implicated as the driver of fluid flow. In this model, the Boulevard and Longline prospects represent the deeper, mesozonal components of the orogenic gold system, while Latte represents the epizonal component.

The anomalous characteristics of Latte can be explained as a result of Latte being the epizonal component of the system. A $CO_2$-rich mineralizing fluid flowed through the region, powered by an anomalous geothermal gradient due to the rapid unroofing of the Dawson Range during the Mid-Cretaceous. This fluid formed sheeted quartz veins rich in Au and with a weak base metal association (Boulevard), depleting the fluid of $SiO_2$. Fluid continued to flow and moved upwards into the epizonal region (Latte), pumping through brittle faults at a temperature of 220-250°C. This fluid retained the dominant characteristics of the original fluid responsible for sheeted quartz veining, but with a simplified composition due to prior mineralization. The original fluid was clearly rich in $CO_2$, As, Sb, S, and Au, but depleted its base metals and silica content during vein formation. As such, the fluid that reached the epizonal domain of the Latte zone was a $CO_2$-As-Sb-S-Au ±Ag orogenic mineralizing fluid, explaining the gold-only nature of Latte mineralization.

While the gold-only nature and lack of significant metal associations of the Latte zone is relatively unique in the Dawson Range, the structural and lithological controls as well as fluid composition and ore and alteration mineralogy as demonstrated in this thesis fit the epizonal orogenic model well. The timing of the orogenic systems in the vicinity of the Latte zone is slightly atypical of a traditional orogenic gold deposit. According to Groves et al., (1998), the timing of most orogenic gold deposits is syn-to-post-peak metamorphic. Peak metamorphism in the Dawson Range is thought to have occurred during the Late Permian, roughly synchronous with the formation of the pervasive and regionally-observed $S_2$ foliation. However, the lack of Ar-Ar dating on amphibole and metamorphic mica at Latte raises the possibility that the unroofing of the Dawson Range was a significant event in the area. Work by McCausland et al. (2006) identified very rapid unroofing of the Dawson Range batholith, which intruded approximately 12km below surface but passed through K-Ar biotite and hornblende closure temperatures (500 and 300˚C) by ~98 Ma. This rapid unroofing and exhumation in the Mid-Cretaceous provides significant context for Dawson Range gold mineralization.

Orogenic gold mineralization at the Golden Saddle deposit occurred at ~160 Ma, following the collision of the YTT with North America (completed by ~180 Ma), which

fits with the typical age relationships observed between orogen development and mineralization (Groves et al., 1998; Bailey, 2013). In contrast, the orogenic mineralized systems at Boulevard and Longline are interpreted to have formed during rapid uplift and exhumation of the Dawson Range within a very tight time frame following magmatism. This uplift occurred syn-to-post-emplacement of the Dawson Range batholith and Coffee Creek granite. Mineralization has been constrained to ~96-95 Ma at Boulevard, and ~93-92 Ma at Longline, with mineralization at Boulevard occurring a minimum of 3 Ma after emplacement of the Coffee Creek granite and ~4 Ma after emplacement of the Dawson Range batholith (McKenzie et al., 2013). While no geochronological study on mineralized rocks at Latte or Coffee has been completed to date, it is inferred that mineralization at Latte formed syn-to-slightly-post Boulevard mineralization as the shallower extension of the system. This estimate dates mineralization at Latte with an upper limit of $\leq$ 96 Ma; however no constraint on a lower limit for mineralization can be applied.

The mineralizing fluid was clearly rich in Au; however a source for the metals has not been identified. Typical orogenic gold models imply that Au is leached from a nearby gold-enriched host rock and subsequently deposited. At Coffee, no gold-enriched host rocks are present. Within the region, however, three possibilities exist: 1) pre-existing VMS mineralization occurring within the Devonian-Mississippian Finlayson assemblage (Touleary occurrence); 2) Jurassic-aged orogenic mineralization such as the Golden Saddle deposit; 3) older, intrusion-related mineralization formed in association with Late Permian metaplutonic rocks. While these are just a few potential sources for gold, it is unknown which, or if any of the above contributed gold to Coffee.

The source of the mineralizing fluid at Latte is difficult to pin down. Most hydrothermal ore deposits are formed from the following styles of fluids: 1) magmatic; 2) meteoric; 3) metamorphic fluid sourced from devolatilization reactions; 4) a deep crustal source. At Latte, the suggested fluid chemistry does not imply a magmatic source as described above. Meteoric fluids were clearly present at the Coffee property as a late, oxidative overprint; however it is unknown whether meteoric fluids played a role with mineralization (ex. fluid mixing). As the true magnitude of the unroofing and exhumation

is currently unknown, it is a possibility that metamorphic devolatilization supplied fluid in the immediate area of the Coffee property during unroofing (Phillips and Powell, 2010). Without study of fluid inclusions and isotopic variations it is difficult to determine the source of mineralizing fluids at Latte. The mineralizing fluid clearly carried gold in excess; however the source of the fluid and Au is currently unknown. Despite the enigmatic fluid and gold source, it is clear that mineralizing fluid at Latte closely resembles orogenic fluids at the Boulevard prospect. Both appear to be $H_2O$-$CO_2$-S-As-Sb-and Au rich, with Boulevard exhibiting weak base metal correlations and Latte showing as gold-only.

# Chapter 7

# 7 Conclusions

The Latte zone is a structurally and lithologically-controlled, epizonal, early-brittle orogenic gold deposit. The deposit is hosted within a corridor of thrust-emplaced slices of Yukon-Tanana terrane rocks. From surface, a thick package of Paleozoic Snowcap assemblage quartz-biotite-feldspar schistose rocks termed the Upper Latte package overlies a package of arc-derived mafic metavolcanic rocks, termed Lower Latte. These rocks are in contact with the Klondike assemblage Sulphur Creek orthogneiss to the NE, a 257.9 +/- 3.5 Ma foliated monzogranite which intruded the Snowcap assemblage schistose rocks during arc volcanism associated with the Klondike orogeny. The corridor of schistose rocks is in contact to the SW with the Coffee Creek granite, a 98.2 +/- 1.3 Ma phase of the Whitehorse Plutonic suite of subduction-related magmatism. The schistose rocks in the corridor were thrust-emplaced during the Jurassic closing of Slide Mountain Ocean along a previously-existing $S_2$ foliation defined by mica and amphibole alignment. This thrust emplacement was accompanied by low-angle shearing and the tectonic incorporation of a thick slice of Slide Mountain assemblage serpentinite into the Upper Latte sequence.

Three distinct mafic rock suites are found throughout Latte: 1) biotite-rich, high-Fe metabasalt within the Upper Latte Snowcap assemblage schist; 2) biotite-rich, low-Fe and high Mg metabasalt within the Lower Latte mafic package; and 3) high-Mg, amphibole-dominant metabasalt and metagabbro within the Lower Latte mafic package. Trace element fingerprinting of the mafic rocks at Coffee demonstrates that the Lower Latte metabasalt and metagabbro have distinct arc signatures, while the Upper Latte metabasalt does not. This implies that the Lower Latte mafic package is a distinct tectonic slice of arc-derived mafic metavolcanic rocks of either the Finlayson or Klondike assemblages, as Snowcap assemblage metabasalt is not arc-derived. Late dikes on the Coffee property include dikes of andesitic, intermediate, and dacitic compositions. All dikes on the property share similar trace element patterns; however two distinct suites can be identified based on varying levels of REE depletion. Based on geochemical similarities to the Coffee Creek granite and limited geochronological work, all dikes in this study are interpreted as components of the Whitehorse Plutonic suite. Dikes analysed

in this study are constrained to intrusive activity occurring between roughly 104 and 101 Ma, however geochronological work is extremely limited and the potential exists for numerous suites of younger dikes.

Mineralization at the Latte zone is hosted by steep, brittle structures dipping steeply (65-85 degrees) to the SSW. These structures are components of the Coffee Creek fault system, a WNW-NW trending dextral strike-slip structural regime activated during Mid-Cretaceous rapid unroofing and uplift of the Dawson Range. This fault system is considered a splay off of the regional-scale Big Creek fault to the SE which is responsible for significant dextral offset. The Latte structures were formed as a relatively passive offshoot of the Coffee Creek fault, a first-order NW-trending fault. A $H_2O$-$CO_2$-As-Sb-S-Au±Ag rich fluid travelled along the steep Latte structures, preferentially reacting with mica-rich schistose rocks in a wall-rock sulphidation reaction. This reaction proceeded with an initial phase of metamorphic biotite or phengite replacement by white mica (illite) in conjunction with complete dolomitization of silicate minerals and deposition of fine-grained, As-rich pyrite and minor arsenopyrite containing micron-scale gold. Following the first phase of white mica formation, secondary hydrothermal mica formed around the rims of mineralized intervals. Continued fluid influx into mineralized zones resulted in consumption of the mineralized sulphide by $CO_2$-rich fluid and remobilization within dolomite-quartz veins. This remobilization resulted in the re-deposition of fine grained Au-bearing arsenian pyrite along vein margins, and as heavy concentrations of “sooty sulphide” in some areas.

The Latte structures appear to have been generally passive during deposition of disseminated Au-bearing pyrite, although breccias of hydrothermal and tectonic character are observed throughout the deposit. Mineralization-phase brecciation appears to be related to the remobilization of sulphide due to continued carbonate fluid influx, and possibly was controlled by changes in lithostatic pressure due to sudden movement along the Latte fault structures. Later breccias cut mineralized intervals and are composed of either a silica-rock flour matrix, or Fe-carbonate unrelated to mineralization.

Host rocks at Latte which contain little-to-no metamorphic biotite or phengite do not react favourably with mineralizing fluid. Some rocks, namely the Slide Mountain serpentinite and the common bands of marble, appear to act as aquitards for mineralizing fluid and channel or concentrate the fluid in a specific area. Amphibole-rich rocks such as those dominating the Lower Latte mafic package do not react with the mineralizing fluid as little-to-no biotite or phengite is present within them to act as a host for sulphidation. Mica-rich host rocks are also highly permeable to the mineralizing fluid with interconnected laths of mica acting as a convenient fluid pathway for sulphidation, volume-reduction, and dolomitization.

Gold occurs as micron-scale inclusions within pyrite of extremely high arsenic content (up to 15 wt. %). Gold is liberated from the sulphide by late oxidative fluids which oxidize the sulphide and release the fine gold. Gold is only found within fine pyrite in association with dolomite and illite; cubic, pre-mineralization metamorphic pyrite grains are not associated with gold mineralization. Elemental enrichment associated with gold mineralization is dominated by arsenic and antimony, although weaker gold-silver and gold-calcium associations are noted at Latte.

Based upon the unique characteristics of the Latte zone, a Mid-Cretaceous epizonal orogenic model is suggested. This model best explains the gold-only and vein poor nature of mineralization at Latte. An orogenic model also accounts for the As, Sb, and weak Ag metal associations observed at Latte, and elegantly represents the shallower equivalent of mesozonal, quartz-vein hosted gold mineralization observed at the Boulevard prospect 10 km to the SW. This interpretation significantly differs from previous interpretations of the deposit as a distal, reduced intrusion-related deposit, an epithermal extension of the Casino porphyry, or as an epithermal analogue to the Golden Saddle deposit (Cruikshank, 2011; Chartier et al., 2013).

## 7.1 Exploration Implications

The results of this study have significant implications for mineral exploration in the Dawson Range, Yukon, as listed below:

- Mineralized fluid flow within the Dawson Range was clearly widespread and resulted in the formation of both meso-and-epizonal orogenic gold deposits. Within the current understanding of these deposits, the epizonal extension (Latte/Coffee) of the deeper orogenic mineralization resulted in a much more significant Au resource (3.2 Moz Au at Coffee). This style of Mid-Cretaceous mineralization has not been identified as such within the Dawson Range. Significant gold intercepts have been intersected surrounding the Coffee property and possibly represent other epizonal orogenic deposits in the area (ex. Comstock Metals Ltd., QV project).
- Mineralization is structurally controlled by a regional fault system and hosted in brittle subsidiary faults which splay off easily mappable, regional-scale dextral strike-slip faults. The identification of these regional-scale structures and their brittle, stress-accommodating counterparts is paramount to discovering gold mineralization of the same style as that of Latte and the Coffee project.
- The host rock composition plays a key role in mineralization. Schistose rock with a high mica content acts as a permeable, reactive host rock for orogenic mineralizing fluid. The identification of areas with schistose rock cut by brittle faults rather than mica-poor rocks increases the chances of a significant discovery.

Mineralized zones do not always have a corresponding surface geochemical signature. Drilling at the Latte zone beyond the westernmost extension of the Au-in-soil geochemical anomaly resulted in the intersection of heavily mineralized structures with no surface geochemical expression. Exploration efforts should not ignore less-prominent Au-in-soil anomalies if the anomaly lies in a structurally and lithologically favourable area.

## 7.2 Recommendations for Further Work

A number of questions are raised by this thesis that should be addressed in future study. Suggested areas of further study include:

- Radiometric dating of the pervasive transpositional fabric observed at Coffee to identify the timing of the development of foliation

- Geochronological study of mineralization-phase (HT1) hydrothermal illite, As-rich pyrite, and later white mica (HT2). The absence of veining associated with disseminated mineralization requires that the mica and pyrite are analysed.
- Fluid inclusion study and micro-thermometry of V3-phase dolomite-quartz veins responsible for remobilization of mineralized sulphide. This study would be useful in comparing mineralization at Latte with that seen at Boulevard and Longline.
- Isotopic study of mineralization-phase disseminated pyrite and remobilized pyrite. This study should be extended to mineralized sulphide at the Supremo and Double Double zones, to examine the extent of remobilized sulphide within the Coffee property.

# References

Allan, M.M., Mortensen, J.K., Hart, C.J.R., Bailey, L.A., Sánchez, M.G., Ciolkiewicz, W., McKenzie, G.G., Creaser, R.A. 2013. Magmatic and metallogenic framework of west-central Yukon and eastern Alaska. *In* Tectonics, Terranes, Metallogeny and Discovery in the northern circum-Pacific region. *Edited by* M. Colpron, T. Bissig, B. Rusk, and J. Thompson. Society of Economic Geologists Special Publication, **17**. pp. 111-168.

Amato, J.M., and Pavlis, T.L. 2010. Detrital zircon ages from the Chugach terrane, southern Alaska, reveal multiple episodes of accretion and erosion in a subduction complex. Geology, **38**(5): 459-462.

Arcus Development Group. 2011. Arcus Makes New VMS Discovery in Yukon White Gold District, Drills 14.15 Metres of 1.44% Cu, 16.5 g/t Ag, and 0.77 g/t Au. Press Release, October 4, 2011.

Bailey, L.A., 2013. Late Jurassic Fault-Hosted Gold Mineralization of the Golden Saddle Deposit, White Gold District, Yukon Territory. M.Sc. Thesis, Department of Earth and Ocean Sciences, The University of British Columbia, Vancouver, B.C.

Bakke, A.A. 1995. The Fort Knox "porphyry" gold deposit—Structurally controlled stockwork and shear quartz vein, sulphide-poor mineralization, hosted by a Late Cretaceous pluton, east-central Alaska. *In* Porphyry deposits of the northwestern Cordillera of North America. *Edited by* T.G. Schroeter. Canadian Institute of Mining, Metallurgy and Petroleum Special Volume, **46**, pp. 795–802.

Bakke, A.A., Morrell, B.G., Odden, J., Bergstrom, T., and Woodman, J. 2000. Kinross Gold USA's activities in the Fairbanks mining district, K2K. *In* The Tintina gold belt—Concepts, exploration, and discoveries. *Edited by* T.L. Tucker and M.T. Smith. British Columbia and Yukon Chamber of Mines, Special Volume **2**. pp. 89–98.

Bazard, D.R., Butler, R.F., Gehrels, G., and Soja, C.M. 1995. Early Devonian paleomagnetic data from the Lower Devonian Karheen Formation suggest Laurentia-Baltica connection for the Alexander terrane. Geology, **23**(8): 707-710.

Bennett, V., Colpron, M., and Burke, M. 2010. Current thinking on Dawson Range tectonics and metallogeny. Yukon Geological Survey, Miscellaneous Report 2: 12.

Benning, L.G., and Seward, T.M. 1996. Hydrosulphide complexing of Au (I) in hydrothermal solutions from 150–400 C and 500–1500 bar. Geochimica et Cosmochimica Acta, **60**(11): 1849-1871.

Beranek, L.P., and Mortensen, J.K. 2011. The timing and provenance record of the Late Permian Klondike orogeny in northwestern Canada and arc-continent collision along western North America. Tectonics, **30**(5).

Beranek, L.P., Mortensen, J.K., Orchard, M.J., and Ullrich, T. 2010a. Provenance of North American Triassic strata from west-central and southeastern Yukon: Correlations with coeval strata in the Western Canada Sedimentary Basin and Canadian Arctic Islands. Canadian Journal of Earth Sciences, **47**(1): 53-73.

Beranek, L.P., Mortensen, J.K., Lane, L.S., Allen, T.L., Fraser, T.A., Hadlari, T., and Zantvoort, W.G. 2010b. Detrital zircon geochronology of the western Ellesmerian clastic wedge, northwestern Canada: Insights on Arctic tectonics and the evolution of the northern Cordilleran miogeocline. Geological Society of America Bulletin, **122**(11-12): 1899-1911.

Berman, R., Ryan, J., Gordey, S., and Villeneuve, M. 2007. Permian to Cretaceous polymetamorphic evolution of the Stewart River region, Yukon-Tanana terrane, Yukon, Canada: P–T evolution linked with in situ SHRIMP monazite geochronology. Journal of Metamorphic Geology, **25**(7): 803-827.

Bradley, D.C., Dumoulin, J.A., Blodgett, R.B., Harris, A.G., Roeske, S.M., McClelland, W.C., and Layer, P.W. 2006. Geology and affinity of Alaska's Farewell terrane. Geological Society of America Abstracts with Programs, **38**(5): 12.

Bradley, D.C., Dumoulin, J., Layer, P., Sunderlin, D., Roeske, S., McClelland, B., Harris, A.G., Abbott, G., Bundtzen, T., and Kusky, T. 2003. Late Paleozoic orogeny in Alaska's Farewell terrane. Tectonophysics, **372**(1): 23-40.

Breitsprecher, K., Mortensen, J., and Villeneuve, M. 2004. YukonAge 2004: A database of isotopic age determinations for rock units from Yukon Territory. Yukon Geological Survey, Department of Energy, Mines and Resources, Government of Yukon.[CD-ROM.].

Cabanis, B., and Lecolle, M. 1989. Le diagramme La/10 Y/15 Nb/8: un outil pour la discrimination des series volcaniques et la mise en evidence des processus de melange et/ou de contamination crustale. Comptes Rendus de l'Académie des Sciences, **309**(ser. II): 2023–2029.

Campbell, J., Armitage, A., and Barnes, W. 2010. Technical report on the Nucleus property, Freegold Mountain Project, including an updated mineral resource estimate. Northern Freegold Resources Ltd., Vancouver, B.C.

Chartier, D., Couture, J.F., Sim, R., and Starkey, J. 2013. Mineral Resource Evaluation, Coffee Gold Project, Yukon, Canada. Technical Report (NI43-101). SRK Consulting, Vancouver, B.C.

Colpron, M., Nelson, J., and Murphy, D.C. 2006a. A tectonostratigraphic framework for the pericratonic terranes of the northern Canadian Cordillera. *In* Paleozoic Evolution and Metallogeny of Pericratonic Terranes at the Ancient Pacific Margin of North America, Canadian and Alaskan Cordillera. *Edited by* M. Colpron and J.L. Nelson. Geological Association of Canada, Special Paper, **45**: 1-23.

Colpron, M., Nelson, J., and Murphy, D.C. 2007. Northern Cordilleran terranes and their interactions through time. GSA Today, **17**(4/5): 4.

Colpron, M., Mortensen, J.K., Gehrels, G.E., and Villeneuve, M. 2006b. Basement complex, Carboniferous magmatism and Paleozoic deformation in Yukon-Tanana terrane of central Yukon: Field, geochemical and geochronological constraints from Glenlyon map area. *In* Paleozoic Evolution and Metallogeny of Pericratonic Terranes at the Ancient Pacific Margin of North America, Canadian and Alaskan Cordillera. *Edited by* M. Colpron and J.L. Nelson. Geological Association of Canada, Special Paper, **45**: 131-151.

Cook, F.A., and Erdmer, P. 2005. An 1800 km cross section of the lithosphere through the northwestern North American plate: lessons from 4.0 billion years of Earth's history. Canadian Journal of Earth Sciences, **42**(6): 1295-1311.

Creaser, R.A., Heaman, L.M., and Erdmer, P. 1997. Timing of high-pressure metamorphism in the Yukon-Tanana terrane, Canadian Cordillera: constraints from U-Pb zircon dating of eclogite from the Teslin tectonic zone. Canadian Journal of Earth Sciences, **34**(5): 709-715.

Creaser, R.A., Goodwin-Bell, J.-A.S., and Erdmer, P. 1999. Geochemical and Nd isotopic constraints for the origin of eclogite protoliths, northern Cordillera: Implications for the Paleozoic tectonic evolution of the Yukon-Tanana terrane. Canadian Journal of Earth Sciences, **36**(10): 1697-1709.

Cruikshank, P. 2011. Hydrothermal alteration and gold mineralization of the Supremo zone, Coffee Property, Yukon, Canada. B.Sc. Thesis, Department of Earth Sciences, The University of Western Ontario, London, ON.

Deer, W.A., Howie, R.A., and Zussman, J. 1966. An Introduction to the Rock-Forming Minerals. John Wiley and Sons, New York, N.Y.

Duk-Rodkin, A., and Shimamura, K. 1999. Glacial limits map of Yukon Territory. Geological Survey of Canada. Open File 3694. Scale 1:1 000 000.

Dusel-Bacon, C., and Cooper, K.M. 1999. Trace-element geochemistry of metabasaltic rocks from the Yukon-Tanana Upland and implications for the origin of tectonic assemblages in east-central Alaska. Canadian Journal of Earth Sciences, **36**(10): 1671-1695.

Dusel-Bacon, C., Lanphere, M.A., Sharp, W.D., Layer, P.W., and Hansen, V.L. 2002. Mesozoic thermal history and timing of structural events for the Yukon-Tanana Upland, east-central Alaska: 40Ar/39Ar data from metamorphic and plutonic rocks. Canadian Journal of Earth Sciences, **39**(6): 1013-1051.

Dusel-Bacon, C., Hopkins, M.J., Mortensen, J.K., Dashevsky, S.S., Bressler, J.R., and Day, W.C. 2006. Paleozoic tectonic and metallogenic evolution of the pericratonic rocks of east-central Alaska and adjacent Yukon Territory. *In* Paleozoic Evolution and Metallogeny of Pericratonic Terranes at the Ancient Pacific Margin of North America, Canadian and Alaskan Cordillera. *Edited by* M. Colpron and J.L. Nelson. Geological Association of Canada Special Paper, **45**: 25-74.

Emsbo, P., Groves, D.I., Hofstra, A.H., and Bierlein, F.P. 2006. The giant Carlin gold province: a protracted interplay of orogenic, basinal, and hydrothermal processes above a lithospheric boundary. Mineralium Deposita, **41**(6): 517-525.

Erdmer, P., Ghent, E.D., Archibald, D.A., and Stout, M.Z. 1998. Paleozoic and Mesozoic high-pressure metamorphism at the margin of ancestral North America in central Yukon. Geological Society of America Bulletin, **110**(5): 615-629.

Fallas, K., Erdmer, P., Archibald, D., Heaman, L., and Creaser, R. 1998. The St. Cyr klippe, south-central Yukon: An outlier of the Teslin tectonic zone. In Lithoprobe: Slave-Northern Cordillera Lithospheric Evolution (SNORCLE) and Cordilleran Tectonics Workshop, Lithoprobe Rep. pp. 131-138.

Gabrielse, H., Murphy, D.C., and Mortensen, J.K. 2006. Cretaceous and Cenozoic dextral orogen-parallel displacements, magmatism, and paleogeography, north-central Canadian Cordillera. *In* Paleogeography of the North American Cordillera: Evidence For and Against Large-Scale Displacements. *Edited by* J.W. Haggart, R.J. Enkin, and J.W.H. Monger. Geological Association of Canada, Special Paper, **46**: 255-276.

Godwin, C.I. 1975. Alternative interpretations for the Casino Complex and Klotassin batholith in the Yukon crystalline terrane. Canadian Journal of Earth Sciences, **12**(11): 1910-1916.

Goldfarb, R.J., Marsh, E.E., Hart, C.J., Mair, J.L., Miller, M., and Johnson, C. 2007. Geology and Origin of Epigenetic Lode Gold Deposits, Tintina Gold Province, Alaska and Yukon. *In* Recent US Geological Survey Studies in the Tintina Gold Province, Alaska, United States, and Yukon, Canada. *Edited by* L.P. Gough and W.C. Day. US Geological Survey Scientific Investigations Report: A1-A18.

Grond, H., Churchill, S., Armstrong, R., Harakal, J., and Nixon, G. 1984. Late Cretaceous age of the Hutshi, Mount Nansen, and Carmacks groups, southwestern Yukon Territory and northwestern British Columbia. Canadian Journal of Earth Sciences, **21**(5): 554-558.

Groves, D.I. 1993. The crustal continuum model for late-Archaean lode-gold deposits of the Yilgarn Block, Western Australia. Mineralium Deposita, **28**(6): 366-374.

Groves, D.I., Goldfarb, R.J., Gebre-Mariam, M., Hagemann, S., and Robert, F. 1998. Orogenic gold deposits: a proposed classification in the context of their crustal distribution and relationship to other gold deposit types. Ore geology reviews, **13**(1): 7-27.

Guidotti, C.V. 1984. Micas in metamorphic rocks. *In* Micas. *Edited by* S.W. Bailey. Reviews in Mineralogy and Geochemistry, **13**(1): 357-467.

Haeussler, P.J., Bradley, D.C., Wells, R.E., and Miller, M.L. 2003. Life and death of the Resurrection plate: Evidence for its existence and subduction in the northeastern Pacific in Paleocene–Eocene time. Geological Society of America Bulletin, **115**(7): 867-880.

Hansen, V., and Dusel-Bacon, C. 1998. Structural and kinematic evolution of the Yukon-Tanana upland tectonites, east-central Alaska: A record of late Paleozoic to Mesozoic crustal assembly. Geological Society of America Bulletin, **110**(2): 211-230.

Hart, C.J. 2007. Reduced intrusion-related gold systems. *In* Mineral deposits of Canada: A synthesis of major deposit types, district metallogeny, the evolution of geological provinces, and exploration methods. *Edited by* W.D. Goodfellow. Geological Association of Canada Special Publication, (5): 95-112.

Hart, C., and Goldfarb, R. 2005. Distinguishing intrusion-related from orogenic gold systems. *In* New Zealand Minerals Conference Proceedings. pp. 125-133.

Hart, C.J., Goldfarb, R.J., Lewis, L.L., and Mair, J.L. 2004. The Northern Cordilleran Mid-Cretaceous Plutonic Province: Ilmenite/Magnetite-series Granitoids and Intrusion-related Mineralisation. Resource Geology, **54**(3): 253-280.

Hart, C., McCoy, D., Goldfarb, R., Smith, M., Roberts, P., Hulstein, R., Bakke, A., and Bundtzen, T. 2002. Geology, exploration, and discovery in the Tintina Gold Province, Alaska and Yukon. *In* Integrated methods for discovery, global exploration in the twenty-first century. *Edited by* R.J. Goldfarb and R.L. Nielsen. Society of Economic Geologists Special Publication **9**: 241-274.

Hedenquist, J.W., Masuhisa, Y., Izawa, E., White, N. C., Giggenbach, W.F., and Aoki, M. 1994. Geology, geochemistry, and origin of high sulphidation Cu-Au mineralization in the Nansatsu District, Japan. Economic Geology, **89**(1): 1-30.

Hietanen, A. 1974. Amphibole Pairs, Epidote Minerals, Chlorite, and Plagioclase in Metamorphic Rocks, Northern Sierra Nevada, California'. American Mineralogist, **59**: 2240.

Jaworski, B.J. and Meyer, B., 2000. Geological and geochemical report on the Coffee Creek Intrusion-related gold project; Yukon Assessment Report 094064, 44p.

Jaworski, B.J. and Vanwermeskerken, M., 2001. Geological and Geochemical report on the Coffee Creek Intrusion-related gold target; Yukon Assessment Report 094207, 53p.

Jenner, G.A. 1996. Trace element geochemistry of igneous rocks: geochemical nomenclature and analytical geochemistry. In Trace element geochemistry of volcanic rocks: Applications for massive sulphide exploration: Geological Association of Canada, Short Course Notes. pp. 51-77.

Jilson, G., 2000. Geochemical and Geological Report on the Dan, Man and lndy Claims, Yukon Assessment Report 0954174, 173 p.

Johnston, S.T., 1995. Geological compilation with interpretation from geophysical surveys of the northern Dawson Range (115 J/9, 115 J/10 and 115 I/12), central Yukon (1:100,000 scale). Exploration and Geological Services Division, Yukon, Indian and Northern Affairs Canada, Open File 1995-2 (G).

Joyce, N.L. 2002. Geological setting, nature, and structural evolution of intrusion-hosted Au-bearing quartz veins at the Longline occurrence, Moosehorn Range area, west-central Yukon Territory. M.Sc. Thesis, Department of Earth and Ocean Sciences, The University of British Columbia, Vancouver, B.C.

Kaminak Gold Corporation, 2012. Kaminak Reports Maiden Inferred Mineral Resource Estimate of 3,236,000 ounces of Gold at the Coffee Project, Yukon. Press Release, December 13, 2012.

Le Maitre, R.W., Bateman, P., Dudek, A., Keller, J., Lameyre, J., Le Bas, M., Sabine, P., Schmid, R., Sorensen, H., and Streckeisen, A. 1989. A classification of igneous rocks and glossary of terms: Recommendations of the International Union of Geological Sciences Subcommission on the Systematics of Igneous Rocks. Blackwell Oxford.

Leake, B., Wooley, A.R., Arps, C.E.S., Birch, W.D., Gilbert, M.C., Grice, J.D., Hawthorne, F.C., Kato, A., Kisch, H.J., Krivovichev, V.G., Linthout, K., Laird, J., Mandarino, J.A., Maresch, W.V., Nickel, E.H., Rock, N.M.S., and Schumacher, J.C. 1997. Nomenclature of amphiboles: report of the subcommittee on amphiboles of the International Mineralogical Association, Commission on New Minerals and Mineral Names. The Canadian Mineralogist, **35**: 219-246.

MacKenzie, D., and Craw, D. 2010. Structural controls on hydrothermal gold mineralization in the White River area, Yukon. *In* Yukon Exploration and Geology 2009. *Edited by* K.E. MacFarlane, L.H. Weston, and L.R. Blackburn. Yukon Geological Survey. pp. 253-263.

MacKenzie, D., and Craw, D. 2012. Contrasting structural settings of mafic and ultramafic rocks in the Yukon-Tanana terrane. *In* Yukon Exploration and Geology 2011. *Edited by* K.E. MacFarlane and P.J. Sack. Yukon Geological Survey. pp. 114-127.

MacKenzie, D., Craw, D., and Mortensen, J. 2008. Thrust slices and associated deformation in the Klondike goldfields, Yukon. *In* Yukon Exploration and Geology 2007. *Edited by* D.S. Emond, L.R. Blackburn, R.P. Hill, and L.H. Weston. Yukon Geological Survey. pp. 199-213.

MacKenzie, D., Craw, D., Cooley, M., and Fleming, A. 2010. Lithogeochemical localisation of disseminated gold in the White River area, Yukon, Canada. Mineralium Deposita, **45**(7): 683-705.

MacKenzie, D., Craw, D., Brodie, C., and Fleming, A. 2013. Foliation development and hydrothermal gold emplacement in metagabbroic rocks, central Yukon, Canada. *In* Yukon Exploration and Geology 2012. *Edited by* K.E. MacFarlane and P.J. Sack. Yukon Geological Survey. pp. 47-64.

Mair, J.L., Hart, C., Goldfarb, R., O'Dea, M., and Harris, S. 1999. Geology and metallogenic signature of gold occurrences at Scheelite Dome, Tombstone gold belt, Yukon. *In* Yukon Exploration and Geology 1998. *Edited by* C.F. Roots and D.S. Emond. Yukon Geological Survey. pp. 165-176.

Mair, J.L., Goldfarb, R.J., Johnson, C.A., Hart, C.J., and Marsh, E.E. 2006. Geochemical constraints on the genesis of the Scheelite Dome intrusion-related gold deposit, Tombstone gold belt, Yukon, Canada. Economic Geology, **101**(3): 523-553.

Maloof, T.L., Baker, T., and Thompson, J.F. 2001. The Dublin Gulch intrusion-hosted gold deposit, Tombstone plutonic suite, Yukon Territory, Canada. Mineralium Deposita, **36**(6): 583-593.

Marsh, E.E., Hart, C.J., Goldfarb, R.J., and Allen, T.L. 1999. Geology and geochemistry of the Clear Creek gold occurrences, Tombstone gold belt, central Yukon Territory. *In* Yukon Exploration and Geology 1998. *Edited by* C.F. Roots and D.S. Emond. Yukon Geological Survey. pp. 185-196.

Marsh, E.E., Goldfarb, R.J., Hart, C.J., and Johnson, C.A. 2003. Geology and geochemistry of the Clear Creek intrusion-related gold occurrences, Tintina Gold Province, Yukon, Canada. Canadian Journal of Earth Sciences, **40**(5): 681-699.

McCuaig, T.C., and Kerrich, R. 1998. P-T-t-deformation-fluid characteristics of lode gold deposits: evidence from alteration systematics. Ore Geology Reviews, **12**(1): 381-453.

McDonough, W., Sun, S.-S., Ringwood, A., Jagoutz, E., and Hofmann, A. 1992. Potassium, rubidium, and cesium in the Earth and Moon and the evolution of the mantle of the Earth. Geochimica et Cosmochimica Acta, **56**(3): 1001-1012.

McKenzie, G.G., Allan, M.M., Mortensen, J.K., Hart, C.J., Sánchez, M., and Creaser, R.A. 2013. Mid-Cretaceous orogenic gold and molybdenite mineralization in the Independence Creek area, Dawson Range, parts of NTS 115J/13 and 14. *In* Yukon Exploration and Geology 2012. *Edited by* K.E. MacFarlane, M.G. Nordling, and P.J. Sack. Yukon Geological Survey. pp. 79-97.

Meschede, M. 1986. A method of discriminating between different types of mid-ocean ridge basalts and continental tholeiites with the Nb- Zr -Y diagram. Chemical Geology, **56**(3): 207-218.

Micklethwaite, S., and Cox, S.F. 2004. Fault-segment rupture, aftershock-zone fluid flow, and mineralization. Geology, **32**(9): 813-816.

Mihalynuk, M.G., Nelson, J., and Diakow, L.J. 1994. Cache Creek terrane entrapment: Oroclinal paradox within the Canadian Cordillera. Tectonics, **13**(3): 575-595.

Mortensen, J. 1990. Geology and U-Pb geochronology of the Klondike District, west-central Yukon Territory. Canadian Journal of Earth Sciences, **27**(7): 903-914.

Mortensen, J. 1992. Pre-mid-Mesozoic tectonic evolution of the Yukon-Tanana terrane, Yukon and Alaska. Tectonics, **11**(4): 836-853.

Mortensen, J.K., 1996. Geological compilation maps of the northern Stewart River map area, Klondike and Sixtymile Districts (115N/15, 16; 115O/13, 14; and parts of 115O/15, 16). Exploration and Geological Services Division, Yukon region, Indian and Northern Affairs Canada. Open File 1996-1 (G), 43 p.

Murphy, D.C., Mortensen, J.K., Piercey, S.J., Orchard, M.J., and Gehrels, G.E. 2006. Mid-Paleozoic to early Mesozoic tectonostratigraphic evolution of Yukon-Tanana and Slide Mountain terranes and affiliated overlap assemblages, Finlayson Lake massive sulphide district, southeastern Yukon. *In* Paleozoic Evolution and Metallogeny of Pericratonic Terranes at the Ancient Pacific margin of North America, Canadian and Alaskan Cordillera. *Edited by* M. Colpron and J.L. Nelson. Geological Association of Canada, Special Paper, **45**: 75-105.

Nelson, J., Colpron, M., Piercey, S.J., Dusel-Bacon, C., Murphy, D.C., and Roots, C.F. 2006. Paleozoic tectonic and metallogenetic evolution of pericratonic terranes in Yukon, northern British Columbia and eastern Alaska. *In* Paleozoic Evolution and Metallogeny of Pericratonic Terranes at the Ancient Pacific margin of North America, Canadian and Alaskan Cordillera. *Edited by* M. Colpron and J.L. Nelson. Geological Association of Canada Special Paper, **45**: 323-360.

Nokleberg, W.J., Parfenov, L.M., Monger, J.W., Norton, I.O., Chanďuk, A.I., Stone, D.B., Scotese, C.R., Scholl, D.W., and Fujita, K. 2000. Phanerozoic tectonic evolution of the Circum-North Pacific. U.S. Geological Survey Professional Paper 1626. US Department of the Interior, US Geological Survey.

Pavlis, T.L., and Roeske, S.M. 2007. The Border Ranges fault system, southern Alaska. *In* Tectonic growth of a collisional continental margin: Crustal evolution of south-central Alaska. *Edited by* K.D. Ridgway. Geological Society of America Special Paper, **431**: 95-128.

Pearce, J., and Cann, J. 1973. Tectonic setting of basic volcanic rocks determined using trace element analyses. Earth and Planetary Science Letters, **19**(2): 290-300.

Phillips, G.N., and Evans, K. 2004. Role of CO2 in the formation of gold deposits. Nature, **429**(6994): 860-863.

Phillips, G.N., and Powell, R. 2010. Formation of gold deposits: a metamorphic devolatilization model. Journal of Metamorphic Geology, **28**(6): 689-718.

Piercey, S.J., and Colpron, M. 2009. Composition and provenance of the Snowcap assemblage, basement to the Yukon-Tanana terrane, northern Cordillera: Implications for Cordilleran crustal growth. Geosphere, **5**(5): 439-464.

Plafker, G. 1987. Regional geology and petroleum potential of the northern Gulf of Alaska continental margin. *In* Geology and resource potential of the continental margin of western North America and adjacent ocean basins – Beaufort Sea to Baja California. *Edited by* D.W. Scholl, A. Grantz, and J.G. Vedder. CircumPacific Council for Energy and Mineral Resources Earth Science Series, **6**: 229-268.

Ross, C.A., and Ross, J.R. 1983. Late Paleozoic accreted terranes of western North America. *In* Pre-Jurassic rocks in western North American suspect terranes. *Edited by* C.H. Stevens. Society of Economic Paleontologists and Mineralogists. pp. 7-22.

Ruks, T.W., Piercey, S.J., Ryan, J.J., Villeneuve, M.E., and Creaser, R.A. 2006. Mid-to late Paleozoic K-feldspar augen granitoids of the Yukon-Tanana terrane, Yukon, Canada: Implications for crustal growth and tectonic evolution of the northern Cordillera. Geological Society of America Bulletin, **118**(9-10): 1212-1231.

Ryan, S., 2007. Geochemical Report, YMIP 06-056, Bridget Area and Coffee Creek Area; 46 p.

Ryan, S., 2008. Geochemical Report, YMIP 07-048, Coffee Creek Area; 43 p.

Ryan, J.J., and Gordey, S.P. 2001a. New geological mapping in Yukon-Tanana Terrane near Thistle Creek, Stewart River map area, Yukon Territory. Geological Survey of Canada Current Research 2001. A2.

Ryan, J.J., and Gordey, S.P. 2001b. Geology, Thistle Creek area, Yukon Territory (115O/3). Geological Survey of Canada. Open File 3690. Scale 1:50,000.

Ryan, J.J., and Gordey, S.P. 2002a. Bedrock geology of Yukon-Tanana terrane in southern Stewart River map area, Yukon Territory. Geological Survey of Canada Current Research 2002: A1.

Ryan, J.J., and Gordey, S.P. 2002b. Geology, southern Stewart River area, Yukon Territory (Parts 115 J/14, 115-O/2,3,4,5,7). Geological Survey of Canada. Open File 4338. Scale 1:100,000.

Ryan, J.J., and Gordey, S.P., 2004. Geology, Stewart River area (Parts of 115N/1,2,7,8, and 115-O/2-12), Yukon Territory. Geological Survey of Canada. Open File 4641. Scale 1:100,000.

Ryan, J.J., Gordey, S.P., Glombick, P., Piercey, S.J., and Villeneuve, M.E. 2003. Update on bedrock geological mapping of the Yukon–Tanana terrane, southern Stewart River map area, Yukon Territory. Geological Survey of Canada. Current Research 2003. A9.

Ryan, J.J., Zagorevski, A., Williams, S.P., Roots, C., Ciolkiewicz, W., Hayward, N., and Chapman, J.B. 2013. Geology, Stevenson Ridge (northwest part), Yukon. Geological Survey of Canada. Canadian Geoscience Map 117 (preliminary). Scale 1:100 000.

Sanchez, M.G., Allan, M.A., Hart, C.J., Mortensen J.K. 2013. Structural Control of Mineralization Recognized by Magnetite-Destructive Faults of the Western Yukon and Eastern Alaska Cordilleran Hinterland (Poster). Society of Economic Geologist (SEG) conference, Whistler 2013: Geoscience for Discovery, September 24-27, 2013, Whistler, BC.

Shives, R.B.K., Carson, J.M., Ford, K.L., Holman, P.B., Gordey, S.P., and Abbott, G. 2002. Airborne multisensory geophysical survey, Stewart River area, Yukon Territory, Phase 1 and 2 (Parts of 115N, O and 116B): 120 digital images of 1:50,000 (110) and 1:250,000 (10) scale colour interval maps, on CD-ROM, in Portable Document Format (PDF). Geological Survey of Canada. Open File 4311. (Also Yukon Exploration and Geological Services Division Open File 2002-17D).

Smith, M., Thompson, J., Bressler, J., Layer, P., Mortensen, J., Abe, I., and Takaoka, H. 1999. Geology of the Liese zone, Pogo property, east-central Alaska. Society of Economic Geologists Newsletter, **38**(1): 12-21.

Smith, P.L., Tipper, H.W., and Ham, D.M. 2001. Lower Jurassic Amaltheidae (Ammonitina) in North America: Paleobiogeography and tectonic implications. Canadian Journal of Earth Sciences, **38**: 1439–1449.

Sun, S.-S., and McDonough, W.F. 1989. Chemical and isotopic systematics of oceanic basalts: implications for mantle composition and processes. *In* Magmatism in the Ocean Basins. *Edited by* A.D. Saunders and M.J. Norry. Geological Society London, Special Publication, **42**(1): 313-345.

Tafti, R., and Mortensen, J.K. 2004. Deformed Early Jurassic Porphyry Cu (-Au) Deposits at Minto and Williams Creek, Carmacks Copper Belt, Western Yukon Territory. Geological Society of America Abstracts with Programs, **36**: 516.

Tempelman-Kluit, D. 1974. Reconnaissance Geology of Aishihik Lake, Snag and Part of Stewart River Map-areas, West Central Yukon (115A, 115F, 115G and 115K). Department of Energy, Mines and Resources.

Tempelman-Kluit, D. 1979. Transported cataclasite, ophiolite, and granodiorite in Yukon: Evidence of arc-continent collision. Geological Survey of Canada Paper, **79**(14): 27.

Unterschutz, J.L., Creaser, R.A., Erdmer, P., Thompson, R.I., and Daughtry, K.L. 2002. North American margin origin of Quesnel terrane strata in the southern Canadian Cordillera: Inferences from geochemical and Nd isotopic characteristics of Triassic metasedimentary rocks. Geological Society of America Bulletin, **114**(4): 462-475.

Villeneuve, M., Ryan, J., Gordey, S., and Piercey, S. 2003. Detailed thermal and provenance history of the Stewart River area (Yukon-Tanana terrane, western Yukon) through application of SHRIMP, Ar-Ar and TIMS. Geological Association of Canada and Mineralogical Association of Canada Abstracts, **28**: 344.

Wainwright, A.J., Simmons, A.T., Finnigan, C.S., Smith, T.R., and Carpenter, R.L. 2011. Geology of new gold discoveries in the Coffee Creek area, White Gold district, west-central Yukon. *In* Yukon Exploration and Geology 2010. *Edited by* K.E. MacFarlane, L.H. Weston, and C. Relf. Yukon Geological Survey. pp. 233-247.

Weiershäuser, L., Nowak, M., and Barnett, W. 2010. White Gold Property, Dawson Range, Yukon, Canada. Technical Report (NI43-101). SRK Consulting. Vancouver, B.C.

White, N.C., and Hedenquist, J.W. 1995. Epithermal gold deposits: Styles, characteristics, and exploration. Society of Economic Geologists Newsletter, **23**(1): 9-13.

Wilson, B.M. 1989. Igneous petrogenesis a global tectonic approach. Springer. Dordrecht, The Netherlands.

Winchester, J., and Floyd, P. 1977. Geochemical discrimination of different magma series and their differentiation products using immobile elements. Chemical Geology, **20**: 325-343.

# Appendix A: Sample Descriptions

| Sample | Description |
|---|---|
| 6-80 | Weakly mineralized and strongly clay altered dacite dike, strong white-mica retrogression. |
| 7-66 | Weakly mineralized and strongly clay altered dacite dike, strongly retrogressed to white-mica/illite. |
| 7-157.8 | Highly deformed and completely carbonate-altered ultramafic. |
| 9-183.5 | Strongly carbonate-altered metagabbro with crosscutting V3-phase dolomite-quartz veins. Veins leave As-rich halo, no Au. |
| 10-180 | Metagabbro, coarse hornblende crystals within a matrix of strongly retrogressed plagioclase. Common epidote, sericite, carbonate. |
| 35-253 | Strongly deformed and retrogressed mafic, strong epidote content, late fractures with calcite infill, minor quartz, feldspar. |
| 38-254 | Strong carbonate replacement, original textures obscured. Strong epidote content. |
| 40-206.9 | Strongly altered mafic, coarse epidote, zoisite, strong deformation fabric. Minor muscovite in patches. Heavily retrogressed. |
| 40-234.8 | Intensely altered ultramafic: near-complete carbonate replacement, minor serpentine. |
| 49-255.7 | Coarse grained tremolite-actinolite with strong carbonate component throughout. |
| 57-128 | Intensely hydrothermally altered metabasalt, coarse epidote, |

| | |
|---|---|
| | chlorite replacement. |
| 57-167.5 | Strongly retrogressed biotite schist, cubic pyrite, coarse epidote. |
| 61-131.15 | Heavily altered ultramafic, common serpentine, tremolite, randomly oriented, no fabric present. |
| 73-9.8 | Strongly altered ultramafic. Serpentine, talc, minor carbonate, Cr-magnetite. |
| 82-104.3 | Muscovite schist, large qtz-carbonate vein sealing a fracture. |
| 82-117.5 | Mineralized mica-schist, strong dolomite-illite replacement of primary mica accompanied by Au-bearing sulphidation. Fine late sericite. |
| 82-133.4 | Mineralized biotite schist, biotite nearly completely replaced by dolomite+illite. Strong arsenian pyrite along foliation. |
| 82-61 | Severely retrogressed biotite schist. Strong chlorite after biotite, minor ilmenite. Common calcite veining. |
| 82-135 | Extremely carbonate-replaced ultramafic. Large domains of chlorite, minor talc, common Cr magnetite. |
| 82-142 | Weakly foliated carbonate-replaced ultramafic. Serpentine, chlorite, magnesite, talc, weak thin calcite veins crosscutting. |
| 82-161.2 | Deformed biotite schist, minor carbonate. Epidote inclusions within feldspar porphyroblasts. |
| 82-168 | Band of foliation-parallel marble. Extremely fine grained carbonate with rare coarse 2mm grains. Minor opaques and quartz dispersed throughout. |
| 82-170.6 | Metabasalt. Up to 15% biotite throughout foliation, 80% |

| | |
|---|---|
| | amphibole, rare euhedral pyrite cubes and patches of quartz. |
| 82-199 | Altered dacite dike, approx. 35% plagioclase with strong kaolinite overprint obscuring rock features. |
| 82-223 | Strained qtz-kspar-biotite gneiss. Augens of K-feldspar and quartz with minor mica wrapping around. Quartz pulled into deformed lozenges. |
| 97-7 | Heavily fractured and dolomitized biotite schist, little to no biotite remaining. Matrix to brecciation consists of super-fine quartz, pyrite. |
| 97-30 | Mineralized quartz-muscovite schist, obliterated by dolomite and later carbonate, brecciated with dolomite-illite infill. |
| 97-45 | Oxidized biotite schist, moderate chlorite after biotite. Plagioclase replaced by fine grained sericite. |
| 97-68 | Quartz-rich muscovite schist, un-oxidized. Minor biotite with chlorite replacement. Minor plagioclase porphyroblasts. |
| 97-78 | Quartz-rich muscovite schist, weaker fabric than 97-68. Minor sericite after plagioclase. |
| 97-92 | Biotite schist, coarse feldspar porphyroblasts with weak sericite alteration. Minor yellow epidote and carbonate along foliation. |
| 97-102 | Mineralized schist, complete dolomite replacement and alteration. Polyphase carbonate veining, remobilization of Au-bearing sulphide. |
| 97-220 | Mineralized schist: complete illite-dolomite replacement, intense sulphidation with Au. |

| | |
|---|---|
| 97-253 | Thin andesite dike, unfoliated. Randomly oriented feldspars, strong kaolinite alteration obscuring 45% of sample. |
| 99-84.5 | Moderately clay altered andesite dike. |
| 99-86 | Moderately clay altered andesite dike. |
| 99-157 | Mineralized sample, domains of V2-phase quartz vein brecciated by dolomite-sulphide fluid, re-precipitation of sulphide. |
| 105-129 | Biotite schist, coarse feldspar porphyroblasts with strong sericite alteration. Minor chlorite after biotite. |
| 105-139 | Highly attenuated quartz-biotite schist. Strong sericitization, moderate pervasive clay alteration. |
| 105-144 | Completely carbonate-replaced ultramafic. Late fractures cut by recrystallized quartz veins. |
| 105-163 | Mineralized breccia, super-fine matrix of rock flour and silica, clasts sulphidized and strongly dolomitized, strong illite replacement. |
| 105-182 | Mineralized breccia, host clasts completely silicified, cut by thin dolomite-sulphide veinlets, later coarse dolomite veinlets. |
| 105-206 | Muscovite-biotite schist, common carbonate throughout. Low strain, minor cubic pyrite and plagioclase with weak sericitization. |
| 105-279 | Carbonate-rich biotite/muscovite schist. Moderately sericitized feldspar porphyroblasts. V2-phase quartz vein with moderate strain. |
| 105-318 | Quartz-biotite schist, green, Mg-rich biotite, minor chlorite, fine |

| | |
|---|---|
| | grained carbonate throughout. Cataclastic texture in quartz. |
| 105-323.5 | Strong talc, carbonate, epidote alteration of mafic protolith. |
| 113-120.4 | Strongly retrogressed ultramafic, coarse magnesite, serpentine, talc, chlorite in the matrix. |
| 113-121 | Intense talc-serpentine after ultramafic, continuation of 113-120.4 |
| 113-121.5 | Coarse brown biotite and epidote within schist. |
| 114-12 | Coarse carbonate occurring as layers within biotite schist in between biotite and quartz. Minor patchy epidote, feldspar with common inclusions. |
| 114-44 | Moderately retrogression biotite schist, common ilmenite along foliation. Moderate clay alteration along foliation (kaolinite), no carbonate. |
| 114-58.5 | Quartz-muscovite schist with highly attenuated brittle overprint on quartz. |
| 114-79 | Quartz-biotite schist with strong carbonate replacement, cut by late calcite veins. |
| 114-114 | Contact between fine-grained andesite dike and quartz-biotite-feldspar schist. |
| 114-116 | Biotite schist, coarse feldspars and cataclastic-textured quartz. |
| 114-162 | Breccia with clasts of sulphidized and dolomitized rock hosted within silica/rock-flour matrix. Fine sulphide within matrix is broken down from communition of clasts. |
| 114-178.9 | Large domains of carbonate within biotite schist. Recrystallized quartz , late carbonate veining. |

| | |
|---|---|
| 114-179 | Patches of carbonate through biotite schist, attenuated and recrystallized quartz, V2-phase quartz vein exhibiting recrystallization. |
| 114-190 | Highly deformed mafic/ultramafic. Long needles of yellow tremolite, minor talc, carbonate. |
| 114-222 | Strongly retrogressed biotite schist. Common zoned epidote, chlorite after biotite. |
| 114-272 | Metabasalt, 15% brown biotite with minor quartz ribbons. Moderate epidote alteration. |
| 114-295 | Metagabbro, coarse hornblende crystals within a matrix of strongly retrogressed plagioclase. Common epidote, sericite, carbonate. |
| 114-296 | Metabasalt, >90% amphibole with minor biotite, quartz. |
| 114-321 | Metabasalt, fine grained chlorite, moderate carbonate component |
| 114-333 | Augen gneiss, coarse quartz-feldspar augen with minor retrogression, blocky domains of carbonate. Foliation defined by muscovite. |
| 164-364.5 | Mineralized schist, complete dolomite-illite replacement of original host mica, strong sulphidation of mica by Au-rich arsenian pyrite. Dolomite veinlets with remobilized sulphide. |
| 164-366.5 | Mineralized schist, complete dolomite-illite replacement of original host mica, strong sulphidation of mica by Au-rich arsenian pyrite |
| 164-438.5 | Mineralized schist, complete dolomite-illite replacement of |

| | |
|---|---|
| | original host mica, strong sulphidation of mica by Au-rich arsenian pyrite |
| 164-456.5 | Mineralized schist, complete dolomite-illite replacement of original host mica, strong sulphidation of mica by Au-rich arsenian pyrite |
| 164-464.5 | Mineralized schist, complete dolomite-illite replacement of original host mica, strong sulphidation of mica by Au-rich arsenian pyrite, minor arsenopyrite. |
| 164-469.5 | Mineralized schist, complete dolomite-illite replacement of original host mica, strong sulphidation of mica by Au-rich arsenian pyrite. Fresh feldspar porphyroblasts. |
| 20-42 | Supremo andesite dike, large porphyritic feldspar crystals. Moderate clay replacement of feldspars. |

# Appendix B: Whole-rock Geochemistry

| SAMPLE | METHOD | ME-ICP06 | ME-ICP06 | ME-ICP06 | ME-ICP06 | ME-ICP06 | ME-ICP06 | ME-ICP06 | ME-ICP06 | ME-ICP06 | ME-ICP06 | ME-ICP06 | ME-ICP06 | ME-ICP06 | ME-ICP06 | C-IR07 |
|---|---|---|---|---|---|---|---|---|---|---|---|---|---|---|---|---|
| | ANALYTE | SiO2 | Al2O3 | Fe2O3 | CaO | MgO | Na2O | K2O | Cr2O3 | TiO2 | MnO | P2O5 | SrO | BaO | C | |
| | UNIT | % | % | % | % | % | % | % | % | % | % | % | % | % | % | |
| L001 | Dac. | 80.4 | 11.65 | 1.22 | 0.05 | 0.17 | 0.03 | 3.07 | <0.01 | 0.11 | <0.01 | 0.01 | <0.01 | 0.19 | 0.01 | |
| L002 | Dac. | 81 | 11.5 | 1.16 | 0.16 | 0.23 | 0.04 | 2.95 | <0.01 | 0.11 | 0.01 | 0.01 | <0.01 | 0.11 | 0.01 | |
| L003 | UM Dike. | 30.8 | 4.51 | 4.77 | 20.2 | 10.25 | 0.03 | 0.19 | 0.28 | 0.11 | 0.24 | 0.01 | 0.04 | 0.01 | 7.73 | |
| L004 | Mgbro. | 44.6 | 17.95 | 5.46 | 14 | 8.57 | 1.58 | 1.55 | 0.13 | 0.2 | 0.1 | <0.01 | 0.05 | 0.03 | 0.85 | |
| L005 | Mbst. | 46.8 | 16.2 | 5.31 | 11 | 7.8 | 3.04 | 2.92 | 0.04 | 0.17 | 0.1 | <0.01 | 0.07 | 0.05 | 1.52 | |
| L006 | Mbst. | 43.9 | 18.45 | 4.92 | 8.21 | 9.58 | 1.73 | 3.45 | 0.11 | 0.21 | 0.07 | 0.05 | 0.06 | 0.06 | 0.94 | |
| L007 | Mbst. | 60.2 | 11.55 | 6.51 | 7.39 | 2.56 | 1.2 | 2.84 | 0.01 | 0.6 | 0.11 | 0.15 | 0.06 | 0.34 | 1.04 | |
| L008 | Tic. Sch. | 46.5 | 4.2 | 3.59 | 15.15 | 8.33 | 0.04 | 0.26 | 0.22 | 0.16 | 0.09 | 0.02 | 0.04 | 0.01 | 5.98 | |
| L009 | Mbst. | 49.7 | 1.65 | 4.25 | 9.32 | 23.2 | 0.13 | 0.05 | 0.26 | 0.03 | 0.09 | <0.01 | 0.02 | 0.03 | 2.29 | |
| L010 | Mbst. | 50.7 | 14.7 | 6.36 | 10.15 | 11 | 3.03 | 1.66 | 0.01 | 0.06 | 0.11 | <0.01 | 0.15 | 0.03 | 0.4 | |
| L011 | Mbst. | 58.9 | 15.9 | 7.84 | 7.39 | 3.87 | 2.38 | 1.58 | <0.01 | 0.49 | 0.1 | 0.04 | 0.33 | 0.05 | 0.06 | |
| L012 | Alt. Mbst. | 46.5 | 0.8 | 7.91 | 3.83 | 28.7 | 0.02 | 0.02 | 0.39 | 0.03 | 0.15 | <0.01 | 0.01 | <0.01 | 0.72 | |
| L013 | Ultramafic | 41.9 | 0.91 | 7.34 | 4.2 | 31.7 | 0.01 | 0.03 | 0.36 | 0.01 | 0.13 | <0.01 | 0.01 | 0.01 | 1.54 | |
| L014 | Ultramafic | 41.1 | 1.24 | 7.95 | 1.12 | 35.9 | <0.01 | <0.01 | 0.42 | 0.06 | 0.07 | 0.01 | 0.01 | <0.01 | 0.58 | |
| L015 | Marble | 2.79 | 0.33 | 0.3 | 54.3 | 0.64 | 0.06 | 0.25 | <0.01 | 0.02 | 0.03 | 0.12 | 0.19 | <0.01 | 11.3 | |
| L016 | Mbst. | 47.6 | 12.3 | 13.2 | 11.1 | 7.9 | 1.94 | 1.61 | 0.06 | 3.57 | 0.16 | 0.45 | 0.06 | 0.05 | 0.22 | |
| L017 | And. | 55.2 | 17.55 | 7.51 | 4.23 | 3.39 | 2.52 | 3.01 | <0.01 | 0.99 | 0.11 | 0.39 | 0.06 | 0.35 | 0.81 | |
| L018 | Ultramafic | 42.6 | 1.22 | 8.03 | 0.95 | 34.8 | 0.01 | 0.02 | 0.48 | 0.03 | 0.1 | <0.01 | 0.01 | <0.01 | 0.71 | |
| L019 | Bt. Sch. | 44.5 | 15.55 | 8.2 | 8.68 | 6.96 | 1.19 | 3.67 | 0.03 | 1.23 | 0.12 | 0.15 | 0.05 | 0.1 | 1.56 | |
| L020 | Mbst. | 53.8 | 17.85 | 8.55 | 9.3 | 5.45 | 1.83 | 1.67 | 0.02 | 0.56 | 0.15 | 0.09 | 0.06 | 0.04 | 0.03 | |
| L021 | Mbst. | 49.9 | 12.25 | 8.22 | 9.63 | 12 | 2.42 | 0.82 | 0.15 | 0.44 | 0.13 | 0.02 | 0.02 | 0.01 | 0.3 | |
| L022 | Sup. And. | 64 | 15.6 | 5.86 | 3.68 | 2.46 | 2.86 | 2.97 | <0.01 | 0.59 | 0.11 | 0.16 | 0.06 | 0.26 | 0.38 | |
| L023 | Kona Dac. | 70.7 | 12.75 | 5.37 | 0.16 | 0.42 | 0.03 | 3.21 | <0.01 | 0.57 | 0.01 | 0.07 | 0.01 | 0.05 | <0.01 | |
| I308657 | Granite | 74.26 | 13.56 | 1.4 | 1.05 | 0.2 | 3.29 | 5.22 | <0.002 | 0.13 | 0.04 | 0.04 | | | <0.02 | |
| I308658 | Granite | 74.54 | 13.36 | 1.66 | 0.89 | 0.23 | 2.84 | 5.09 | <0.002 | 0.14 | 0.08 | 0.04 | | | 0.05 | |
| 400378 | Granite | 75.53 | 13.12 | 1.27 | 0.06 | 0.12 | 0.1 | 4.58 | <0.002 | 0.15 | <0.01 | 0.05 | | | <0.02 | |
| 78816B | Granite | 93.71 | 3.19 | 0.89 | 0.05 | 0.08 | 0.02 | 0.75 | <0.002 | 0.04 | <0.01 | 0.02 | | | <0.02 | |
| 78816A | Granite | 74.77 | 12.87 | 1.89 | 0.19 | 0.03 | 3.78 | 5.28 | <0.002 | 0.13 | 0.02 | 0.06 | | | 0.02 | |
| I308672 | Kona And. | 62.51 | 16.51 | 5.99 | 2.11 | 1.96 | 3.11 | 3.18 | 0.004 | 0.6 | 0.08 | 0.2 | | | <0.02 | |
| I308673 | Kona Dac. | 67.83 | 20.09 | 0.83 | 0.06 | 0.06 | 0.06 | 2.51 | 0.004 | 0.76 | <0.01 | 0.1 | | | <0.02 | |
| I308668 | Sup. Inter. | 61.29 | 15.77 | 5.62 | 4.53 | 2.59 | 2.91 | 3.04 | 0.003 | 0.57 | 0.1 | 0.16 | | | 0.38 | |
| 400421 | Sup. Inter. | 55.76 | 19.68 | 10.46 | 0.06 | 0.28 | 0.03 | 2.33 | 0.003 | 1.28 | 0.15 | 0.26 | | | 0.1 | |
| 59353 | Sup. Inter. | 62.6 | 15.99 | 6.05 | 3.87 | 2.53 | 2.88 | 2.77 | 0.003 | 0.58 | 0.11 | 0.17 | | | 0.08 | |
| 59446 | Sup. Inter. | 53.75 | 15.46 | 18.77 | 0.03 | 0.17 | 0.03 | 1.53 | 0.003 | 1 | 0.08 | 0.29 | | | 0.08 | |
| 59449 | Sup. Inter. | 60.75 | 18.65 | 7.84 | 0.08 | 0.53 | 0.05 | 3.09 | <0.002 | 1.06 | 0.06 | 0.12 | | | 0.02 | |
| 59551 | Sup. Dior. | 52.41 | 17.18 | 8.21 | 5.65 | 3.57 | 2.74 | 2.78 | <0.002 | 0.99 | 0.19 | 0.36 | | | 0.49 | |

| SAMPLE | METHOD | S-IR08 | ME-MS81 | ME-MS81 | ME-MS81 | ME-MS81 | ME-MS81 | ME-MS81 | ME-MS81 | ME-MS81 | ME-MS81 | ME-MS81 | ME-MS81 | ME-MS81 | ME-MS81 |
|---|---|---|---|---|---|---|---|---|---|---|---|---|---|---|---|
| | ANALYTE | S | Ba | Ce | Cr | Cs | Dy | Er | Eu | Ga | Gd | Hf | Ho | La | Lu |
| | UNIT | % | ppm | ppm | ppm | ppm | ppm | ppm | ppm | ppm | ppm | ppm | ppm | ppm | ppm |
| L001 | Dac. | 0.13 | 1565 | 69 | 20 | 2.46 | 4.28 | 2.59 | 0.87 | 10.8 | 4.76 | 4.7 | 0.85 | 36.6 | 0.35 |
| L002 | Dac. | 0.13 | 967 | 59.6 | 10 | 4.61 | 2.46 | 1.71 | 0.59 | 11.8 | 2.69 | 2.9 | 0.52 | 34.6 | 0.29 |
| L003 | UM Dike. | 0.24 | 49.7 | 14.1 | 1910 | 15.75 | 1.15 | 0.72 | 0.17 | 7.6 | 1.16 | 1.2 | 0.23 | 8.4 | 0.09 |
| L004 | Mgbro. | 0.01 | 229 | 2.4 | 930 | 1.43 | 0.98 | 0.62 | 0.43 | 12.7 | 0.87 | 0.3 | 0.21 | 1.2 | 0.09 |
| L005 | Mbslt. | 0.11 | 432 | 8.2 | 310 | 2.85 | 1.16 | 0.75 | 0.29 | 13.1 | 1.07 | 0.6 | 0.24 | 4.2 | 0.11 |
| L006 | Mbslt. | 0.02 | 528 | 1.7 | 680 | 7.88 | 1.03 | 0.59 | 0.44 | 12.9 | 0.85 | 0.4 | 0.21 | 0.6 | 0.08 |
| L007 | Mbslt. | 0.52 | 2910 | 74.2 | 100 | 4.96 | 4.18 | 2.43 | 1.37 | 17.4 | 4.9 | 5.2 | 0.81 | 37.8 | 0.34 |
| L008 | Tlc. Sch. | 0.06 | 43.7 | 14.9 | 1560 | 5.99 | 1.33 | 0.82 | 0.25 | 6.8 | 1.23 | 1.5 | 0.26 | 8.4 | 0.1 |
| L009 | Mbslt. | 0.44 | 234 | 10.6 | 1800 | 0.43 | 0.85 | 0.46 | 0.19 | 2.9 | 1.04 | 1.8 | 0.17 | 5 | 0.05 |
| L010 | Mbslt. | 0.55 | 288 | 2.6 | 110 | 1.41 | 0.3 | 0.21 | 0.19 | 10.8 | 0.27 | 0.2 | 0.07 | 1.5 | 0.06 |
| L011 | Mbslt. | 0.12 | 379 | 28.1 | 40 | 1.29 | 2.54 | 1.64 | 0.6 | 18.5 | 2.57 | 1.9 | 0.53 | 14.5 | 0.22 |
| L012 | Alt. Mbslt. | 0.23 | 1.5 | 2.3 | 2760 | 0.21 | 0.1 | 0.05 | 0.03 | 2 | 0.15 | <0.2 | 0.02 | 1.7 | 0.01 |
| L013 | Ultramafic | <0.01 | 102.5 | 0.5 | 2510 | 2.19 | 0.15 | 0.13 | <0.03 | 2.6 | 0.12 | <0.2 | 0.04 | <0.5 | 0.03 |
| L014 | Ultramafic | 0.08 | 5.1 | 1.5 | 2990 | 0.19 | 0.2 | 0.16 | 0.03 | 2.1 | 0.19 | 0.2 | 0.05 | 0.8 | 0.02 |
| L015 | Marble | 0.01 | 39.9 | 5.4 | 30 | 0.08 | 0.47 | 0.26 | 0.18 | 0.6 | 0.51 | <0.2 | 0.1 | 4.1 | 0.03 |
| L016 | Mbslt. | 0.19 | 407 | 85.8 | 410 | 2.12 | 6.7 | 3.22 | 2.84 | 21.9 | 9.01 | 6.6 | 1.2 | 39.5 | 0.3 |
| L017 | And. | 0.06 | 2930 | 55 | 20 | 11.45 | 4.14 | 2.41 | 1.46 | 19.5 | 5.2 | 4.1 | 0.79 | 27.5 | 0.34 |
| L018 | Ultramafic | 0.24 | 10.4 | 0.6 | 3350 | 0.2 | 0.07 | 0.05 | <0.03 | 2.8 | 0.05 | 0.2 | 0.02 | <0.5 | 0.01 |
| L019 | Bt. Sch. | 0.01 | 881 | 27.9 | 230 | 9.1 | 4.41 | 2.76 | 1.34 | 16.4 | 4.55 | 2.9 | 0.93 | 14 | 0.34 |
| L020 | Mbslt. | 0.19 | 342 | 16.5 | 190 | 1.66 | 2.09 | 1.29 | 0.67 | 18.1 | 2.03 | 1.5 | 0.46 | 8.7 | 0.22 |
| L021 | Mbslt. | 0.14 | 82.4 | 3.4 | 1250 | 2.14 | 1.92 | 1.27 | 0.43 | 12.4 | 1.52 | 0.9 | 0.43 | 1.3 | 0.19 |
| L022 | Sup. And. | <0.01 | 2180 | 49.8 | 40 | 0.9 | 3.2 | 1.99 | 0.94 | 17.8 | 3.54 | 3.9 | 0.68 | 28.3 | 0.32 |
| L023 | Kona Dac. | 0.02 | 451 | 44.8 | 40 | 5.96 | 1.95 | 1.22 | 0.71 | 19.5 | 2.28 | 3.9 | 0.42 | 26 | 0.21 |
| I308657 | Granite | <0.02 | 821 | 17.7 | | 4.6 | 2.2 | 1.8 | 0.38 | 13.8 | 1.71 | 3.2 | 0.53 | 8 | 0.35 |
| I308658 | Granite | <0.02 | 696 | 17.4 | | 5 | 1.41 | 1.02 | 0.31 | 14.3 | 1.23 | 2.7 | 0.31 | 9.1 | 0.21 |
| 400378 | Granite | 0.15 | 712 | 59.4 | | 2 | 1.04 | 0.55 | 0.25 | 13.1 | 1.55 | 3.2 | 0.2 | 32.7 | 0.11 |
| 78816B | Granite | <0.02 | 105 | 6.2 | | 0.8 | 0.51 | 0.44 | 0.07 | 4.3 | 0.41 | 0.4 | 0.12 | 3.4 | 0.07 |
| 78816A | Granite | <0.02 | 724 | 9.5 | | 2.2 | 0.95 | 0.72 | 0.11 | 11.3 | 0.66 | 3.5 | 0.22 | 3.2 | 0.19 |
| I308672 | Kona And. | <0.02 | 1854 | 54.5 | | 4.1 | 2.95 | 1.69 | 1.01 | 17.4 | 3.32 | 4.4 | 0.56 | 27.4 | 0.25 |
| I308673 | Kona Dac. | <0.02 | 1093 | 65.1 | | 1.8 | 3.09 | 1.65 | 1.39 | 22.8 | 4.44 | 5.3 | 0.55 | 29.9 | 0.29 |
| I308668 | Sup. Inter. | <0.02 | 2326 | 49.5 | | 1.5 | 3.02 | 1.94 | 0.93 | 15.7 | 3.25 | 3.4 | 0.62 | 25.5 | 0.32 |
| 400421 | Sup. Inter. | <0.02 | 716 | 57.6 | | 2.6 | 4.48 | 2.43 | 1.37 | 19 | 4.41 | 2.7 | 0.86 | 23.7 | 0.39 |
| 59353 | Sup. Inter. | <0.02 | 2331 | 52.1 | | 2.8 | 3.11 | 1.91 | 0.95 | 16.3 | 3.48 | 3.5 | 0.67 | 26.6 | 0.3 |
| 59446 | Sup. Inter. | <0.02 | 313 | 35 | | 2 | 4.13 | 2.73 | 1.27 | 14.9 | 4.56 | 2.1 | 0.89 | 15.5 | 0.38 |
| 59449 | Sup. Inter. | <0.02 | 1449 | 59.5 | | 2.5 | 4.08 | 2.36 | 1.36 | 17.7 | 4.47 | 3.3 | 0.8 | 29.1 | 0.35 |
| 59551 | Sup. Dior. | 0.1 | 2879 | 57.3 | | 1.7 | 4.02 | 2.36 | 1.46 | 17 | 4.98 | 3.2 | 0.85 | 27 | 0.34 |

| SAMPLE | METHOD | ME-MS81 | ME-MS81 | ME-MS81 | ME-MS81 | ME-MS81 | ME-MS81 | ME-MS81 | ME-MS81 | ME-MS81 | ME-MS81 | ME-MS81 | ME-MS81 | ME-MS81 | ME-MS81 |
|---|---|---|---|---|---|---|---|---|---|---|---|---|---|---|---|
| | ANALYTE | Nb | Nd | Pr | Rb | Sm | Sn | Sr | Ta | Tb | Th | Tl | Tm | U | V |
| | UNIT | ppm | ppm | ppm | ppm | ppm | ppm | ppm | ppm | ppm | ppm | ppm | ppm | ppm | ppm |
| L001 | Dac. | 9.1 | 29.4 | 7.76 | 128.5 | 5.58 | <1 | 22.3 | 0.7 | 0.7 | 15.3 | 1.1 | 0.37 | 2.74 | 15 |
| L002 | Dac. | 9.8 | 21 | 6.17 | 134 | 3.54 | <1 | 23.9 | 1 | 0.41 | 19.15 | 1 | 0.27 | 4.47 | 10 |
| L003 | UM Dike. | 3 | 6.1 | 1.53 | 20 | 1.25 | <1 | 302 | 0.2 | 0.17 | 3.61 | 0.5 | 0.1 | 0.61 | <5 |
| L004 | Mgbro. | 0.4 | 1.6 | 0.32 | 48.3 | 0.56 | <1 | 357 | <0.1 | 0.15 | 0.11 | <0.5 | 0.09 | 0.11 | 106 |
| L005 | Mbslt. | 1.7 | 3.8 | 0.94 | 110.5 | 0.94 | 1 | 543 | 0.2 | 0.17 | 3.61 | 0.6 | 0.11 | 2 | 76 |
| L006 | Mbslt. | <0.2 | 1.5 | 0.26 | 146 | 0.6 | <1 | 480 | <0.1 | 0.15 | 0.05 | 0.8 | 0.09 | 0.05 | 88 |
| L007 | Mbslt. | 11.3 | 31.5 | 8.34 | 92.5 | 5.88 | 3 | 505 | 0.9 | 0.68 | 13.3 | 0.5 | 0.36 | 3.07 | 85 |
| L008 | Tlc. Sch. | 3.9 | 6 | 1.65 | 17.3 | 1.23 | <1 | 301 | 0.2 | 0.2 | 3.04 | <0.5 | 0.11 | 1.04 | <5 |
| L009 | Mbslt. | 0.8 | 5.2 | 1.31 | 2.1 | 1.14 | <1 | 135 | <0.1 | 0.15 | 4.48 | 1.1 | 0.07 | 0.46 | <5 |
| L010 | Mbslt. | 0.8 | 1.1 | 0.28 | 41.6 | 0.29 | 1 | 1195 | <0.1 | 0.04 | 0.19 | <0.5 | 0.04 | 0.43 | 80 |
| L011 | Mbslt. | 4.9 | 12.3 | 3.21 | 60.3 | 2.83 | 2 | 2670 | 0.6 | 0.4 | 9.37 | <0.5 | 0.24 | 4.32 | 268 |
| L012 | Alt. Mbslt. | <0.2 | 1 | 0.24 | 1.6 | 0.18 | <1 | 79.4 | <0.1 | 0.02 | 0.22 | 2 | 0.01 | <0.05 | <5 |
| L013 | Ultramafic | 0.5 | 0.3 | 0.07 | 3.1 | 0.11 | <1 | 80.8 | <0.1 | 0.02 | 0.46 | <0.5 | 0.02 | 0.44 | <5 |
| L014 | Ultramafic | 1.2 | 0.7 | 0.17 | 0.6 | 0.19 | <1 | 43.7 | 0.1 | 0.03 | 0.64 | <0.5 | 0.03 | 0.33 | <5 |
| L015 | Marble | 0.7 | 3 | 0.73 | 5.5 | 0.6 | <1 | 1505 | <0.1 | 0.08 | 0.34 | <0.5 | 0.04 | 0.64 | 7 |
| L016 | Mbslt. | 45.1 | 45.1 | 10.65 | 52.2 | 9.84 | 2 | 441 | 2.9 | 1.22 | 3.47 | <0.5 | 0.4 | 1.03 | 340 |
| L017 | And. | 8.2 | 28.3 | 6.77 | 115 | 5.92 | 1 | 480 | 0.5 | 0.72 | 13.5 | 0.9 | 0.35 | 4.15 | 218 |
| L018 | Ultramafic | 0.8 | 0.3 | 0.08 | 1.4 | 0.09 | <1 | 38.6 | <0.1 | 0.01 | 0.24 | <0.5 | 0.01 | 0.28 | <5 |
| L019 | Bt. Sch. | 2.8 | 16.5 | 3.72 | 148 | 4.09 | <1 | 417 | 0.2 | 0.71 | 1.2 | 0.8 | 0.38 | 1.81 | 202 |
| L020 | Mbslt. | 2 | 8.5 | 2.06 | 61.7 | 1.99 | 1 | 460 | 0.1 | 0.34 | 2.17 | <0.5 | 0.2 | 0.95 | 247 |
| L021 | Mbslt. | 0.6 | 3.1 | 0.56 | 25.3 | 1.16 | <1 | 179 | <0.1 | 0.28 | 0.18 | <0.5 | 0.19 | 0.17 | 236 |
| L022 | Sup. And. | 7.3 | 20.8 | 5.62 | 94.5 | 4 | 1 | 442 | 0.7 | 0.54 | 13.7 | 0.5 | 0.3 | 3.42 | 152 |
| L023 | Kona Dac. | 10.4 | 16.5 | 4.77 | 219 | 3.03 | 1 | 96.4 | 0.6 | 0.34 | 8.91 | 2.9 | 0.19 | 41.9 | 109 |
| I308657 | Granite | 12.9 | 6.9 | 1.93 | 169.8 | 1.49 | 1 | 108.7 | 1 | 0.35 | 31.6 | 0.3 | 0.29 | 6.3 | <8 |
| I308658 | Granite | 12.4 | 6.5 | 1.83 | 165.8 | 1.29 | 1 | 98 | 0.9 | 0.23 | 31.8 | 0.3 | 0.17 | 4.1 | <8 |
| 400378 | Granite | 12.8 | 16.6 | 5.39 | 160.3 | 2.61 | 1 | 91.5 | 0.9 | 0.22 | 29.2 | 0.2 | 0.09 | 3.1 | <8 |
| 78816B | Granite | 5.6 | 2.2 | 0.61 | 35 | 0.5 | <1 | 9 | 0.3 | 0.08 | 5.4 | <0.1 | 0.08 | 4.1 | <8 |
| 78816A | Granite | 16.5 | 2.4 | 0.8 | 224.8 | 0.69 | 2 | 92.5 | 1.4 | 0.15 | 29.8 | <0.1 | 0.14 | 3.8 | <8 |
| I308672 | Kona And. | 8.5 | 21.1 | 5.76 | 92.6 | 3.92 | 1 | 464.4 | 0.7 | 0.51 | 10 | <0.1 | 0.27 | 2.7 | 92 |
| I308673 | Kona Dac. | 16.1 | 28.8 | 7.15 | 130 | 5.44 | 2 | 199.4 | 0.7 | 0.64 | 12 | <0.1 | 0.26 | 7.7 | 84 |
| I308668 | Sup. Inter. | 6.8 | 19.7 | 5.28 | 83.7 | 3.71 | <1 | 442.8 | 0.5 | 0.55 | 14 | 0.2 | 0.29 | 4.2 | 114 |
| 400421 | Sup. Inter. | 8 | 23.6 | 5.81 | 127.1 | 4.91 | 1 | 1150.5 | 0.4 | 0.71 | 5.7 | 1 | 0.38 | 50.7 | 247 |
| 59353 | Sup. Inter. | 7.4 | 20.8 | 5.49 | 90.8 | 3.91 | 1 | 452.4 | 0.5 | 0.56 | 13.9 | 0.4 | 0.29 | 3 | 122 |
| 59446 | Sup. Inter. | 6.5 | 19.4 | 4.3 | 82.9 | 4.37 | 1 | 102 | 0.3 | 0.76 | 3.9 | 0.1 | 0.39 | 23.9 | 266 |
| 59449 | Sup. Inter. | 7.3 | 26.2 | 6.75 | 126.5 | 5.31 | 2 | 259.7 | 0.4 | 0.71 | 8.1 | 0.3 | 0.35 | 7.2 | 249 |
| 59551 | Sup. Dior. | 6.9 | 25.9 | 6.58 | 73 | 5.19 | 2 | 610.7 | 0.3 | 0.77 | 7.4 | <0.1 | 0.35 | 2.6 | 222 |

| SAMPLE | METHOD | ME-MS81 | ME-MS81 | ME-MS81 | ME-MS81 | ME-MS42 | ME-MS42 | ME-MS42 | ME-MS42 | ME-MS42 | ME-MS42 | OA GRA05 | TOT-ICP06 | ME4ACD81 | ME4ACD81 |
|---|---|---|---|---|---|---|---|---|---|---|---|---|---|---|---|
| | ANALYTE | W | Y | Yb | Zr | As | Bi | Hg | Sb | Se | Te | LOI | Total | Ag | Cd |
| | UNIT | ppm | ppm | ppm | ppm | ppm | ppm | ppm | ppm | ppm | ppm | % | % | ppm | ppm |
| L001 | Dac. | 2 | 24.5 | 2.41 | 161 | 136 | 0.29 | 0.192 | 32.5 | 0.2 | 0.03 | 2.65 | 99.55 | 1.1 | <0.5 |
| L002 | Dac. | 2 | 16.1 | 1.87 | 86 | 183.5 | 0.07 | 0.081 | 5.29 | 0.4 | 0.04 | 2.43 | 99.71 | <0.5 | <0.5 |
| L003 | UM Dike. | <1 | 7.6 | 0.67 | 43 | >250 | 0.23 | 0.205 | 4.22 | 1 | 0.04 | 29.9 | 101.34 | <0.5 | <0.5 |
| L004 | Mgbro. | <1 | 6.1 | 0.6 | 3 | 3.6 | 0.06 | <0.005 | 0.25 | 0.4 | 0.02 | 4.85 | 99.07 | <0.5 | <0.5 |
| L005 | Mbslt. | <1 | 7.2 | 0.77 | 13 | 6.4 | 0.18 | <0.005 | 0.17 | 0.5 | <0.01 | 7.98 | 101.48 | <0.5 | <0.5 |
| L006 | Mbslt. | 1 | 5.3 | 0.51 | 8 | 2.2 | 0.05 | 0.007 | 0.4 | 0.7 | 0.01 | 7.34 | 98.14 | <0.5 | <0.5 |
| L007 | Mbslt. | 1 | 23.1 | 2.21 | 192 | 3.5 | 0.63 | <0.005 | 0.37 | 0.8 | 0.07 | 5.14 | 98.66 | <0.5 | <0.5 |
| L008 | Tlc. Sch. | <1 | 7.9 | 0.69 | 55 | >250 | 0.13 | 0.075 | 2.02 | 0.8 | 0.07 | 23.3 | 101.91 | <0.5 | <0.5 |
| L009 | Mbslt. | <1 | 5.5 | 0.4 | 58 | 66 | 0.57 | 0.006 | 0.2 | 0.7 | 0.12 | 11.65 | 100.38 | <0.5 | <0.5 |
| L010 | Mbslt. | <1 | 2 | 0.35 | 2 | 15.4 | 0.19 | 0.008 | 0.15 | 0.6 | 0.03 | 3.23 | 101.19 | <0.5 | <0.5 |
| L011 | Mbslt. | 1 | 15.5 | 1.53 | 56 | 5.8 | 0.05 | <0.005 | 0.07 | 0.5 | 0.02 | 1.82 | 100.69 | <0.5 | <0.5 |
| L012 | Alt. Mbslt. | <1 | 0.7 | 0.06 | <2 | 21.5 | 0.33 | <0.005 | 0.44 | 0.4 | 0.15 | 10.4 | 98.76 | <0.5 | <0.5 |
| L013 | Ultramafic | <1 | 1.6 | 0.15 | <2 | 11.1 | 0.16 | <0.005 | 1.98 | 0.8 | 0.08 | 14.5 | 101.11 | <0.5 | <0.5 |
| L014 | Ultramafic | <1 | 1.5 | 0.16 | 3 | 11.6 | 0.14 | <0.005 | <0.05 | 0.7 | 0.11 | 12.4 | 100.28 | <0.5 | <0.5 |
| L015 | Marble | <1 | 3.5 | 0.22 | <2 | <0.1 | 0.03 | 0.01 | 0.07 | 0.7 | 0.03 | 42.7 | 101.73 | <0.5 | <0.5 |
| L016 | Mbslt. | 1 | 31.5 | 2.3 | 262 | 2.1 | 0.06 | <0.005 | 0.19 | 1 | 0.02 | 1.72 | 101.72 | <0.5 | <0.5 |
| L017 | And. | 1 | 22.1 | 2.21 | 148 | 3 | 0.1 | 0.006 | 0.65 | 1.5 | 0.03 | 5.84 | 101.15 | <0.5 | <0.5 |
| L018 | Ultramafic | <1 | 0.5 | 0.09 | 3 | 4.2 | 0.3 | <0.005 | 0.1 | 1.1 | 0.18 | 11.6 | 99.85 | <0.5 | <0.5 |
| L019 | Bt. Sch. | 1 | 26.6 | 2.4 | 118 | 1.3 | 0.04 | <0.005 | 2.15 | 1.8 | 0.04 | 10.65 | 101.08 | <0.5 | <0.5 |
| L020 | Mbslt. | 1 | 13.1 | 1.36 | 46 | 4.8 | 0.04 | <0.005 | 0.27 | 0.9 | 0.01 | 1.74 | 101.11 | <0.5 | <0.5 |
| L021 | Mbslt. | <1 | 12.3 | 1.24 | 19 | 2.2 | 0.01 | <0.005 | 0.21 | 0.7 | 0.02 | 2.4 | 98.41 | <0.5 | <0.5 |
| L022 | Sup. And. | 1 | 20.4 | 1.99 | 128 | 2.5 | 0.06 | <0.005 | 0.45 | 1 | 0.02 | 3.28 | 101.89 | <0.5 | <0.5 |
| L023 | Kona Dac. | 3 | 13 | 1.24 | 144 | >250 | 0.01 | 1.16 | 14.75 | 0.5 | 0.03 | 4.31 | 97.66 | <0.5 | <0.5 |
| I308657 | Granite | 0.5 | 20 | 2.02 | 99.1 | 2.2 | 0.1 | <0.01 | 0.4 | <0.5 | | 0.7 | 99.9 | <0.1 | <0.1 |
| I308658 | Granite | <0.5 | 9.7 | 1.26 | 86.3 | 1.4 | <0.1 | <0.01 | 0.7 | <0.5 | | 1.1 | 99.92 | <0.1 | <0.1 |
| 400378 | Granite | 0.5 | 5.4 | 0.72 | 101.9 | 1606.7 | <0.1 | 1.59 | 1.2 | <0.5 | | 4.9 | 99.86 | <0.1 | <0.1 |
| 78816B | Granite | <0.5 | 3.5 | 0.49 | 16 | 273.2 | 1.7 | 0.24 | 0.8 | <0.5 | | 1.2 | 99.96 | 0.5 | 0.1 |
| 78816A | Granite | <0.5 | 5.7 | 1.13 | 99.8 | 122.3 | 0.2 | 0.01 | 0.3 | <0.5 | | 0.9 | 99.86 | <0.1 | <0.1 |
| I308672 | Kona And. | 0.6 | 17.9 | 1.68 | 167.2 | 3 | <0.1 | <0.01 | 0.5 | <0.5 | | 3.4 | 99.67 | <0.1 | <0.1 |
| I308673 | Kona Dac. | 5.7 | 14.9 | 1.81 | 190.2 | 207.2 | 0.1 | 0.31 | 1.4 | <0.5 | | 7.5 | 99.83 | <0.1 | <0.1 |
| I308668 | Sup. Inter. | 1.1 | 18.7 | 1.95 | 121.3 | 4.2 | <0.1 | <0.01 | 0.3 | <0.5 | | 3 | 99.63 | <0.1 | <0.1 |
| 400421 | Sup. Inter. | 9.4 | 18.7 | 2.58 | 88.2 | 900.3 | <0.1 | 0.29 | 15.9 | <0.5 | | 9.3 | 99.61 | 0.1 | 0.2 |
| 59353 | Sup. Inter. | 1.4 | 19.5 | 2.01 | 122.6 | 15.6 | 0.1 | 0.02 | 0.5 | <0.5 | | 2 | 99.57 | <0.1 | 0.1 |
| 59446 | Sup. Inter. | 9.8 | 25.7 | 2.63 | 74.9 | 511 | <0.1 | 0.19 | 5.6 | 0.7 | | 8.7 | 99.83 | <0.1 | 0.1 |
| 59449 | Sup. Inter. | 2.2 | 21 | 2.45 | 127.6 | 480.1 | <0.1 | 0.2 | 4.2 | <0.5 | | 7.5 | 99.71 | <0.1 | 0.2 |
| 59551 | Sup. Dior. | 0.8 | 24 | 2.22 | 120.4 | 10.4 | 0.1 | 0.11 | 0.3 | <0.5 | | 5.4 | 99.44 | <0.1 | 0.1 |

| SAMPLE | METHOD | ME4ACD81 | ME4ACD81 | ME4ACD81 | ME4ACD81 | ME4ACD81 | ME4ACD81 | ME4ACD81 | ME4ACD81 |
|---|---|---|---|---|---|---|---|---|---|
| | ANALYTE | Co | Cu | Li | Mo | Ni | Pb | Sc | Zn |
| | UNIT | ppm | ppm | ppm | ppm | ppm | ppm | ppm | ppm |
| L001 | Dac. | <1 | <1 | <10 | <1 | 1 | 44 | 6 | 3 |
| L002 | Dac. | 1 | 25 | <10 | <1 | 23 | 8 | 2 | 9 |
| L003 | UM Dike. | 74 | 20 | 10 | <1 | 1130 | 8 | 6 | 69 |
| L004 | Mgbro. | 29 | 12 | 10 | <1 | 112 | 2 | 32 | 25 |
| L005 | Mbslt. | 24 | 27 | 30 | <1 | 111 | 5 | 15 | 34 |
| L006 | Mbslt. | 28 | 18 | 40 | <1 | 158 | 3 | 19 | 33 |
| L007 | Mbslt. | 15 | 63 | 10 | <1 | 36 | 28 | 10 | 156 |
| L008 | Tlc. Sch. | 30 | 16 | 10 | <1 | 681 | 10 | 8 | 28 |
| L009 | Mbslt. | 83 | 18 | 10 | 1 | 1900 | 3 | 5 | 35 |
| L010 | Mbslt. | 45 | 75 | 10 | <1 | 220 | 6 | 5 | 37 |
| L011 | Mbslt. | 21 | 75 | 20 | <1 | 15 | 13 | 26 | 47 |
| L012 | Alt. Mbslt. | 96 | 25 | 10 | <1 | 1670 | <2 | 10 | 51 |
| L013 | Ultramafic | 75 | 19 | <10 | <1 | 1580 | 2 | 7 | 48 |
| L014 | Ultramafic | 103 | 2 | <10 | <1 | 2200 | <2 | 6 | 45 |
| L015 | Marble | 2 | <1 | <10 | <1 | 13 | 10 | <1 | <2 |
| L016 | Mbslt. | 48 | 76 | 20 | <1 | 174 | <2 | 25 | 132 |
| L017 | And. | 14 | 8 | 20 | 1 | 27 | 14 | 15 | 84 |
| L018 | Ultramafic | 93 | 11 | <10 | <1 | 2390 | 2 | 5 | 63 |
| L019 | Bt. Sch. | 31 | <1 | 30 | <1 | 41 | 7 | 23 | 64 |
| L020 | Mbslt. | 25 | 53 | 20 | <1 | 42 | 11 | 25 | 68 |
| L021 | Mbslt. | 45 | 76 | 10 | <1 | 224 | 2 | 36 | 57 |
| L022 | Sup. And. | 13 | 8 | 10 | <1 | 4 | 30 | 13 | 69 |
| L023 | Kona Dac. | 2 | <1 | 10 | <1 | <1 | 16 | 15 | 21 |
| I308657 | Granite | 1 | 1.7 | | 0.5 | 0.8 | 6.9 | 2 | 35 |
| I308658 | Granite | 0.8 | 1.9 | | 0.8 | 0.6 | 5.5 | 2 | 35 |
| 400378 | Granite | 0.5 | <0.1 | | 0.5 | 0.6 | 13.5 | 3 | 3 |
| 78816B | Granite | <0.2 | 0.7 | | 0.2 | 0.5 | 79 | <1 | 8 |
| 78816A | Granite | 1 | 0.7 | | 0.2 | 1.5 | 11.6 | 2 | 19 |
| I308672 | Kona And. | 11.2 | 1.9 | | 1.1 | 13.7 | 5 | 13 | 83 |
| I308673 | Kona Dac. | 0.3 | 1.4 | | 0.2 | 0.6 | 7.6 | 12 | 4 |
| I308668 | Sup. Inter. | 12.5 | 9.3 | | 0.6 | 3.8 | 11.2 | 17 | 55 |
| 400421 | Sup. Inter. | 45.6 | 47.9 | | 1.6 | 15.3 | 6.5 | 36 | 83 |
| 59353 | Sup. Inter. | 15.1 | 14.2 | | 0.3 | 7.3 | 10.9 | 17 | 52 |
| 59446 | Sup. Inter. | 29 | 26 | | 1.9 | 24.5 | 12.3 | 26 | 94 |
| 59449 | Sup. Inter. | 16.1 | 6.8 | | 0.4 | 4 | 5.3 | 26 | 65 |
| 59551 | Sup. Dior. | 17.4 | 9 | | 0.2 | 3.9 | 6.2 | 23 | 74 |

# Appendix C: EPMA Analyses

TABLE 1, AMPHIBOLE, KAMINAK GOLD, ERIC BUITENHUIS, JUNE 2013, R.L.B.

| | 1 | | 2 | | 3 | | 4 | | 5 | | 6 | | 7 | | 8 |
|---|---|---|---|---|---|---|---|---|---|---|---|---|---|---|---|
| SIO2 | 43.80 | | 43.98 | | 43.49 | | 46.03 | | 44.68 | | 43.37 | | 42.92 | | 44.32 |
| TIO2 | .42 | | .42 | | .45 | | .33 | | .44 | | .40 | | .42 | | .36 |
| A2O3 | 13.52 | | 12.33 | | 13.68 | | 12.03 | | 13.05 | | 13.34 | | 13.00 | | 12.82 |
| C2O3 | .07 | | .00 | | .02 | | .06 | | .23 | | .12 | | .39 | | .02 |
| FEO | 16.58 | | 16.58 | | 16.34 | | 15.49 | | 16.44 | | 17.23 | | 16.97 | | 17.10 |
| MGO | 9.75 | | 10.70 | | 9.87 | | 10.83 | | 10.34 | | 10.15 | | 10.42 | | 9.58 |
| MNO | .28 | | .25 | | .33 | | .24 | | .35 | | .36 | | .23 | | .26 |
| CAO | 11.39 | | 11.60 | | 11.27 | | 11.54 | | 11.48 | | 11.32 | | 11.34 | | 11.49 |
| K2O | .55 | | .42 | | .57 | | .36 | | .51 | | .52 | | .54 | | .50 |
| NA2O | 1.63 | | 1.41 | | 1.74 | | 1.53 | | 1.47 | | 1.53 | | 1.50 | | 1.35 |
| SUM | 97.99 | | 97.69 | | 97.76 | | 98.44 | | 98.99 | | 98.34 | | 97.73 | | 97.80 |
| SI | 6.500 | * | 6.548 | * | 6.468 | * | 6.731 | * | 6.551 | * | 6.441 | * | 6.419 | * | 6.593 | * |
| AL | 1.500 | 8.000 | 1.452 | 8.000 | 1.532 | 8.000 | 1.269 | 8.000 | 1.449 | 8.000 | 1.559 | 8.000 | 1.581 | 8.000 | 1.407 | 8.000 |
| AL | .844 | * | .711 | * | .865 | * | .805 | * | .805 | * | .776 | * | .710 | * | .840 | * |
| TI | .047 | * | .047 | * | .050 | * | .036 | * | .049 | * | .045 | * | .047 | * | .040 | * |
| CR | .008 | * | .000 | * | .002 | * | .007 | * | .027 | * | .014 | * | .046 | * | .002 | * |
| FE | 2.058 | * | 2.064 | * | 2.032 | * | 1.894 | * | 2.016 | * | 2.140 | * | 2.122 | * | 2.127 | * |
| MG | 2.157 | * | 2.374 | * | 2.188 | * | 2.361 | * | 2.260 | * | 2.247 | * | 2.323 | * | 2.124 | * |
| MN | .035 | 5.168 | .032 | 5.229 | .042 | 5.180 | .030 | 5.133 | .043 | 5.199 | .045 | 5.267 | .029 | 5.278 | .033 | 5.167 |
| CA | 1.811 | * | 1.850 | * | 1.796 | * | 1.808 | * | 1.803 | * | 1.801 | * | 1.817 | * | 1.831 | * |
| K | .104 | * | .080 | * | .108 | * | .067 | * | .095 | * | .099 | * | .103 | * | .095 | * |
| NA | .469 | 2.384 | .407 | 2.337 | .502 | 2.406 | .434 | 2.309 | .418 | 2.317 | .441 | 2.340 | .435 | 2.355 | .389 | 2.316 |
| O | 23.000 | * | 23.000 | * | 23.000 | * | 23.000 | * | 23.000 | * | 23.000 | * | 23.000 | * | 23.000 | * |
| | CUMM | 35.79 | | 37.75 | | 36.37 | | 38.93 | | 37.17 | | 36.31 | | 37.09 | | 34.92 |
| | WO | 30.06 | | 29.42 | | 29.85 | | 29.82 | | 29.67 | | 29.11 | | 29.02 | | 30.11 |
| | GRUN | 34.15 | | 32.82 | | 33.78 | | 31.24 | | 33.16 | | 34.58 | | 33.89 | | 34.97 |
| | F/M | .970 | | .883 | | .948 | | .815 | | .911 | | .973 | | .926 | | 1.017 |
| | F/FM | .492 | | .469 | | .487 | | .449 | | .477 | | .493 | | .481 | | .504 |

1 ***** SAMPLE DDH82-170.6m C-1
2 AT MARGIN
3 AT MARGIN
4 AT MARGIN
5 INT W BIO
6 INT W BIO
7 INT W BIO
8 C PLATE C-2

TABLE 1, AMPHIBOLE, KAMINAK GOLD, ERIC BUITENHUIS, JUNE 2013, R.L.B.

| | 9 | 10 | 11 | 12 | 13 | 14 | 15 | 16 |
|---|---|---|---|---|---|---|---|---|
| SIO2 | 44.70 | 45.66 | 44.28 | 45.13 | 45.56 | 45.36 | 44.72 | 45.26 |
| TIO2 | .27 | .27 | .30 | .32 | .29 | .34 | .29 | .29 |
| A2O3 | 16.61 | 16.10 | 16.14 | 15.50 | 15.29 | 15.84 | 15.78 | 15.68 |
| C2O3 | .00 | .00 | .06 | .07 | .03 | .00 | .00 | .00 |
| FEO | 11.93 | 12.23 | 12.52 | 11.57 | 11.47 | 12.03 | 12.03 | 11.54 |
| MGO | 10.95 | 11.07 | 11.67 | 12.16 | 12.17 | 11.65 | 11.94 | 12.29 |
| MNO | .31 | .32 | .19 | .17 | .21 | .26 | .20 | .22 |
| CAO | 11.48 | 10.98 | 10.87 | 10.81 | 10.78 | 11.03 | 10.97 | 10.92 |
| K2O | .32 | .30 | .33 | .27 | .29 | .31 | .34 | .27 |
| NA2O | 1.50 | 1.55 | 1.62 | 1.73 | 1.65 | 1.66 | 1.56 | 1.62 |
| SUM | 98.07 | 98.48 | 97.98 | 97.73 | 97.74 | 98.48 | 97.83 | 98.09 |
| SI | 6.438 * | 6.537 * | 6.402 * | 6.503 * | 6.555 * | 6.500 * | 6.457 * | 6.495 * |
| AL | 1.562 8.000 | 1.463 8.000 | 1.598 8.000 | 1.497 8.000 | 1.445 8.000 | 1.500 8.000 | 1.543 8.000 | 1.505 8.000 |
| AL | 1.257 * | 1.253 * | 1.152 * | 1.135 * | 1.147 * | 1.174 * | 1.142 * | 1.146 * |
| TI | .029 * | .029 * | .033 * | .035 * | .031 * | .037 * | .031 * | .031 * |
| CR | .000 * | .000 * | .007 * | .008 * | .003 * | .000 * | .000 * | .000 * |
| FE | 1.437 * | 1.464 * | 1.514 * | 1.394 * | 1.380 * | 1.442 * | 1.453 * | 1.385 * |
| MG | 2.351 * | 2.362 * | 2.515 * | 2.612 * | 2.610 * | 2.488 * | 2.570 * | 2.629 * |
| MN | .038 5.112 | .039 5.148 | .023 5.244 | .021 5.205 | .026 5.197 | .032 5.172 | .024 5.221 | .027 5.218 |
| CA | 1.771 * | 1.684 * | 1.684 * | 1.669 * | 1.662 * | 1.693 * | 1.697 * | 1.679 * |
| K | .059 * | .055 * | .061 * | .050 * | .053 * | .057 * | .063 * | .049 * |
| NA | .419 2.249 | .430 2.169 | .454 2.199 | .483 2.202 | .460 2.175 | .461 2.211 | .437 2.196 | .451 2.179 |
| O | 23.000 * | 23.000 * | 23.000 * | 23.000 * | 23.000 * | 23.000 * | 23.000 * | 23.000 * |
| CUMM | 42.28 | 42.87 | 44.02 | 46.02 | 46.18 | 44.25 | 44.93 | 46.18 |
| WO | 31.87 | 30.56 | 29.48 | 29.41 | 29.40 | 30.11 | 29.67 | 29.49 |
| GRUN | 25.85 | 26.57 | 26.50 | 24.57 | 24.42 | 25.64 | 25.40 | 24.33 |
| F/M | .627 | .636 | .611 | .542 | .539 | .592 | .575 | .537 |
| F/FM | .386 | .389 | .379 | .351 | .350 | .372 | .365 | .349 |

9 ***** SAMPLE DDH114-272.0m STRONG FABRIC
10 HIGH METAM GRADE AMPHIBOLITE
11 C AMPH SHEAF C-1
12 C AMPH SHEAF C-1
13 C AMPH SHEAF C-1
14 C AMPH SHEAF C-1
15 C AMPH SHEAF C-1
16 C AMPH SHEAF C-1

TABLE 1, AMPHIBOLE, KAMINAK GOLD, ERIC BUITENHUIS, JUNE 2013, R.L.B.

| | 17 | | 18 | | 19 | | 20 | | 21 | | 22 | | 23 | | 24 | |
|---|---|---|---|---|---|---|---|---|---|---|---|---|---|---|---|---|
| SIO2 | 46.66 | | 53.90 | | 53.18 | | 55.56 | | 54.78 | | 52.60 | | 52.20 | | 48.88 | |
| TIO2 | .24 | | .28 | | .14 | | .00 | | .03 | | .17 | | .71 | | .24 | |
| A2O3 | 13.90 | | 3.77 | | 5.31 | | 3.10 | | 3.92 | | 5.38 | | 4.66 | | 11.01 | |
| C2O3 | .02 | | .19 | | .21 | | .11 | | .10 | | .09 | | .11 | | .10 | |
| FEO | 11.68 | | 6.63 | | 6.47 | | 6.14 | | 6.41 | | 7.12 | | 7.17 | | 9.09 | |
| MGO | 12.47 | | 18.82 | | 18.76 | | 20.18 | | 19.48 | | 18.81 | | 18.77 | | 15.25 | |
| MNO | .37 | | .03 | | .04 | | .06 | | .14 | | .12 | | .06 | | .08 | |
| CAO | 10.87 | | 12.62 | | 12.79 | | 13.24 | | 12.95 | | 12.78 | | 12.56 | | 11.83 | |
| K2O | .26 | | .01 | | .03 | | .03 | | .01 | | .03 | | .00 | | .19 | |
| NA2O | 1.42 | | .41 | | .54 | | .25 | | .41 | | .40 | | .59 | | 1.45 | |
| SUM | 97.89 | | 96.66 | | 97.47 | | 98.67 | | 98.23 | | 97.50 | | 96.83 | | 98.12 | |
| SI | 6.702 | * | 7.621 | * | 7.464 | * | 7.678 | * | 7.615 | * | 7.410 | * | 7.416 | * | 6.927 | * |
| AL | 1.298 | 8.000 | .379 | 8.000 | .536 | 8.000 | .322 | 8.000 | .385 | 8.000 | .590 | 8.000 | .584 | 8.000 | 1.073 | 8.000 |
| AL | 1.054 | * | .250 | * | .343 | * | .182 | * | .257 | * | .303 | * | .196 | * | .765 | * |
| TI | .026 | * | .030 | * | .015 | * | .000 | * | .003 | * | .018 | * | .076 | * | .026 | * |
| CR | .002 | * | .021 | * | .023 | * | .012 | * | .011 | * | .010 | * | .012 | * | .011 | * |
| FE | 1.403 | * | .784 | * | .759 | * | .710 | * | .745 | * | .839 | * | .852 | * | 1.077 | * |
| MG | 2.670 | * | 3.966 | * | 3.925 | * | 4.156 | * | 4.036 | * | 3.950 | * | 3.975 | * | 3.221 | * |
| MN | .045 | 5.200 | .004 | 5.055 | .005 | 5.070 | .007 | 5.067 | .016 | 5.070 | .014 | 5.134 | .007 | 5.118 | .010 | 5.110 |
| CA | 1.673 | * | 1.912 | * | 1.923 | * | 1.960 | * | 1.929 | * | 1.929 | * | 1.912 | * | 1.796 | * |
| K | .048 | * | .002 | * | .005 | * | .005 | * | .002 | * | .005 | * | .000 | * | .034 | * |
| NA | .395 | 2.116 | .112 | 2.026 | .147 | 2.076 | .067 | 2.033 | .111 | 2.041 | .109 | 2.044 | .163 | 2.074 | .398 | 2.229 |
| O | 23.000 | * | 23.000 | * | 23.000 | * | 23.000 | * | 23.000 | * | 23.000 | * | 23.000 | * | 23.000 | * |
| | CUMM | 46.47 | | 59.54 | | 59.40 | | 60.89 | | 60.15 | | 58.80 | | 58.99 | | 52.85 |
| | WO | 29.12 | | 28.70 | | 29.11 | | 28.72 | | 28.74 | | 28.72 | | 28.37 | | 29.47 |
| | GRUN | 24.42 | | 11.77 | | 11.49 | | 10.39 | | 11.11 | | 12.49 | | 12.64 | | 17.68 |
| | F/M | .542 | | .199 | | .195 | | .172 | | .189 | | .216 | | .216 | | .337 |
| | F/FM | .352 | | .166 | | .163 | | .147 | | .159 | | .178 | | .178 | | .252 |

17 C AMPH SHEAF C-1
18 ***** SAMPLE DDH114-295m C PLATE C-1 IM1546
19 AGAIN
20 AT MARGIN W MICA
21 CENTRAL RIBBED ZONE IM1550 C-3
22 AT MARGIN
23 RIBBED CENTRAL
24 BRIGHT RELIC CENTRAL IM0003,1552

TABLE 1, AMPHIBOLE, KAMINAK GOLD, ERIC BUITENHUIS, JUNE 2013, R.L.B.

| | 25 | | 26 | | 27 | | 28 | | 29 | | 30 | | 31 | | 32 | |
|---|---|---|---|---|---|---|---|---|---|---|---|---|---|---|---|---|
| SIO2 | 51.84 | | 49.05 | | 50.29 | | 50.30 | | 54.80 | | 55.02 | | 51.36 | | 49.38 | |
| TIO2 | .31 | | .25 | | .16 | | .35 | | .03 | | .00 | | .30 | | .24 | |
| A2O3 | 6.36 | | 10.39 | | 8.20 | | 6.96 | | 3.28 | | 2.73 | | 7.73 | | 10.59 | |
| C2O3 | .10 | | .24 | | .13 | | .50 | | .28 | | .26 | | .43 | | .24 | |
| FEO | 7.62 | | 9.11 | | 8.17 | | 7.84 | | 6.03 | | 6.29 | | 8.68 | | 8.38 | |
| MGO | 17.73 | | 14.96 | | 16.53 | | 17.17 | | 19.74 | | 19.75 | | 16.91 | | 15.39 | |
| MNO | .09 | | .08 | | .17 | | .10 | | .07 | | .02 | | .14 | | .17 | |
| CAO | 12.90 | | 12.31 | | 12.47 | | 12.63 | | 12.75 | | 12.69 | | 11.51 | | 12.01 | |
| K2O | .11 | | .25 | | .14 | | .12 | | .02 | | .00 | | .08 | | .12 | |
| NA2O | .64 | | 1.22 | | 1.03 | | .84 | | .30 | | .28 | | 1.20 | | 1.27 | |
| SUM | 97.70 | | 97.86 | | 97.29 | | 96.81 | | 97.30 | | 97.04 | | 98.34 | | 97.79 | |
| SI | 7.319 | * | 6.979 | * | 7.160 | * | 7.200 | * | 7.673 | * | 7.728 | * | 7.226 | * | 6.994 | * |
| AL | .681 | 8.000 | 1.021 | 8.000 | .840 | 8.000 | .800 | 8.000 | .327 | 8.000 | .272 | 8.000 | .774 | 8.000 | 1.006 | 8.000 |
| AL | .378 | * | .721 | * | .536 | * | .374 | * | .214 | * | .179 | * | .507 | * | .761 | * |
| TI | .033 | * | .027 | * | .017 | * | .038 | * | .003 | * | .000 | * | .032 | * | .026 | * |
| CR | .011 | * | .027 | * | .015 | * | .057 | * | .031 | * | .029 | * | .048 | * | .027 | * |
| FE | .900 | * | 1.084 | * | .973 | * | .938 | * | .706 | * | .739 | * | 1.021 | * | .993 | * |
| MG | 3.731 | * | 3.173 | * | 3.508 | * | 3.663 | * | 4.120 | * | 4.135 | * | 3.546 | * | 3.249 | * |
| MN | .011 | 5.063 | .010 | 5.041 | .021 | 5.069 | .012 | 5.082 | .008 | 5.082 | .002 | 5.084 | .017 | 5.171 | .020 | 5.075 |
| CA | 1.951 | * | 1.877 | * | 1.902 | * | 1.937 | * | 1.913 | * | 1.910 | * | 1.735 | * | 1.822 | * |
| K | .020 | * | .045 | * | .025 | * | .022 | * | .004 | * | .000 | * | .014 | * | .022 | * |
| NA | .175 | 2.146 | .337 | 2.259 | .284 | 2.212 | .233 | 2.192 | .081 | 1.998 | .076 | 1.986 | .327 | 2.077 | .349 | 2.193 |
| O | 23.000 | * | 23.000 | * | 23.000 | * | 23.000 | * | 23.000 | * | 23.000 | * | 23.000 | * | 23.000 | * |
| | CUMM | 56.68 | | 51.73 | | 54.96 | | 56.02 | | 61.14 | | 60.95 | | 56.27 | | 53.58 |
| | WO | 29.65 | | 30.60 | | 29.80 | | 29.62 | | 28.38 | | 28.15 | | 27.53 | | 30.05 |
| | GRUN | 13.67 | | 17.67 | | 15.24 | | 14.35 | | 10.48 | | 10.89 | | 16.20 | | 16.37 |
| | F/M | .244 | | .345 | | .283 | | .260 | | .173 | | .179 | | .293 | | .312 |
| | F/FM | .196 | | .256 | | .221 | | .206 | | .148 | | .152 | | .226 | | .238 |

25 RELIC DOMAIN CENTRAL
26 RELIC DOMAIN CENTRAL
27 RELIC DOMAIN CENTRAL
28 SURROUNDING HOST ZONED
29 SURROUNDING HOST ZONED
30 SURROUNDING HOST ZONED
31 ***** SAMPLE DDH114-296.0m C-1 ATTEN AMPHIBOLITE W BIO
32 INT W CHROMIAN MG MICA

TABLE 1, AMPHIBOLE, KAMINAK GOLD, ERIC BUITENHUIS, JUNE 2013, R.L.B.

| | 33 | | 34 | | 35 | | 36 | | 37 | | 38 | |
|---|---|---|---|---|---|---|---|---|---|---|---|---|
| SIO2 | 49.40 | | 48.79 | | 47.30 | | 48.11 | | 51.43 | | 50.23 | |
| TIO2 | .19 | | .23 | | .24 | | .26 | | .24 | | .17 | |
| A2O3 | 10.48 | | 11.39 | | 13.59 | | 12.89 | | 8.49 | | 9.53 | |
| C2O3 | .30 | | .23 | | .24 | | .09 | | .33 | | .07 | |
| FEO | 8.26 | | 8.42 | | 9.24 | | 9.11 | | 7.89 | | 8.07 | |
| MGO | 15.82 | | 15.39 | | 14.16 | | 14.62 | | 16.94 | | 16.18 | |
| MNO | .09 | | .18 | | .17 | | .18 | | .19 | | .13 | |
| CAO | 11.74 | | 11.65 | | 11.30 | | 11.33 | | 11.42 | | 11.95 | |
| K2O | .13 | | .17 | | .20 | | .20 | | .08 | | .07 | |
| NA2O | 1.42 | | 1.49 | | 1.77 | | 1.76 | | 1.11 | | 1.24 | |
| SUM | 97.83 | | 97.94 | | 98.21 | | 98.55 | | 98.12 | | 97.64 | |
| SI | 6.989 | * | 6.905 | * | 6.707 | * | 6.787 | * | 7.213 | * | 7.102 | * |
| AL | 1.011 | 8.000 | 1.095 | 8.000 | 1.293 | 8.000 | 1.213 | 8.000 | .787 | 8.000 | .898 | 8.000 |
| AL | .736 | * | .805 | * | .978 | * | .929 | * | .616 | * | .690 | * |
| TI | .020 | * | .024 | * | .026 | * | .028 | * | .025 | * | .018 | * |
| CR | .034 | * | .026 | * | .027 | * | .010 | * | .037 | * | .008 | * |
| FE | .977 | * | .997 | * | 1.096 | * | 1.075 | * | .925 | * | .954 | * |
| MG | 3.336 | * | 3.247 | * | 2.993 | * | 3.074 | * | 3.541 | * | 3.410 | * |
| MN | .011 | 5.114 | .022 | 5.120 | .020 | 5.139 | .022 | 5.137 | .023 | 5.167 | .016 | 5.095 |
| CA | 1.780 | * | 1.767 | * | 1.717 | * | 1.712 | * | 1.716 | * | 1.810 | * |
| K | .023 | * | .031 | * | .036 | * | .036 | * | .014 | * | .013 | * |
| NA | .389 | 2.192 | .409 | 2.206 | .487 | 2.240 | .481 | 2.230 | .302 | 2.032 | .340 | 2.163 |
| O | 23.000 | * | 23.000 | * | 23.000 | * | 23.000 | * | 23.000 | * | 23.000 | * |
| CUMM | 54.75 | | 54.02 | | 51.55 | | 52.45 | | 57.28 | | 55.23 | |
| WO | 29.21 | | 29.40 | | 29.57 | | 29.22 | | 27.76 | | 29.32 | |
| GRUN | 16.04 | | 16.58 | | 18.87 | | 18.34 | | 14.97 | | 15.45 | |
| F/M | .296 | | .314 | | .373 | | .357 | | .268 | | .284 | |
| F/FM | .229 | | .239 | | .272 | | .263 | | .211 | | .221 | |

33 INT W MG MICA
34 INT W MG MICA
35 INT W MG MICA
36 INT W MG MICA
37 C ATTEN C-2
38 C ATTEN C-2

TABLE 2: PHLOGOPITE-BIOTITEss., KAMINAK GOLD, ERIC BUTENHUIS, JUNE 2013, R.L.B.

| | 1 | 2 | 3 | 4 | 5 | 6 | 7 | 8 |
|---|---|---|---|---|---|---|---|---|
| SIO2 | 38.33 | 38.34 | 37.14 | 37.09 | 37.98 | 38.49 | 37.82 | 38.20 |
| TIO2 | 1.34 | 1.36 | 1.43 | 1.45 | 1.42 | 1.61 | 1.56 | 1.48 |
| A2O3 | 16.48 | 16.84 | 16.90 | 16.78 | 17.47 | 16.37 | 17.04 | 17.59 |
| C2O3 | .03 | .13 | .09 | .25 | .16 | .03 | .00 | .00 |
| FEO | 13.98 | 14.09 | 17.78 | 17.31 | 15.90 | 18.74 | 19.47 | 19.10 |
| MGO | 15.03 | 14.52 | 12.84 | 13.27 | 13.88 | 11.61 | 10.82 | 10.02 |
| MNO | .19 | .06 | .11 | .11 | .10 | .11 | .08 | .08 |
| BAO | .02 | .07 | .11 | .15 | .21 | .00 | .00 | .00 |
| CAO | .00 | .00 | .08 | .02 | .00 | .00 | .00 | .00 |
| K2O | 10.01 | 9.82 | 9.24 | 9.87 | 9.67 | 9.95 | 10.07 | 10.22 |
| NA2O | .08 | .18 | .19 | .08 | .19 | .11 | .09 | .07 |
| SUM | 95.49 | 95.41 | 95.91 | 96.38 | 96.98 | 97.02 | 96.95 | 96.76 |

| | | | | | | | | | | | | | | | | |
|---|---|---|---|---|---|---|---|---|---|---|---|---|---|---|---|---|
| SI | 5.676 | * | 5.676 | * | 5.569 | * | 5.546 | * | 5.582 | * | 5.725 | * | 5.656 | * | 5.706 | * |
| AL | 2.324 | 8.000 | 2.324 | 8.000 | 2.431 | 8.000 | 2.454 | 8.000 | 2.418 | 8.000 | 2.275 | 8.000 | 2.344 | 8.000 | 2.294 | 8.000 |
| AL | .551 | * | .614 | * | .554 | * | .502 | * | .608 | * | .594 | * | .659 | * | .801 | * |
| TI | .149 | * | .151 | * | .161 | * | .163 | * | .157 | * | .180 | * | .175 | * | .166 | * |
| CR | .004 | * | .015 | * | .011 | * | .030 | * | .019 | * | .004 | * | .000 | * | .000 | * |
| FE | 1.731 | * | 1.744 | * | 2.229 | * | 2.165 | * | 1.954 | * | 2.331 | * | 2.435 | * | 2.386 | * |
| MG | 3.317 | * | 3.204 | * | 2.869 | * | 2.957 | * | 3.041 | * | 2.574 | * | 2.412 | * | 2.231 | * |
| MN | .024 | 5.776 | .008 | 5.737 | .014 | 5.839 | .014 | 5.831 | .012 | 5.791 | .014 | 5.697 | .010 | 5.691 | .010 | 5.594 |
| CA | .000 | * | .000 | * | .013 | * | .003 | * | .000 | * | .000 | * | .000 | * | .000 | * |
| BA | .001 | * | .004 | * | .006 | * | .009 | * | .012 | * | .000 | * | .000 | * | .000 | * |
| K | 1.890 | * | 1.854 | * | 1.767 | * | 1.882 | * | 1.813 | * | 1.888 | * | 1.921 | * | 1.947 | * |
| NA | .023 | 1.915 | .052 | 1.910 | .055 | 1.842 | .023 | 1.918 | .054 | 1.879 | .032 | 1.919 | .026 | 1.947 | .020 | 1.967 |
| O | 22.000 | * | 22.000 | * | 22.000 | * | 22.000 | * | 22.000 | * | 22.000 | * | 22.000 | * | 22.000 | * |
| | FE | 34.29 | | 35.25 | | 43.72 | | 42.26 | | 39.13 | | 47.52 | | 50.24 | | 51.68 |
| | MG | 65.71 | | 64.75 | | 56.28 | | 57.74 | | 60.87 | | 52.48 | | 49.76 | | 48.32 |
| | F/M | .529 | | .547 | | .782 | | .737 | | .647 | | .911 | | 1.014 | | 1.074 |
| | F/FM | .346 | | .354 | | .439 | | .424 | | .393 | | .477 | | .503 | | .518 |

1 **** DDH82-161.2m C FOL C-1
2 C FOL C-1
3 **** DDH82-170.6m C-1 INT W AMPH
4 INT W AMPH
5 C PLATE C-2
6 **** DDH82-223.0m GREEN BIO, C-1 IM1505.6
7 C-2
8 C-2

TABLE 2: PHLOGOPITE-BIOTITEss., KAMINAK GOLD, ERIC BUTENHUIS, JUNE 2013, R.L.B.

| | 9 | 10 | 11 | 12 | 13 | 14 | 15 | 16 |
|---|---|---|---|---|---|---|---|---|
| SIO2 | 36.94 | 37.66 | 37.59 | 38.23 | 38.08 | 38.28 | 38.58 | 38.19 |
| TIO2 | .98 | 1.86 | 1.20 | 1.13 | 1.14 | .95 | 1.18 | 1.17 |
| A2O3 | 16.88 | 17.15 | 16.27 | 16.40 | 15.68 | 15.97 | 16.35 | 15.76 |
| C2O3 | .06 | .00 | .02 | .02 | .02 | .06 | .01 | .09 |
| FEO | 20.10 | 19.67 | 14.11 | 13.62 | 12.56 | 13.45 | 13.18 | 13.62 |
| MGO | 11.01 | 10.05 | 15.43 | 15.97 | 15.51 | 15.89 | 16.02 | 15.23 |
| MNO | .10 | .02 | .08 | .08 | .07 | .10 | .11 | .07 |
| BAO | .00 | .01 | .00 | .00 | .00 | .00 | .04 | .10 |
| CAO | .00 | .00 | .00 | .01 | .09 | .09 | .39 | .05 |
| K2O | 10.18 | 10.19 | 9.59 | 9.10 | 8.27 | 9.28 | 9.45 | 9.95 |
| NA2O | .08 | .09 | .24 | .28 | .30 | .17 | .32 | .23 |
| SUM | 96.33 | 96.70 | 94.53 | 94.84 | 91.72 | 94.24 | 95.63 | 94.46 |

| | | | | | | | | | | | | | | | | |
|---|---|---|---|---|---|---|---|---|---|---|---|---|---|---|---|---|
| SI | 5.599 | * | 5.656 | * | 5.626 | * | 5.662 | * | 5.779 | * | 5.710 | * | 5.673 | * | 5.718 | * |
| AL | 2.401 | 8.000 | 2.344 | 8.000 | 2.374 | 8.000 | 2.338 | 8.000 | 2.221 | 8.000 | 2.290 | 8.000 | 2.327 | 8.000 | 2.282 | 8.000 |
| AL | .614 | * | .691 | * | .495 | * | .525 | * | .583 | * | .516 | * | .505 | * | .499 | * |
| TI | .112 | * | .210 | * | .135 | * | .126 | * | .130 | * | .107 | * | .130 | * | .132 | * |
| CR | .007 | * | .000 | * | .002 | * | .002 | * | .002 | * | .007 | * | .001 | * | .011 | * |
| FE | 2.548 | * | 2.471 | * | 1.766 | * | 1.687 | * | 1.594 | * | 1.678 | * | 1.621 | * | 1.705 | * |
| MG | 2.487 | * | 2.250 | * | 3.442 | * | 3.526 | * | 3.508 | * | 3.533 | * | 3.511 | * | 3.399 | * |
| MN | .013 | 5.780 | .003 | 5.624 | .010 | 5.851 | .010 | 5.876 | .009 | 5.827 | .013 | 5.853 | .014 | 5.782 | .009 | 5.755 |
| CA | .000 | * | .000 | * | .000 | * | .002 | * | .015 | * | .014 | * | .061 | * | .008 | * |
| BA | .000 | * | .001 | * | .000 | * | .000 | * | .000 | * | .000 | * | .002 | * | .006 | * |
| K | 1.968 | * | 1.952 | * | 1.831 | * | 1.719 | * | 1.601 | * | 1.765 | * | 1.772 | * | 1.900 | * |
| NA | .024 | 1.992 | .026 | 1.979 | .070 | 1.900 | .080 | 1.801 | .088 | 1.704 | .049 | 1.829 | .091 | 1.927 | .067 | 1.981 |
| O | 22.000 | * | 22.000 | * | 22.000 | * | 22.000 | * | 22.000 | * | 22.000 | * | 22.000 | * | 22.000 | * |
| | FE | 50.60 | | 52.34 | | 33.91 | | 32.36 | | 31.24 | | 32.20 | | 31.58 | | 33.41 |
| | MG | 49.40 | | 47.66 | | 66.09 | | 67.64 | | 68.76 | | 67.80 | | 68.42 | | 66.59 |
| | F/M | 1.029 | | 1.099 | | .516 | | .481 | | .457 | | .478 | | .466 | | .504 |
| | F/FM | .507 | | .524 | | .340 | | .325 | | .314 | | .324 | | .318 | | .335 |

9 C-2
10 C-2
11 **** DDH114-44.0m C PLATE
12 C PLATE
13 C PLATE
14 C PLATE
15 C PLATE
16 C PLATE

TABLE 2: PHLOGOPITE-BIOTITEss., KAMINAK GOLD, ERIC BUTENHUIS, JUNE 2013, R.L.B.

| | 17 | | 18 | | 19 | | 20 | | 21 | | 22 | | 23 | | 24 | |
|---|---|---|---|---|---|---|---|---|---|---|---|---|---|---|---|---|
| SIO2 | 38.03 | | 38.79 | | 38.14 | | 37.72 | | 37.37 | | 38.44 | | 38.31 | | 37.38 | |
| TIO2 | 1.50 | | 1.44 | | 1.25 | | 1.77 | | 1.74 | | 1.20 | | 1.21 | | 1.26 | |
| A2O3 | 16.49 | | 16.06 | | 16.74 | | 15.79 | | 15.86 | | 16.74 | | 18.44 | | 18.30 | |
| C2O3 | .10 | | .00 | | .02 | | .00 | | .04 | | .07 | | .03 | | .10 | |
| FEO | 13.67 | | 13.45 | | 13.61 | | 16.89 | | 17.58 | | 13.82 | | 13.90 | | 13.47 | |
| MGO | 14.81 | | 14.25 | | 14.64 | | 12.90 | | 12.85 | | 15.11 | | 14.92 | | 14.87 | |
| MNO | .30 | | .18 | | .22 | | .16 | | .21 | | .13 | | .21 | | .16 | |
| BAO | .00 | | .00 | | .00 | | .00 | | .01 | | .00 | | .00 | | .01 | |
| CAO | .08 | | .14 | | .02 | | .00 | | .00 | | .00 | | .01 | | .00 | |
| K2O | 9.59 | | 9.48 | | 10.18 | | 10.06 | | 10.10 | | 9.33 | | 9.84 | | 10.18 | |
| NA2O | .22 | | .18 | | .16 | | .14 | | .18 | | .10 | | .13 | | .09 | |
| SUM | 94.79 | | 93.97 | | 94.98 | | 95.43 | | 95.94 | | 94.94 | | 97.00 | | 95.82 | |
| SI | 5.662 | * | 5.799 | * | 5.675 | * | 5.681 | * | 5.627 | * | 5.691 | * | 5.562 | * | 5.509 | * |
| AL | 2.338 | 8.000 | 2.201 | 8.000 | 2.325 | 8.000 | 2.319 | 8.000 | 2.373 | 8.000 | 2.309 | 8.000 | 2.438 | 8.000 | 2.491 | 8.000 |
| AL | .555 | * | .628 | * | .611 | * | .484 | * | .441 | * | .611 | * | .716 | * | .687 | * |
| TI | .168 | * | .162 | * | .140 | * | .200 | * | .197 | * | .134 | * | .132 | * | .140 | * |
| CR | .012 | * | .000 | * | .002 | * | .000 | * | .005 | * | .008 | * | .003 | * | .012 | * |
| FE | 1.702 | * | 1.682 | * | 1.694 | * | 2.127 | * | 2.214 | * | 1.711 | * | 1.688 | * | 1.660 | * |
| MG | 3.286 | * | 3.175 | * | 3.247 | * | 2.896 | * | 2.884 | * | 3.334 | * | 3.229 | * | 3.266 | * |
| MN | .038 | 5.761 | .023 | 5.670 | .028 | 5.721 | .020 | 5.728 | .027 | 5.768 | .016 | 5.814 | .026 | 5.794 | .020 | 5.784 |
| CA | .013 | * | .022 | * | .003 | * | .000 | * | .000 | * | .000 | * | .002 | * | .000 | * |
| BA | .000 | * | .000 | * | .000 | * | .000 | * | .001 | * | .000 | * | .000 | * | .001 | * |
| K | 1.821 | * | 1.808 | * | 1.932 | * | 1.933 | * | 1.940 | * | 1.762 | * | 1.822 | * | 1.914 | * |
| NA | .064 | 1.897 | .052 | 1.882 | .046 | 1.981 | .041 | 1.974 | .053 | 1.993 | .029 | 1.790 | .037 | 1.860 | .026 | 1.940 |
| O | 22.000 | * | 22.000 | * | 22.000 | * | 22.000 | * | 22.000 | * | 22.000 | * | 22.000 | * | 22.000 | * |
| | FE | 34.12 | | 34.62 | | 34.28 | | 42.35 | | 43.43 | | 33.91 | | 34.33 | | 33.70 |
| | MG | 65.88 | | 65.38 | | 65.72 | | 57.65 | | 56.57 | | 66.09 | | 65.67 | | 66.30 |
| | F/M | .529 | | .537 | | .530 | | .742 | | .777 | | .518 | | .531 | | .514 |
| | F/FM | .346 | | .349 | | .346 | | .426 | | .437 | | .341 | | .347 | | .340 |

17 **** DDH114-114.0m C-1 iNT W PHENG MUSC
18 RELICT METAM BIO REPL BY CHL
19 RELICT METAM BIO REPL BY CHL
20 **** DDH114-179.0m C GREEN PLATE C-2
21 INST PLAG
22 **** DDH114-272.0m STRONG FABRIC
23 BRIGHT
24 BRIGHT

TABLE 2: PHLOGOPITE-BIOTITEss., KAMINAK GOLD, ERIC BUTENHUIS, JUNE 2013, R.L.B.

| | 25 | | 26 | | 27 | | 28 | | 29 | | 30 | | 31 | | 32 | |
|---|---|---|---|---|---|---|---|---|---|---|---|---|---|---|---|---|
| SIO2 | 37.59 | | 37.59 | | 39.17 | | 38.95 | | 39.01 | | 39.01 | | 39.02 | | 38.96 | |
| TIO2 | 1.23 | | 1.02 | | .99 | | .99 | | .97 | | .86 | | .98 | | 1.04 | |
| A2O3 | 17.84 | | 17.83 | | 17.71 | | 17.56 | | 17.81 | | 17.53 | | 18.01 | | 18.03 | |
| C2O3 | .05 | | .06 | | .00 | | .00 | | .12 | | 1.00 | | 1.05 | | .32 | |
| FEO | 13.36 | | 14.16 | | 10.12 | | 9.97 | | 10.13 | | 10.16 | | 10.68 | | 8.90 | |
| MGO | 14.73 | | 14.69 | | 16.37 | | 17.08 | | 17.27 | | 16.16 | | 16.05 | | 16.56 | |
| MNO | .15 | | .18 | | .00 | | .03 | | .12 | | .01 | | .04 | | .00 | |
| BAO | .13 | | .00 | | .03 | | .01 | | .05 | | .00 | | .00 | | .00 | |
| CAO | .00 | | .11 | | .00 | | .02 | | .01 | | .00 | | .00 | | .00 | |
| K2O | 9.91 | | 10.06 | | 9.41 | | 9.83 | | 8.89 | | 9.78 | | 10.03 | | 10.05 | |
| NA2O | .12 | | .08 | | .17 | | .18 | | .24 | | .12 | | .09 | | .14 | |
| SUM | 95.11 | | 95.78 | | 93.97 | | 94.62 | | 94.62 | | 94.63 | | 95.95 | | 94.00 | |
| SI | 5.573 | * | 5.557 | * | 5.738 | * | 5.685 | * | 5.670 | * | 5.705 | * | 5.648 | * | 5.698 | * |
| AL | 2.427 | 8.000 | 2.443 | 8.000 | 2.262 | 8.000 | 2.315 | 8.000 | 2.330 | 8.000 | 2.295 | 8.000 | 2.352 | 8.000 | 2.302 | 8.000 |
| AL | .690 | * | .663 | * | .795 | * | .705 | * | .720 | * | .725 | * | .720 | * | .806 | * |
| TI | .137 | * | .113 | * | .109 | * | .109 | * | .106 | * | .095 | * | .107 | * | .114 | * |
| CR | .006 | * | .007 | * | .000 | * | .000 | * | .014 | * | .116 | * | .120 | * | .037 | * |
| FE | 1.657 | * | 1.751 | * | 1.240 | * | 1.217 | * | 1.231 | * | 1.242 | * | 1.293 | * | 1.089 | * |
| MG | 3.255 | * | 3.237 | * | 3.574 | * | 3.716 | * | 3.741 | * | 3.522 | * | 3.463 | * | 3.610 | * |
| MN | .019 | 5.764 | .023 | 5.793 | .000 | 5.718 | .004 | 5.750 | .015 | 5.828 | .001 | 5.701 | .005 | 5.708 | .000 | 5.656 |
| CA | .000 | * | .017 | * | .000 | * | .003 | * | .002 | * | .000 | * | .000 | * | .000 | * |
| BA | .008 | * | .000 | * | .002 | * | .001 | * | .003 | * | .000 | * | .000 | * | .000 | * |
| K | 1.874 | * | 1.897 | * | 1.758 | * | 1.830 | * | 1.648 | * | 1.824 | * | 1.852 | * | 1.875 | * |
| NA | .034 | 1.916 | .023 | 1.937 | .048 | 1.808 | .051 | 1.885 | .068 | 1.720 | .034 | 1.858 | .025 | 1.877 | .040 | 1.915 |
| O | 22.000 | * | 22.000 | * | 22.000 | * | 22.000 | * | 22.000 | * | 22.000 | * | 22.000 | * | 22.000 | * |
| FE | 33.73 | | 35.10 | | 25.75 | | 24.67 | | 24.76 | | 26.08 | | 27.19 | | 23.17 | |
| MG | 66.27 | | 64.90 | | 74.25 | | 75.33 | | 75.24 | | 73.92 | | 72.81 | | 76.83 | |
| F/M | .515 | | .548 | | .347 | | .329 | | .333 | | .353 | | .375 | | .302 | |
| F/FM | .340 | | .354 | | .258 | | .247 | | .250 | | .261 | | .273 | | .232 | |

25 C BIOT-PHLOG AMPH SHEAF C-1
26 C AMPH SHEAF C-1
27 **** DDH114-295m LARGE PLATE IM1548 C-2
28 C PLATE W AMPH, C-3 IM1549
29 C PLATE W AMPH, C-3 IM1549
30 **** DDH114-296.0m C-1 C-1 ATTEN AMPHIGOLITE W BIO
31 C-1 ATTEN AMPHIGOLITE W BIO
32 C NEAR PLAG W APAT

TABLE 2: PHLOGOPITE-BIOTITEss., KAMINAK GOLD, ERIC BUTENHUIS, JUNE 2013, R.L.B.

| | 33 | |
|---|---|---|
| SIO2 | 38.54 | |
| TIO2 | .75 | |
| A2O3 | 18.45 | |
| C2O3 | .25 | |
| FEO | 10.64 | |
| MGO | 16.75 | |
| MNO | .00 | |
| BAO | .00 | |
| CAO | .01 | |
| K2O | 9.38 | |
| NA2O | .12 | |
| SUM | 94.89 | |
| SI | 5.611 | * |
| AL | 2.389 | 8.000 |
| AL | .777 | * |
| TI | .082 | * |
| CR | .029 | * |
| FE | 1.296 | * |
| MG | 3.635 | * |
| MN | .000 | 5.818 |
| CA | .002 | * |
| BA | .000 | * |
| K | 1.742 | * |
| NA | .034 | 1.777 |
| O | 22.000 | * |
| FE | 26.28 | |
| MG | 73.72 | |
| F/M | .356 | |
| F/FM | .263 | |

33 C ATTEN C-2

TABLE 3: PHENGITIC MUSC, KAMINAK GOLD, ERIC BUITENHUIS, JUNE 2013, R.L.B.

| | 1 | | 2 | | 3 | | 4 | | 5 | | 6 | | 7 | | 8 | |
|---|---|---|---|---|---|---|---|---|---|---|---|---|---|---|---|---|
| SIO2 | 52.29 | | 51.97 | | 52.14 | | 52.22 | | 53.15 | | 52.33 | | 52.07 | | 53.09 | |
| TIO2 | 1.41 | | 2.71 | | .31 | | .28 | | .48 | | .26 | | .21 | | .31 | |
| A2O3 | 31.27 | | 30.35 | | 33.34 | | 33.44 | | 30.99 | | 34.19 | | 34.26 | | 33.77 | |
| C2O3 | .02 | | .00 | | .00 | | .06 | | .00 | | .02 | | .04 | | .04 | |
| FEO | 1.04 | | .84 | | 1.21 | | .60 | | 1.15 | | .38 | | .43 | | .37 | |
| MGO | 1.87 | | 2.56 | | 1.22 | | 2.12 | | 2.19 | | 1.68 | | 1.48 | | 2.03 | |
| MNO | .00 | | .00 | | .00 | | .00 | | .00 | | .01 | | .00 | | .00 | |
| BAO | .00 | | .00 | | .00 | | .00 | | .00 | | .00 | | .00 | | .00 | |
| CAO | .02 | | .05 | | .00 | | .06 | | .10 | | .06 | | .00 | | .03 | |
| K2O | 8.40 | | 6.08 | | 7.70 | | 7.94 | | 8.08 | | 6.06 | | 8.32 | | 6.33 | |
| NA2O | .05 | | .05 | | .01 | | .01 | | .01 | | .00 | | .00 | | .04 | |
| SUM | 96.37 | | 94.61 | | 95.93 | | 96.73 | | 96.15 | | 94.99 | | 96.81 | | 96.01 | |
| SI | 6.723 | * | 6.718 | * | 6.690 | * | 6.646 | * | 6.825 | * | 6.682 | * | 6.623 | * | 6.718 | * |
| AL | 1.277 | 8.000 | 1.282 | 8.000 | 1.310 | 8.000 | 1.354 | 8.000 | 1.175 | 8.000 | 1.318 | 8.000 | 1.377 | 8.000 | 1.282 | 8.000 |
| AL | 3.461 | * | 3.342 | * | 3.732 | * | 3.661 | * | 3.515 | * | 3.827 | * | 3.758 | * | 3.754 | * |
| TI | .136 | * | .263 | * | .030 | * | .027 | * | .046 | * | .025 | * | .020 | * | .030 | * |
| CR | .002 | * | .000 | * | .000 | * | .006 | * | .000 | * | .002 | * | .004 | * | .004 | * |
| FE | .112 | * | .091 | * | .130 | * | .064 | * | .124 | * | .041 | * | .046 | * | .039 | * |
| MG | .358 | * | .493 | * | .233 | * | .402 | * | .419 | * | .320 | * | .281 | * | .383 | * |
| MN | .000 | 4.070 | .000 | 4.189 | .000 | 4.125 | .000 | 4.160 | .000 | 4.104 | .001 | 4.215 | .000 | 4.109 | .000 | 4.210 |
| CA | .003 | * | .007 | * | .000 | * | .008 | * | .014 | * | .008 | * | .000 | * | .004 | * |
| BA | .000 | * | .000 | * | .000 | * | .000 | * | .000 | * | .000 | * | .000 | * | .000 | * |
| K | 1.378 | * | 1.003 | * | 1.260 | * | 1.289 | * | 1.323 | * | .987 | * | 1.350 | * | 1.022 | * |
| NA | .012 | 1.393 | .013 | 1.022 | .002 | 1.263 | .002 | 1.300 | .002 | 1.340 | .000 | .995 | .000 | 1.350 | .010 | 1.036 |
| O | 22.000 | * | 22.000 | * | 22.000 | * | 22.000 | * | 22.000 | * | 22.000 | * | 22.000 | * | 22.000 | * |
| | FE | 23.78 | | 15.55 | | 35.75 | | 13.70 | | 22.76 | | 11.26 | | 14.02 | | 9.28 |
| | MG | 76.22 | | 84.45 | | 64.25 | | 86.30 | | 77.24 | | 88.74 | | 85.98 | | 90.72 |
| | F/M | .312 | | .184 | | .556 | | .159 | | .295 | | .130 | | .163 | | .102 |
| | F/FM | .238 | | .155 | | .358 | | .137 | | .228 | | .115 | | .140 | | .093 |

1 **** DDH82-117.5m ALT MICA IM0614
2 ALTERED MICA W PY SULPHURIZED
3 VERY DARK
4 PYRITE-MUSC ALT C-2 IM1619, BSE0009
5 INT W DOLOMITE-ANK
6 INT W DOLOMITE-ANK
7 INT W DOLOMITE-ANK
8 INT W DOLOMITE-ANK

TABLE 3: PHENGITIC MUSC, KAMINAK GOLD, ERIC BUITENHUIS, JUNE 2013, R.L.B.

| | 9 | | 10 | | 11 | | 12 | | 13 | | 14 | | 15 | | 16 | |
|---|---|---|---|---|---|---|---|---|---|---|---|---|---|---|---|---|
| SIO2 | 51.84 | | 51.64 | | 50.95 | | 49.03 | | 52.75 | | 53.46 | | 50.35 | | 52.72 | |
| TIO2 | .78 | | .36 | | .14 | | .20 | | .84 | | 1.15 | | 1.60 | | 1.59 | |
| A2O3 | 33.58 | | 35.10 | | 30.09 | | 28.94 | | 32.93 | | 32.41 | | 32.31 | | 31.34 | |
| C2O3 | .37 | | .30 | | .07 | | .03 | | .09 | | .16 | | .08 | | .13 | |
| FEO | .59 | | .25 | | 3.12 | | 2.96 | | .30 | | .32 | | .62 | | .62 | |
| MGO | 1.88 | | 1.54 | | 2.66 | | 2.84 | | 1.81 | | 1.86 | | 2.19 | | 2.20 | |
| MNO | .00 | | .00 | | .00 | | .03 | | .00 | | .00 | | .00 | | .00 | |
| BAO | .00 | | .00 | | .00 | | .03 | | .00 | | .00 | | .00 | | .00 | |
| CAO | .00 | | .02 | | .00 | | .00 | | .05 | | .07 | | .00 | | .02 | |
| K2O | 6.38 | | 7.78 | | 8.69 | | 11.01 | | 7.31 | | 5.87 | | 7.38 | | 8.61 | |
| NA2O | .02 | | .00 | | .29 | | .17 | | .04 | | .01 | | .00 | | .00 | |
| SUM | 95.44 | | 96.99 | | 96.01 | | 95.24 | | 96.12 | | 95.31 | | 94.53 | | 97.23 | |
| SI | 6.629 | * | 6.539 | * | 6.680 | * | 6.597 | * | 6.716 | * | 6.798 | * | 6.561 | * | 6.715 | * |
| AL | 1.371 | 8.000 | 1.461 | 8.000 | 1.320 | 8.000 | 1.403 | 8.000 | 1.284 | 8.000 | 1.202 | 8.000 | 1.439 | 8.000 | 1.285 | 8.000 |
| AL | 3.688 | * | 3.777 | * | 3.329 | * | 3.186 | * | 3.656 | * | 3.654 | * | 3.523 | * | 3.419 | * |
| TI | .075 | * | .034 | * | .014 | * | .020 | * | .080 | * | .110 | * | .157 | * | .152 | * |
| CR | .037 | * | .030 | * | .007 | * | .003 | * | .009 | * | .016 | * | .008 | * | .013 | * |
| FE | .063 | * | .026 | * | .342 | * | .333 | * | .032 | * | .034 | * | .068 | * | .066 | * |
| MG | .358 | * | .291 | * | .520 | * | .570 | * | .343 | * | .353 | * | .425 | * | .418 | * |
| MN | .000 | 4.222 | .000 | 4.158 | .000 | 4.212 | .003 | 4.115 | .000 | 4.121 | .000 | 4.166 | .000 | 4.181 | .000 | 4.069 |
| CA | .000 | * | .003 | * | .000 | * | .000 | * | .007 | * | .010 | * | .000 | * | .003 | * |
| BA | .000 | * | .000 | * | .000 | * | .002 | * | .000 | * | .000 | * | .000 | * | .000 | * |
| K | 1.041 | * | 1.257 | * | 1.453 | * | 1.890 | * | 1.187 | * | .952 | * | 1.227 | * | 1.399 | * |
| NA | .005 | 1.045 | .000 | 1.259 | .074 | 1.527 | .044 | 1.935 | .010 | 1.204 | .002 | .964 | .000 | 1.227 | .000 | 1.402 |
| O | 22.000 | * | 22.000 | * | 22.000 | * | 22.000 | * | 22.000 | * | 22.000 | * | 22.000 | * | 22.000 | * |
| FE | 14.97 | | 8.35 | | 39.69 | | 36.90 | | 8.51 | | 8.80 | | 13.71 | | 13.65 | |
| MG | 85.03 | | 91.65 | | 60.31 | | 63.10 | | 91.49 | | 91.20 | | 86.29 | | 86.35 | |
| F/M | .176 | | .091 | | .658 | | .591 | | .093 | | .097 | | .159 | | .158 | |
| F/FM | .150 | | .083 | | .397 | | .371 | | .085 | | .088 | | .137 | | .137 | |

9 INT W FE-RICH DOL
10 INT W FE-RICH DOL
11 ATTEN REL IM 0010 S 1
12 STILL BRIGHT SPOT 2
13 DARK MARGIN SPOT 3
14 DARK AT M W ELEV TI
15 DARK AT M W ELEV TI
16 DARK AT M W ELEV TI

TABLE 3: PHENGITIC MUSC, KAMINAK GOLD, ERIC BUITENHUIS, JUNE 2013, R.L.B.

| | 17 | | 18 | | 19 | | 20 | | 21 | | 22 | | 23 | | 24 | |
|---|---|---|---|---|---|---|---|---|---|---|---|---|---|---|---|---|
| SIO2 | 45.89 | | 50.25 | | 50.19 | | 51.90 | | 50.58 | | 51.91 | | 50.78 | | 52.50 | |
| TIO2 | .18 | | .16 | | .14 | | 1.67 | | 1.14 | | 1.43 | | 1.30 | | 1.36 | |
| A2O3 | 29.66 | | 29.90 | | 28.67 | | 32.14 | | 31.58 | | 31.69 | | 33.28 | | 31.50 | |
| C2O3 | .00 | | .00 | | .11 | | .11 | | .00 | | .02 | | .00 | | .04 | |
| FEO | 3.10 | | 2.97 | | 3.19 | | .65 | | 1.09 | | 1.04 | | .69 | | .57 | |
| MGO | 2.75 | | 2.78 | | 2.62 | | 2.19 | | 2.36 | | 2.45 | | 1.83 | | 2.17 | |
| MNO | .00 | | .00 | | .01 | | .00 | | .00 | | .01 | | .00 | | .00 | |
| BAO | .03 | | .03 | | .02 | | .00 | | .00 | | .00 | | .00 | | .00 | |
| CAO | .00 | | .00 | | .00 | | .03 | | .03 | | .02 | | .04 | | .01 | |
| K2O | 10.33 | | 8.01 | | 10.63 | | 6.77 | | 7.22 | | 6.01 | | 7.29 | | 7.17 | |
| NA2O | .39 | | .49 | | .26 | | .05 | | .03 | | .04 | | .01 | | .03 | |
| SUM | 92.33 | | 94.59 | | 95.84 | | 95.51 | | 94.03 | | 94.62 | | 95.22 | | 95.35 | |
| SI | 6.383 | * | 6.666 | * | 6.690 | * | 6.658 | * | 6.631 | * | 6.700 | * | 6.557 | * | 6.750 | * |
| AL | 1.617 | 8.000 | 1.334 | 8.000 | 1.310 | 8.000 | 1.342 | 8.000 | 1.369 | 8.000 | 1.300 | 8.000 | 1.443 | 8.000 | 1.250 | 8.000 |
| AL | 3.244 | * | 3.340 | * | 3.194 | * | 3.517 | * | 3.510 | * | 3.520 | * | 3.621 | * | 3.522 | * |
| TI | .019 | * | .016 | * | .014 | * | .161 | * | .112 | * | .139 | * | .126 | * | .131 | * |
| CR | .000 | * | .000 | * | .012 | * | .011 | * | .000 | * | .002 | * | .000 | * | .004 | * |
| FE | .361 | * | .330 | * | .356 | * | .070 | * | .120 | * | .112 | * | .075 | * | .061 | * |
| MG | .570 | * | .550 | * | .521 | * | .419 | * | .461 | * | .471 | * | .352 | * | .416 | * |
| MN | .000 | 4.194 | .000 | 4.236 | .001 | 4.097 | .000 | 4.178 | .000 | 4.203 | .001 | 4.245 | .000 | 4.174 | .000 | 4.135 |
| CA | .000 | * | .000 | * | .000 | * | .004 | * | .004 | * | .003 | * | .006 | * | .001 | * |
| BA | .002 | * | .002 | * | .001 | * | .000 | * | .000 | * | .000 | * | .000 | * | .000 | * |
| K | 1.833 | * | 1.355 | * | 1.807 | * | 1.108 | * | 1.207 | * | .989 | * | 1.201 | * | 1.176 | * |
| NA | .105 | 1.939 | .126 | 1.483 | .067 | 1.876 | .012 | 1.124 | .008 | 1.219 | .010 | 1.002 | .003 | 1.209 | .007 | 1.185 |
| O | 22.000 | * | 22.000 | * | 22.000 | * | 22.000 | * | 22.000 | * | 22.000 | * | 22.000 | * | 22.000 | * |
| FE | 38.74 | | 37.48 | | 40.59 | | 14.28 | | 20.58 | | 19.24 | | 17.46 | | 12.84 | |
| MG | 61.26 | | 62.52 | | 59.41 | | 85.72 | | 79.42 | | 80.76 | | 82.54 | | 87.16 | |
| F/M | .632 | | .599 | | .685 | | .167 | | .259 | | .240 | | .212 | | .147 | |
| F/FM | .387 | | .375 | | .407 | | .143 | | .206 | | .194 | | .175 | | .128 | |

17 BRIGHT REL IM0011
18 BRIGHT REL IM0011
19 BRIGHT REL IM0011
20 DARK MARGIN ZONE
21 W V F GR PYRITE
22 W V F GR PYRITE
23 W V F GR PYRITE
24 INT W PY AND TI PHASE IM0013

TABLE 3: PHENGITIC MUSC, KAMINAK GOLD, ERIC BUITENHUIS, JUNE 2013, R.L.B.

| | 25 | | 26 | | 27 | | 28 | | 29 | | 30 | | 31 | | 32 | |
|---|---|---|---|---|---|---|---|---|---|---|---|---|---|---|---|---|
| SIO2 | 52.23 | | 51.68 | | 51.87 | | 52.82 | | 51.12 | | 51.99 | | 49.49 | | 48.47 | |
| TIO2 | 1.42 | | 1.55 | | 1.21 | | .00 | | .00 | | .12 | | .22 | | .31 | |
| A2O3 | 32.10 | | 31.57 | | 31.78 | | 36.41 | | 36.81 | | 35.49 | | 29.90 | | 31.04 | |
| C2O3 | .07 | | .08 | | .01 | | .07 | | .01 | | .10 | | .00 | | .00 | |
| FEO | .65 | | .77 | | .67 | | .09 | | .09 | | .13 | | 3.77 | | 4.16 | |
| MGO | 2.21 | | 2.33 | | 2.62 | | .80 | | .77 | | .97 | | 2.72 | | 2.33 | |
| MNO | .00 | | .00 | | .00 | | .00 | | .00 | | .00 | | .00 | | .00 | |
| BAO | .00 | | .00 | | .00 | | .00 | | .00 | | .00 | | .00 | | .00 | |
| CAO | .04 | | .05 | | .05 | | .13 | | .16 | | .16 | | .00 | | .00 | |
| K2O | 6.06 | | 6.02 | | 7.29 | | 6.39 | | 7.62 | | 7.50 | | 10.45 | | 8.68 | |
| NA2O | .05 | | .05 | | .00 | | .05 | | .03 | | .03 | | .18 | | .13 | |
| SUM | 94.83 | | 94.10 | | 95.50 | | 96.76 | | 96.61 | | 96.49 | | 96.73 | | 95.12 | |
| SI | 6.710 | * | 6.701 | * | 6.676 | * | 6.616 | * | 6.477 | * | 6.590 | * | 6.550 | * | 6.466 | * |
| AL | 1.290 | 8.000 | 1.299 | 8.000 | 1.324 | 8.000 | 1.384 | 8.000 | 1.523 | 8.000 | 1.410 | 8.000 | 1.450 | 8.000 | 1.534 | 8.000 |
| AL | 3.570 | * | 3.525 | * | 3.496 | * | 3.990 | * | 3.974 | * | 3.890 | * | 3.213 | * | 3.346 | * |
| TI | .137 | * | .151 | * | .117 | * | .000 | * | .000 | * | .011 | * | .022 | * | .031 | * |
| CR | .007 | * | .008 | * | .001 | * | .007 | * | .001 | * | .010 | * | .000 | * | .000 | * |
| FE | .070 | * | .083 | * | .072 | * | .009 | * | .010 | * | .014 | * | .417 | * | .464 | * |
| MG | .423 | * | .450 | * | .503 | * | .149 | * | .145 | * | .183 | * | .537 | * | .463 | * |
| MN | .000 | 4.208 | .000 | 4.218 | .000 | 4.188 | .000 | 4.156 | .000 | 4.130 | .000 | 4.109 | .000 | 4.189 | .000 | 4.304 |
| CA | .006 | * | .007 | * | .007 | * | .017 | * | .022 | * | .022 | * | .000 | * | .000 | * |
| BA | .000 | * | .000 | * | .000 | * | .000 | * | .000 | * | .000 | * | .000 | * | .000 | * |
| K | .993 | * | .996 | * | 1.197 | * | 1.021 | * | 1.232 | * | 1.212 | * | 1.764 | * | 1.477 | * |
| NA | .012 | 1.011 | .013 | 1.015 | .000 | 1.204 | .012 | 1.050 | .007 | 1.261 | .007 | 1.242 | .046 | 1.810 | .034 | 1.511 |
| O | 22.000 | * | 22.000 | * | 22.000 | * | 22.000 | * | 22.000 | * | 22.000 | * | 22.000 | * | 22.000 | * |
| FE | 14.16 | | 15.64 | | 12.55 | | 5.94 | | 6.15 | | 6.99 | | 43.75 | | 50.04 | |
| MG | 85.84 | | 84.36 | | 87.45 | | 94.06 | | 93.85 | | 93.01 | | 56.25 | | 49.96 | |
| F/M | .165 | | .185 | | .143 | | .063 | | .066 | | .075 | | .778 | | 1.002 | |
| F/FM | .142 | | .156 | | .125 | | .059 | | .062 | | .070 | | .437 | | .500 | |

25 INT W PY AND TI PHASE IM0013
26 INT W PY AND TI PHASE IM0013
27 INT W PY ANDTI PHASE IM0013
28 AWAY
29 AWAY
30 INT W MN DOL
31 **** DDH82-223.0m W GREEN BIO, C-1 IM1505,6
32 W BIO AND KSPAR

TABLE 3: PHENGITIC MUSC, KAMINAK GOLD, ERIC BUITENHUIS, JUNE 2013, R.L.B.

| | 33 | | 34 | | 35 | | 36 | | 37 | | 38 | | 39 | | 40 | |
|---|---|---|---|---|---|---|---|---|---|---|---|---|---|---|---|---|
| SIO2 | 48.52 | | 46.51 | | 47.45 | | 46.56 | | 47.81 | | 47.89 | | 47.29 | | 52.40 | |
| TIO2 | .20 | | .37 | | .23 | | .25 | | .00 | | .01 | | .00 | | .00 | |
| A2O3 | 32.32 | | 33.11 | | 33.54 | | 33.94 | | 32.77 | | 32.84 | | 33.50 | | 35.96 | |
| C2O3 | .02 | | .05 | | .00 | | .00 | | .00 | | .03 | | .02 | | .00 | |
| FEO | 3.32 | | 4.04 | | 3.48 | | 3.47 | | 3.86 | | 3.81 | | 4.02 | | .12 | |
| MGO | 1.24 | | 1.50 | | 1.33 | | 1.37 | | 1.92 | | 1.32 | | 1.47 | | .72 | |
| MNO | .00 | | .00 | | .00 | | .00 | | .01 | | .00 | | .00 | | .00 | |
| BAO | .00 | | .00 | | .00 | | .00 | | .00 | | .00 | | .00 | | .00 | |
| CAO | .00 | | .00 | | .00 | | .00 | | .00 | | .01 | | .00 | | .21 | |
| K2O | 10.33 | | 9.25 | | 10.37 | | 10.16 | | 9.51 | | 10.06 | | 10.12 | | 7.26 | |
| NA2O | .12 | | .07 | | .12 | | .13 | | .09 | | .09 | | .11 | | .07 | |
| SUM | 96.07 | | 94.90 | | 96.52 | | 95.88 | | 95.97 | | 96.06 | | 96.53 | | 96.74 | |
| SI | 6.436 | * | 6.248 | * | 6.282 | * | 6.206 | * | 6.343 | * | 6.363 | * | 6.269 | * | 6.607 | * |
| AL | 1.564 | 8.000 | 1.752 | 8.000 | 1.718 | 8.000 | 1.794 | 8.000 | 1.657 | 8.000 | 1.637 | 8.000 | 1.731 | 8.000 | 1.393 | 8.000 |
| AL | 3.488 | * | 3.489 | * | 3.514 | * | 3.536 | * | 3.467 | * | 3.505 | * | 3.502 | * | 3.950 | * |
| TI | .020 | * | .037 | * | .023 | * | .025 | * | .000 | * | .001 | * | .000 | * | .000 | * |
| CR | .002 | * | .005 | * | .000 | * | .000 | * | .000 | * | .003 | * | .002 | * | .000 | * |
| FE | .368 | * | .454 | * | .385 | * | .387 | * | .428 | * | .423 | * | .446 | * | .013 | * |
| MG | .245 | * | .300 | * | .262 | * | .272 | * | .380 | * | .261 | * | .290 | * | .135 | * |
| MN | .000 | 4.124 | .000 | 4.286 | .000 | 4.185 | .000 | 4.220 | .001 | 4.276 | .000 | 4.194 | .000 | 4.240 | .000 | 4.098 |
| CA | .000 | * | .000 | * | .000 | * | .000 | * | .000 | * | .001 | * | .000 | * | .028 | * |
| BA | .000 | * | .000 | * | .000 | * | .000 | * | .000 | * | .000 | * | .000 | * | .000 | * |
| K | 1.748 | * | 1.585 | * | 1.751 | * | 1.727 | * | 1.609 | * | 1.705 | * | 1.711 | * | 1.168 | * |
| NA | .031 | 1.779 | .018 | 1.603 | .031 | 1.782 | .034 | 1.761 | .023 | 1.632 | .023 | 1.730 | .028 | 1.739 | .017 | 1.213 |
| O | 22.000 | * | 22.000 | * | 22.000 | * | 22.000 | * | 22.000 | * | 22.000 | * | 22.000 | * | 22.000 | * |
| FE | 60.04 | | 60.18 | | 59.48 | | 58.70 | | 53.01 | | 61.82 | | 60.54 | | 8.55 | |
| MG | 39.96 | | 39.82 | | 40.52 | | 41.30 | | 46.99 | | 38.18 | | 39.46 | | 91.45 | |
| F/M | 1.502 | | 1.511 | | 1.468 | | 1.421 | | 1.131 | | 1.619 | | 1.534 | | .094 | |
| F/FM | .600 | | .602 | | .595 | | .587 | | .531 | | .618 | | .605 | | .086 | |

33 W BIO AND KSPAR
34 W BIO AND KSPAR
35 W BIO AND KSPAR
36 W BIO AND KSPAR
37 C-2
38 C-2
39 C-2
40 **** DDH97-102.0m MICA IN PERV CARB ALT

TABLE 3: PHENGITIC MUSC, KAMINAK GOLD, ERIC BUITENHUIS, JUNE 2013, R.L.B.

| | 41 | | 42 | | 43 | | 44 | | 45 | | 46 | | 47 | | 48 | |
|---|---|---|---|---|---|---|---|---|---|---|---|---|---|---|---|---|
| SIO2 | 51.37 | | 51.34 | | 53.44 | | 50.57 | | 52.76 | | 52.45 | | 53.20 | | 53.59 | |
| TIO2 | .00 | | 1.24 | | 1.40 | | .00 | | .00 | | 1.58 | | .00 | | .00 | |
| A2O3 | 35.04 | | 30.81 | | 31.20 | | 36.44 | | 36.32 | | 31.60 | | 35.66 | | 35.37 | |
| C2O3 | .00 | | .04 | | .04 | | .00 | | .00 | | .07 | | .00 | | .00 | |
| FEO | .08 | | .75 | | .71 | | .16 | | .23 | | .77 | | .31 | | .37 | |
| MGO | .67 | | 2.63 | | 2.39 | | .77 | | .72 | | 2.42 | | 1.16 | | 1.35 | |
| MNO | .00 | | .00 | | .00 | | .00 | | .00 | | .00 | | .00 | | .01 | |
| BAO | .00 | | .00 | | .00 | | .00 | | .00 | | .00 | | .00 | | .00 | |
| CAO | .16 | | .09 | | .12 | | .25 | | .22 | | .12 | | .16 | | .21 | |
| K2O | 7.20 | | 7.43 | | 5.88 | | 7.70 | | 6.83 | | 7.25 | | 7.03 | | 6.39 | |
| NA2O | .10 | | .02 | | .04 | | .08 | | .12 | | .05 | | .07 | | .07 | |
| SUM | 94.62 | | 94.35 | | 95.22 | | 95.97 | | 97.20 | | 96.31 | | 97.59 | | 97.36 | |
| SI | 6.623 | * | 6.704 | * | 6.824 | * | 6.464 | * | 6.606 | * | 6.697 | * | 6.644 | * | 6.683 | * |
| AL | 1.377 | 8.000 | 1.296 | 8.000 | 1.176 | 8.000 | 1.536 | 8.000 | 1.394 | 8.000 | 1.303 | 8.000 | 1.356 | 8.000 | 1.317 | 8.000 |
| AL | 3.947 | * | 3.445 | * | 3.519 | * | 3.953 | * | 3.964 | * | 3.452 | * | 3.891 | * | 3.880 | * |
| TI | .000 | * | .122 | * | .134 | * | .000 | * | .000 | * | .152 | * | .000 | * | .000 | * |
| CR | .000 | * | .004 | * | .004 | * | .000 | * | .000 | * | .007 | * | .000 | * | .000 | * |
| FE | .009 | * | .082 | * | .076 | * | .017 | * | .024 | * | .082 | * | .032 | * | .039 | * |
| MG | .129 | * | .512 | * | .455 | * | .147 | * | .134 | * | .461 | * | .216 | * | .251 | * |
| MN | .000 | 4.085 | .000 | 4.165 | .000 | 4.189 | .000 | 4.116 | .000 | 4.123 | .000 | 4.154 | .000 | 4.140 | .001 | 4.171 |
| CA | .022 | * | .013 | * | .016 | * | .034 | * | .030 | * | .016 | * | .021 | * | .028 | * |
| BA | .000 | * | .000 | * | .000 | * | .000 | * | .000 | * | .000 | * | .000 | * | .000 | * |
| K | 1.184 | * | 1.238 | * | .958 | * | 1.255 | * | 1.091 | * | 1.181 | * | 1.120 | * | 1.016 | * |
| NA | .025 | 1.231 | .005 | 1.255 | .010 | .984 | .020 | 1.309 | .029 | 1.149 | .012 | 1.210 | .017 | 1.158 | .017 | 1.061 |
| O | 22.000 | * | 22.000 | * | 22.000 | * | 22.000 | * | 22.000 | * | 22.000 | * | 22.000 | * | 22.000 | * |
| | FE | 6.28 | | 13.79 | | 14.29 | | 10.44 | | 15.20 | | 15.15 | | 13.04 | | 13.33 |
| | MG | 93.72 | | 86.21 | | 85.71 | | 89.56 | | 84.80 | | 84.85 | | 86.96 | | 86.67 |
| | F/M | .067 | | .160 | | .167 | | .117 | | .179 | | .179 | | .150 | | .158 |
| | F/FM | .063 | | .138 | | .143 | | .104 | | .152 | | .151 | | .130 | | .136 |

41 MICA IN PERV CARB ALT
42 MICA IN PERV CARB ALT
43 MICA IN PERV CARB ALT
44 MICA IN PERV CARB ALT
45 MICA IN PERV CARB ALT
46 MICA IN PERV CARB ALT
47 MICA IN PERV CARB ALT
48 MICA IN PERV CARB ALT

TABLE 3: PHENGITIC MUSC, KAMINAK GOLD, ERIC BUITENHUIS, JUNE 2013, R.L.B.

| | 49 | | 50 | | 51 | | 52 | | 53 | | 54 | | 55 | | 56 | |
|---|---|---|---|---|---|---|---|---|---|---|---|---|---|---|---|---|
| SIO2 | 52.47 | | 54.41 | | 52.83 | | 52.32 | | 54.44 | | 53.90 | | 51.95 | | 53.01 | |
| TIO2 | .23 | | .37 | | .00 | | .00 | | .00 | | .00 | | 2.26 | | 2.05 | |
| A2O3 | 35.54 | | 33.14 | | 35.09 | | 36.06 | | 36.07 | | 34.37 | | 30.41 | | 31.74 | |
| C2O3 | .03 | | .15 | | .05 | | .00 | | .00 | | .08 | | .44 | | .31 | |
| FEO | .38 | | .45 | | .29 | | .09 | | .02 | | .08 | | .61 | | .63 | |
| MGO | 1.11 | | 1.32 | | 1.07 | | 1.00 | | 1.00 | | 1.38 | | 2.93 | | 2.46 | |
| MNO | .00 | | .00 | | .00 | | .00 | | .04 | | .00 | | .00 | | .00 | |
| BAO | .00 | | .00 | | .00 | | .00 | | .00 | | .00 | | .00 | | .00 | |
| CAO | .09 | | .08 | | .17 | | .07 | | .06 | | .04 | | .16 | | .02 | |
| K2O | 7.47 | | 6.61 | | 7.21 | | 7.35 | | 4.97 | | 6.64 | | 7.27 | | 5.72 | |
| NA2O | .07 | | .05 | | .07 | | .02 | | .02 | | .07 | | .03 | | .04 | |
| SUM | 97.39 | | 96.58 | | 96.78 | | 96.91 | | 96.62 | | 96.56 | | 96.06 | | 95.98 | |
| SI | 6.594 | * | 6.846 | * | 6.662 | * | 6.587 | * | 6.749 | * | 6.771 | * | 6.672 | * | 6.722 | * |
| AL | 1.406 | 8.000 | 1.154 | 8.000 | 1.338 | 8.000 | 1.413 | 8.000 | 1.251 | 8.000 | 1.229 | 8.000 | 1.328 | 8.000 | 1.278 | 8.000 |
| AL | 3.857 | * | 3.760 | * | 3.877 | * | 3.936 | * | 4.019 | * | 3.858 | * | 3.274 | * | 3.464 | * |
| TI | .022 | * | .035 | * | .000 | * | .000 | * | .000 | * | .000 | * | .218 | * | .195 | * |
| CR | .003 | * | .015 | * | .005 | * | .000 | * | .000 | * | .008 | * | .045 | * | .031 | * |
| FE | .040 | * | .047 | * | .031 | * | .009 | * | .002 | * | .008 | * | .066 | * | .067 | * |
| MG | .208 | * | .248 | * | .201 | * | .188 | * | .185 | * | .258 | * | .561 | * | .465 | * |
| MN | .000 | 4.129 | .000 | 4.104 | .000 | 4.113 | .000 | 4.133 | .004 | 4.210 | .000 | 4.133 | .000 | 4.163 | .000 | 4.223 |
| CA | .012 | * | .011 | * | .023 | * | .009 | * | .008 | * | .005 | * | .022 | * | .003 | * |
| BA | .000 | * | .000 | * | .000 | * | .000 | * | .000 | * | .000 | * | .000 | * | .000 | * |
| K | 1.197 | * | 1.061 | * | 1.160 | * | 1.180 | * | .786 | * | 1.064 | * | 1.191 | * | .925 | * |
| NA | .017 | 1.227 | .012 | 1.084 | .017 | 1.200 | .005 | 1.195 | .005 | .799 | .017 | 1.086 | .007 | 1.220 | .010 | .938 |
| O | 22.000 | * | 22.000 | * | 22.000 | * | 22.000 | * | 22.000 | * | 22.000 | * | 22.000 | * | 22.000 | * |
| | FE | 16.11 | | 16.06 | | 13.20 | | 4.81 | | 1.11 | | 3.15 | | 10.46 | | 12.56 |
| | MG | 83.89 | | 83.94 | | 86.80 | | 95.19 | | 98.89 | | 96.85 | | 89.54 | | 87.44 |
| | F/M | .192 | | .191 | | .152 | | .050 | | .034 | | .033 | | .117 | | .144 |
| | F/FM | .161 | | .161 | | .132 | | .048 | | .033 | | .032 | | .105 | | .126 |

49 MICA IN PERV CARB ALT
50 MICA IN PERV CARB ALT
51 MICA IN PERV CARB ALT
52 MICA IN PERV CARB ALT
53 MICA IN PERV CARB ALT
54 MICA IN PERV CARB ALT
55 **** DDH97-220.0m C-1 FOL & INT W FE DOL C-1
56 FOL AAND INT W FE DOL C-1

TABLE 3: PHENGITIC MUSC, KAMINAK GOLD, ERIC BUITENHUIS, JUNE 2013, R.L.B.

| | 57 | | 58 | | 59 | | 60 | | 61 | | 62 | | 63 | | 64 | |
|---|---|---|---|---|---|---|---|---|---|---|---|---|---|---|---|---|
| SIO2 | 50.42 | | 51.55 | | 53.63 | | 52.61 | | 52.04 | | 54.09 | | 50.82 | | 51.95 | |
| TIO2 | 1.72 | | 2.19 | | 1.46 | | 1.93 | | 2.00 | | 2.00 | | 2.01 | | 2.01 | |
| A2O3 | 31.66 | | 30.73 | | 31.02 | | 31.08 | | 31.06 | | 31.38 | | 30.87 | | 31.14 | |
| C2O3 | .77 | | .38 | | .20 | | .34 | | .50 | | .50 | | .50 | | .50 | |
| FEO | .45 | | .61 | | .48 | | .86 | | .53 | | .53 | | .53 | | .53 | |
| MGO | 2.18 | | 2.70 | | 2.34 | | 2.70 | | 2.60 | | 2.59 | | 2.60 | | 2.59 | |
| MNO | .02 | | .00 | | .00 | | .00 | | .01 | | .01 | | .01 | | .01 | |
| BAO | .00 | | .00 | | .00 | | .00 | | .00 | | .00 | | .00 | | .00 | |
| CAO | .00 | | .03 | | .07 | | .15 | | .14 | | .14 | | .14 | | .14 | |
| K2O | 7.36 | | 7.14 | | 7.00 | | 7.21 | | 4.79 | | 4.74 | | 7.09 | | 7.31 | |
| NA2O | .02 | | .05 | | .03 | | .00 | | .01 | | .01 | | .01 | | .01 | |
| SUM | 94.60 | | 95.38 | | 96.23 | | 96.88 | | 93.68 | | 95.99 | | 94.58 | | 96.19 | |
| SI | 6.576 | * | 6.657 | * | 6.820 | * | 6.691 | * | 6.729 | * | 6.809 | * | 6.621 | * | 6.656 | * |
| AL | 1.424 | 8.000 | 1.343 | 8.000 | 1.180 | 8.000 | 1.309 | 8.000 | 1.271 | 8.000 | 1.191 | 8.000 | 1.379 | 8.000 | 1.344 | 8.000 |
| AL | 3.442 | * | 3.334 | * | 3.468 | * | 3.349 | * | 3.461 | * | 3.464 | * | 3.361 | * | 3.357 | * |
| TI | .169 | * | .213 | * | .140 | * | .185 | * | .194 | * | .189 | * | .197 | * | .194 | * |
| CR | .079 | * | .039 | * | .020 | * | .034 | * | .051 | * | .050 | * | .052 | * | .051 | * |
| FE | .049 | * | .066 | * | .051 | * | .091 | * | .057 | * | .056 | * | .058 | * | .057 | * |
| MG | .424 | * | .520 | * | .444 | * | .512 | * | .501 | * | .486 | * | .505 | * | .495 | * |
| MN | .002 | 4.165 | .000 | 4.171 | .000 | 4.122 | .000 | 4.171 | .001 | 4.266 | .001 | 4.246 | .001 | 4.173 | .001 | 4.154 |
| CA | .000 | * | .004 | * | .010 | * | .020 | * | .019 | * | .019 | * | .020 | * | .019 | * |
| BA | .000 | * | .000 | * | .000 | * | .000 | * | .000 | * | .000 | * | .000 | * | .000 | * |
| K | 1.224 | * | 1.176 | * | 1.135 | * | 1.170 | * | .790 | * | .761 | * | 1.178 | * | 1.195 | * |
| NA | .005 | 1.229 | .013 | 1.193 | .007 | 1.152 | .000 | 1.190 | .003 | .812 | .002 | .782 | .003 | 1.200 | .002 | 1.216 |
| O | 22.000 | * | 22.000 | * | 22.000 | * | 22.000 | * | 22.000 | * | 22.000 | * | 22.000 | * | 22.000 | * |
| FE | 10.38 | | 11.25 | | 10.32 | | 15.16 | | 10.26 | | 10.30 | | 10.26 | | 10.30 | |
| MG | 89.62 | | 88.75 | | 89.68 | | 84.84 | | 89.74 | | 89.70 | | 89.74 | | 89.70 | |
| F/M | .121 | | .127 | | .115 | | .179 | | .117 | | .117 | | .117 | | .117 | |
| F/FM | .108 | | .113 | | .103 | | .152 | | .104 | | .105 | | .104 | | .105 | |

57 AGAINST FABRIC, OLDER
58 INT W TI-MUSC FE DOL
59 INT W TI-MUSC, FE DOL
60 W FOL DOL C-2
61 W FOL DOL C-2
62 W NFOL DOL C-2
63 W FOL DOL C-2
64 W BFOL DOL C-2

TABLE 3: PHENGITIC MUSC, KAMINAK GOLD, ERIC BUITENHUIS, JUNE 2013, R.L.B.

| | 65 | | 66 | | 67 | | 68 | | 69 | | 70 | | 71 | | 72 | |
|---|---|---|---|---|---|---|---|---|---|---|---|---|---|---|---|---|
| SIO2 | 51.85 | | 51.84 | | 53.31 | | 52.15 | | 48.17 | | 47.79 | | 49.37 | | 48.09 | |
| TIO2 | 2.01 | | 2.01 | | 2.00 | | 2.01 | | .19 | | .29 | | .15 | | .16 | |
| A2O3 | 31.16 | | 30.81 | | 30.54 | | 30.32 | | 32.18 | | 34.27 | | 35.71 | | 33.54 | |
| C2O3 | .50 | | .50 | | .50 | | .50 | | .04 | | .00 | | .00 | | .00 | |
| FEO | .52 | | .53 | | .53 | | .53 | | 2.69 | | 2.76 | | 2.94 | | 2.90 | |
| MGO | 2.59 | | 2.60 | | 2.60 | | 2.60 | | 1.18 | | 1.15 | | 1.29 | | 1.33 | |
| MNO | .01 | | .01 | | .01 | | .01 | | .01 | | .02 | | .02 | | .05 | |
| BAO | .00 | | .00 | | .00 | | .00 | | .29 | | .45 | | .36 | | .00 | |
| CAO | .14 | | .14 | | .14 | | .14 | | .00 | | .00 | | .00 | | .00 | |
| K2O | 7.40 | | 7.20 | | 5.17 | | 7.07 | | 10.35 | | 7.75 | | 9.41 | | 10.31 | |
| NA2O | .01 | | .01 | | .01 | | .01 | | .31 | | .17 | | .36 | | .31 | |
| SUM | 96.19 | | 95.65 | | 94.81 | | 95.34 | | 95.41 | | 94.65 | | 99.61 | | 96.69 | |
| SI | 6.647 | * | 6.675 | * | 6.818 | * | 6.728 | * | 6.438 | * | 6.336 | * | 6.278 | * | 6.333 | * |
| AL | 1.353 | 8.000 | 1.325 | 8.000 | 1.182 | 8.000 | 1.272 | 8.000 | 1.562 | 8.000 | 1.664 | 8.000 | 1.722 | 8.000 | 1.667 | 8.000 |
| AL | 3.355 | * | 3.350 | * | 3.421 | * | 3.337 | * | 3.506 | * | 3.690 | * | 3.629 | * | 3.538 | * |
| TI | .194 | * | .195 | * | .192 | * | .195 | * | .019 | * | .029 | * | .014 | * | .016 | * |
| CR | .051 | * | .051 | * | .051 | * | .051 | * | .004 | * | .000 | * | .000 | * | .000 | * |
| FE | .056 | * | .057 | * | .057 | * | .057 | * | .301 | * | .306 | * | .313 | * | .319 | * |
| MG | .495 | * | .499 | * | .496 | * | .500 | * | .235 | * | .227 | * | .245 | * | .261 | * |
| MN | .001 | 4.151 | .001 | 4.153 | .001 | 4.218 | .001 | 4.142 | .001 | 4.066 | .002 | 4.254 | .002 | 4.203 | .006 | 4.140 |
| CA | .019 | * | .019 | * | .019 | * | .019 | * | .000 | * | .000 | * | .000 | * | .000 | * |
| BA | .000 | * | .000 | * | .000 | * | .000 | * | .015 | * | .023 | * | .018 | * | .000 | * |
| K | 1.210 | * | 1.182 | * | .843 | * | 1.163 | * | 1.764 | * | 1.311 | * | 1.526 | * | 1.732 | * |
| NA | .002 | 1.232 | .002 | 1.204 | .002 | .865 | .003 | 1.185 | .080 | 1.860 | .044 | 1.378 | .089 | 1.633 | .079 | 1.811 |
| O | 22.000 | * | 22.000 | * | 22.000 | * | 22.000 | * | 22.000 | * | 22.000 | * | 22.000 | * | 22.000 | * |
| | FE | 10.12 | | 10.26 | | 10.26 | | 10.26 | | 56.12 | | 57.38 | | 56.12 | | 55.02 |
| | MG | 89.88 | | 89.74 | | 89.74 | | 89.74 | | 43.88 | | 42.62 | | 43.88 | | 44.98 |
| | F/M | .115 | | .117 | | .117 | | .117 | | 1.284 | | 1.356 | | 1.288 | | 1.245 |
| | F/FM | .103 | | .104 | | .104 | | .104 | | .562 | | .576 | | .563 | | .555 |

65 BRIGHT ZONE DOLOMITE IM0020
66 INTERLEAVED W QTZ, DOL, AS-PYRITE W ASP
67 MATRIX
68 MATRIX
69 **** DDH105-182.0m INT W QTZ KAOLINITE
70 INT W QTZ KAOL
71 INT W QTZ KAOL
72 INT W QTZ KAOL

TABLE 3: PHENGITIC MUSC, KAMINAK GOLD, ERIC BUITENHUIS, JUNE 2013, R.L.B.

| | 73 | | 74 | | 75 | | 76 | | 77 | | 78 | | 79 | | 80 | |
|---|---|---|---|---|---|---|---|---|---|---|---|---|---|---|---|---|
| SIO2 | 48.26 | | 46.28 | | 47.63 | | 48.65 | | 50.40 | | 50.78 | | 49.48 | | 46.71 | |
| TIO2 | .13 | | .15 | | .15 | | .55 | | .27 | | .21 | | .20 | | .58 | |
| A2O3 | 33.49 | | 33.21 | | 32.76 | | 29.30 | | 26.56 | | 26.64 | | 26.98 | | 29.76 | |
| C2O3 | .00 | | .02 | | .11 | | .03 | | .00 | | .05 | | .04 | | .00 | |
| FEO | 3.37 | | 2.91 | | 2.87 | | 3.93 | | 3.36 | | 3.54 | | 3.20 | | 3.88 | |
| MGO | 2.19 | | 1.66 | | 1.31 | | 2.71 | | 3.58 | | 3.49 | | 3.52 | | 2.32 | |
| MNO | .05 | | .06 | | .00 | | .00 | | .06 | | .00 | | .00 | | .00 | |
| BAO | .00 | | .00 | | .10 | | .00 | | .00 | | .07 | | .00 | | .03 | |
| CAO | .00 | | .00 | | .00 | | .00 | | .00 | | .00 | | .00 | | .00 | |
| K2O | 10.97 | | 9.09 | | 10.72 | | 11.00 | | 9.92 | | 10.68 | | 10.76 | | 11.01 | |
| NA2O | .13 | | .10 | | .37 | | .21 | | .18 | | .14 | | .22 | | .20 | |
| SUM | 98.59 | | 93.48 | | 96.02 | | 96.38 | | 94.33 | | 95.60 | | 94.40 | | 94.49 | |
| SI | 6.276 | * | 6.270 | * | 6.346 | * | 6.506 | * | 6.808 | * | 6.804 | * | 6.719 | * | 6.389 | * |
| AL | 1.724 | 8.000 | 1.730 | 8.000 | 1.654 | 8.000 | 1.494 | 8.000 | 1.192 | 8.000 | 1.196 | 8.000 | 1.281 | 8.000 | 1.611 | 8.000 |
| AL | 3.407 | * | 3.572 | * | 3.488 | * | 3.123 | * | 3.035 | * | 3.011 | * | 3.036 | * | 3.185 | * |
| TI | .013 | * | .015 | * | .015 | * | .055 | * | .027 | * | .021 | * | .020 | * | .060 | * |
| CR | .000 | * | .002 | * | .012 | * | .003 | * | .000 | * | .005 | * | .004 | * | .000 | * |
| FE | .366 | * | .330 | * | .320 | * | .439 | * | .380 | * | .397 | * | .363 | * | .444 | * |
| MG | .424 | * | .335 | * | .260 | * | .540 | * | .721 | * | .697 | * | .712 | * | .473 | * |
| MN | .006 | 4.216 | .007 | 4.261 | .000 | 4.095 | .000 | 4.161 | .007 | 4.170 | .000 | 4.131 | .000 | 4.136 | .000 | 4.162 |
| CA | .000 | * | .000 | * | .000 | * | .000 | * | .000 | * | .000 | * | .000 | * | .000 | * |
| BA | .000 | * | .000 | * | .005 | * | .000 | * | .000 | * | .004 | * | .000 | * | .002 | * |
| K | 1.819 | * | 1.571 | * | 1.822 | * | 1.876 | * | 1.709 | * | 1.825 | * | 1.864 | * | 1.921 | * |
| NA | .033 | 1.852 | .026 | 1.597 | .096 | 1.922 | .054 | 1.931 | .047 | 1.756 | .036 | 1.865 | .058 | 1.922 | .053 | 1.975 |
| O | 22.000 | * | 22.000 | * | 22.000 | * | 22.000 | * | 22.000 | * | 22.000 | * | 22.000 | * | 22.000 | * |
| FE | 46.33 | | 49.59 | | 55.14 | | 44.86 | | 34.49 | | 36.27 | | 33.78 | | 48.41 | |
| MG | 53.67 | | 50.41 | | 44.86 | | 55.14 | | 65.51 | | 63.73 | | 66.22 | | 51.59 | |
| F/M | .876 | | 1.004 | | 1.229 | | .814 | | .536 | | .569 | | .510 | | .938 | |
| F/FM | .467 | | .501 | | .551 | | .449 | | .349 | | .363 | | .338 | | .484 | |

73 INT W QTZ KAOL
74 INT W QTZ KAOL
75 INT W QTZ KAOL
76 **** DDH114-114.0m C-1 INT W CHL AFTER BIO
77 PROG DARKER
78 PROG DARKER
79 INT W PHENG MUSC
80 INT W PHENG MUSC

TABLE 3: PHENGITIC MUSC, KAMINAK GOLD, ERIC BUITENHUIS, JUNE 2013, R.L.B.

| | 81 | | 82 | | 83 | |
|---|---|---|---|---|---|---|
| SIO2 | 50.09 | | 49.38 | | 47.49 | |
| TIO2 | .17 | | .56 | | .52 | |
| A2O3 | 26.59 | | 30.52 | | 29.82 | |
| C2O3 | .00 | | .00 | | .00 | |
| FEO | 3.15 | | 3.51 | | 4.01 | |
| MGO | 3.53 | | 2.39 | | 2.41 | |
| MNO | .02 | | .00 | | .05 | |
| BAO | .05 | | .00 | | .00 | |
| CAO | .00 | | .00 | | .00 | |
| K2O | 10.09 | | 10.29 | | 9.24 | |
| NA2O | .13 | | .25 | | .19 | |
| SUM | 93.82 | | 96.90 | | 93.73 | |
| SI | 6.804 | * | 6.510 | * | 6.467 | * |
| AL | 1.196 | 8.000 | 1.490 | 8.000 | 1.533 | 8.000 |
| AL | 3.061 | * | 3.251 | * | 3.252 | * |
| TI | .017 | * | .056 | * | .053 | * |
| CR | .000 | * | .000 | * | .000 | * |
| FE | .358 | * | .387 | * | .457 | * |
| MG | .715 | * | .470 | * | .489 | * |
| MN | .002 | 4.153 | .000 | 4.164 | .006 | 4.257 |
| CA | .000 | * | .000 | * | .000 | * |
| BA | .003 | * | .000 | * | .000 | * |
| K | 1.748 | * | 1.730 | * | 1.605 | * |
| NA | .034 | 1.785 | .064 | 1.794 | .050 | 1.655 |
| O | 22.000 | * | 22.000 | * | 22.000 | * |
| FE | 33.36 | | 45.18 | | 48.28 | |
| MG | 66.64 | | 54.82 | | 51.72 | |
| F/M | .504 | | .824 | | .945 | |
| F/FM | .335 | | .452 | | .486 | |

81 C PLATE W BA-KSPAR
82 C PLATE W BA-KSPAR
83 C PLATE W BA-KSPAR

TABLE 4: CARBONATE, KAMINAK GOLD, ERIC BUITENHUIS, JUNE 2013, R,L.B.

| | 1 | 2 | 3 | 4 | 5 | 6 | 7 | 8 |
|---|---|---|---|---|---|---|---|---|
| SIO2 | .00 | .00 | .79 | .57 | .00 | .00 | .00 | .03 |
| TIO2 | .00 | .00 | .00 | .00 | .00 | .00 | .00 | .00 |
| A2O3 | .04 | .09 | .56 | .56 | .07 | .12 | .15 | .23 |
| C2O3 | .00 | .00 | .02 | .00 | .00 | .00 | .00 | .00 |
| FEO | .99 | .97 | 9.48 | 1.40 | 7.02 | 6.48 | 5.30 | 5.66 |
| MGO | 21.35 | 22.29 | 15.40 | 21.39 | 16.87 | 17.35 | 18.36 | 18.21 |
| MNO | 1.23 | 1.36 | .19 | 1.48 | .36 | .24 | .23 | .23 |
| CAO | 32.29 | 32.96 | 27.32 | 32.77 | 31.90 | 31.24 | 31.04 | 28.71 |
| K2O | .01 | .06 | .20 | .03 | .00 | .00 | .00 | .00 |
| NA2O | .00 | .00 | .00 | .00 | .01 | .03 | .00 | .00 |
| SUM | 55.91 | 57.73 | 53.17 | 57.63 | 56.23 | 55.46 | 55.08 | 53.04 |

| | | | | | | | | | | | | | | | | |
|---|---|---|---|---|---|---|---|---|---|---|---|---|---|---|---|---|
| AL | .015 | .015 | .033 | .033 | .236 | .236 | .206 | .206 | .028 | .028 | .048 | .048 | .059 | .059 | .094 | .094 |
| AL | .000 | * | .000 | * | .000 | * | .000 | * | .000 | * | .000 | * | .000 | * | .000 | * |
| TI | .000 | * | .000 | * | .000 | * | .000 | * | .000 | * | .000 | * | .000 | * | .000 | * |
| CR | .000 | * | .000 | * | .006 | * | .000 | * | .000 | * | .000 | * | .000 | * | .000 | * |
| FE | .266 | * | .252 | * | 2.838 | * | .366 | * | 1.968 | * | 1.829 | * | 1.488 | * | 1.647 | * |
| MG | 10.240 | * | 10.339 | * | 8.217 | * | 9.959 | * | 8.429 | * | 8.727 | * | 9.189 | * | 9.443 | * |
| MN | .335 | 10.842 | .358 | 10.949 | .058 | 11.118 | .392 | 10.717 | .102 | 10.499 | .069 | 10.624 | .065 | 10.743 | .068 | 11.157 |
| CA | 11.133 | * | 10.989 | * | 10.479 | * | 10.968 | * | 11.457 | * | 11.295 | * | 11.168 | * | 10.701 | * |
| K | .004 | * | .024 | * | .091 | * | .012 | * | .000 | * | .000 | * | .000 | * | .000 | * |
| NA | .000 | 11.137 | .000 | 11.013 | .000 | 10.570 | .000 | 10.980 | .006 | 11.463 | .020 | 11.314 | .000 | 11.168 | .000 | 10.701 |
| O | 22.000 | * | 22.000 | * | 22.000 | * | 22.000 | * | 22.000 | * | 22.000 | * | 22.000 | * | 22.000 | * |

| | | | | | | | | |
|---|---|---|---|---|---|---|---|---|
| DOL | 47.32 | 47.91 | 38.16 | 46.77 | 38.57 | 39.94 | 42.07 | 43.33 |
| CAL | 51.45 | 50.92 | 48.66 | 51.51 | 52.43 | 51.69 | 51.12 | 49.11 |
| ANK | 1.23 | 1.17 | 13.18 | 1.72 | 9.01 | 8.37 | 6.81 | 7.56 |
| M/M | .059 | .059 | .352 | .076 | .246 | .217 | .169 | .182 |
| F/FM | .055 | .056 | .261 | .071 | .197 | .179 | .145 | .154 |

1 **** DDH82-117.5m W PYRITE-MUSC ALT C-2 IM1619, BSE0009
2 DOLOMITE-ANK INT W MUSC-PYRITE
3 SMALL DOMAIN IN MUSC
4 W HIGHLY ALTERED HYD MICA
5 **** DDH97-102.0m LATE CARB VEIN IN BLEACHED DOMAIN
6 FE DOLOMITE LATE
7 INT W PY IN DEFORMED DOMAIN
8 **** DDH97-220.0m C-1 INT W MUSC

TABLE 4: CARBONATE, KAMINAK GOLD, ERIC BUITENHUIS, JUNE 2013, R,L.B.

| | 9 | 10 | 11 | 12 | 13 | 14 | 15 | 16 |
|---|---|---|---|---|---|---|---|---|
| SIO2 | .03 | .03 | .03 | .03 | .03 | .03 | .03 | .03 |
| TIO2 | .00 | .00 | .00 | .00 | .00 | .00 | .00 | .00 |
| A2O3 | .23 | .23 | .23 | .23 | .23 | .23 | .23 | .23 |
| C2O3 | .00 | .00 | .00 | .00 | .00 | .00 | .00 | .00 |
| FEO | 5.34 | 5.76 | 5.38 | 6.47 | 5.35 | 5.95 | 4.04 | 6.98 |
| MGO | 18.18 | 18.10 | 19.32 | 15.18 | 15.95 | 15.16 | 17.11 | 16.01 |
| MNO | .20 | .29 | .25 | .16 | .18 | .11 | .05 | .08 |
| CAO | 27.40 | 29.57 | 29.37 | 31.23 | 31.96 | 31.63 | 32.48 | 30.39 |
| K2O | .00 | .00 | .00 | .00 | .00 | .00 | .00 | .00 |
| NA2O | .00 | .00 | .00 | .00 | .00 | .00 | .00 | .00 |
| SUM | 51.35 | 53.95 | 54.55 | 53.27 | 53.67 | 53.08 | 53.91 | 53.69 |

| | | | | | | | | | | | | | | | | |
|---|---|---|---|---|---|---|---|---|---|---|---|---|---|---|---|---|
| AL | .097 | .097 | .093 | .093 | .091 | .091 | .096 | .096 | .095 | .095 | .096 | .096 | .093 | .093 | .095 | .095 |
| AL | .000 | * | .000 | * | .000 | * | .000 | * | .000 | * | .000 | * | .000 | * | .000 | * |
| TI | .000 | * | .000 | * | .000 | * | .000 | * | .000 | * | .000 | * | .000 | * | .000 | * |
| CR | .000 | * | .000 | * | .000 | * | .000 | * | .000 | * | .000 | * | .000 | * | .000 | * |
| FE | 1.598 | * | 1.653 | * | 1.514 | * | 1.919 | * | 1.561 | * | 1.767 | * | 1.159 | * | 2.047 | * |
| MG | 9.694 | * | 9.255 | * | 9.690 | * | 8.023 | * | 8.295 | * | 8.023 | * | 8.749 | * | 8.368 | * |
| MN | .061 | 11.352 | .084 | 10.992 | .071 | 11.275 | .048 | 9.990 | .053 | 9.910 | .033 | 9.823 | .015 | 9.922 | .024 | 10.439 |
| CA | 10.502 | * | 10.869 | * | 10.588 | * | 11.866 | * | 11.948 | * | 12.033 | * | 11.938 | * | 11.418 | * |
| K | .000 | * | .000 | * | .000 | * | .000 | * | .000 | * | .000 | * | .000 | * | .000 | * |
| NA | .000 | 10.502 | .000 | 10.869 | .000 | 10.588 | .000 | 11.866 | .000 | 11.948 | .000 | 12.033 | .000 | 11.938 | .000 | 11.418 |
| O | 22.000 | * | 22.000 | * | 22.000 | * | 22.000 | * | 22.000 | * | 22.000 | * | 22.000 | * | 22.000 | * |
| | DOL | 44.48 | | 42.50 | | 44.46 | | 36.79 | | 38.04 | | 36.77 | | 40.05 | | 38.33 |
| | CAL | 48.19 | | 49.91 | | 48.59 | | 54.41 | | 54.80 | | 55.14 | | 54.65 | | 52.30 |
| | ANK | 7.33 | | 7.59 | | 6.95 | | 8.80 | | 7.16 | | 8.10 | | 5.31 | | 9.38 |
| | F/M | .171 | | .188 | | .164 | | .245 | | .195 | | .224 | | .134 | | .247 |
| | F/FM | .146 | | .158 | | .141 | | .197 | | .163 | | .183 | | .118 | | .198 |

9 C-1 INT W MUSC
10 C-1 INT W MUSC
11 C-1 INT W MUSC
12 **** DDH99-157.0m WIDE VEINLET
13 WIDE VEINLET IN QTZ
14 BRIGHTER
15 BRIGHTER
16 BRIGHTER

TABLE 4: CARBONATE, KAMINAK GOLD, ERIC BUITENHUIS, JUNE 2013, R,L.B.

| | 17 | 18 | 19 | 20 | 21 | 22 | 23 | 24 |
|---|---|---|---|---|---|---|---|---|
| SIO2 | .03 | .03 | .03 | .03 | .03 | .03 | .03 | .03 |
| TIO2 | .00 | .00 | .00 | .00 | .00 | .00 | .00 | .00 |
| A2O3 | .23 | .23 | .23 | .23 | .23 | .23 | .23 | .23 |
| C2O3 | .00 | .00 | .00 | .00 | .00 | .00 | .00 | .00 |
| FEO | 6.70 | 3.25 | 3.27 | 5.54 | .86 | 3.68 | 4.00 | 5.70 |
| MGO | 15.81 | 18.47 | 19.44 | 15.44 | 19.53 | 17.69 | 17.68 | 15.56 |
| MNO | .13 | .33 | .21 | .12 | .00 | .00 | .05 | .16 |
| CAO | 31.39 | 28.55 | 29.30 | 31.05 | 31.60 | 31.49 | 32.98 | 33.05 |
| K2O | .00 | .00 | .00 | .00 | .00 | .00 | .00 | .00 |
| NA2O | .00 | .00 | .00 | .00 | .00 | .00 | .00 | .00 |
| SUM | 54.26 | 50.83 | 52.45 | 52.38 | 52.22 | 53.09 | 54.94 | 54.70 |

| | | | | | | | | | | | | | | | | |
|---|---|---|---|---|---|---|---|---|---|---|---|---|---|---|---|---|
| AL | .094 | .094 | .097 | .097 | .094 | .094 | .097 | .097 | .093 | .093 | .094 | .094 | .091 | .091 | .093 | .093 |
| AL | .000 | * | .000 | * | .000 | * | .000 | * | .000 | * | .000 | * | .000 | * | .000 | * |
| TI | .000 | * | .000 | * | .000 | * | .000 | * | .000 | * | .000 | * | .000 | * | .000 | * |
| CR | .000 | * | .000 | * | .000 | * | .000 | * | .000 | * | .000 | * | .000 | * | .000 | * |
| FE | 1.947 | * | .972 | * | .945 | * | 1.659 | * | .247 | * | 1.065 | * | 1.124 | * | 1.641 | * |
| MG | 8.188 | * | 9.844 | * | 10.009 | * | 8.243 | * | 9.992 | * | 9.122 | * | 8.854 | * | 7.983 | * |
| MN | .038 | 10.173 | .100 | 10.916 | .061 | 11.015 | .036 | 9.939 | .000 | 10.239 | .000 | 10.187 | .014 | 9.992 | .047 | 9.671 |
| CA | 11.686 | * | 10.938 | * | 10.844 | * | 11.916 | * | 11.621 | * | 11.672 | * | 11.872 | * | 12.189 | * |
| K | .000 | * | .000 | * | .000 | * | .000 | * | .000 | * | .000 | * | .000 | * | .000 | * |
| NA | .000 | 11.686 | .000 | 10.938 | .000 | 10.844 | .000 | 11.916 | .000 | 11.621 | .000 | 11.672 | .000 | 11.872 | .000 | 12.189 |
| O | 22.000 | * | 22.000 | * | 22.000 | * | 22.000 | * | 22.000 | * | 22.000 | * | 22.000 | * | 22.000 | * |

| | | | | | | | | |
|---|---|---|---|---|---|---|---|---|
| DOL | 37.52 | 45.25 | 45.92 | 37.78 | 45.71 | 41.73 | 40.52 | 36.60 |
| CAL | 53.55 | 50.28 | 49.75 | 54.61 | 53.16 | 53.40 | 54.33 | 55.88 |
| ANK | 8.92 | 4.47 | 4.33 | 7.61 | 1.13 | 4.87 | 5.14 | 7.52 |
| | | | | | | | | |
| F/M | .242 | .109 | .101 | .206 | .025 | .117 | .129 | .211 |
| F/FM | .195 | .098 | .091 | .171 | .024 | .105 | .114 | .174 |

17 BRIGHTER
18 EXT F GRAINED, C-2
19 EXT F GRAINED, C-2
20 ADJ C VEIBNLIKE
21 VERY DARK BSE IM0018
22 INTERIOR OF ZONED GRAIN
23 INTERIOR OF ZONED GRAIN
24 IN BRIGHT ZONES

TABLE 4: CARBONATE, KAMINAK GOLD, ERIC BUITENHUIS, JUNE 2013, R,L.B.

| | 25 | | 26 | |
|---|---|---|---|---|
| SIO2 | .03 | | .03 | |
| TIO2 | .00 | | .00 | |
| A2O3 | .23 | | .23 | |
| C2O3 | .00 | | .00 | |
| FEO | 5.38 | | 6.77 | |
| MGO | 15.96 | | 14.06 | |
| MNO | .05 | | .21 | |
| CAO | 32.99 | | 32.46 | |
| K2O | .00 | | .00 | |
| NA2O | .00 | | .00 | |
| SUM | 54.61 | | 53.73 | |
| AL | .093 | .093 | .096 | .096 |
| AL | .000 | * | .000 | * |
| TI | .000 | * | .000 | * |
| CR | .000 | * | .000 | * |
| FE | 1.545 | * | 2.010 | * |
| MG | 8.167 | * | 7.438 | * |
| MN | .015 | 9.726 | .063 | 9.511 |
| CA | 12.134 | * | 12.344 | * |
| K | .000 | * | .000 | * |
| NA | .000 | 12.134 | .000 | 12.344 |
| O | 22.000 | * | 22.000 | * |
| DOL | 37.38 | | 34.13 | |
| CAL | 55.55 | | 56.65 | |
| ANK | 7.07 | | 9.22 | |
| F/M | .191 | | .279 | |
| F/FM | .160 | | .218 | |

25 IN BRIGHT ZONES
26 IN BRIGHT ZONES

## LATTE ZONE: PIMA SPECTRAL ANALYSIS

| Sample | Lith | Au g/t | Min1 | Min2 | Error | hqd1900 | hqd2200 | w2200 | width2200 | hqd2250 | w2250 | hqd2350 | w2350 | width2350 |
|---|---|---|---|---|---|---|---|---|---|---|---|---|---|---|
| LAT85-205.50 | PyF | 3.34 | Illite | NULL | 75.57 | 0.0546 | 0.142 | 2205.83 | 31545 | NULL | NULL | 0.0477 | 2343.84 | 36.292 |
| | | | Illite | NULL | 47.431 | 0.0719 | 0.15 | 2202.06 | 33.107 | NULL | NULL | 0.0472 | 2348.77 | 39.497 |
| | | | Illite | Kaolinite | 60.773 | 0.0621 | 0.134 | 2206.76 | 29.678 | NULL | NULL | 0.0398 | 2349.28 | 37.919 |
| | | | Illite | Kaolinite | 94.009 | 0.0584 | 0.12 | 2207.3 | 27.643 | 0.0243 | 2242.83 | 0.0272 | 2349.96 | 37.541 |
| LAT82-55.50 | HU | 156 | Kaolinite | NULL | 82.337 | 0.375 | 0.263 | 2207.6 | 27.509 | NULL | NULL | 0.0383 | 2326.11 | 35.946 |
| | | | Kaolinite | NULL | 53.299 | 0.358 | 0.361 | 2207.82 | 26.489 | NULL | NULL | 0.0622 | 2323.8 | 32.041 |
| LAT82-94.60 | RQM | 4.44 | Illite | DryVegetation | 52.832 | 0.323 | 0.314 | 2196.63 | 34.187 | NULL | NULL | 0.0988 | 2338.49 | 38.32 |
| | | | Illite | DryVegetation | 50.428 | 0.319 | 0.305 | 2196.91 | 34.263 | NULL | NULL | 0.0966 | 2339.53 | 39.289 |
| | | | Gypsum | Illite | 86.059 | 0.374 | 0.142 | 2206.66 | 33.411 | NULL | NULL | 0.00666 | 2332.91 | 28.805 |
| LAT82-131.50 | RQM | 0.337 | Illite | NULL | 70.038 | 0.354 | 0.251 | 2199.18 | 35.147 | NULL | NULL | 0.0635 | 2345.78 | 36.028 |
| | | | Illite | Jarosite | 64.706 | 0.45 | 0.282 | 2197.04 | 34.843 | 0.0479 | 2257.71 | 0.0436 | 2339.59 | 34.073 |
| | | | Illite | Jarosite | 73.398 | 0.372 | 0.228 | 2197.06 | 34.56 | 0.0419 | 2258.21 | 0.0316 | 2342.93 | 32.525 |
| LAT82-183.40 | RQM | 2.12 | Kaolinite | Illite | 297.65 | 0.0763 | 0.0709 | 2206.38 | 29.5 | 0.00855 | 2242.64 | 0.0151 | 2344.87 | 38.395 |
| | | | Illite | Gypsum | 338.31 | 0.137 | 0.0666 | 2205.55 | 30.665 | NULL | NULL | 0.0101 | 2356.49 | 29.437 |
| LAT82-184.70 | SZ | 0.028 | Serpentine | Talc | 93.475 | 0.141 | NULL | NULL | NULL | NULL | NULL | 0.262 | 2312.93 | 35.179 |
| | | | Talc | NULL | 190.13 | 0.105 | NULL | NULL | NULL | NULL | NULL | 0.351 | 2311.63 | 24.862 |
| | | | Serpentine | Talc | 94.77 | 0.141 | NULL | NULL | NULL | NULL | NULL | 0.295 | 2312.26 | 31.371 |
| LAT78-268.40 | YC | 0.6 | Illite | NULL | 27.473 | 0.313 | 0.466 | 2197.44 | 33.85 | NULL | NULL | 0.217 | 2348.02 | 38.731 |
| | | | Illite | NULL | 41.078 | 0.232 | 0.337 | 2200.47 | 34.379 | NULL | NULL | 0.159 | 2346.7 | 40.081 |
| LAT78-270.50 | HU | 0.366 | Muscovite | Gypsum | 466.32 | 0.27 | 0.0897 | 2208.75 | 25.205 | NULL | NULL | 0.00792 | 2325.95 | 21.358 |
| | | | Muscovite | Kaolinite | 144.33 | 0.0557 | 0.0921 | 2207.81 | 24.917 | 0.0253 | 2240.88 | 0.0248 | 2350.44 | 35.801 |
| | | | Kaolinite | Gypsum | 274.33 | 0.166 | 0.119 | 2207.94 | 25.014 | NULL | NULL | 0.00773 | 2321.47 | 22.985 |
| LAT89-46.70 | RQM | 0.086 | Dickite | Muscovite | 65.962 | 0.244 | 0.207 | 2206.88 | 28.336 | NULL | NULL | 0.0442 | 2352.49 | 33.904 |
| | | | Muscovite | Dickite | 74.334 | 0.224 | 0.2 | 2206.74 | 27.477 | NULL | NULL | 0.0414 | 2353.67 | 32.981 |
| | | | Muscovite | Dickite | 66.596 | 0.344 | 0.192 | 2206.34 | 28.355 | NULL | NULL | 0.0397 | 2354.38 | 30.413 |
| | | | Muscovite | Dickite | 61.442 | 0.27 | 0.155 | 2206.62 | 28.665 | NULL | NULL | 0.0237 | 2350.72 | 27.835 |
| LAT89-47.80 | HU | 0.082 | Kaolinite | Paragonite | 88.822 | 0.235 | 0.205 | 2207.68 | 31003 | 0.0292 | 224154 | NULL | NULL | NULL |
| | | | Kaolinite | NULL | 115.41 | 0.223 | 0.192 | 2207.71 | 29.956 | NULL | NULL | 0.0294 | 2357.95 | 34.471 |
| LAT89-111.50 | YC | 4.23 | Illite | Palygorskite | 44.596 | 0.402 | 0.202 | 2207.47 | 31715 | NULL | NULL | 0.0751 | 2343.56 | 37.326 |
| | | | Illite | Phengite | 36.279 | 0.223 | 0.223 | 2206.31 | 31204 | NULL | NULL | 0.0902 | 2345.49 | 37.969 |
| | | | Illite | Kaolinite | 46.159 | 0.271 | 0.356 | 2207.52 | 27.94 | NULL | NULL | 0.129 | 2344.74 | 39.274 |
| LAT102-30.90 | HU | 0.023 | Kaolinite | Opal | 50.246 | 0.42 | 0.195 | 2207.86 | 23.903 | NULL | NULL | 0.0238 | 2300.4 | 32.052 |
| | | | Kaolinite | Opal | 33.231 | 0.401 | 0.283 | 2207.72 | 25.245 | NULL | NULL | 0.0301 | 2356.15 | 35.44 |
| | | | Kaolinite | NULL | 55.472 | 0.393 | 0.223 | 2207.73 | 25.566 | 0.00607 | 2240.36 | 0.0234 | 2319.39 | 34.411 |
| LAT102-50.0 | RQM | 1.475 | Illite | NULL | 90.168 | 0.416 | 0.311 | 2197.69 | 35.496 | NULL | NULL | 0.0814 | 2347.43 | 38.689 |
| | | | Illite | NULL | 124.86 | 0.442 | 0.273 | 2198.27 | 35.67 | NULL | NULL | 0.0581 | 2346.97 | 38.213 |
| | | | Illite | NULL | 33.73 | 0.429 | 0.296 | 2196.82 | 35.24 | NULL | NULL | 0.0769 | 2344.98 | 38.951 |

Note: "LAT85-205.50" corresponds to CFD0085, 205.50m

# Appendices E, F

Appendix E consists of a Microsoft Excel worksheet with complete 35-element ICP-AES assay data for the Latte zone.

Appendix F consists of a Leapfrog Viewer file containing a 3D model of the Latte Zone (Leapfrog – ARANZ Geo Limited). To view the file, Leapfrog Viewer is available as a free download from: http://www.leapfrog3d.com/products/Leapfrog-Viewer

# Curriculum Vitae

| | |
|---|---|
| **Name:** | Eric Buitenhuis |
| **Post-secondary Education and Degrees:** | University of Western Ontario<br>London, Ontario, Canada<br>2007-2011 HBSc<br><br>The University of Western Ontario<br>London, Ontario, Canada<br>2011-2014 MSc |
| **Honours and Awards:** | Society of Economic Geologists: Graduate Student Fellowship 2012<br><br>Yukon Geological Survey: The Geoffrey Bradshaw Memorial Scholarship 2012 |
| **Related Work Experience** | Exploration Geologist<br>Kaminak Gold Corporation<br>2011-Present<br><br>Graduate Teaching Assistant<br>The University of Western Ontario<br>2011-2013<br><br>Research Assistant<br>The University of Western Ontario<br>May 2010 – August 2010 |

**Publications:**

Sapers, H.M., Osinski, G.R., Buitenhuis, E., Banerjee, N.R., Flemming, R.L., Hainge, J., and Blain, S. 2012. The Ries Post-Impact Hydrothermal System: Spatial and Temporal Mineralogical Variation. 43rd Lunar and Plentary Science Conference. #1915.